

THE REACTIVE ABSORPTION OF CO₂ INTO SOLUTIONS OF MEA/2-PROPANOL

by

Louis Jacobus du Preez

Thesis submitted in fulfillment of the requirements for the Degree

The crest of the University of Stellenbosch, featuring a shield with various symbols, topped with a crown and flanked by two figures.

of
MASTER OF SCIENCE IN ENGINEERING
(CHEMICAL ENGINEERING)

in the Department of Process Engineering at the University of
Stellenbosch

Supervised by

Prof. J.H. Knoetze

STELLENBOSCH

March 2010

Declaration

I, L.J. du Preez, hereby declare that the work contained in this thesis is my own original work and that I have not previously in its entirety or in part submitted it at any university for a degree.

.....

Signature

.....

Date

ABSTRACT

The discovery that the reaction of CO₂ with primary amines in both aqueous and non-aqueous media provides a viable chemical method for determining the effective interfacial mass transfer area for separation column internals has led to an increase in the interest of studying the reaction kinetics and determining the governing reaction rate expressions. For the absorption studies conducted on these systems, many authors assumed that power rate law reaction kinetics govern the reaction rate, which simplified the derivation of absorption correlations. This has already been proven to be an over simplifying assumption, since many authors suggest a non-elementary rate expression based on the pseudo-steady state hypothesis for the reactive zwitterion intermediate to be valid.

An evaluation of the existing reaction rate expressions for the homogeneous liquid phase reaction of CO₂ and mono-ethanolamine (MEA) in a 2-propanol solvent system was performed. The reaction rate profiles of CO₂ and MEA at 25°C, 30°C and 35°C, and relative initial concentrations of [MEA]_i = [CO₂]_i, [MEA]_i = 2.5[CO₂]_i, [MEA]_i = 4[CO₂]_i were determined by means of an isothermal CSTR set-up. Scavenging of the unreacted MEA with benzoyl chloride provided the means to be able to stop the reaction in the product stream. This in turn allowed for the construction of concentration- and reaction rate profiles.

The reaction rate data was modelled on various rate expressions by means of a MATLAB[®] non-linear estimation technique, employing the Levenberg-Marquard algorithm for minimizing the loss function. It was concluded that the rate expressions proposed in literature are insufficient and a rate expression derived fundamentally from first principals is proposed:

$$-r_{\text{MEA}} = k_1 [\text{CO}_2][\text{RNH}_2] - k_2 [\text{Z}] + k_3 [\text{Z}][\text{RNH}_2] - k_4 [\text{S}]^2$$

where k_i are the reaction rate constants, Z is the zwitterion reactive intermediate and S the salt product of the overall reaction mechanism.

In order to be able to determine the effective interfacial mass transfer area, the absorption rate per unit area or specific rate of absorption for the solute gas as a

rate expression function of species concentration must firstly be determined. This is achieved by performing experimental absorption runs on a gas-liquid contactor of known surface area. This study incorporated the well known wetted wall experimental set-up. The aim was to construct and implement a wetted wall set-up and conduct absorption experiments for a gas side CO₂ concentration range stretching from pure CO₂ to diluted gas mixtures absorbing into solutions of varying MEA concentrations.

Validation of the set-up was done by performing experiments at similar conditions to a previous study. The study then proceeded to determine the absolute and specific absorption rates at CO₂ mass percentages of 100%, 78%, 55% and 30% into solutions of MEA concentrations of 0.25 and 0.3 mol/L. These runs were conducted at 25°C and 30°C. The wetted wall was designed to facilitate absorption studies at column heights of 60, 90 and 105mm. This allowed the investigation of the effect that surface area and column height has on the absolute rate of absorption as well as the CO₂ and MEA concentrations in the liquid phase

It was found that the specific absorption rate is independent of contact time, which is consistent with the rapid nature of the reaction. It was furthermore found that an increase in MEA concentration caused an increase in the absorption rate. The effect of temperature is linked with the solubility of CO₂ in the solution. As the temperature increases, the solubility of CO₂ decreases, but the absorption rate increases. The result is that it seems as if a change in temperature has no effect on the absorption rate, when in actual fact it does. An increase in the amount of CO₂ absorbed is noticed for an increase in wetted wall surface area. This is expected and indicates that there is an increase in the amount of CO₂ absorbed as the column length increases.

Stopping the absorption reaction by means of MEA scavenging with benzoyl chloride at various column heights will allow for the construction of a concentration profile for both CO₂ and MEA as a function of column height. These profiles will allow for the derivation of a non-elementary rate expression governing the specific absorption rate. This has been identified as 'n area of great interest for future investigation.

OPSOMMING

'n Groot navorsingsbelangstelling in die reaksiekinetika van CO₂ en monoethanolamien (MEA) het ontstaan sedert die ontdekking dat hierdie reaktiewe sisteem ook 'n goeie metode is vir die bepaling van die effektiewe massaoordragsoppervlakte van gestruktureerde pakkingsmateriaal. Die klem val op die bepaling van eerstens die mees geskikte en akkurate model om die reaksiekinetika te beskryf wat dan gebruik kan word om die absorpsiekinetika deeglik te karakteriseer. Sommige van die vorige navorsers het vereenvoudigende aannames gemaak rakende die reaksiekinetika ten einde die bepaling van geskikte absorpsievergelykings te vergemaklik. Ander het gevind dat die nie-elementêre, pseudo-gestadigde toestand hipotese gebaseer op die reaktiewe zwitterioon tussenproduk van die reaksie 'n meer verteenwoordigende kinetiese model is.

Hierdie studie is eerstens gemik op die evaluasie van die bestaande reaksiekinetikavergelykings deur die homogene vloeistoffase reaksie van CO₂ met mono-etanolamien (MEA) in die oplosmiddel, 2-propanol te ondersoek. Die studie is uitgevoer in 'n isoterme CSTR sisteem by onderskeidelik 25°C, 30°C en 35°C en MEA konsentrasies van [MEA]_i = [CO₂]_i, [MEA]_i = 2.5[CO₂]_i en [MEA]_i = 4[CO₂]_i.

Die voorgestelde reaksiekinetikavergelykings was gemodelleer met 'n nie-lineêre datapassingstegniek verskaf deur die sagtewarepakket, MATLAB[®] wat die Levenberg-Marquard algoritme gebruik om die resfunksie te minimeer. Uit die teorie en datapassing word die volgende vergelyking voorgestel:

$$-r_{\text{MEA}} = k_1 [\text{CO}_2][\text{RNH}_2] - k_2 [\text{Z}] + k_3 [\text{Z}][\text{RNH}_2] - k_4 [\text{S}]^2$$

waar k_1 die reaksietempokonstante voorstel, Z die zwitterioontussenproduk en S die soutproduk.

Die eerste stap in die bepaling van die effektiewe massaoordragsarea van gestruktureerde pakkingsmateriaal is om 'n geskikte vergelyking of korrelasie vir die spesifieke absorpsie van die gas te bepaal. Dit word gedoen deur absorpsie eksperimente te doen op toerusting van bekende oppervlakarea. Hierdie studie het die reeds bekende 'wetted wall' opstelling gebruik. Die hoof doelwit van hierdie

absorpsiestudie was om 'n werkende opstelling te bou en absorpsie eksperimente vir CO₂ konsentrasies wat strek van suiwer CO₂ tot verdunde mengsels uit te voer. Die konsentrasie MEA is ook gevarieër.

Die geskiktheid van die opstelling is eerstens getoets deur eksperimentele lopies uit te voer by soortgelyke toestande as 'n vorige studie. Die doel van die studie is om die absolute en spesifieke absorpsietempos van CO₂ by gasfase massapersentasies van 100%, 78%, 55% en 30% in MEA/2-propanol oplossings met MEA konsentrasies van 0.25 en 0.3 mol/L te bepaal. Die lopies is uitgevoer by beide 25°C en 30°C. Die opstelling is ook ontwerp om absorpsie eksperimente by verskillende kolomhoogtes uit te voer. Hierdie hoogtes is 60, 90 en 105mm. Hierdie studie het tweedens gefokus op die effek wat absorpsiearea en kolomhoogte op die absorpsietempo van CO₂ het.

Die resultate van die studie toon dat die absorpsietempo onafhanklik is van kontaktyd. Dit stem saam met die vinnige reaksietempo. 'n Toename in MEA konsentrasie het 'n toename in spesifieke absorpsietempo tot gevolg, terwyl die effek van temperatuur gekoppel kan word aan die oplosbaarheid van CO₂. Soos die temperatuur toeneem, neem die absolute absorpsietempo toe, maar die oplosbaarheid van CO₂ neem af, dit het beide 'n toenemende en afnemende effek op die spesifieke absorpsietempo. Die hoeveelheid CO₂ geabsorbeer neem toe met 'n toename in kolomhoogte.

Die konsentrasie MEA in die uitlaatvloeistof toon 'n skynbare eksponensiële afname met 'n toename in kolomhoogte. 'n Studie gemik om die konsentrasieprofiele van CO₂ en MEA as 'n funksie van kolomhoogte te bepaal, word voorgestel. Absorpsiemodelle en korrelasies kan dan afgelei word uit hierdie profiele, wat die berekening van die effektiewe massa-oordragsarea akkuraat sal maak. Dit sal deel vorm van toekomstige navorsing.

ACKNOWLEDGEMENTS

Prof. J.H. Knoetze: I would like to express my immense gratitude for die guidance and limitless input that you have provided as my study leader in this project. The project has taken me on an adventure of discovery and without you as the tour guide; it would definitely not have been as valuable an experience. Thank you.

Dr. C.E. Schwarz: Cara, your support and guidance through all the nitty, gritty aspects of a research project gave me the necessary boost when I needed it most. Thank you for the very inspirational role that you fulfilled.

Dr. J.P. Barnard: My friend, thank you very much for your MATLAB[®] expertise. Without your help, I doubt it if I would have been able to complete this thesis successfully. When all is said and done, we shall philosophise once more over a cold one. Thank you once again.

Eben Uys: Thank you for your seemingly endless knowledge of process automation which helped me a lot during the design stages of this project. I wish you the best of luck and thank you for your friendship.

Process Engineering Workshop: Oom Jannie, Anton, Howard, Alvin en Vincent. Baie dankie vir 'n baie opwindende paar jaar. Ek sal nooit die grappies en Vrydagmiddag-braaisessies vergeet nie.

Sasol Ltd: I would like to thank my sponsors of the project for the financial support granted, which of course was the life blood of this research project.

Louis and Annelien du Preez: My beautiful parents; thank you very much for the endless love and support through God Almighty. I love you.

TABLE OF CONTENTS

Abstract.....i

Opsommingiii

Acknowledgements..... v

Table of Contents vi

Nomenclature.....xiii

CHAPTER 1: Introduction and Project Outline..... - 1 -

 1.1 Background - 1 -

 1.2 Objectives..... - 2 -

 1.3 Scope and Limitations - 3 -

 1.4 Mind Map..... - 4 -

CHAPTER 2: Reactive Absorption Theory..... - 5 -

 2.1 Background - 5 -

 2.2 Homogeneous Reaction Kinetics Theory - 5 -

 2.2.1 Proposed Reaction Mechanism - 5 -

 2.2.2 Reaction Rate Law..... - 7 -

 2.2.3 Applicable Reaction Regimes..... - 17 -

 2.3 Diffusive Mass Transfer Theory - 18 -

2.3.1 Physical Absorption.....	- 18 -
2.3.2 Absorption with Chemical Reaction: Existing Models	- 21 -
2.3.3 Effective Interfacial Mass Transfer Theory	- 31 -
CHAPTER 3: Reaction Kinetic Experimental Design and Procedure.....	- 34 -
3.1 Choice of Amine	- 34 -
3.2 Choice of Solvent.....	- 35 -
3.3 Reactor Design.....	- 37 -
3.3.1 Short Residence Time CSTR.....	- 37 -
3.3.2 Long Residence Time CSTR	- 41 -
3.4 CSTR Modeling	- 42 -
3.4.1 Mole Balance	- 43 -
3.4.2 Energy Balance	- 44 -
3.5 Stopping the Reaction	- 46 -
3.5.1 Main Scavenging Reactions.....	- 46 -
3.5.2 Possible Side Reactions and Product Species Validation.....	- 48 -
3.5.3 Achieving Desired MEA Scavenging.....	- 55 -
3.6 Design of Experiments.....	- 59 -
3.6.1 Solubility of CO ₂ in 2-propanol.....	- 59 -
3.6.2 Experimental Design Parameters	- 60 -
3.7 Reaction Kinetic Process P&ID	- 61 -

3.7.1 Materials of Construction	- 63 -
3.7.2 Liquid Flow Rate Calibration	- 63 -
3.7.3 Experimental Procedure and Control Philosophy.....	- 64 -
3.8 Method of Analysis	- 65 -
3.8.1 CO ₂ Analysis.....	- 65 -
3.8.2 CO ₂ Sensitivity and Repeatability in Analysis.....	- 66 -
3.8.3 MEA Analysis.....	- 67 -
3.8.4 MEA Error and Repeatability in Analysis	- 70 -
CHAPTER 4: Diffusive Mass Transfer Experimental Design and Procedure-	71 -
4.1.1 Wetted Wall Column Design.....	- 71 -
4.1.2 Experimental Design Parameters.....	- 74 -
4.2 Diffusive Mass Transfer P&ID	- 77 -
4.2.1 Materials of Construction	- 79 -
4.2.2 Experimental Procedure and Control Philosophy.....	- 79 -
4.3 Diffusive Mass Transfer Method of Analysis.....	- 80 -
4.3.1 CO ₂ Analysis.....	- 80 -
4.3.2 MEA Analysis.....	- 84 -
4.3.3 CO ₂ Error and Sensitivity of Analysis	- 85 -
4.3.4 MEA Error and Sensitivity of Analysis	- 85 -
CHAPTER 5: Results and Discussion: Reaction Kinetics.....	- 86 -

5.1 Concentration – Residence Time Profiles	- 86 -
5.1.1 CO ₂ Concentration Profiles	- 86 -
5.1.2 MEA Concentration Profile	- 88 -
5.2 Conversion and Reaction Rate Profiles	- 89 -
5.2.1 Conversion Profiles	- 89 -
5.2.2 Reaction Rate Profiles	- 91 -
5.3 Temperature and Relative Initial Concentration Effect	- 93 -
5.3.1 Temperature/Concentration Effect	- 94 -
5.3.2 Relative Initial Concentration Effect	- 97 -
5.4 Zwitterion and Salt Concentrations	- 102 -
5.5 Chapter Conclusions	- 107 -
CHAPTER 6: Modelling of a Reaction Rate Expression	- 109 -
6.1 Power Rate Law Expression	- 110 -
6.2 Non-Elementary PSSH Rate Expression	- 117 -
6.3 Proposed Rate Expression.....	- 120 -
6.4 Chapter Conclusions	- 127 -
CHAPTER 7: Results and Discussion: Reactive Absorption.....	- 128 -
7.1 Validation Results.....	- 128 -
7.2 Temperature/Concentration Effect	- 132 -

7.3 Specific Absorption Model Proposed by Erasmus, 2004 - 136 -

7.4 Relevance of Reaction Kinetics - 137 -

CHAPTER 8: Conclusions - 140 -

CHAPTER 9: Recommended Future Work..... - 143 -

9.1 Continuous Time Concentration Profiles - 143 -

9.2 Effective Interfacial Mass Transfer Area - 143 -

9.3 Modifications of the Wetted Wall Set-up - 144 -

References - 145 -

Appendix..... - 149 -

APPENDIX A: Physical and Chemical Properties - 150 -

A.1 Properties of CO₂ (g) - 150 -

A.2 Properties of Argon - 150 -

A.3 Properties of MEA - 151 -

A.4 Properties of 2-Propanol - 151 -

A.5 Properties of Benzoyl Chloride - 151 -

A.6 Density and Viscosity Data for MEA/2-propanol mixtures - 152 -

APPENDIX B: Calibration Data and Design Calculations..... - 154 -

B.1 Reaction Kinetics Pump Calibration - 154 -

B.2 Sample Collection Times in Scavenging Unit - 156 -

B.3	Mass Flow Controller Calibration Data	- 156 -
B.4	Gas Mixture Calibration Data.....	- 160 -
B.5	Calculating CSTR Water Jacket Flow Rate.....	- 162 -
APPENDIX C: Reaction Kinetics Experimental Data and Sample Calculations		- 163 -
C.1	Derivation of the PSSH Rate Expression	- 163 -
C.2	Calculating MEA Concentration from HPLC Data	- 164 -
C.3	Calculating Zwitterion and Salt Concentrations from HPLC Data.....	- 166 -
C.4	Reaction Kinetic Data at 25°C	- 168 -
C.5	Reaction Kinetic Data at 30°C	- 171 -
C.6	Reaction Kinetic Data at 35°C	- 174 -
APPENDIX D: Absorption Experimental Data and Sample Calculations		- 177 -
D.1	Calculating Specific Absorption Rate	- 177 -
D.2	Absorption Experimental Data.....	- 179 -
APPENDIX E: Equipment Specifications and Illustrations		- 184 -
E.1	Mass Flow Controller	- 184 -
Figure E1: Components of MFC		- 184 -
E.2	Temperature Sensors.....	- 187 -
E.3	Wetted Wall Liquid Pump	- 189 -
E.4	Reaction Kinetics Pump	- 192 -

E.5 Mechanical Drawings of CSTRs and Wetted Wall..... - 194 -

APPENDIX F: Statistical Parameters of Interest for Model Evaluation - 198 -

F.1 Mean Squared Error..... - 198 -

F.2 Pearson R^2 -value - 198 -

F.3 Jacobian Matrix..... - 199 -

APPENDIX G: Model Data - 201 -

NOMENCLATURE

Symbol	Description	Units
A	Area	m ²
C _i	Concentration of i	mol/L
D _i	Diffusivity of i	m ² /s
E (eq. 2.7)	Reaction Activation Energy	J
E (eq. 2.58)	Enhancement Factor	-
E _{sys}	System Energy	J
F _i	Molar Flow Rate	mol/s
G _A	Rate of Generation	mol/s
H (eq. 2.64)	Henry's Law Constant	Pa.m ³ /mol
H _j (eq. 3.10)	Enthalpy of j	J/mol
K _C	Reaction Equilibrium Constant	-
M _r	Molecular Mass	kg/kmol
MFC _{out}	Outlet Mass Flow Controller Reading	
N _i	Specific Absorption Rate	mol/m ² .s

Symbol	Description	Units
P	Pressure	Pa
Q (eq. 2.44)	Gas Absorbed	mol/s
Q	Heat Energy	J
R	Universal Gas Constant	kJ/mol.K
T	Absolute Temperature	Kelvin
T_{ref}	Reference Temperature	Kelvin
V	Volume	m^3
\dot{V}	Volumetric Flow Rate	m^3/s
W_s	Shaft Work	J
X_i	Chemical Conversion	-
a	Interfacial Area	m^2
a_e	Effective Interfacial Area	m^2/m^3
C_p	Heat Capacity	J/mol.K
f	Calibration Factor for MFC	-
g	Gravitational Acceleration	m/s^2
h	Height	m

Symbol	Description	Units
k	Reaction Rate Constant	Depends on Reaction Order
k_A^0	Reaction Rate Constant at Reference Temperature	Depends on Reaction Order
k_L	Liquid Mass Transfer Coefficient	m/s
k_g	Gas side Mass Transfer Coefficient	m/s
m	Mass	kg
\dot{m}	Mass Flow Rate	kg/hr
n_i	Rate of Absorption	mol/s
p_i	Partial Pressure	Pa
r	Reaction Rate	mol/L.s
r^0	Reaction Rate at Reference Temperature	mol/L.s
s	Rate of Surface Renewal	s^{-1}
t_c	Contact Time	s
u	Velocity	m/s
x	Volume%	-
y	Mass%	-
γ, ν	Stoichiometric Coefficient	-

Symbol	Description	Units
τ	Residence Time	s
ρ	Density	kg/m ³
μ	Dynamic Viscosity	Pa.s
δ	Film Thickness	m

CHAPTER 1: INTRODUCTION AND PROJECT OUTLINE

1.1 Background

The reactive absorption of CO₂ with primary amines has long been identified as a viable chemical method for determining the effective interfacial mass transfer area of separation column internals such as structured packing (Danckwerts, 1970). The absorption is accompanied by a chemical reaction which, for many operating conditions, is the limiting step in the reactive absorption process (Davis and Sandall, 1993). This has sparked intensive research to define and derive the applicable reaction mechanism and rate expressions to best represent this reactive system.

Certain non-aqueous solvent systems, such as various alcohol solvents, have been proven to provide better wetting of the separation column internals than aqueous solvents (Danckwerts, 1970). This discovery has sparked even further interest into the characterization of the reactive absorption kinetics of CO₂ into non-aqueous solutions of primary amines.

This project forms part of the greater science of separation technology. Its location within the bigger picture of this science is best illustrated in **Figure 1.1**:

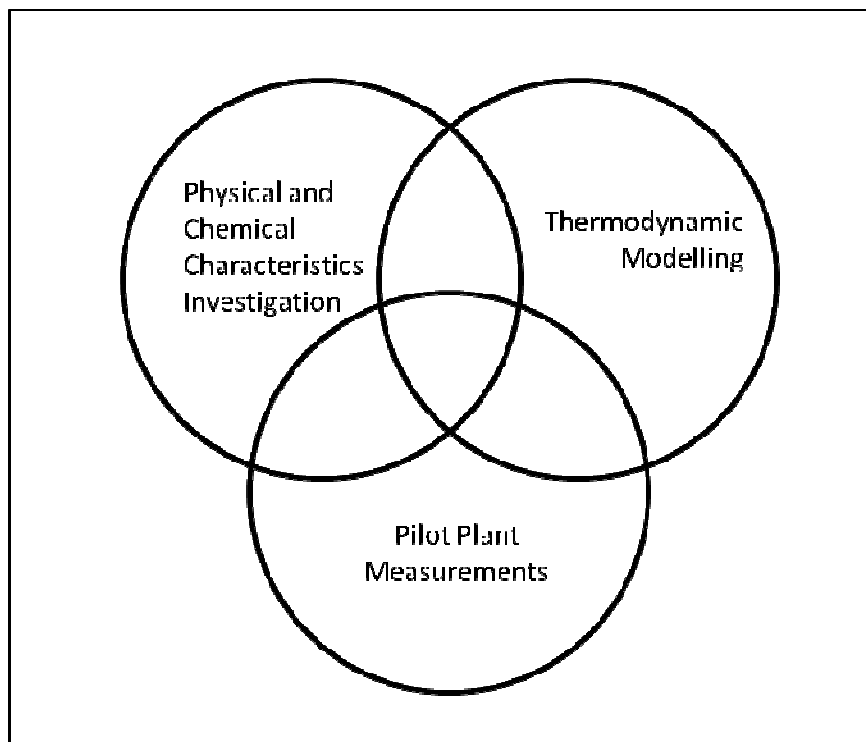


Figure 1.1: Schematic of Separation Technology Research Categories

The determination of the effective interfacial mass transfer area of separation column internals (in this case structured packing) falls in the Physical and Chemical Characteristics Investigation category in **Figure 1.1**. The method for determining effective interfacial mass transfer area rests strongly on a good knowledge of the reactive absorption kinetics of the system chosen to develop this method. The main goal of this project is therefore to determine the reaction kinetics and specific absorption characteristics of CO₂ in a non-aqueous MEA solution.

1.2 Objectives

The first objective of the research is to characterise the homogeneous, liquid phase reaction kinetics of CO₂ with a primary amine (MEA) in a non-aqueous, 2-propanol solution, since no homogeneous reaction kinetic data exists for the reaction of CO₂ with MEA. The choice of amine and solvent is discussed in detail in section 3.1 of this thesis. The reaction kinetic characterization will firstly consist of an evaluation of the existing rate expression proposed in literature and if these are proved to be inaccurate, a more suitable and accurate rate expression will be derived and modelled.

The second objective of this study is to investigate the absorption of CO₂ in various solutions of MEA in 2-propanol on a wetted wall experimental set-up. The data obtained from the study will be modelled on an existing absorption rate expression to test its validity for a wide range of CO₂ partial pressures. The results obtained from this comparative study will shed light on whether more accurate absorption rate expressions for determining the effective interfacial mass transfer area on separation column internals are required.

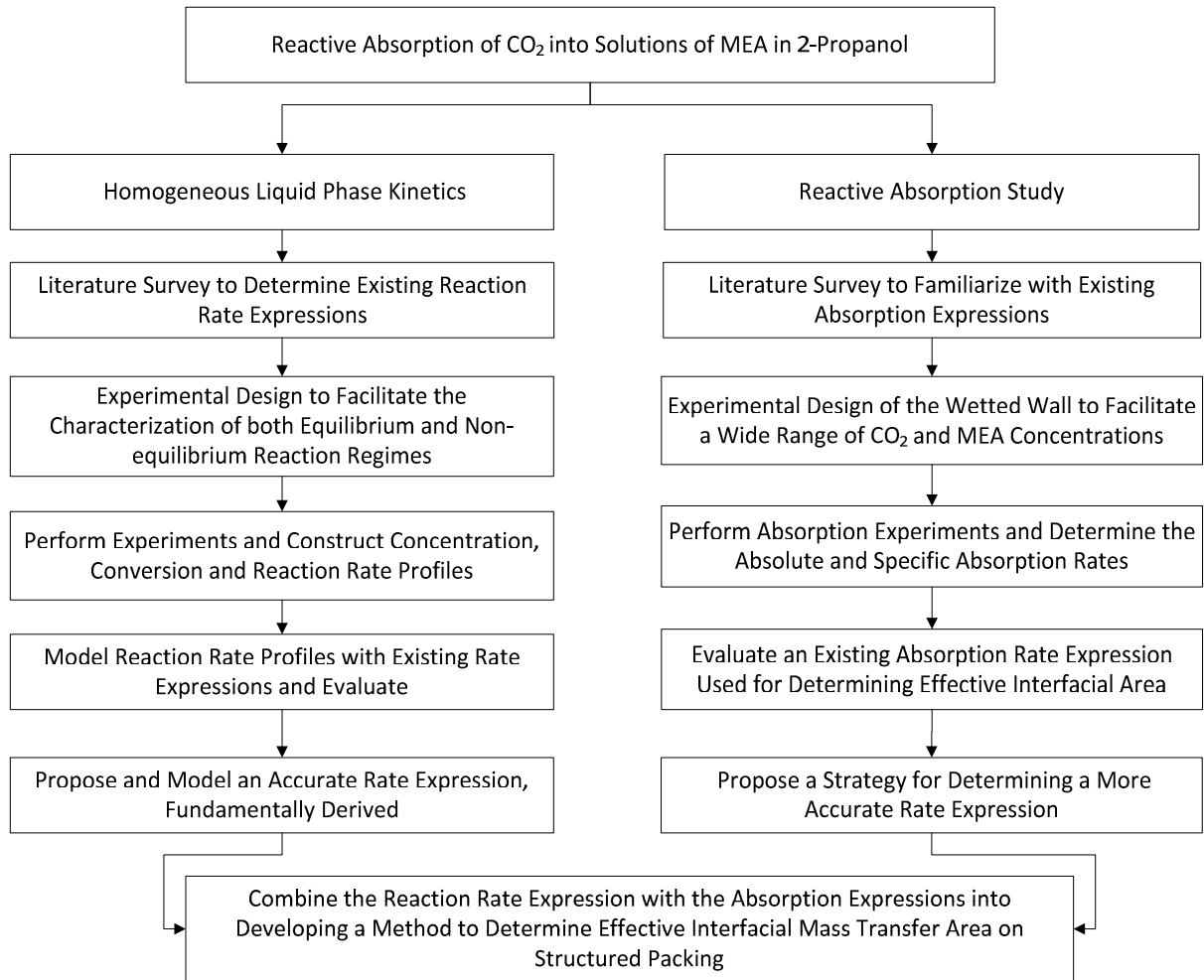
1.3 Scope and Limitations

The scope of this thesis has two focus points which in the end is integrated towards the one main project goal:

1. The homogeneous liquid phase reaction kinetics of CO₂ with MEA in solution with 2-propanol is investigated and determined using isothermal CSTR kinetics. This is done for a temperature range of 25 - 35°C at a pressure of 1 atm (abs).
2. The reactive absorption of CO₂ into the same solution is investigated on a wetted wall absorber. This is done over the same temperature range and system pressure to be able to integrate the data into a method for determining effective interfacial mass transfer area on structured packing material.

The thesis is limited to the study of only CO₂ as acid gas reactively absorbing into a solution containing only one primary amine (MEA) in one solvent (2-propanol). The study is further limited to a temperature range of 25 - 35°C and a system pressure of 1 atm (abs).

1.4 Mind Map



CHAPTER 2: REACTIVE ABSORPTION THEORY

2.1 Background

In all previous studies conducted on the reactive absorption of CO₂ into alcohol amines (Charpentier, 1981, Danckwerts, 1970) many simplifying assumption are made in deriving the governing expressions and correlations of which two will be highlighted. It is firstly assumed that both the gas side en liquid side mass transfer limitations between gaseous CO₂ and the liquid amine are negligible when characterising the kinetics of the reaction. The second main assumption is that the reaction kinetics may be simplified to elementary kinetics when deriving the mass transfer correlations. The study conducted in this project is aimed at testing the legitimacy and accuracy of these assumptions over a specified operating temperature and concentration range.

2.2 Homogeneous Reaction Kinetics Theory

Based on the work completed by previous authors and the results obtained from their comparative studies, the following theory for the reaction of CO₂ with a range of amines in both aqueous and non-aqueous solvents may be presented:

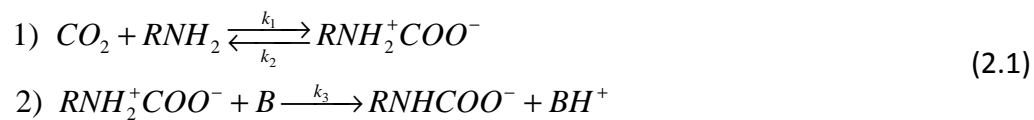
2.2.1 Proposed Reaction Mechanism

Since the discovery of the reactive properties of CO₂ with various amines, a need to determine and characterize the appropriate reaction mechanism has existed. Danckwerts (1970) confirmed that the reaction mechanism proposed by Caplow (1968) describes the dynamics of the reaction most accurately (Davis and Sandall, 1993). Other authors, most notably Alvarez-Fuster *et al.* (1981), Sridharan and Sharma (1976), Oyevaar *et al.* (1990), Sada *et al.* (1985) and Versteeg & van Swaaij (1988a) confirmed Danckwerts' findings. The mechanism proposed by Caplow involves two steps:

1. The formation of a reactive zwitterion intermediate followed by
2. The removal of a proton from the zwitterion by a base

This is true for both primary and secondary amines, but not for tertiary amines. The reaction with tertiary amines follows a different mechanism which can be described as the base catalysis of CO₂ hydration. For the tertiary amine reaction to occur the hydroxide ion derived from the water used as solvent is vital, therefore no reaction takes place in a non-aqueous solvent system (Versteeg and van Swaaij, 1987). Since the reaction with tertiary amines falls outside the project scope, it will not be investigated.

The reaction mechanism for the reaction of CO₂ with a primary amine may be illustrated as follows:



where *R* is the functional group attached to and characterizing the amine, contributing to its chemical properties. *B* is the base responsible for the deprotonation of the zwitterion intermediate.

The required base for both mechanisms may come from several sources. In aqueous solvent systems the hydroxide ion (OH⁻) derived from the dissociation of water is the strongest base present in solution and is therefore mostly responsible for the deprotonation step (Barth *et al.* 1984, Versteeg and Oyevaar, 1988 and Little *et al.* 1992). In a non-aqueous solvent system where no stronger natural bases are present, the amine itself acts as the deprotonating base due to the basic properties of the nitrogen (N) atom present in the molecule (Little *et al.*, 1992, Sada *et al.*, 1985, and Alvarez-Fuster *et al.*, 1980). The nitrogen atom in the neutral amine molecule possesses two available valence electrons for accepting a proton (H⁺) and gaining a positive charge. This is in accordance with the behaviour of a Brønsted-Lawry base and is illustrated as follows (McMurry, 2004):

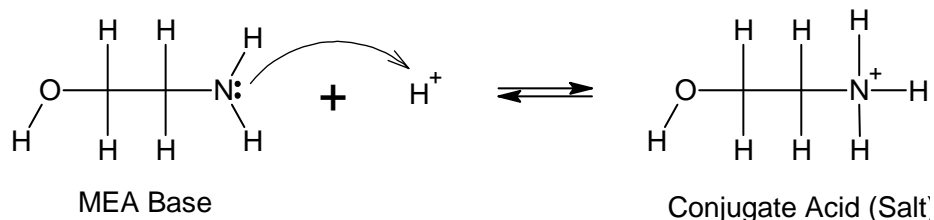
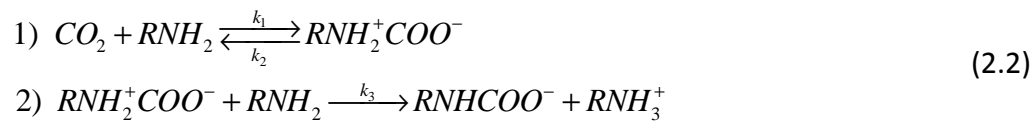


Figure 2.1: Mechanism for a Primary Amine acting as a Base

As an example of a primary amine acting as a base and deprotonating the zwitterion the following reaction mechanism is proposed:



Since only the reaction of a primary amine (MEA) in a non-aqueous solvent system (2-propanol) is investigated in this kinetic study, equation 2.2 will form the basis of the proposed reaction mechanism applicable to the reactions occurring during the experimental procedure.

2.2.2 Reaction Rate Law

The rate at which any chemical reaction occurs is characterised by a reaction rate law. The rate law proportionally correlates the reaction rate with either the reactant or product concentration and may be expressed as (Fogler, 1999):

$$r_i \propto C_i^\alpha \tag{2.3}$$

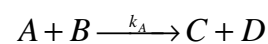
The proportionality is equated by introducing the reaction rate constant, k_j :

$$r_i = k_i C_i^\alpha \tag{2.4}$$

The rate constant accounts for the time dependence of the reaction rate and for the dependence of the chemical reaction on certain extensive thermodynamic properties, such as pressure and temperature. Equation 2.4 is however the simplest example of a reaction rate law and it is therefore necessary to study the two main groups of chemical reactions separately to be able to understand the rate laws associated with each. The two main groups are known as power rate law - and non-elementary reaction kinetics groups.

2.2.2.1 Power rate law and Power Law Reaction Kinetics

Power rate law reaction kinetics is best described by a hypothetical example. Consider the following hypothetical reaction:



For simplification it is assumed that the reaction is irreversible and homogeneous in the liquid phase. The first step in determining the rate law for this specific reaction is to define the rate of reaction. In this case the rate of the disappearance of reactant A will form the basis for the rate of reaction and k_A will accordingly serve as the reaction rate constant. The reaction rate law may now be expressed as:

$$-r_A = k_A C_A^\alpha C_B^\beta \quad (2.5)$$

The rate of the reaction is almost without exception determined experimentally, but is functionally represented by the reaction order. The exponents, α and β , depict the order of the reaction with respect to each of the reactants. The numerical value of these exponents represents the relative activity of each of the reactants during the chemical reaction. The overall reaction order is therefore determined by the sum of the individual reaction orders (Fogler, 1999):

$$n = \alpha + \beta \quad (2.6)$$

The reaction order can however not be determined without characterising the rate constant, k_A . In contrast to its name, the rate constant is in actual fact not a constant, but is merely independent of the concentrations of the species involved in the reaction (Fogler, 1999). As previously stated, the rate constant takes the effect of the extensive thermodynamic properties affecting the chemical reaction into account. For the homogeneous reaction under consideration the rate constant will almost exclusively be a function of temperature.

The temperature dependence of k_A is best correlated by means of the Arrhenius equation (Fogler, 1999):

$$k_A(T) = k_A^0(T_{\text{ref}}) \exp \left[\frac{E}{R} \left(\frac{1}{T_{\text{ref}}} - \frac{1}{T} \right) \right] \quad (2.7)$$

It now becomes apparent that in order to be able to calculate k_A , the parameters, k_A^0 and E must first be known. This is achieved through simple algebra:

k_A^0 is the reaction rate constant at a certain reference temperature, thus, if the reaction were to be carried out at this temperature, the rate law would be:

$$-r_A^0 = k_A^0 C_A^\alpha C_B^\beta \quad (2.8)$$

By taking the natural logarithm on both sides of the equation and implementing the logarithmic product law, equation 2.8 could be written as:

$$\ln(r_A^0) = \ln(k_A^0) + \alpha \cdot \ln(C_A) + \beta \cdot \ln(C_B) \quad (2.9)$$

Equation 2.9 may now either be solved iteratively with the available experimental data or the following method may be implemented:

If a number of reaction runs are completed at the reference temperature with C_B kept relatively constant by having it in large excess and C_A varied, equation 2.9 may be simplified to:

$$\ln(r_A^0) = \ln(k^*) + \alpha \cdot \ln(C_A) \quad (2.10)$$

with

$$k^* = k_A^0 C_B^\beta \text{ used as a proportionality constant.}$$

The rate of each reaction is determined experimentally by measuring the reactant concentrations at various times during the progress of the reaction. A plot of $\ln(r_A^0)$ vs. $\ln(C_A)$ will now yield a straight line with a slope of α and an intercept equal to $\ln(k^*)$. The same procedure can be followed to determine β , by varying C_B and keeping C_A in high excess. With both α and β known, equation 2.9 is solved for k_A^0 .

A very similar method is used to determine E . If the natural logarithm is taken on both sides of equation 2.7, it translates to:

$$\ln(k_A) = \ln(k_A^0) + 1/T(-E/R)$$

but

$$k_A = \frac{-r_A}{C_A^\alpha C_B^\beta} \quad (2.11)$$

$$\therefore \ln\left(\frac{-r_A}{C_A^\alpha C_B^\beta}\right) = \ln(k_A^0) + 1/T(-E/R)$$

A plot of $\ln\left(\frac{-r_A}{C_A^\alpha C_B^\beta}\right)$ vs. $1/T$ will yield straight line with slope $-E/R$ and intercept, $\ln(k_A^0)$, from which it is easy to determine the activation energy for the reaction.

This method, known as the method of excess, is however not the best method available, since it is only modelled on the extreme conditions prevailing and intermediary interactions during the reaction may not be accounted for. The discussion of this method is however valid, since many of the mathematical techniques such as the linearization of the rate expression and executing linear plots to determine the rate constants, have been incorporated by authors such as Hikita *et al.*, (1977) Alvarez-Fuster *et al.* (1980) and Davis and Sandall (1993) on more complex rate expressions.

It is important to note that this method is only applicable for a reaction proceeding in either the forward or reverse direction, hence the assumption of an irreversible reaction made at the beginning of this example. The reason for this is that different reaction rate constants apply to both the forward and reverse reaction (Fogler, 1999).

Consider the following hypothetical reaction:



This reaction is once again assumed to be homogeneous in the liquid phase and completely reversible. A reaction is considered to be completely reversible when a state of reaction equilibrium is achieved. Reaction equilibrium is defined as a reactive system which has an equal forward and reverse rate of reaction, thus the effective rate of reaction for each of the species is identically zero. This means that each of the individual species collectively remain at a constant concentration. The equilibrium is therefore controlled by a thermodynamic relationship in concentration (Fogler, 1999):

$$K_C = \frac{C_{C,eq}^c \cdot C_{D,eq}^d}{C_{A,eq}^a \cdot C_{B,eq}^b} \quad (2.13)$$

It is important to always ensure that the rate law determined for an equilibrium reaction is in accordance with the equilibrium constant at the same temperature.

2.2.2.2 Non-Elementary Reaction Kinetics

It is well known by now that not all chemical reactions are complete in just one step. There exist many chemical reactions (heterogeneous and homogeneous) which involve the formation and subsequent reaction of an intermediate species (Fogler, 1999). The reaction rate law that results for a reaction mechanism involving more than one reaction step more often than not follows non-elementary reaction kinetics. This phenomenon is once again best described by a hypothetical example. Consider the following reaction mechanism:



The sum of reaction mechanism 2.14 results in the net overall reaction:



The formation and reaction of the so called reactive intermediate, C^* , may not be omitted from the overall reaction rate law expression, since it is obvious that the rate of formation of the products D and E depends strongly on the kinetic behaviour of the reactive intermediate. Simply put: the products will not come to exist without the formation and reaction of the reactive intermediate (Fogler, 1999).

The overall reaction rate law for this two step mechanism is derived by firstly treating each of the reactions as elementary. The individual rate laws based on equation 2.14 therefore are:

$$-r_A = k_1 [A]^a [B]^b - k_2 [C^*] \quad (2.16)$$

$$-r_{C^*} = k_3 [C^*] - k_4 [D]^d [E]^e \quad (2.17)$$

The net rate of formation for the reactive intermediate is deduced from equations 2.16 and 2.17:

$$r^* = -r_A - (-r_{C^*}) \tag{2.18}$$

$$\therefore r^* = k_1 [A]^a [B]^b - k_2 [C^*] - k_3 [C^*] + k_4 [D]^d [E]^e$$

The second step in determining the overall reaction rate law is assuming the pseudo-steady-state hypothesis (PSSH) for reactive intermediates. According to the PSSH the lifetime of the reactive intermediate is very short relative to the other species present. It therefore furthermore assumes a very low concentration of reactive intermediate at any time during the reaction. As a result, it is assumed that the rate of formation of the reactive intermediate is equal to its rate of disappearance and thus its overall rate of formation at equilibrium is equal to zero (Fogler, 1999). Mathematically it means:

$$r^* = 0 = k_1 [A]^a [B]^b - k_2 [C^*] - k_3 [C^*] + k_4 [D]^d [E]^e \tag{2.19}$$

Rearranging equation 2.19 leads to:

$$[C^*] = \frac{k_1 [A]^a [B]^b + k_4 [D]^d [E]^e}{k_2 + k_3} \tag{2.20}$$

Substituting equation 2.20 into equation 2.16 and rearranging reveals the overall reaction rate law expression:

$$-r_A = \frac{k_1 k_3 [A]^a [B]^b - k_2 k_4 [D]^d [E]^e}{k_2 + k_3} \tag{2.21}$$

The rate law in equation 2.21 is just one example of a non-elementary reaction rate expression.

2.2.2.3 Existing CO₂ – Amine Rate Law

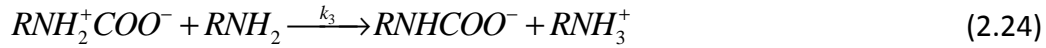
As illustrated in section 2.2.1, the reaction of CO₂ with either a primary or secondary amine follows a two step reaction mechanism. The formation of the zwitterion intermediate in the first step follows a reversible reaction regime, in this case with a primary amine:



The deprotonation of the zwitterion is mostly regarded as irreversible (Davis and Sandall, 1993; Laddha and Danckwerts, 1980):



In non-aqueous solvent systems equation 2.23 may be written as:



The summation of equations 2.22 and 2.24 results in the net overall reaction expression:



Since equation 2.24 states an irreversible reaction, it should result in equation 2.25 also being irreversible, but since the reactive intermediate concentration is so small, the effect is that the overall reaction remains reversible as originally assumed by Caplow (1968). This assumption will be challenged in this project. It may now be concluded that the equilibrium rate law for the reaction of CO₂ with a primary amine in a non-aqueous solvent system follows non-elementary reaction kinetics which leads to the following assumptions in deriving a reaction rate law: It is firstly assumed that enough time is allowed for equilibrium to have been achieved in the formation of the zwitterion intermediate. The second very critical assumption is that the order of reaction with respect to each species is assumed to be one:

$$-r_{CO_2} = k_1[CO_2][RNH_2] - k_2[RNH_2^+COO^-] \quad (2.26)$$

$$-r_{RNH_2} = k_1[CO_2][RNH_2] - k_2[RNH_2^+COO^-] - k_3[RNH_2][RNH_2^+COO^-] \quad (2.27)$$

The basis for this assumption is the elementary nature of the formation of the zwitterion, even though the overall reaction is non-elementary (Davis and Sandall, 1993). It is assumed to be elementary since its formation consists of one reaction pathway in which the nucleophilic nitrogen atom attacks the delta positively charged carbon atom in CO₂ shifting an electron to one of the vacant valence orbitals of one of the oxygen atoms. The nitrogen atom attaches on to the carbon atom causing it to adopt a positive charge. The added electron to the oxygen atom now

has a negative charge, which causes an overall neutral molecule charge (McMurry, 2004). This mechanism is illustrated in **Figure 2.2**:

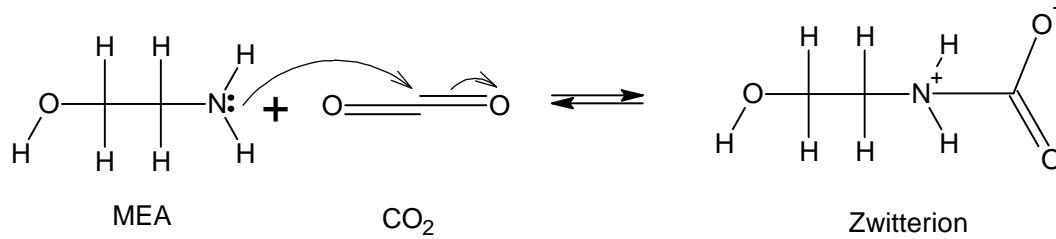


Figure 2.2: Elementary Reaction Mechanism for the Formation of the Zwitterion

The third assumption proposes the implementation of the pseudo-steady-state approximation for the reactive zwitterion intermediate (Danckwerts, 1979). This means that it is assumed that the zwitterion concentration is small and that it does not accumulate as the overall reaction proceeds (Davis and Sandall, 1993). The reaction rate of the zwitterion is therefore zero:

$$r_z = 0 = k_1 [\text{CO}_2][\text{RNH}_2] - k_2 [\text{RNH}_2^+\text{COO}^-] - k_3 [\text{RNH}_2^+\text{COO}^-][\text{RNH}_2] \quad (2.28)$$

At equilibrium equation 2.28 may be rearranged to give:

$$[\text{RNH}_2^+\text{COO}^-] = \frac{k_1 [\text{CO}_2][\text{RNH}_2]}{k_2 + k_3 [\text{RNH}_2]} \quad (2.29)$$

Substituting equation 2.29 into equation 2.26 and simplifying:

$$\begin{aligned}
 -r_{\text{CO}_2} &= \frac{k_1 k_2 [\text{CO}_2][\text{RNH}_2] + k_1 k_3 [\text{CO}_2][\text{RNH}_2]^2 - k_1 k_2 [\text{CO}_2][\text{RNH}_2]}{k_2 + k_3 [\text{RNH}_2]} \\
 \therefore -r_{\text{CO}_2} &= \frac{k_1 k_3 [\text{CO}_2][\text{RNH}_2]^2}{k_2 + k_3 [\text{RNH}_2]} \\
 \therefore -r_{\text{CO}_2} &= \frac{[\text{CO}_2][\text{RNH}_2]}{\frac{k_2}{k_1 k_3 [\text{RNH}_2]} + \frac{1}{k_1}} \quad (2.30)
 \end{aligned}$$

The rate constants can however not be determined individually, but are expressed as product groups in the form illustrated in equation 2.30. The rate constants can now either be determined by non-linear regression from experimental data or by linearizing the rate expression and implementing the method of excess (Davis and Sandall 1993).

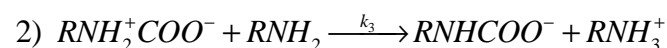
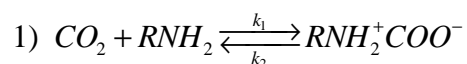
It is important to note that equation 2.30 does not grant absolute clarity on the order of the reaction. It is believed by many authors that the order of the reaction with respect to CO₂ is close to 1 and that it varies from 1 – 2 with respect to the amine (Versteeg, *et al.*, 1989). Equation 2.30 seems to be in accordance with these findings. With respect to primary amines it is believed that the reaction order is close to 1.

It may now be seen how different the approaches are to determining an applicable reaction rate law. Many authors, most notably Danckwerts (1970), Charpentier (1981) and Erasmus (2004) have all opted to assume power rate law reaction kinetics and proceeded in solving rate expressions such as that of Equation 2.9 (see section 2.3.2.1), whilst others, most notably Versteeg, Kuipers, van Beckum or van Swaij (Versteeg *et al.*, 1989) maintain that the PSSH is a valid assumption and have modelled their kinetic data accordingly.

One of the main tasks of this study now becomes the critical assessment of these proposed approaches. The validity of these assumptions will be challenged and an effort made to derive a rate law that will be the best representative of this reactive system.

2.2.2.4 Proposed Reaction Rate Law

With a firm knowledge of both power rate law and non-elementary reaction kinetics now in place, it becomes necessary to try and determine the most accurate reaction rate law to describe the kinetics of the reaction of CO₂ with MEA. Reconsidering the proposed applicable reaction mechanism:



The fundamental rate law with respect to each reagent species should thus be:

$$-r_{CO_2} = k_1 [CO_2]^m [RNH_2]^n - k_2 [RNH_2^+COO^-]^p \quad (2.31)$$

$$-r_{RNH_2} = k_1 [CO_2]^m [RNH_2]^n - k_2 [RNH_2^+COO^-]^p + k_3 [RNH_2]^q [RNH_2^+COO^-]^v \quad (2.32)$$

$$-r_z = -k_1 [CO_2]^m [RNH_2]^n + k_2 [RNH_2^+COO^-]^p + k_3 [RNH_2]^q [RNH_2^+COO^-]^v \quad (2.33)$$

Manipulation of equations 2.31 – 2.33 leads to the following simplified system of applicable rate laws:

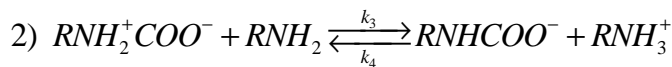
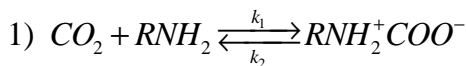
$$-r_{CO_2} = k_1 [CO_2]^m [RNH_2]^n - k_2 [RNH_2^+COO^-]^p$$

$$-r_{RNH_2} = -r_{CO_2} - k_3 [RNH_2]^q [RNH_2^+COO^-]^v \quad (2.34)$$

$$-r_z = -r_{RNH_2} - 2(-r_{CO_2}) \quad (2.35)$$

From CSTR kinetics it is possible to determine $-r_{CO_2}$ and $-r_{RNH_2}$. The only challenge that remains is to determine a concentration profile for the active zwitterion intermediate.

There also exists the possibility to investigate the reversibility of the second reaction in the proposed mechanism. This would alter the mechanism to the form:



This implies that the product concentrations of reaction (2) must be included in the proposed reaction rate expression:

$$-r_{RNH_2} = k_1 [CO_2]^m [RNH_2]^n - k_2 [RNH_2^+COO^-]^p + k_3 [RNH_2]^q [RNH_2^+COO^-]^v - k_4 [RNH_3^+]^w \quad (2.36)$$

$$-r_z = -k_1 [CO_2]^m [RNH_2]^n + k_2 [RNH_2^+ COO^-]^p + k_3 [RNH_2]^q [RNH_2^+ COO^-]^v - k_4 [RNH_3^+]^w \quad (2.37)$$

with

$$r_s = k_3 [RNH_2]^q [RNH_2^+ COO^-]^s - k_4 [RNH_3^+]^w = (-r_{MEA}) - (-r_{CO_2}) \quad (2.38)$$

It is important to note that since the salt products of reaction (2) will always be present in equal molar quantities, it is only necessary to include the concentration of one in the reaction rate expression. The concentration of the salt is calculated by means of a carbon and nitrogen atomic balance.

The rate law system of equations 2.36 – 2.38 will be solved by means of non-linear regression to quantify the rate constants as well as the reaction orders. It is important to note that this system is obviously non-elementary which means that the method of excess is not applicable. The solution to this rate law will be implemented on an expression similar to that of equation 2.30 to test the accuracy of its assumptions.

2.2.3 Applicable Reaction Regimes

The reasoning behind discussing both power rate law and non-elementary reaction kinetics is to complete the argument of which regime should be considered for the purpose of deriving correlations and models for reactive absorption. Charpentier, Erasmus and others assumed power rate law kinetics for their correlations, purely because of its greater simplicity (Charpentier, 1981, Erasmus, 2004). Many authors, such as Versteeg *et al.*, Onda *et al.* and Davies *et al.* (Versteeg *et al.*, 1989), to name a few, have however incorporated the more accurate and complicated non-elementary kinetics to model the reactive absorption of CO₂ into amine solutions.

This study is aimed at critically evaluating the existing models for accuracy and suggesting an alternative approach to determining the appropriate reaction kinetics model. To achieve this, the rate law system derived in section 2.2.2.4 will be evaluated on concentration-residence time profiles of the reagent species from initial contact until reaction equilibrium is reached. This is why no simplifying assumptions were made during its derivation. As it is stated, the rate law represents

a system proceeding from pure species concentrations reacting until equilibrium is reached and maintained.

2.3 Diffusive Mass Transfer Theory

There have been a vast number of studies done on the phenomenon of gas-liquid absorption, since it plays a vital role in many industrial processes, especially in the field of separation technology (Astarita, 1967, Danckwerts, 1970, Charpentier, 1981).

2.3.1 Physical Absorption

The basic mechanics of a gas diffusively absorbing into an appropriate absorbing liquid agent is well known and will therefore only be described briefly.

As a gas comes into contact with a liquid, a boundary layer is formed on both sides of the gas-liquid interface; as illustrated in **Figure 2.3**.

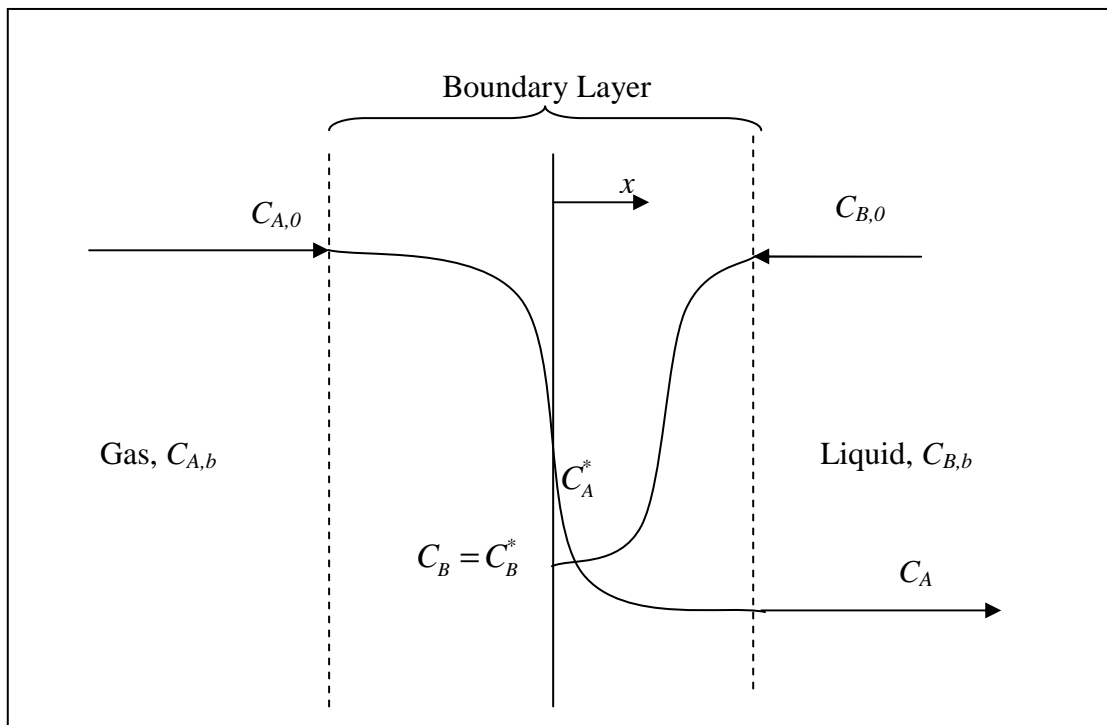


Figure 2.3: Schematic of Diffusive Mass Transfer

The mass transfer from the gas to the liquid occurs in this boundary layer. The driving force behind the mass transfer is a concentration difference or gradient

between the two phases. In order to balance the difference in concentration, the gas diffuses through the boundary layer, along the concentration gradient into the liquid phase. The rate of diffusion is characterised by a diffusion-time profile which takes the following form (Danckwerts, 1970):

$$D_A \frac{\partial^2 C_A}{\partial x^2} - \frac{\partial C_A}{\partial t} = 0 \quad (2.39)$$

where x is the direction of diffusion and absorption, as illustrated in Figure 2.3, D_A is the diffusivity of species A in the liquid and t denotes time. It is recognised by many authors that three absorption models with equation 2.39 as basis exist (Charpentier, 1981). These three models will be discussed briefly and their relevance to this study duly noted.

2.3.1.1 The Stagnant Film Model

The stagnant film model assumes that the gas – liquid boundary layer is a stagnant film with no convection present within the film leaving molecular diffusion as the only means for mass transfer that takes place. The bulk liquid and gas is kept uniform in composition. The rate at which the dissolved gas is transferred perpendicular to the gas - liquid interface is determined from:

$$(N_A)_x = n_A a = -D_A \frac{dC_A}{dx} \quad (2.40)$$

Where a is the effective interfacial mass transfer area and n_A the average rate of absorption per unit area. Integrating equation 2.40 by assuming the concentration of species A to decline linearly from C_A^* at the interface to $C_{A,0}$ in the bulk liquid through a film thickness of δ_L results in the following expression:

$$n_A a = a \left(\frac{D_A}{\delta_L} \right) (C_A^* - C_{A,0}) \quad (2.41)$$

From the basic absorption equation:

$$(N_A)_x = n_A a = k_L a (C_A^* - C_{A,0}) \quad (2.42)$$

With k_L being the liquid phase mass transfer coefficient and therefore:

$$k_L = \frac{D_A}{\delta_L} \quad (2.43)$$

This model, however, is not very realistic since it has been shown that experimentally k_L is not directly proportional to D_A but that the relation is better described by $D_A^{0.5}$ (Charpentier, 1981). This is shown by the surface-renewal models discussed in section 2.3.1.2.

2.3.1.2 The Surface-Renewal Models

The surface renewal model assumes that the liquid side boundary layer is constantly replaced or refreshed with elements from the bulk liquid with the same composition of the bulk liquid. This means that the gas is effectively being absorbed into a stagnant layer of infinite depth. The rate of absorption now becomes a function of the time of exposure of each liquid element to the absorbing gas, with rapid initial absorption decreasing with time (Charpentier, 1970). The liquid layer of infinite depth is described by a model proposed by Higbie (1935).

The model assumes that each liquid element at the gas – liquid interface has equal time of exposure, t_c before being replaced. This means that each element absorbs the same amount Q of gas per unit area and the average rate of absorption is thus Q/t_c . The following absorption equations are subsequently derived (Higbie, 1935; Charpentier, 1981):

$$Q = 2(C_A^* - C_{A,0}) \left(\frac{D_A t_c}{\pi} \right)^{0.5} \quad (2.44)$$

$$n_A = \frac{Q}{t_c} = 2(C_A^* - C_{A,0}) \left(\frac{D_A}{t_c \pi} \right)^{0.5} \quad (2.45)$$

$$k_L = 2 \left(\frac{D_A}{t_c \pi} \right)^{0.5} \quad (2.46)$$

Equation 2.46 provides an improved description of the experimentally determined proportional relationship of k_L and D_A . However, Danckwerts discovered that the Higbie uniform-time model is unrealistic for industrial gas – liquid contactors because of the probability that the replacement of an interfacial liquid element is

independent of the length of time it was exposed to the gas (Danckwerts, 1970). He therefore introduced a third model, replacing exposure time with the rate of surface renewal, s . Danckwerts assumes that the probability of an element to be replaced in the time between t and $t + dt$ is equal to the probability that it will still be present. This probability is derived as $s \cdot dt$ and relates to:

$$n_A = (C_A^* - C_{A,0})(D_A s)^{0.5} \quad (2.47)$$

$$k_L = (D_A s)^{0.5} \quad (2.48)$$

This model is however restricted to cases where the rate of renewal is known and its application is therefore very limited (Charpentier, 1981).

Each of the three proposed models has advantages and disadvantages. All three contain an empirical parameter which could prove difficult to determine: effective film thickness (δ_L), effective exposure (t_c) time and effective rate of surface renewal (s). The stagnant film model is the simplest to incorporate since it involves solving simple differential equations but the surface renewal models give a more accurate relationship for k_L and D_A . Charpentier states that in the end it is a matter of convenience (Charpentier, 1981).

The theory regarding the different proposed diffusion models for physical absorption is the starting point for deriving any correlation or model for gas absorption processes from first principles. When dealing with reactive absorption processes, the choice of the physical absorption model to use as basis for the rate based model will greatly determine the complexity of the model.

2.3.2 Absorption with Chemical Reaction: Existing Models

In many cases the absorption of a gas into the liquid phase is followed by a chemical reaction between the species present. The governing equation for absorption followed by chemical reaction in one dimension, x , is expressed as (Danckwerts, 1970):

$$D_A \frac{\partial^2 C_A}{\partial x^2} = \frac{\partial C_A}{\partial t} + r(x,t) \quad (2.49)$$

where $r(x,t)$ is the reaction rate law for the specific chemical reaction. Equation 2.49 is derived from first principles and forms the basis for most existing models. The difference between the models is the assumptions made regarding the reaction rate law.

2.3.2.1 Correlations Proposed By Charpentier and Danckwerts

Danckwerts has developed analytical solutions for equation 2.49 if the reaction is first order (Danckwerts, 1970). It becomes more difficult as the reaction order increases. For the sake of an even further simplified approach, the reference reaction for the derivation of the existing reactive absorption models is assumed to be irreversible and follows power rate law reaction rate kinetics (Charpentier, 1981). If, for example, a second order reaction ($\alpha = \beta = 1$) with the following rate law:

$$-r_A = kC_A C_B \quad (2.50)$$

governs the reaction kinetics, the diffusion equation is expressed as a series of material balances for both the dissolved gas (species A) and the reactive absorbing liquid (species B). The material balance equation for species A is determined as (Charpentier, 1981; Erasmus, 2004):

$$D_A \frac{\partial^2 C_A}{\partial x^2} - kC_A C_B = 0 \quad (2.51)$$

and for species B:

$$D_B \frac{\partial^2 C_B}{\partial x^2} - z kC_A C_B = 0 \quad (2.52)$$

D_A and D_B are the liquid phase diffusivities of species A and B respectively and z is the number of moles of B reacting with exactly one mole of A. The same method is used for higher order reactions, the only difference being the value of α and β in the reaction rate law, otherwise the material balances have the same form (Danckwerts, 1970). In order to be able to solve this system of differential equations, the boundary conditions must first be specified. At the gas-liquid interface the following boundary conditions apply (Erasmus, 2004):

$$C_A = C_{A,i} \quad \text{and} \quad \frac{dC_B}{dx} = 0 \quad (2.53)$$

At the edge of the liquid film ($x = \delta_L$) the boundary conditions for species B is:

$$C_B = C_{B,b} \quad (2.54)$$

Since the chemical reaction commences at the gas-liquid interface, some of A is consumed in the boundary layer and that which does not react, diffuses through the liquid film edge to react within the bulk liquid phase. It therefore becomes very difficult to determine the boundary conditions for A at the liquid film edge. Charpentier developed a correlation to calculate the boundary conditions for species A as a function of liquid hold-up (h_t), specific interfacial area (a) and liquid film thickness (δ) (Charpentier, 1981, Erasmus, 2004):

$$-D_A \left(\frac{dC_A}{dx} \right)_{x=\delta} = k C_{A,0} C_{B,0} \left(\frac{h_t}{a} - \delta_L \right) \quad (2.55)$$

The complexity of the boundary conditions prohibits the system from being solved analytically and it is therefore necessary to incorporate numerical techniques. A convenient method proposed by Danckwerts and supported by Charpentier involves the use of an enhancement factor, E :

$$E = \frac{N_{A,\text{chemical reaction}}}{N_{A,\text{physical absorption}}} \quad (2.56)$$

The results may now be expressed in terms of the ratio of gas absorbed in the presence of a chemical reaction to the amount absorbed in the absence of a chemical reaction (Danckwerts, 1970; Charpentier, 1981; Erasmus, 2004):

$$N_A = Ek_L (C_A^* - C_{A,0}) \quad (2.57)$$

The enhancement factor is determined by absorbing a non-reactive gas with molecules of approximately the same size and orientation as CO_2 . Equation 2.56 is then applied to determine the enhancement factor.

The numerical solution for the system of differential equation may now be expressed as:

$$E = \frac{\text{Ha} \left[\frac{(E_i - E)}{(E_i - 1)} \right]^{0.5}}{\tanh \left\{ \text{Ha} \left[\frac{(E_i - E)}{(E_i - 1)} \right]^{0.5} \right\}} \quad (2.58)$$

Ha is known as the dimensionless Hatta number which relates the absorption of a gas in a reactive system to the physical absorption of the same gas. It is defined as:

$$\text{Ha} = \frac{\sqrt{D_A k C_{B,b}}}{k_L} \quad (2.59)$$

Charpentier and Danckwerts assumed the reaction of CO₂ and MEA in any solvent medium to obey rapid elementary (m-n)th order kinetics. For this case they derived a limiting value for the Enhancement factor, E_i . It is defined as:

$$E_i = 1 + \left(\frac{D_B}{z D_A} \right) \left(\frac{C_{B,b}}{C_{A,i}} \right) \quad (2.60)$$

The numerical solution for a generalized rapid pseudo m,nth order reversible reaction ($r_A = k_{m,n} C_A^m C_B^n$) may now further be developed. The enhancement factor is now approximated as (Hikita and Asai, 1964; Charpentier, 1981; Danckwerts, 1970; Erasmus 2004):

$$E = \frac{\text{Ha} \left[\frac{(E_i - E)}{(E_i - 1)} \right]^{n/2}}{\tanh \left\{ \text{Ha} \left[\frac{(E_i - E)}{(E_i - 1)} \right]^{n/2} \right\}} \quad (2.61)$$

with an altered definition for the Hatta number:

$$\text{Ha} = \left(\frac{1}{k_L} \right) \left[\left(\frac{2}{m+1} \right) (k_{m,n} D_A C_{A,i}^{m-1} C_{B,b}^n) \right]^{0.5} \quad (2.62)$$

If the reaction falls under the regime of moderately fast as is assumed for the reaction of diluted CO₂ with MEA in non-aqueous solvent systems (Charpentier,

1980) the average rate of absorption is now independent of the liquid side mass transfer coefficient and may be determined from:

$$n_A = aN_A = a \left[\left(\frac{2}{m+1} \right) (k_{m,n} D_A C_{A,i}^{m+1} C_{B,b}^n) \right]^{0.5} \quad (2.63)$$

In order to maintain this reaction regime, the soluble gas is diluted with an insoluble non-reacting gas. This will ensure that the reaction regime does not pass over into the fast reaction regime (Charpentier 1981, Danckwerts, 1970). The dilution of the gas may give rise to gas phase mass transfer limitations, which forces the incorporation of the gas side mass transfer coefficient (k_G) in the equations for determining the average rate of absorption (Charpentier, 1970):

$$n_A = aN_A = \frac{p}{\frac{1}{k_G a} + \frac{H}{a \left[\left(\frac{2}{m+1} \right) (k_{m,n} D_A C_{A,i}^{m+1} C_{B,b}^n) \right]^{0.5}}} \quad (2.64)$$

Where p is the partial pressure of the soluble gas in the bulk gas phase and H is the Henry's law constant for the soluble gas.

It should now be noted that the correlations derived by Charpentier are tedious to apply, since so many conditions must be satisfied for each of the many identifiable regimes that exist. It is furthermore based on the stagnant film model for physical absorption, which is an over simplification as well as assuming power rate law kinetics for all the reactive absorption correlations. There, therefore, definitely exists the need for more accurate models.

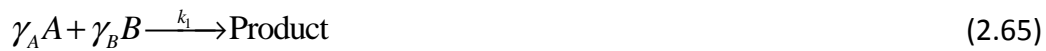
2.3.2.2 Correlations Proposed By Onda et al. (1969)

Onda *et al.* (1969) sought out to derive approximate solutions for gas absorption accompanied by (m,n)-(p,q)-th order reversible, consecutive and parallel complex chemical reactions. They derived correlations for all three transfer models as discussed in section 2.3.1. Their assumptions are as follows:

1. Mass transfer resistance in the gas phase is negligible.
2. The species in the liquid phase are non-volatile for the conditions at which the correlations are applied.

3. The concentration of reactants and products in the bulk are equal to that of their respective equilibrium concentrations.
4. The reaction terms in the material balance equations can be linearised in terms of the concentrations at the gas – liquid interface.

The first system under consideration is the (m,n)-th order irreversible chemical reaction. The reaction under consideration is:



Where A is the gaseous species, ν_B is the stoichiometric coefficient ratio $\frac{\gamma_B}{\gamma_A}$.

Applying the penetration theory, the following differential equations can be derived (Onda *et al.*, 1969):

$$D_A \frac{\partial^2 C_A}{\partial x^2} - \frac{\partial C_A}{\partial t} = k_1 C_A^m C_B^n = -r_A \quad (2.67)$$

$$D_B \frac{\partial^2 C_A}{\partial x^2} - \frac{\partial C_A}{\partial t} = \nu_B k_1 C_A^m C_B^n = \nu_B (-r_A) \quad (2.68)$$

The following boundary conditions are imposed:

$$\text{for } t = 0, x \geq 0: C_A = C_{A,0}, C_B = C_{B,0}$$

$$\text{for } t \geq 0, x = 0: C_A = C_A^*, C_B = C_B^*, \frac{\partial C_B}{\partial t} = 0$$

$$\text{for } t \geq 0, x \rightarrow \infty: C_A = C_{A,0}, C_B = C_{B,0}$$

Following on assumption (4) the rate expression is linearised according to the correlation proposed by Hikita and Asai (1964) as well as Danckwerts (1970) and Charpentier (1981):

$$-r_A = \frac{2}{m+1} k_1 (C_A^*)^{m-1} (C_B^*)^n C_A \quad (2.69)$$

An approximate solution to the system of partial differential equations is given by:

$$N_A = k_L \left(1 - C_{A,0} + \frac{D_B}{D_A} \cdot \frac{C_{B,0}}{\nu_B} \left(1 - \frac{C_B^*}{C_{B,0}} \right) \right) \quad (2.70)$$

The second system under consideration would be a system governed by a reversible chemical reaction of the form:



with the following partial differential equations applying:

$$D_A \frac{\partial^2 C_A}{\partial x^2} - \frac{\partial C_A}{\partial t} = k_1 C_A^m C_B^n - k_2 C_E^p C_F^q = -r_A \quad (2.72)$$

$$D_B \frac{\partial^2 C_B}{\partial x^2} - \frac{\partial C_B}{\partial t} = \nu_B (k_1 C_A^m C_B^n - k_2 C_E^p C_F^q) = \nu_B (-r_A) \quad (2.73)$$

$$D_E \frac{\partial^2 C_E}{\partial x^2} - \frac{\partial C_E}{\partial t} = -\nu_E (k_1 C_A^m C_B^n - k_2 C_E^p C_F^q) = -\nu_E (-r_A) \quad (2.74)$$

$$D_F \frac{\partial^2 C_F}{\partial x^2} - \frac{\partial C_F}{\partial t} = -\nu_F (k_1 C_A^m C_B^n - k_2 C_E^p C_F^q) = -\nu_F (-r_A) \quad (2.75)$$

The initial and boundary values for this system of equations would be:

$$\text{for } t = 0, x \geq 0: C_A = C_{A,0}, C_B = C_{B,0}, C_E = 0, C_F = 0$$

$$\text{for } t \geq 0, x = 0: C_A = C_A^*, C_B = C_B^*, \frac{\partial C_B}{\partial t} = \frac{\partial C_E}{\partial t} = \frac{\partial C_F}{\partial t} = 0$$

$$\text{for } t \geq 0, x \rightarrow \infty: C_A = C_{A,0}, C_B = C_{B,0}, C_E = C_{E,0}, C_F = C_{F,0}$$

The linearised form of the rate expression is now given by Hikita and Asai (1964):

$$-r_A = \frac{2}{m+1} \gamma_A k_1 (C_A^*)^{m-1} (C_B^*)^n C_A - \frac{2}{p+1} \gamma_A k_2 (C_E^*)^{p-1} (C_F^*)^q C_E \quad (2.76)$$

This leads to the very complex correlation for the approximate solution given by:

$$N_A = k_L \left[\frac{(1 - C_{A,0}) \left(T + \frac{D_E}{v_E D_A} \right) + \frac{D_E}{v_E D_A} (C_{A,0} - T C_{E,0}) (1 - \zeta)}{T + \frac{D_E}{v_E D_A} \cdot \frac{1}{\Phi_0}} \right] \quad (2.77)$$

where

$$T = \frac{k_2}{k_1} (C_A^*)^{p+q-m-n} \cdot \left(\frac{C_{B,0}}{C_A^*} \right)^{p+q-n-1} \cdot \frac{\left(\frac{C_E^*}{C_{B,0}} \right)^{p-1} \cdot \left(\frac{C_F^*}{C_{B,0}} \right)^q}{\left(\frac{C_B^*}{C_{B,0}} \right)^n} \quad (2.78)$$

$$\Phi_0 = \frac{\sqrt{M_1}}{\tanh \sqrt{M_1}} \quad (2.79)$$

$$M_1 = M \cdot \left(\frac{C_B^*}{C_{B,0}} \right)^n \cdot \left(1 + v_E T \cdot \frac{D_A}{D_E} \right) \quad (2.80)$$

$$M = \frac{2}{m+1} \cdot \frac{k_1 D_A (C_A^*)^{m-1} (C_{B,0})^n}{(k_L)^2} \quad (2.81)$$

It is firstly noticeable how complex these correlations become as the complexity of the reaction increases. It is furthermore important to note that these correlations are only approximate solutions to a system of reactive absorption. These correlations are all based on the assumption of a linearised version of the reaction rate expression which is why a more modern and accurate rate-based approach is necessary to achieve more accurate results.

2.3.2.3 Rate Based Model Proposed By Vas Bat et al. (1999)

It is clear that none of the existing correlations addresses the unique nature of reaction mechanism governing the reactive absorption of CO₂ into a solution containing MEA. The closest approximation to solving the system was determined by Vas Bat et al. (1999). They propose a generalized model for the mass transfer accompanied by two step complex chemical reaction for the following systems:

1. Both reactions are irreversible
2. First reaction is irreversible, second reaction is reversible
3. First reaction is reversible, second reaction is irreversible
4. Both reactions reversible.

Their model starts off by depicting the appropriate reactions:



The next step is to perform material balances for all species present:

$$D_A \frac{\partial^2 C_A}{\partial x^2} - \frac{\partial C_A}{\partial t} = k_1 C_A^m C_B^n - k_2 C_C^p C_D^q \quad (2.85)$$

$$D_B \frac{\partial^2 C_B}{\partial x^2} - \frac{\partial C_B}{\partial t} = k_1 C_A^m C_B^n - k_2 C_C^p C_D^q + k_3 C_B^r C_C^s - k_4 C_E^u C_F^v \quad (2.86)$$

$$D_C \frac{\partial^2 C_C}{\partial x^2} - \frac{\partial C_C}{\partial t} = -k_1 C_A^m C_B^n + k_2 C_C^p C_D^q + k_3 C_B^r C_C^s - k_4 C_E^u C_F^v \quad (2.87)$$

$$D_D \frac{\partial^2 C_D}{\partial x^2} - \frac{\partial C_D}{\partial t} = -k_1 C_A^m C_B^n + k_2 C_C^p C_D^q \quad (2.88)$$

$$D_E \frac{\partial^2 C_E}{\partial x^2} - \frac{\partial C_E}{\partial t} = -k_3 C_B^r C_C^s + k_4 C_E^u C_F^v \quad (2.89)$$

$$D_F \frac{\partial^2 C_F}{\partial x^2} - \frac{\partial C_F}{\partial t} = -k_3 C_B^r C_C^s + k_4 C_E^u C_F^v \quad (2.90)$$

The system of partial differential equations is solved in accordance with the following initial and boundary conditions:

$$\text{for } t = 0, x \geq 0: C_A = C_{A,0}, C_B = C_{B,0}, C_C = C_{C,0}, C_D = C_{D,0}, C_E = C_{E,0}, C_F = C_{F,0}$$

$$\text{for } t \geq 0, x = 0: C_A = C_A^*, C_B = C_B^*, \frac{\partial C_B}{\partial t} = \frac{\partial C_C}{\partial t} = \frac{\partial C_D}{\partial t} = \frac{\partial C_E}{\partial t} = \frac{\partial C_F}{\partial t} = 0$$

$$\text{for } t \geq 0, x \rightarrow \infty: C_A = C_{A,0}, C_B = C_{B,0}, C_C = C_{C,0}, C_D = C_{D,0}, C_E = C_{E,0}, C_F = C_{F,0}$$

The bulk concentration, $C_{i,0}$ of all the species present may be calculated for a given bulk concentration of A and B by means of the equilibrium constant, K_j for each of the reactions and definitions of the total mass balances:

$$K_1 = \frac{C_{C,0} C_{D,0}}{C_{A,0} C_{B,0}} \quad (2.91)$$

$$K_2 = \frac{C_{E,0} C_{F,0}}{C_{B,0} C_{C,0}} \quad (2.92)$$

$$C_{D,0} - C_{C,0} - C_{E,0} = 0 \quad (2.93)$$

$$C_{E,0} - C_{F,0} = 0 \quad (2.94)$$

This leaves 4 equations with 4 unknowns which may be solved simultaneously to determine the bulk concentrations for the specified boundary conditions.

The model also incorporates dimensionless parameters to account for the underlying mass transfer phenomena, the first of which is the enhancement factor which is once again the ratio of absorption with chemical reaction to that without:

$$E_A = \frac{N_A}{k_L (C_A^* - C_{A,0})} \quad (2.95)$$

As indicated in section 2.3.2.1 the enhancement factor is used in accordance with the Hatta number, which in this case is defined by:

$$\text{Ha} = \frac{\sqrt{k_1 C_{B,0} D_A}}{k_L} \quad (2.96)$$

The Hatta number is varied by varying the value for k_L or k_1 . The ratio of the forward reaction rate constants ($k_3:k_1$) is kept constant and the kinetic orders assumed to be unity. This is a simplification, but serves as a good first approximation.

The results of the model are typically presented as plots of dimensionless concentrations, $\frac{C_i}{C_{i,0}}$ vs. penetration depth x for the different values of the Hatta number to evaluate the effect of k_L and k_1 on the concentration profiles.

The three methods of determining absorption rate expressions and models described in this section were derived for general implementation of any reactive absorption system. They are all derived from a sound basis of first principles and modified to be representative for a wide range of conditions by implementing various simplifying assumptions.

A focused approach is necessary to achieve the most accurate model or correlation to be representative of the system under investigation in this study. Such a method is proposed by Erasmus (2004) and involves the calculation of the effective interfacial mass transfer area of structured packing material from an absorption rate expression. The accuracy of this method rests strongly on the accuracy of the reaction rate expression.

2.3.3 Effective Interfacial Mass Transfer Theory

One of the most important parameters to consider when designing and implementing structured packing for the purpose of separation processes is the effective interfacial mass transfer area (a_e) achieved for a certain system.

Erasmus provides a detailed survey on the different types of structured packing used in industry, each with its own semi-empirical correlation in terms of various dimensionless numbers to calculate the ratio of the geometric to effective surface area of the packing (Erasmus, 2004). These correlations are however tedious since they firstly only serve as an approximation and secondly are only applicable to a specific type of packing material.

Erasmus sought to find a fundamental method for determining the effective interfacial mass transfer area of FLEXIPAC 350Y. Since the current study is ultimately aimed at incorporating fundamental methods for modeling the reactive absorption of CO₂ in MEA, his method will serve as theoretical background.

Erasmus firstly sought out to determine the effective absorption rate of CO₂ in a non-aqueous solution of MEA by measuring the absolute absorption rate on a wetted wall of known effective mass transfer area. The effective absorption rate could thus be calculated from:

$$N_{CO_2} = \frac{n_{CO_2}}{a_{Wetted\ Wall}} \quad (2.97)$$

He then proceeded to find a functional relationship for the effective absorption rate in terms of the concentration of MEA and the partial pressure of CO₂. The functional relationship is as follows:

$$N_{CO_2} = k \cdot p_{CO_2}^{0.9} \cdot C_{MEA}^{0.93} \quad (2.98)$$

with the temperature dependence of k expressed as:

$$k = -3.818 \times 10^{-6} \cdot T + 2.985 \times 10^{-3} \quad (2.99)$$

With the effective absorption rate determined, he proceeded to perform several experimental runs at similar conditions to that done of the wetted wall on the structured packing, FLEXIPAC 350Y. He then implemented a material balance along the height of the packing to determine the effective interfacial mass transfer area. The material balance may be stipulated as:

$$Vdy = a_e N_{CO_2} A_s dz \quad (2.100)$$

where

V = Molar Gas Flow Rate (mol/s)

y = Mole Fraction of CO₂ in the Gass Phase

A_s = Cross Sectional Area of the Column (m²)

The absolute absorption rate may now be expressed as:

$$n_{\text{CO}_2} = \int_{z=0}^{z=h} a_e N_{\text{CO}_2} A_s dz \quad (2.101)$$

where h is the height of the packing material. He then assumes that gas phase resistance is negligible, since this is the assumption made for deriving equation 2.98 and that the effective mass transfer area is uniform throughout the packing. Incorporating these assumptions, the effective interfacial mass transfer area may be calculated from:

$$a_e = \frac{n_{\text{CO}_2}}{A_s \int_{z=0}^{z=h} N_{\text{CO}_2} dz} \quad (2.102)$$

The integral in equation 2.102 was solved numerically by assuming linear concentration profiles for CO_2 and MEA along the height of packing material. This is an over simplifying assumption but was deemed valid since very short sections of packing material was investigated.

The need is therefore identified to investigate the correct concentration profiles of CO_2 and MEA in the liquid phase along the height of the packing material to be able to determine the effective interfacial area to a higher accuracy. The two main effects on the shape and dynamics of these profiles are of course the diffusion and reaction kinetic profiles.

The method used by Erasmus has a sound fundamental basis, which makes it a viable choice for a focused approach to derive the equations and correlations for determining effective interfacial mass transfer area. The use of a power rate law to describe the reactive absorption kinetics of CO_2 into a non-aqueous MEA solution will be investigated in this study to try and determine its accuracy in application. The homogenous reaction kinetics of CO_2 with MEA in a non-aqueous solvent system must therefore firstly be determined followed by an absorption study.

CHAPTER 3: REACTION KINETIC EXPERIMENTAL DESIGN AND PROCEDURE

With a sound theoretical foundation in place, the design of experiments for the homogeneous reaction kinetic study may be done. This chapter will focus on the design of the equipment, the material and energy balances performed, the motivation for the choice of amine and the appropriate solvent and finally the experimental parameters and method of analysis for the experimental runs performed.

The experimental design for the reaction kinetic study incorporates a similar rapid mixing method as that used by Hikita *et al.*, (1976). The main purpose of the rapidly mixed reaction system is to render any gas side mass transfer limitations which may exist, negligible. The experimental design ensures that the system is rapidly mixed, operates isothermally and the products are efficiently separated and accurately analysed without compromising the equilibrium of the reaction where applicable.

It is however firstly important to decide which system to investigate. As mentioned previously, the reaction of CO₂ with MEA in 2-propanol will be investigated. The validation of this choice is discussed before any other experimental design is done.

3.1 Choice of Amine

The reaction of CO₂ with a vast range of amines in both aqueous and non-aqueous solvents has been investigated by previous authors (Blauwhoff *et al.*, 1982; Sada *et al.*, 1976; Danckwerts, 1979; Little *et al.*, 1992). All these studies were in an effort to discover and characterize the most effective, safe and most cost efficient reactive system for the sequestration of CO₂. Two very important amine characteristics that are vital to the design of the structured packing used in the gas-liquid reactive absorption column were recognised (Davis and Sandall, 1993). The selected amine must firstly ensure that the zwitterion formation reaction proceeds in the rapid pseudo m,n^{th} order kinetics ($r_A = k_{m,n} C_A^m C_B^n$) in order to achieve fast reaction equilibrium. It is secondly required that the amine has good wetting characteristics when used in combination with the choice of solvent. Better wetting of the packing

material will cause an increase in the effective interfacial mass transfer area within the column, ensuring more efficient mass transfer (Erasmus, 2004).

The best suited range of amines identified to possess these characteristics are known as alcohol amines (Alvarez-Fuster *et al.*, 1981; Bratzler and Doegres, 1974; Erasmus, 2004). Like many other groups of amines, alcohol amines are divided into three distinct groups: primary, secondary and tertiary alcohol amines. Since the reaction of CO₂ and tertiary amines does not occur in non-aqueous solvents, only the primary and secondary amines will be considered for selection. The following criteria were considered in choosing the amine:

1. The absorption rate of CO₂ decreases in the order primary amines>secondary amines>tertiary amines (Erasmus, 2004)
2. The stability of the zwitterion intermediate decreases in the order primary amines>secondary amines>tertiary amines (Davis and Sandall, 1993)

Since a stable zwitterion intermediate is required for the kinetic study and rapid CO₂ absorption is more desirable when determining effective interfacial mass transfer area with a reactive system (Charpentier, 1981) a primary amine is the best candidate. In deciding which primary amine, the safety and economic factors must be considered.

All alcohol amines have corrosive properties and are toxic. All primary alcohol amines are in the liquid phase at ambient conditions and are therefore very manageable with the correct personal protective equipment (PPE) and having safety measures in tact. After considering the availability and cost of various primary amines, it was decided that the reaction between CO₂ and mono-ethanolamine (MEA) will be investigated in this study.

The full specifications sheet as well as the hazard analysis sheet for MEA is available in Appendix A.

3.2 Choice of Solvent

A part of the scope of this study is to investigate the reaction of CO₂ with an amine in a non-aqueous solvent system. The need for alternative solvent systems to the current aqueous based systems have long been recognised (Danckwerts, 1970).

Studies already conducted on systems utilizing a range of hydrocarbon-, polar- and viscous solvents found that these systems are suitable for the reaction of CO₂ with both primary and secondary alcohol amines (Sridharan and Sharma, 1976; Erasmus, 2004). A good example of a CO₂ – amine reactive system utilizing an organic solvent is the Amisol process which uses methanol as solvent (Bratzler and Doegres, 1974). From the results obtained from this industrial process, it became apparent that alcohols are an excellent choice of solvent.

The choice of solvent is strongly influenced by the following criteria:

1. Both the amine and CO₂ must be soluble, or partly soluble in the alcohol, otherwise the homogeneous liquid phase reaction is impossible.
2. The alcohol must have a relatively low vapour pressure at the experimental conditions, to avoid losses due to evaporation. This is especially important for the kinetic study, since solvent evaporation will influence the product concentrations.
3. The zwitterion intermediate was found to be more stable in polar solvents (Davis and Sandall, 1993), thus polar solvents will be more suitable for the kinetic study.
4. The solvent should not have any reactive tendencies with any of the species involved within the system, including the chemicals used during the analysis procedure.

A range of alcoholic solvents were considered, including ethanol, n-butanol, n-propanol and 2-propanol. Erasmus (Erasmus, 2004) determined absorption rates with n-propanol as solvent, but after consulting the solvent criteria, it was decided to use the relatively higher boiling, more polar, less reactive 2-propanol as solvent. Both n-propanol and 2-propanol have similar densities and viscosities over the same temperature range, which renders these solvents appropriate for comparative studies.

The full specifications sheet as well as the hazard analysis sheet for 2-propanol is available in Appendix A.

3.3 Reactor Design

A rapidly mixed reactive system is best achieved in a Continuously Stirred Tank Reactor (CSTR) (Hikita *et al.*, 1976). The reagent streams will be fed separately, one consisting of dissolved CO₂ in 2-propanol, the other of dissolved mono-ethanolamine (MEA) in 2-propanol, allowing a homogeneous liquid phase for the reaction to take place in. The kinetic study is divided into two sections. Each of these sections will require a different size reactor since the reactant residence times differ greatly. For the purpose of this kinetic study a CSTR was chosen as the most suitable reactor mainly because of two vital reasons:

1. Rapid and complete mixing within the reactor is necessary to ensure that the reactants are evenly distributed and the mixing action will break up any gas bubbles that may have formed on the way to the reactor which will eliminate any form of gas side mass transfer limitations which may arise.
2. A continuous flow system is required to be able to stop the reaction after a specified and desired residence time.

There is however two crucial drawbacks to this choice of reactor:

1. The rate of reaction can only be expressed in terms of residence time and not continuous time.
2. All concentration measurements are therefore independent in continuous time, which means that the data points gathered may not be plotted as a continuous profile in the time domain.

3.3.1 Short Residence Time CSTR

To accurately determine the kinetics of the reaction of CO₂ with MEA from initial reactant contact up until equilibrium is reached, it is of utmost importance to have the correct reactor volume for a range of flow rates. The reason for this is to be able to study the reaction at various residence times and by measuring the exit concentrations of each of the species in the product stream; it would be possible to construct a concentration - residence time profile for the reaction as it approaches equilibrium.

The design of the short residence time reactor depended firstly on the pumps available for the experiment. The range of flow rates were chosen on the basis of the pump capacity available. The pumps chosen for the delivery of the reactants to the short residence time CSTR are the Sera diaphragm pumps which are able to deliver a flow rate of 50 L/hr at full capacity (see Appendix F for the full pump characteristics and process specifications).

The appropriate size of the short residence time CSTR is determined by calculating the residence time of the reactants within the reactor at the various specified flow rates delivered. Since the reactants are separately fed to the reactor, the pumps work in a parallel configuration. This means that the flow rate within the reactor is the sum of the individual pump flow rates, causing a maximum delivery of 100 L/hr to the reactor. The maximum flow rate to the reactor will coincide with the shortest possible residence time and *visa versa*.

Previous authors have estimated the time required for reaching equilibrium to lie between 3 – 4 seconds from initial reactant contact (Hikita *et al.*, 1976) but it is strongly dependant on temperature. The gas side mass transfer limitations in their studies could also have influenced the required time. This study will therefore try and determine the time required for equilibrium to be reached at the various operating temperatures without the mass transfer limitations. The dimensions of the short residence time reactor were therefore determined for a residence time varying from 0.46 to 4.65 seconds. It may at first seem risky to limit the maximum residence time to only 4.65 seconds, but it was found that increasing the maximum residence by merely 1 second (by enlarging the reactor) would greatly compromise the minimum residence time and increase the time steps noted for each flow rate. The reactor was also limited by mechanical construction.

A non dimensioned sectional schematic of the jacketed short residence time CSTR is illustrated in **Figure 3.1**. Refer to Appendix E for the dimensioned drawings of both CSTRs.

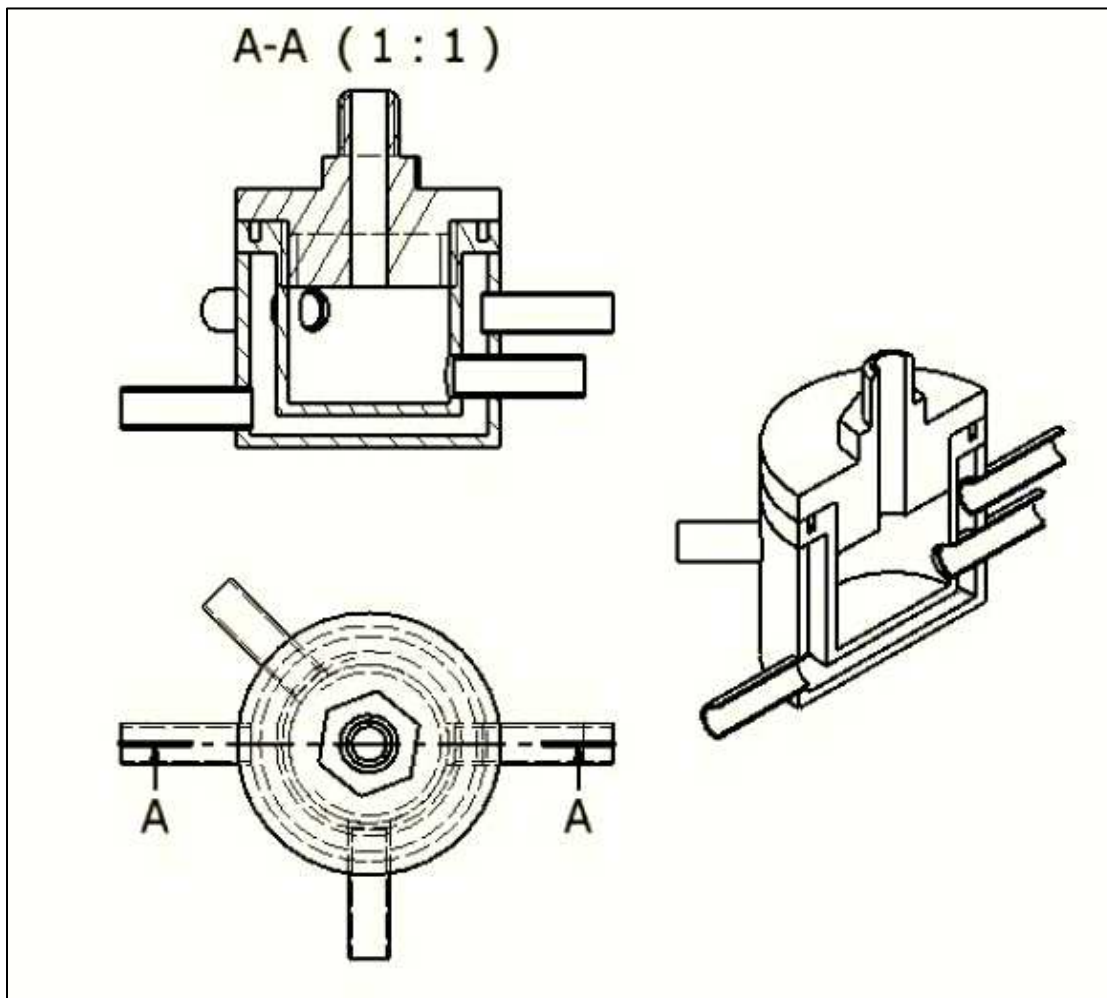


Figure 3.1: Schematic of the short residence time CSTR

The entry port for the pressure sensor on top of the reactor was identified as dead volume, which would compromise the accuracy of the results. The dead volume was therefore filled with inert Teflon with a small centre hole for the liquid to still reach the diaphragm of the pressure sensor. The short residence time reactor dimensions are tabulated in **Table 3.1**:

Table 3.1: Short Residence Time CSTR Dimensions

Short Residence Time Reactor Sizing	
Void Height (cm)	2
Diameter (cm)	2.5
Void Volume (L)	0.0129
Max Residence Time (s)	4.65
Min Residence Time (s)	0.46
Material of Construction	316 Stainless Steel

(100 L/hr Flow Rate)
(10 L/hr Flow Rate)

Stainless Steel 316 was chosen as the material of construction due to the corrosive nature of MEA. It should be noted that the calculated *Total Void Volume* takes the volume of the exit tube as well as the volume occupied by the magnetic stirrer into account. The residence time (τ) can now be calculated with equation 3.1:

$$\tau = \frac{\text{Total Void Volume}}{\text{Total Flow Rate}} = \frac{V}{F} \quad (\text{s}) \quad (3.1)$$

In calculating the residence time it was assumed that the change in volume from mixing (ΔV_{mix}) within the reactor is zero. The basis of this assumption is that both reagent streams consists predominantly of 2-propanol. It is now appropriate to determine the residence time steps for each flow rate. For each time step each pump capacity is changed by 5 L/hr, inducing a total delivery change of 10 L/hr to the reactor. The residence time for each flow rate is tabulated in **Table 3.2**:

Table 3.2: Short Residence Time CSTR Residence Times

Residence Time Steps	
Total Capacity (L/hr)	Residence Time (s)
100	0.46
90	0.52
80	0.58
70	0.66
60	0.77
50	0.93
40	1.16
30	1.55
20	2.32
10	4.65

These 10 time steps represent 10 data points on the concentration – residence time profile for each of the operating temperatures. This profile will then be analysed and the reaction kinetic parameters for the reaction approaching equilibrium determined, via CSTR modelling from basic mass and mole balance principles. For these data points to be deemed valid, isothermal conditions within the reactor must be ensured. This is achieved by jacketing the reactor with temperature controlled water. The temperature range for both reactors is 25°C – 35°C at a reactor pressure of 1 atm (abs).

Another vital consideration for the design of the reactor is the location of the entry and exit streams on the reactor. To ensure that proper mixing is achieved the entry streams are located at the bottom of the reactor at a 90° angle to each other (Refer to the top view in **Figure 3.1**) and mixed rapidly with a magnetic stirrer. To avoid possible reactant by-pass through the reactor, the exit stream is located at the top end of the reactor opposite the entry streams. It is also necessary to conduct a residence time distribution study, to ensure that the product stream is representative of the species concentrations within the reactor. Such a study was not done, but the degree of mixing within the reactor is discussed in further detail in Chapter 5.

3.3.2 Long Residence Time CSTR

Once again, the first consideration is the flow rates available to the reactor. It is of value to size the long residence time reactor to allow for an overlap in the residence times of the short residence time reactor. This overlap will serve as a means to two desirable ends: It will firstly ensure a continuous concentration – residence time profile which will clarify the time required for complete equilibrium to set in at each operating temperature and it will secondly nullify the risk of under-designing the short residence time reactor for a too short maximum residence time.

Since both reactors are schematically similar, **Figure 3.1** also depicts the schematic of the long residence time CSTR. The dimensions of the long residence time CSTR are tabulated in **Table 3.3**:

Table 3.3: Long Residence Time CSTR Dimensions

Long Residence Time Reactor Sizing		
Void Height (cm)	5	
Diameter (cm)	4.8	
Void Volume (L)	0.09	
Max Residence Time (s)	32.57	(10 L/hr Flow Rate)
Min Residence Time (s)	3.26	(100 L/hr Flow Rate)
Material of Construction	316 Stainless Steel	

Once again the total flow rate is changed by 10 L/hr for each residence time data point. The residence times are calculated with equation 3.1 and are listed in **Table 3.4**:

Table 3.4: Long Residence Time CSTR Residence Times

Residence Time Steps	
Total Capacity (L/hr)	Residence Time (s)
100	3.26
90	3.62
80	4.07
70	4.65
60	5.43
50	6.51
40	8.14
30	10.86
20	16.29
10	32.57

The overlap in residence times for the non-equilibrium and long residence time reactor is achieved as well as enough residence time allowed within the long residence time reactor to ensure that chemical equilibrium is reached. Complete Mechanical Drawings of both jacketed CSTRs are included in Appendix E

3.4 CSTR Modeling

To be able to interpret the data gathered from a reaction within a CSTR accurately, the theory of this reactor must be understood. The same theory will also be implemented in modeling the reaction rate law equations and parameters needed to characterize the reaction kinetics for the homogeneous reaction of CO₂ with MEA.

3.4.1 Mole Balance

Consider the following diagram of a CSTR:

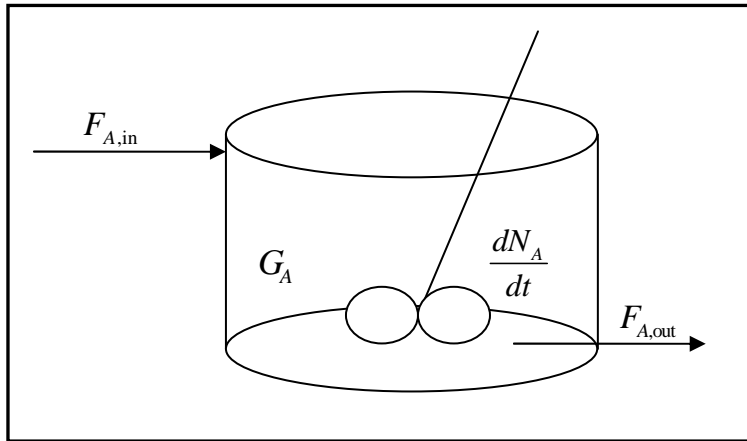


Figure 3.2: CSTR Schematic Diagram

F_A is the molar flow rate of species A. The general mole balance may be written as:

$$F_{A,in} + G_A - F_{A,out} = \frac{dN_A}{dt} \quad (3.2)$$

The generation of species A within the reactor is dependent on the rate of the reaction it is involved in, r_A . At isothermal conditions within the reactor, product generation is strongly influenced by the volume available for reaction, reagent concentration as well as the degree of mixing of the reagents. In a CSTR it is assumed that complete mixing is achieved and the generation of species A may be expressed as the total reactor volume integral of its function of the rate of reaction:

$$G_A = \int_V r_A \cdot dV \quad (3.3)$$

Equation 3.2 may now be expressed as:

$$F_{A,in} + \int_V r_A \cdot dV - F_{A,out} = \frac{dN_A}{dt} \quad (3.4)$$

With the assumption of steady state and no spatial variations in the reaction rate, the design equation for a CSTR may be expressed as (Fogler, 1999):

$$V = \frac{F_{A,in} - F_{A,out}}{-r_A} \quad (3.5)$$

since a reaction is taking place within the reactor, it is of great use to define a conversion term, X_A :

$$X_A = \frac{F_{A,in} - F_{A,out}}{F_{A,in}} \quad (3.6)$$

Substituting equation 3.6 into 3.5 reveals:

$$V = \frac{F_{A,in} \cdot X_A}{(-r_A)_{\text{exit}}} \quad (3.7)$$

However, for the purpose of this kinetic study, it would be more appropriate to have an expression in terms of reactant residence time and concentration. From basic definitions the following rate expression in terms of residence time may be derived:

$$(-r_A)_{\text{exit}} = \frac{C_{A,out} \cdot X_A}{\tau} \quad (3.8)$$

It is important to note that conversion may also be defined in terms of concentration (Fogler, 1999):

$$X_A = \frac{C_{A,in} - C_{A,out}}{C_{A,in}} \quad (3.9)$$

The mole balance of the CSTR will form the basis of the kinetic model to determine the rate law parameters for both the non-equilibrium and equilibrium reaction regime. Equation 3.8 is of utmost importance since the concentration is measured and the conversion and residence time calculated, which will reveal the reaction rate. The calculated reaction rate is the dependant variable for modeling the proposed reaction rate expression.

3.4.2 Energy Balance

The mole balance, especially concerning the equation for defining conversion as a function of inlet and outlet concentrations, rests strongly on the assumption of

isothermal conditions prevailing. Isothermal conditions within each of the reactors are ensured by means of a water jacket constructed around the reactor. Water at the desirable process temperature is circulated from an isothermal water bath to within the water jacket. The temperature within the reactor is monitored by means of a PT-100 temperature sensor (accuracy: $\pm 0.5^\circ\text{C}$).

The water is circulated in the jacket before the reagents are introduced to heat or cool the reactor to the desired operating temperature. An energy balance on the system is however still necessary to reveal the minimum flow rate of water in the reactor jacket during an experimental run to ensure that the temperature within the reactor is maintained.

The general energy balance may be written as:

$$\frac{dE_{\text{sys}}}{dt} = \sum_{j=1}^n (F_{j,\text{in}} \cdot H_{j,\text{in}}) - \sum_{j=1}^m (F_{j,\text{out}} \cdot H_{j,\text{out}}) + Q - W_s \quad (3.10)$$

where H_j is the enthalpy of species j . At steady state the accumulation of energy is zero, the work done by the system negligible and since $T_{\text{in}} = T_{\text{out}}$ the enthalpy change for each species is zero resulting in the following energy balance expression (Fogler 1999):

$$Q = F_{A,\text{in}} \cdot X \cdot \Delta H_{\text{rxn}}(T) \quad (3.11)$$

From equation 3.11 it is possible to determine the amount of heat generated or consumed by the reaction which must be counterbalanced by the water in the jacket of the CSTR. The flow rate of the water may be determined from:

$$Q = n_{\text{water}} \cdot c_{P,\text{water}} \cdot \Delta T_{\text{water}} \quad (3.12)$$

The actual energy balance equation of concern to the reactor thus becomes:

$$n_{\text{water}} = \frac{F_{A,\text{in}} \cdot X \cdot \Delta H_{\text{rxn}}(T)}{c_{P,\text{water}} \cdot \Delta T_{\text{water}}} \quad (3.13)$$

Taking the published ΔH_{rxn} for the absorption reaction of CO_2 with MEA and by means of using a theoretical 100% conversion and the highest inlet flow rate of CO_2 from the experimental design it is possible to determine the minimum mass flow

rate of water to the jacket to keep ΔT_{water} down to 0.5 K. Refer to Appendix B for the full calculation. These flow rates are tabulated in **Table 3.5**:

Table 3.5: Minimum Water Flow Rate in Reactor Jacket

Jacket Water Flow Rate	
ΔH_{rxn} (kJ/kg)	1919
$C_{p,water}$ (kJ/kg.K)	4.81
$C_{p,2-propanol}$ (kJ/kg.K)	2.57
$F_{CO_2, in}$ (kg/hr)	0.183
ΔT (K)	0.5
$m_{minimum}$ (kg/hr)	146
m_{actual} (kg/hr)*	252

*4.2 L/min water

From **Table 3.5** it can be seen that the actual flow rate of water exceeds the minimum required flow rate of water to counter an increase of 0.5 K in temperature. It was found from measuring the outlet temperature of the reactors that isothermal conditions did prevail for all circumstances.

3.5 Stopping the Reaction

In order to be able to construct a concentration - residence time profile for the species in the rate law, it is necessary to stop the reaction immediately at the product stream of the reactor. This was previously attempted by means of rapid evaporation of the unreacted CO_2 under vacuum, but it was found that 99% CO_2 liberation could not be achieved unless 80% vacuum was drawn. This large pressure drop could have a significant effect on the reaction rate parameters and an alternative method for stopping the reaction was investigated. The investigation led to scavenging the unreacted MEA with an excess amount of benzoyl chloride.

3.5.1 Main Scavenging Reactions

MEA reacts very rapidly with benzoyl chloride according to the following reaction mechanism (McMurry, 2004):

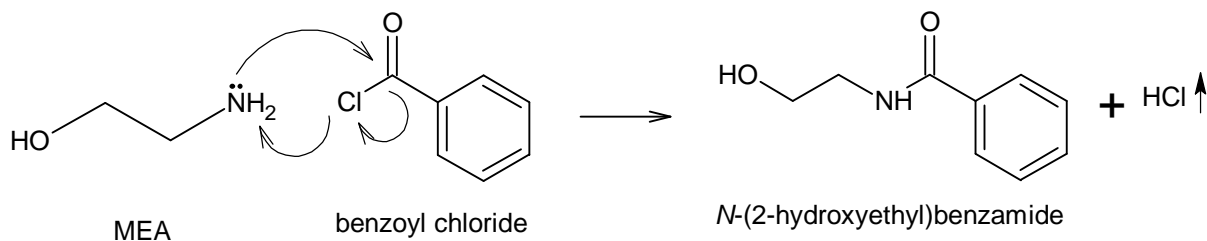


Figure 3.3: Reaction Mechanism of Benzoyl Chloride with MEA

According to McMurry (2004) the reaction rate of MEA with benzoyl chloride is in the order of 200 times faster than the reaction of MEA with CO₂ making it a viable scavenging reaction. This is firstly due to the carbon atom of benzoyl chloride attached to the benzene ring gaining a delta positive charge because of the electron withdrawing characteristics of the electronegative Cl atom attached to it. This delta positive charge causes the carbon atom to be more susceptible for nucleophilic attack from the valence electrons on the nitrogen atom of MEA. The second reason for a more rapid reaction is because the leaving group, Cl⁻, in benzoyl chloride is much more stable than the zwitterion, causing MEA to rather react with benzoyl chloride than CO₂. In the scavenging unit, the concentration of benzoyl chloride is much higher than that of CO₂, further enhancing the selectivity and reaction rate of MEA with it.

N-(2-hydroxyethyl)benzamide is a white crystal amide precipitate. Amides are the least reactive of the carboxylic acid derivatives (McMurry, 2004) because of the following resonance structure:

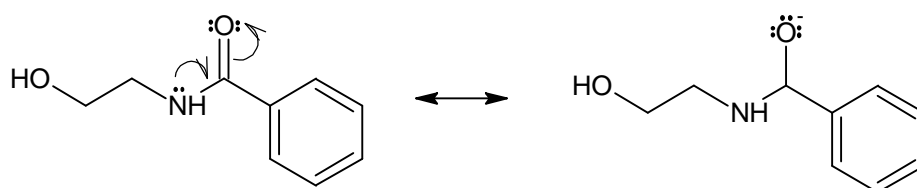


Figure 3.4: Resonance Structure of N-(2-hydroxyethyl) benzamide

The resonance structure indicates that the electron density around the nitrogen atom is reduced greatly, prohibiting its nucleophilic attack on the carbon atom of CO₂. It is thus reasonable to assume that the reaction of CO₂ with MEA is stopped completely. The validation of this assumption however also rests in part on whether all of the amine reacts with the benzoyl chloride. According to McMurry, some of the amine reacts with the HCl formed in the main reaction (**Figure 3.5**) to form an

amino chloride ion. This is because MEA acts as a base. The amino chloride ion is formed according to the following mechanism:

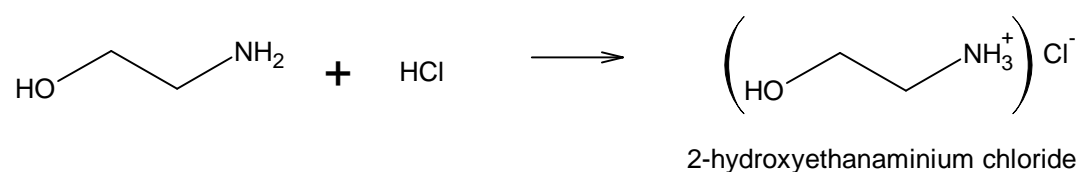


Figure 3.5: Formation of the amino chloride ion

It is important to note that the amino chloride ion is also unable to react with CO₂ since the valence electrons responsible for nucleophilic attack is occupied by a proton.

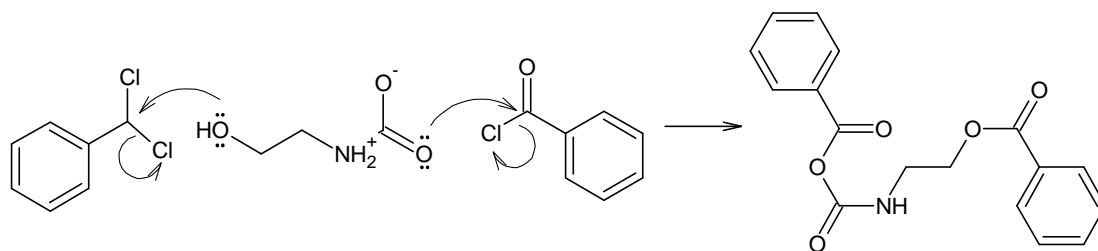
According to McMurry approximately 92% of the amine is converted to the amide. 99% conversion could be achieved by adding a base such as NaOH to neutralize the HCl and thus preventing the amino chloride ion from forming. This was investigated in this study but it was found that water, either that formed in the neutralization reaction or that serving as the solvent for NaOH prevented the formation of the amide precipitate. The reason for this is that benzoyl chloride preferably reacts with water to form benzoic acid, which is water soluble.

An investigation was also made into dissolving the base in 2-propanol to avoid any water contamination. Potassium hydroxide (KOH) showed promise since it is soluble in 2-propanol, but it was found that KOH reacts with the amide precipitate resulting in the decomposition of the crystal structure back to the original amine.

It was therefore decided to perform precipitation studies with benzoyl chloride in great excess (20:1 – 30:1 mole ratios of benzoyl chloride (BC):MEA) to achieve the desired 99% amide yield. It was further found that using 2-propanol as solvent proved favourable in achieving this desired yield.

3.5.2 Possible Side Reactions and Product Species Validation

Benzoyl chloride will also react with the hydroxyl functional group of 2-propanol to form an ester and HCl (not shown), according to the following mechanism:



2-(((phenylcarbonyl)oxy)carbonyl)amino)ethyl benzoate

Figure 3.8: Reaction of the Zwitterion with Benzoyl Chloride

The salt product has one less proton than the zwitterion, which means that the same molecule is formed in the reaction with benzoyl chloride.

The validation of this theory lies in combined MS and NMR data obtained for the precipitate formed for a typical experimental run at 25°C and equal relative initial concentrations. The MS data is presented in **Figure 3.9**:

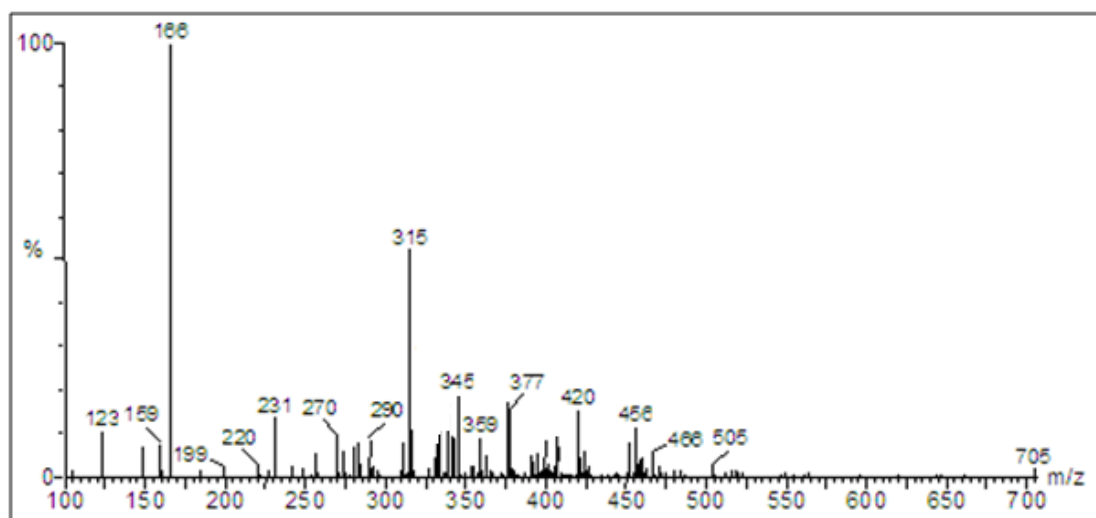


Figure 3.9: MS Data for an Experimental Run at 25°C and Equal Initial Concentrations

The MS data shows that a molecule with a molecular weight of 165 g/mol is predominantly formed with the second most abundant molecule having a molecular weight in the order of 313 – 314 g/mol. This is consistent with the reaction theory, since the amide precipitate (N-(2-hydroxyethyl)benzamide) has a molecular weight of 165 g/mol and the zwitterion or salt product precipitate (refer to **Figure 3.8**) has a molecular weight of 313 – 314 g/mol. Since the zwitterion precipitate has a molecular weight of 314 g/mol, it is assumed to be the predominant contributor to the component identified in the MS analysis. This assumption plays an important role in determining the zwitterion concentration from the HPLC analysis. It is important to note that the ester formed in **Figure 3.6** also has a molecular weight of

165 g/mol, but since it passes through as liquid filtrate during precipitate preparation for HPLC analysis, it is assumed to have an insignificant mass in the sample analysed and thus an insignificant influence on the MS data.

The samples were prepared for HPLC analysis by firstly washing with benzoyl chloride whilst filtrating through a buchner vacuum filter until nearly all of the liquid was sucked through (enough to have the filter paper almost dry). The precipitate was then weighed in a closed container on scales with an accuracy of 4 decimal figures and the sample mass dissolved in methanol. The weight of the almost dry filter paper was taken into account. A test was done by wetting a number of filter papers with the ester, placing each on the buchner filter with no precipitate and drawing vacuum until the paper is almost dry. The weights of the paper were within 0.8% of each other for 13 papers investigated. The amount of ester still clinging to the solid precipitate was detected in the HPLC chromatograms and since the HPLC was calibrated for it, a mass balance on the precipitate could be performed. The effect of the number of washes was indirectly tested since the same volume of benzoyl chloride was not used for washing each time, yet the repeatability in the HPLC analysis remained the same (see section 3.8.4).

In order to be sure of the physical structure of the precipitates formed, the same sample was sent for NMR analysis. The result of an overnight analysis in a 600 MHz NMR revealed the following ^{13}C spectra:

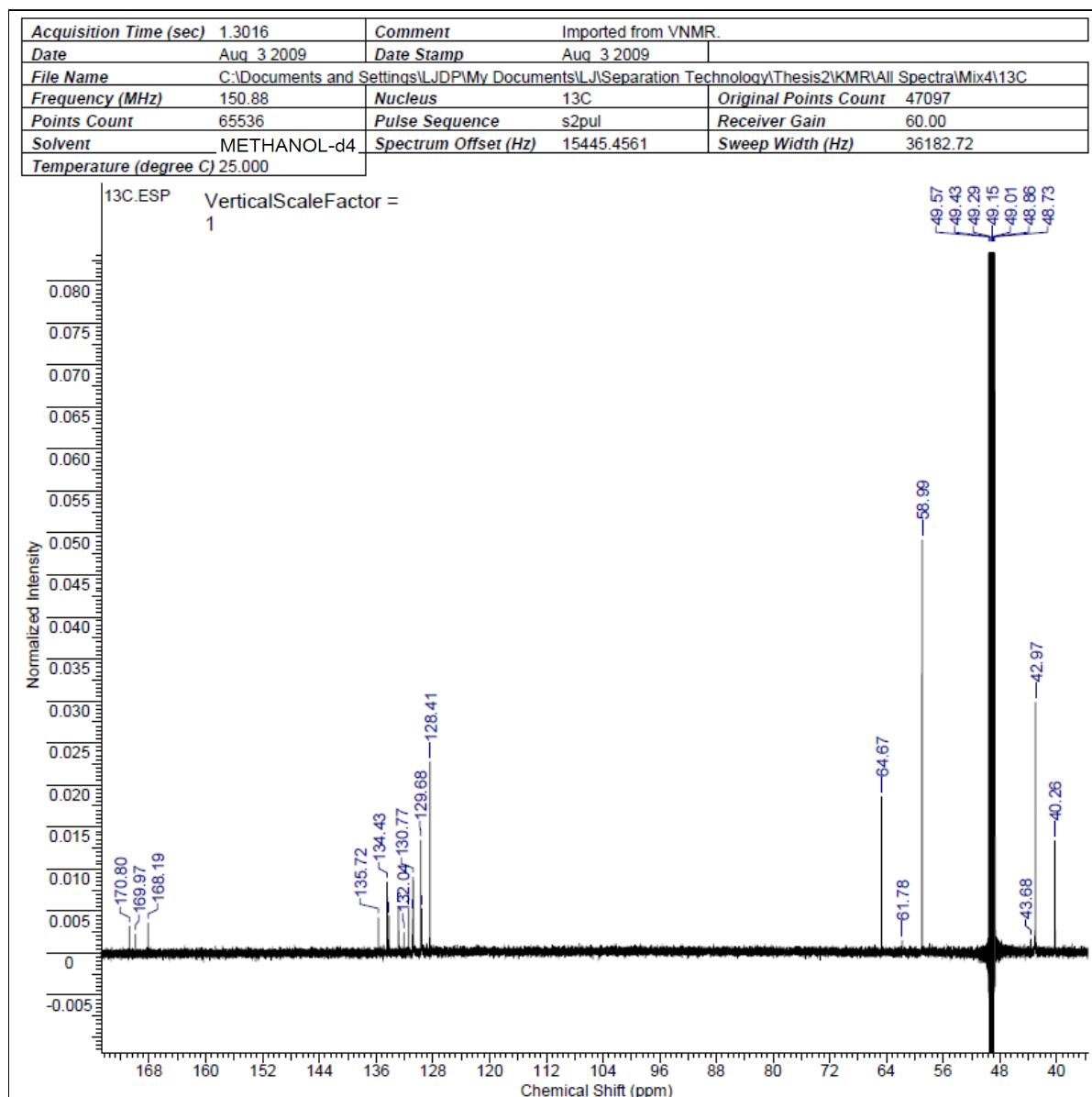


Figure 3.10: ¹³C Spectra for an Experimental Run at 25°C and Equal Initial Concentrations

All the peaks identified in the ¹³C spectra are labeled in **Figure 3.10** and may be tabulated to allow for comparison with data in literature. All the peaks identified are tabulated in **Table 3.6** with the peaks of interest to identify N-(2-hydroxyethyl) benzamide in bold print. In order to achieve a positive identification, all of the peaks documented in literature must be present in the spectra:

Table 3.6: List of ¹³C NMR peaks

No	Chemical Shift (ppm)	Literature* Shift (ppm)
1	40.26	42.5
2	42.97	
3	48.73	
4	48.86	
5	49.01	
6	49.15	
7	49.29	
8	49.43	
9	49.57	
10	58.99	61.1
11	61.78	
12	64.67	
13	128.41	128.2
14	129.59	128.6
15	129.68	
16	130.77	
17	130.83	
18	131.45	131.3
19	132.04	
20	132.85	
21	134.17	133.7
22	134.43	
23	135.72	
24	168.19	168.7
25	169.97	
26	170.8	

*Morcuende *et al*, 1996

It is firstly important to note that the literature data used chloroform-d as solvent, whilst this study used methanol-d4 since the precipitate is insoluble in chloroform. The peaks filled in grey in **Table 3.6** represent the solvent, which is used as the reference peak during peak identification. Because of the difference in solvent systems, the peaks will not overlap exactly, but as is seen from **Table 3.6** the peaks are all present and in close enough vicinity to those from literature to be able to conclude that the precipitate contains N-(2-hydroxyethyl) benzamide.

Three of the NMR peaks documented in literature to be able to identify 2-[(phenyl carbonyl)amino]ethyl benzoate are absent from the spectra, which is in accordance with its relative absence in the MS data for the sample. No NMR spectral data for the zwitterion and salt precipitate products could be found, but since the MS data indicates its presence, it is assumed to exist in the precipitate mixture.

An investigation was made as to why no NMR data could be found for the zwitterion precipitate and the conclusion was that it is impossible to synthesize it to 99% purity since it is a very unstable pure compound, especially in solid form as it will decompose and release CO₂. It was found in this study that it remains stable in a precipitate mixture dissolved in methanol, since repeated MS spectra showed very similar amounts of it each time.

The final part of the precipitate species validation, is to investigate the HPLC data obtained from a typical experimental run. The HPLC chromatogram for such a run is illustrated in **Figure 3.11**:

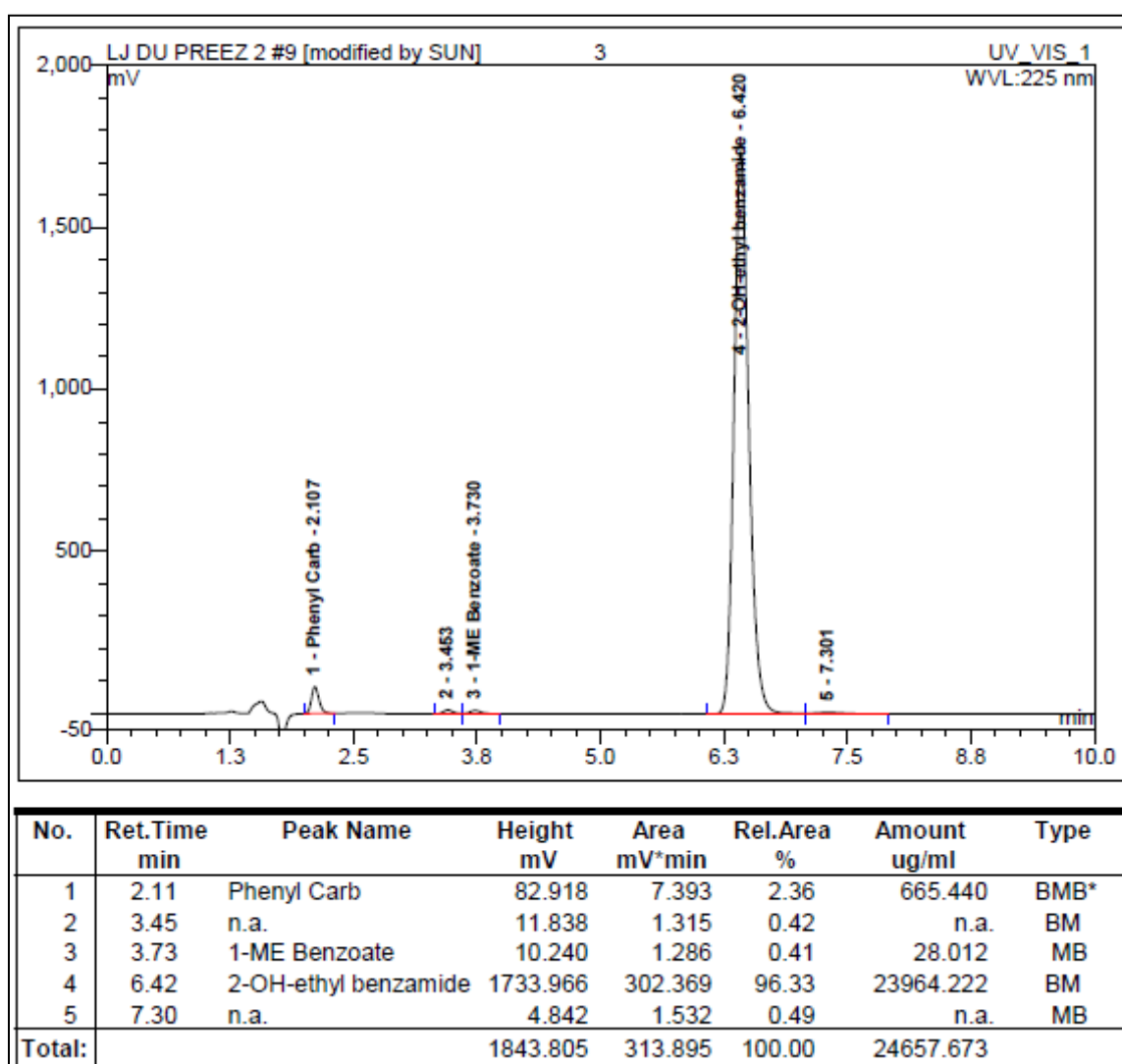


Figure 3.11: HPLC chromatogram for a Typical Experimental Run

From the chromatogram the three components of interest are identified and labeled. The peak identification was done from chromatograms for solutions of high

purity for 1-methylethyl benzoate and N-(2-hydroxyethyl) benzamide. The chromatogram in **Figure 3.11** is for a run performed at 25°C and equal initial concentration to be comparable with the MS data. The two peaks of main interest are firstly the peak at 2.1 min and secondly the peak at 6.4 min. The latter represents N-(2-hydroxyethyl) benzamide and the former that of the precipitate from the zwitterion and salt products (abbreviated as phenyl carb). The peak at 3.7 min represents 1-methylethyl benzoate and is not always present in the chromatograms, since most of it reports to the liquid filtrate.

Usually molecules with larger molecular weight have longer retention times in HPLC analysis. In this case it is noticed that the zwitterion precipitate has a shorter retention time than that of N-(2-hydroxyethyl) benzamide. This is possible since it has been found that molecules that are easily protonated in acidic solutions have shorter than expected retention times and as the mobile phase contains some acetic acid, the short retention time can be explained. This could not be verified since the zwitterion precipitate could not be isolated and purified.

3.5.3 Achieving Desired MEA Scavenging

Before the reaction kinetic experiments can be designed, it is firstly necessary to determine the volume of benzoyl chloride needed to achieve 99% MEA scavenging. As mentioned in the previous section, precipitation tests were carried out at various benzoyl chloride (BC) to MEA ratio's to obtain the ratio that will provide the desired degree of MEA scavenging.

The first study was done at a mole ratio of 1:1 with only BC and MEA. This study yielded a highest MEA scavenging of 83% (range = 48 – 83%) on the basis of assuming only N-(2-hydroxyethyl) benzamide formed as precipitate. The MS analysis of this precipitate shows that some of the N-(2-hydroxyethyl) benzamide reacted further with BC to form 2-[(phenyl carbonyl)amino]ethyl benzoate, proving the assumption incorrect. It was decided to repeat the precipitation study at mole ratio's of 10:1, 20:1 and 30:1. The results are illustrated in **Figure 3.12**. The yield was once again calculated by assuming all of the precipitate to be N-(2-hydroxyethyl) benzamide. The yield was calculated with a mole balance for N-(2-hydroxyethyl) benzamide.

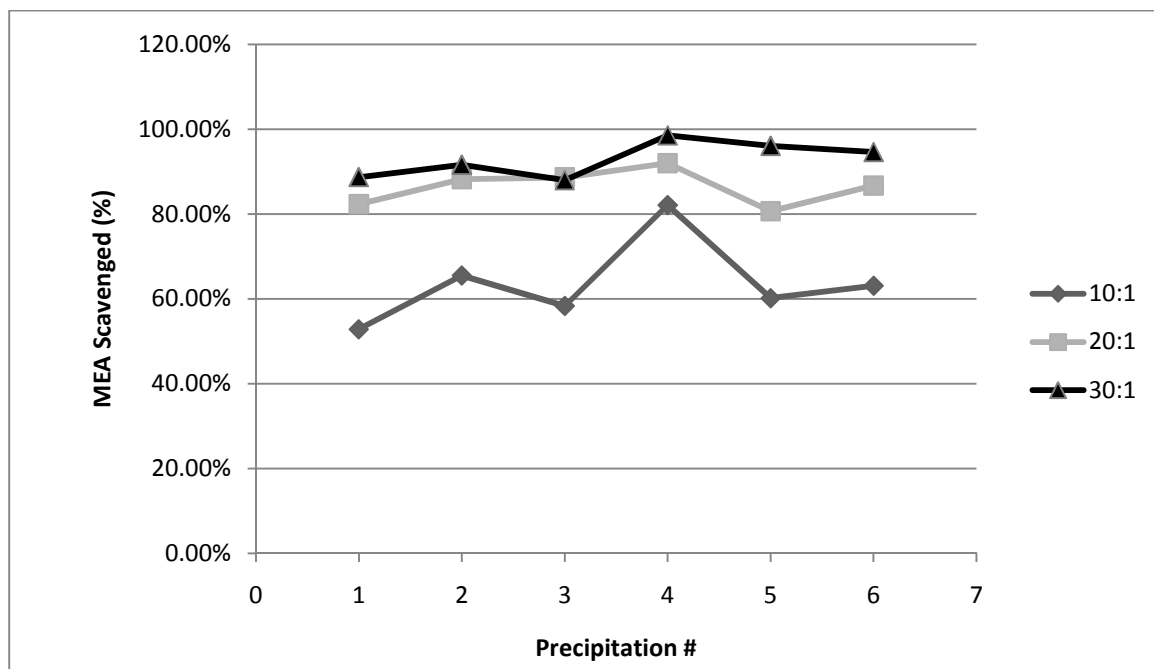


Figure 3.12: Pure MEA and Benzoyl Chloride Precipitation Study

Figure 3.12 shows an increase in the percentage MEA scavenged with an increase in BC:MEA ratio. It also shows an improvement in repeatability as the ratio increases. To validate the assumption that most of the precipitate consists of N-(2-hydroxyethyl) benzamide a sample of the 30:1 ratio was analysed with MS. The results are illustrated in Figure 3.13:

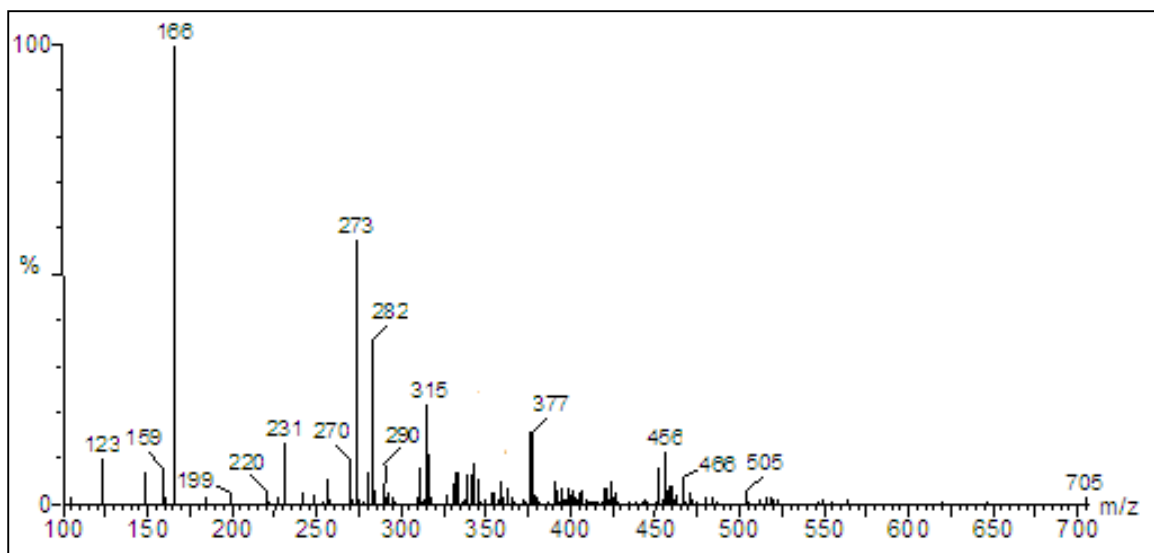


Figure 3.13: MS data for 30:1 pure MEA and Benzoyl chloride Precipitation Study

2-[(phenyl carbonyl)amino]ethyl benzoate has a molar mass in the range of 269 -272 g/mol depending on the degree of protonation. As seen from Figure 3.13 there are a

significant amount of 2-[(phenyl carbonyl)amino]ethyl benzoate in the pure precipitate study, nullifying the assumption made in the pure study.

Based on the results obtained in validating the chemical structure of the precipitate formed in a typical experimental run, it was decided to repeat the precipitation study in the presence of 2-propanol as solvent. The same BC:MEA mole ratios were used and the results are illustrated in **Figure 3.14**:

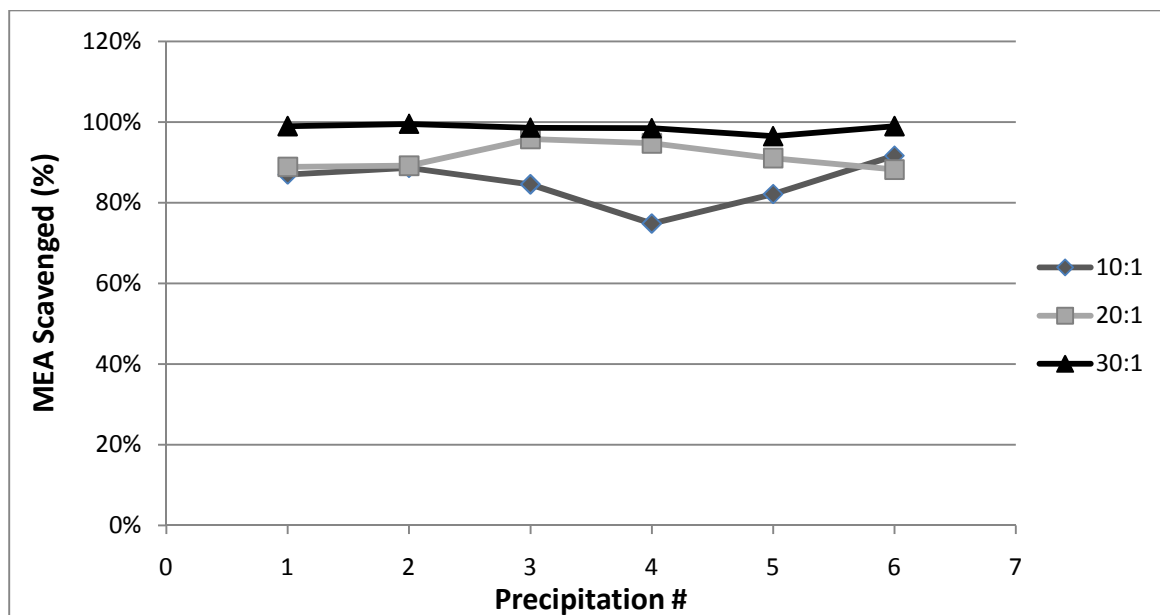


Figure 3.14: MEA and Benzoyl Chloride in 2-Propanol Precipitation Study

The percentage MEA scavenged was once again calculated on the basis that the precipitate consists mainly of N-(2-hydroxyethyl) benzamide. **Figure 3.14** shows the same trends as **Figure 3.12** but with even better repeatability and the desired 99% MEA scavenged. Validation of the assumption that most of the precipitate is in fact N-(2-hydroxyethyl) benzamide is illustrated in **Figure 3.15**:

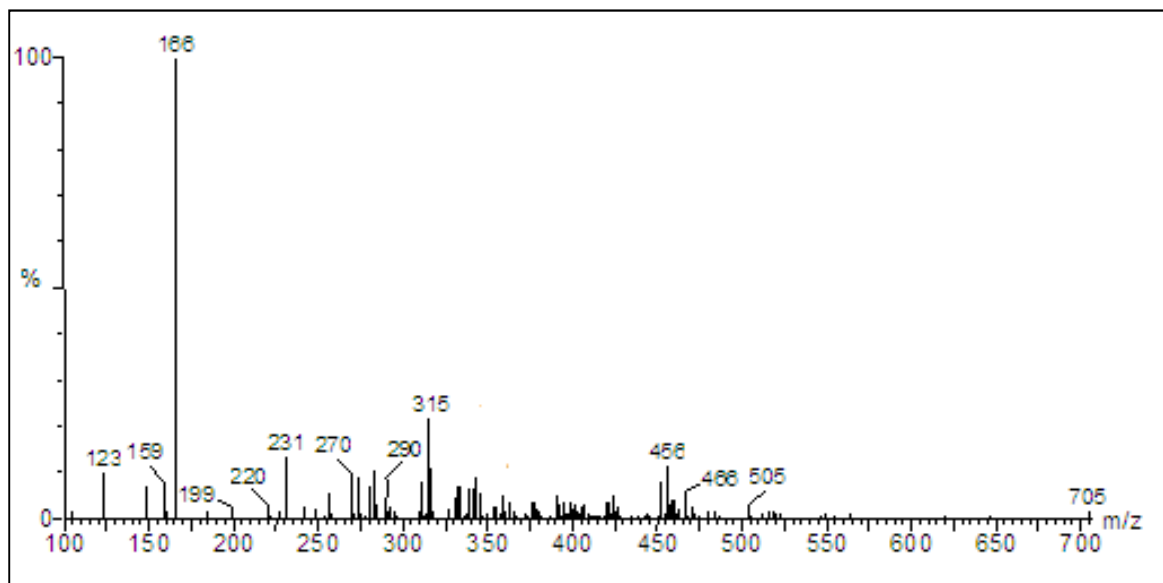


Figure 3.15: MS data for 30:1 MEA and Benzoyl Chloride in 2-Propanol Precipitation Study

All the other peaks present in **Figure 3.15** has a relative abundance of 20% or less. This means that if the N-(2-hydroxyethyl) benzamide is detected 10 times out of 10, the other components in the sample are detected less than twice. This is a good basis for assuming that most of the sample consists of N-(2-hydroxyethyl) benzamide from where a pure species mole balance may be performed to determine the %MEA scavenged. The exact reason why 2-propanol suppresses the formation of 2-[(phenyl carbonyl)amino]ethyl benzoate is not clear.

A conservative mole balance was done based on the results obtained in the mole ratio study to determine the correct benzoyl chloride to MEA ratio for achieving 99% scavenging. This test was done using 2-propanol as solvent and enough benzoyl chloride was added, on top of the amount needed for MEA scavenging, to completely convert the 2-propanol to the ester in a 1.05:1 mole ratio of benzoyl chloride to 2-propanol. The propanol was completely converted, which is desirable, since the precipitate may be partially soluble in 2-propanol due to it being completely soluble in methanol. From the results obtained in **Figure 3.14**, it may be concluded that the precipitate is insoluble in the 1-methylethyl benzoate present in the scavenging unit after complete reaction with the excess benzoyl chloride. 99% of the MEA is scavenged and captured in the solid precipitate.

3.6 Design of Experiments

After completing the design for the CSTRs and MEA scavenging, it is necessary to design the experimental parameters. The most important parameters are the relative reagent concentrations, which are controlled by the relative reagent flow rates. The experimental design must allow for the widest range of reagent concentrations realistically possible to ensure that the most complete reaction kinetic study is done.

3.6.1 Solubility of CO₂ in 2-propanol

The importance of knowing the solubility of CO₂ in 2-propanol is twofold:

1. CO₂ must be introduced to the reactor dissolved in liquid 2-propanol to nullify any gas phase mass transfer resistance.
2. The maximum solubility of CO₂ in 2-propanol will determine the maximum concentration of CO₂ introduced to the reactor at each temperature. The concentration of MEA must therefore be altered to achieve the desired range of relative reagent concentrations.

The solubility of CO₂ in 2-propanol has already been determined by other researchers and the data collected by Tokunaga (1975) was used in this study. The solubility data published by Tokunaga was tested with the data available in the NIST data base and found to be accurate

The functional relationship of the concentration of CO₂ in 2-propanol over the specified temperature range of 25 – 55°C is a power series which may be expressed as:

$$[\text{CO}_2] = 0.2256 \cdot T^{-0.3077} \quad (3.14)$$

The power-law series fit has an R^2 – value of 0.997

It is now possible to determine the concentration of CO₂ in the solvent at any of the intermittent temperatures if necessary.

3.6.2 Experimental Design Parameters

With the concentration of CO₂ known and fixed for each operating temperature, it now becomes possible to specify the relative MEA concentrations. The choice of MEA concentrations must adhere to the following criteria to ensure a complete reaction kinetic study:

The reaction rate model must be tested for consistency over a wide enough concentration range. Since the initial concentration of CO₂ is fixed at the solubility limits, the MEA concentration must be varied. It was decided to have a minimum initial MEA concentration equal to that of the initial CO₂ concentration. This is to allow for a large enough concentration of unreacted MEA to facilitate precipitation.

A maximum initial MEA concentration of 4 times the CO₂ initial concentration was chosen in order not to use too much benzoyl chloride since each run will be conducted at a benzoyl chloride to MEA mole ratio of 30:1 with the initial MEA concentration as basis. The reaction kinetic study was carried out at three temperatures (25°C, 30°C, 35°C) and three relative initial concentrations (1, 2.5, 4)

In order to be able to construct continuous concentration-time profiles, the same experimental parameters must apply for both the non-equilibrium and equilibrium reaction regimes

A large enough volume must be passed through the reactor to allow for measureable amount of unreacted MEA and CO₂. The sample volume must however not be too large to avoid wasting benzoyl chloride. It was found that a sample volume of 60 mL proved sufficient. The volume of benzoyl chloride was determined with a conservative mole balance based on all the possible reactions taking place in the scavenging unit. A volume of 150 mL results in at least a 30:1 benzoyl chloride to unreacted MEA ratio to ensure that 99% of the unreacted MEA is scavenged.

In order to achieve complete precipitation of the unreacted MEA, 500µL of pure MEA is added to the scavenging unit. From inspection, fine crystal formation was immediately noticed once the product stream came in contact with the benzoyl chloride. The 500µL of pure MEA acts as seed crystals to facilitate larger crystals to form. This is necessary for an accurate analysis of the precipitate. Since the zwitterion precipitate (abbreviated as phenyl carb) could not be analysed very accurately, it was decided to add a sufficient enough amount of pure MEA to render the mass of phenyl carb formed insignificant to that of the total mass of precipitate.

With a volume of 500 μ L it was found that the mass of phenyl carb precipitated calculated from HPLC analysis is less than 1% of the total precipitate mass. This is essential for determining the concentration of unreacted MEA. Refer to Appendix C for clarification in the sample calculation.

3.7 Reaction Kinetic Process P&ID

The reaction kinetic study piping and instrumentation diagram (P&ID) is illustrated in **Figure 3.16**. The process fundamentals may be summarised as follows:

- The reagent mixtures are prepared to the appropriate concentration in their separate 5L reservoirs. Argon gas blankets the MEA to prevent reaction with atmospheric CO₂. Argon is also directed to the vacuum separation unit to blanket the unreacted MEA.
- From the reservoirs the reagents are pumped through 316-stainless steel coils submerged in a water bath heated to the desired operating temperature.
- The reagents are circulated through the heated water bath and back to the reservoirs until the temperature within the reservoirs are equal to the operating temperature maintained in the bath. This is determined with the temperature sensors (PT-100). Refer to Appendix E for the calibration certificate.
- Once isothermal conditions prevail, the reagents are directed to the jacketed CSTR via the T-junction valve system. The unreacted CO₂ and MEA are separated upon exiting the reactor in the separation unit and analysed.

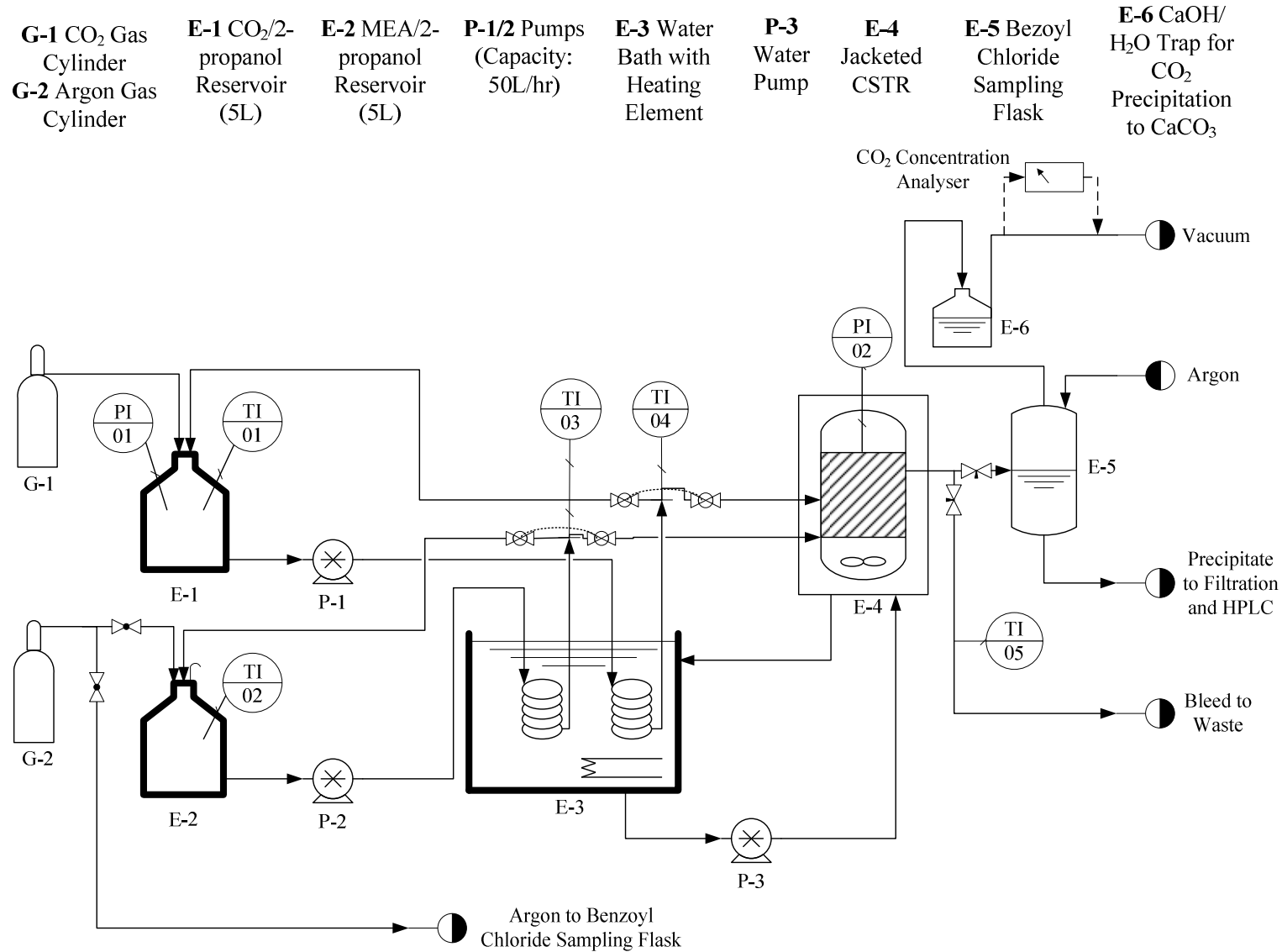


Figure 3.16 P&ID of Reaction Kinetic Experimental Set-up

3.7.1 Materials of Construction

Due to the corrosive nature of MEA care must be taken regarding the choice of the most appropriate materials of construction. After testing a range of commonly used materials, the following were decided on based on their compatibility as well as cost:

- The 5 L reservoirs are glass Erlenmeyer flasks to enable visibility of the reagent mixtures. Each flask is fitted with a custom designed stainless steel cap with the necessary entry and exit ports.
- The pumps used are fitted with Teflon type diaphragms within stainless steel casings, shielding the pump motor from the reagent mixture.
- All tubing is made from 316-stainless steel and insulated.
- Both CSTRs were constructed from 316-stainless steel.
- All of the valves in the system are made from 316-stainless steel.

3.7.2 Liquid Flow Rate Calibration

The liquid flow rates for the reaction kinetic study were determined by pumping 2-propanol through both reactors at various pump settings and all three temperatures and measuring the time for a fixed volume (300 ml) to collect from the product stream. Each pump was calibrated separately. The combined flow rate of the pumps was also verified at various pump settings with a stopwatch and volume measuring cylinder. The calibration curves were consistent for the temperature range (25 - 35 °C) and are illustrated in Appendix B.

The times required to collect approximately 60ml reactor product at each flow rate were calculated from the total flow rate through the reactor. Validation runs were performed to practice opening and closing the valves in the allotted times. The set-up was designed to have the bleed stream valve and scavenging unit valve very close to one another to ensure the simultaneous opening and closing of each. During an experimental run, the product stream is firstly bled to allow for steady state to be achieved in the reactor. Once four or more reactor volumes have passed through, the bleed stream valve is closed, the scavenging unit valve opened and the stopwatch started simultaneously. The time for approximately 60 ml sample is allowed and the valves switched back and stopwatch stopped simultaneously. It takes a lot of practice to get the timing of the valves right, since the shortest collection time is in the region of 2.16 seconds. After enough practice, 2.16 seconds

becomes a long time. The volume collected from the reactor was calculated from the time measured for collecting the product in the scavenging unit. The times needed for 60 mL sample collection is tabulated in Appendix B

3.7.3 Experimental Procedure and Control Philosophy

To ensure safe and accurate operation of the reaction kinetic experimental set-up, an experimental procedure along with a control philosophy is designed and must be followed during the course of an experiment. The procedure followed is duly summarized:

The very first task is filling the water bath to the correct depth and switching on the heating element to the desired temperature. All tubing connections should be checked whilst waiting for thermal equilibrium in the water bath. Start circulating water to the reactor jacket. Prepare the MEA scavenging unit to the correct benzoyl chloride volume and start purging with argon whilst drawing slight vacuum. Add 500 μ L of pure MEA to the scavenging unit. This acts as seed crystals to facilitate complete precipitation. Start stirring the contents of the scavenging unit. Allow the HCL liberated from the scavenging unit to bubble through three pure water traps.

Fill each reservoir to the correct volume and concentration. Do not exceed the specified amine volume to prevent waste. Then mount the reservoirs in place. Blanket the MEA/2-propanol reservoir with argon immediately.

Before starting the pumps, check that all the tubing is connected properly and that the T-junction valve systems are in the position to allow circulation of the reagent mixtures through the water bath. Prepare the CO₂ traps with a sufficient volume of CaOH solution. Put the CO₂ traps in place and purge with argon whilst drawing slight vacuum. Open the CO₂ cylinder safely and allow the gas to bubble through. Once thermal equilibrium is achieved the experimental run may be performed.

Before directing flow to the reactor, first ensure that the product stream valves are set to allow the system to bleed until steady state is achieved within the reactor. Once steady state is achieved, direct the product flow to the scavenging unit and allow for an approximate 60 mL sample to flow to the scavenging unit.

Allow enough time for the unreacted CO₂ to evaporate whilst continuously stirring the mixture. Filtrate the mixture and prepare the precipitate sample after weighing for HPLC analysis by dissolving it in methanol.

Vacuum filter the CaOH traps, dry and weigh the CaCO₃ precipitate.

To prepare for the next run, ensure that all residual product mixture is cleared from the product line. Flush the CaOH traps with distilled water. Flush the MEA scavenging unit with acetone and dry with compressed air.

3.8 Method of Analysis

3.8.1 CO₂ Analysis

After the reaction of CO₂ with MEA is stopped by scavenging the MEA with benzoyl chloride, the unreacted CO₂ is allowed to evaporate off under vacuum with inert argon as carrier gas. The minimum time needed for 99% CO₂ evaporation was determined by allowing the evaporating gas to firstly pass through three water traps to dissolve all the HCl formed in the scavenging reaction, and then through a CO₂ concentration analyser until a zero reading was achieved. The minimum time varied between 5 and 7 minutes and thus 15 minutes was allowed during each experimental run.

For CO₂ analysis, the unreacted CO₂ is bubbled through three traps in series containing solutions of CaOH in water. A CaCO₃ precipitate is formed according to the following reaction:



The first trap acted as an acid trap as well, dissolving the HCl formed in the scavenging reaction. The effect of the acid was studied, since HCl decomposed some of the CaCO₃ in the first trap back to CO₂. It was found that the acid helped prevent the CO₂ from dissolving in water since the pH was lowered already and the liberated CO₂ in the first trap was precipitated in the second and third. Since the CaCl₂ formed

by the HCl is water soluble, it reports to the liquid filtrate. The precipitate is filtered off as soon as possible to avoid the formation of calcium bicarbonate, which is also water soluble:



The precipitate is dried and weighed to determine the number of moles of unreacted CO₂. The concentration of unreacted CO₂ may now be determined from the known volume passed through the reactor for the particular experimental run.

3.8.2 CO₂ Sensitivity and Repeatability in Analysis

As with all scientific studies, care must be taken when interpreting the accuracy of the data collected. This accuracy depends on how accurate the instrumentation used in the analysis is, as well as how accurately the system conditions have been maintained through the entire course of the experimental run. This section will only address the accuracy involved with the analysis procedure.

In order to be able to ensure that the experimental run was done at the correct predicted initial CO₂ concentration, the CO₂/2-propanol mixture was pumped through the short residence time reactor and the evaporated CO₂ analysed. The results of the test at 30°C are listed in **Table 3.7**:

Table 3.7: Test for Solubility of CO₂ in 2-propanol at 30 °C and 1 atm

Volume of sample (L)	Mass CaCO ₃ (g)	n _{CO2} (mol)	[CO ₂] (mol/L)	Error %
0.062	0.486	0.0049	0.0787	-0.437
0.060	0.473	0.0047	0.0794	-1.310
0.061	0.481	0.0048	0.0786	-0.307
0.063	0.478	0.0048	0.0763	2.707
0.062	0.496	0.0050	0.0806	-2.781

This is in good agreement with the solubility data in literature (Tokunaga, 1975). This was also a good test for regulating the pressure within the system at 1 atm. From **Table 3.7** it is seen that good repeatability was achieved with each repetition. The repeatability of the CO₂ measurements was found to be within 2.8% of the average measurement of the 5 repetitions. To ensure that an acceptable degree of repeatability was achieved over the entire CO₂ concentration range, a study was

done at initial concentrations of $[MEA]_i = 2.5[CO_2]_i$ at 30 °C in the long residence time reactor at the lowest volumetric flow rate. The results obtained are tabulated in **Table 3.8**:

Table 3.8: Test for Repeatability of CO₂ Measurements

Volume of sample (L)	Mass CaCO ₃ (g)	n _{CO₂} (mol)	[CO ₂] (mol/L)	Deviation from Average Concentration (%)
0.060	0.065	0.0006	0.0108	-0.807
0.060	0.069	0.0007	0.0115	4.85
0.060	0.071	0.0007	0.0118	8.25
0.059	0.063	0.0006	0.0107	-2.09
0.060	0.059	0.0006	0.0098	-10.2

From **Table 3.8** it shows that the repeatability of the CO₂ measurement at low CO₂ concentrations lies within 10.2% of the average for the 5 repetitions. Taking into consideration that the range of CaCO₃ mass measurements lies within 0.012 g and that some inaccuracy must be attributed to some of the CaCO₃ further reacting with CO₂ (eq. 3.16), the error is relatively low. It results in a confidence interval of ±0.002 mol/L for the CO₂ concentration measurements. Further investigation into more advanced methods for CO₂ analysis should be investigated in future to be able to eliminate the inaccuracies of further reaction.

3.8.3 MEA Analysis

The precipitate formed from the unreacted MEA and formed zwitterion was analysed with High Performance Liquid Chromatography (HPLC). The first task was identifying the appropriate solvent for the mobile phase. It was found that the precipitate is completely soluble in methanol. Accordingly, the HPLC equipment used for analysis may be summarized as follows:

- **Column:** Phenomenex Luna C18(2), 100A, 150x4.6mm, 5u
- **Guard Column:** Phenomenex SecurityGuard C18, 4mm x 3.0mm ID
- **Injection Volume:** 10 µl
- **HPLC System:** TSP SpectraSystem P2000 Pump, AS3000 Autosampler and UV1000 UV-VIS Detector set to 225 nm
- **Mobile Phase Flow Rate:** 1.0 ml/min
- **Mobile Phase:** Methanol / Water, Volume ratio 59:41
- **Run Time:** 0 – 10 min.

After filtration, the precipitate was weighed and a solution with a concentration of approximately 0.1 – 0.12 g/mL in methanol, prepared. Then dilute 10µL of the sample to 1ml with methanol. The stock sample is kept in a closed container in a refrigerator to prevent decomposition. It was found that the samples maintained its composition well with no noticeable decomposition within 4 days of preparation and an approximate 17% decomposition after 3 weeks in the refrigerator. All samples were analysed within 24 hours of preparation.

In order to be able to quantify the HPLC analysis of each sample, an internal standard must be prepared. For this purpose, a sample of high purity of each component of interest to the analysis must be prepared. The purity of the samples used to prepare the internal standard is tabulated in **Table 3.9**

Table 3.9: Purity of the Stock Solutions Used for the Internal Standard

Stock Solution	Purity (%)	Concentration (mg/ml)
1-methylethyl benzoate	93.23	7.3
N-(2-hydroxyethyl) benzamide	96.94	39.086

The purity is on a mass basis and is accounted for in the calibration factor calculated for each component. Since the zwitterion precipitate (abbreviated as phenyl carb) could not be prepared to the desirable purity, its calibration factor was determined from its relative concentration in the N-(2-hydroxyethyl) benzamide stock solution, which does not invest a lot of confidence in the accuracy of the factor, but serves as the best approximation. The calibration factor is derived from injecting 6 different concentrations of a mixture of known composition and integrating the chromatogram peaks of each of the analysis. The outliers are rejected and a plot of concentration vs. area then yields a straight line with the slope of the line

representing the calibration factor. The calibration factor plot for N-(2-hydroxyethyl) benzamide is illustrated in **Figure 3.17** and the calibration factors of the three components of interest are tabulated in **Table 3.10**:

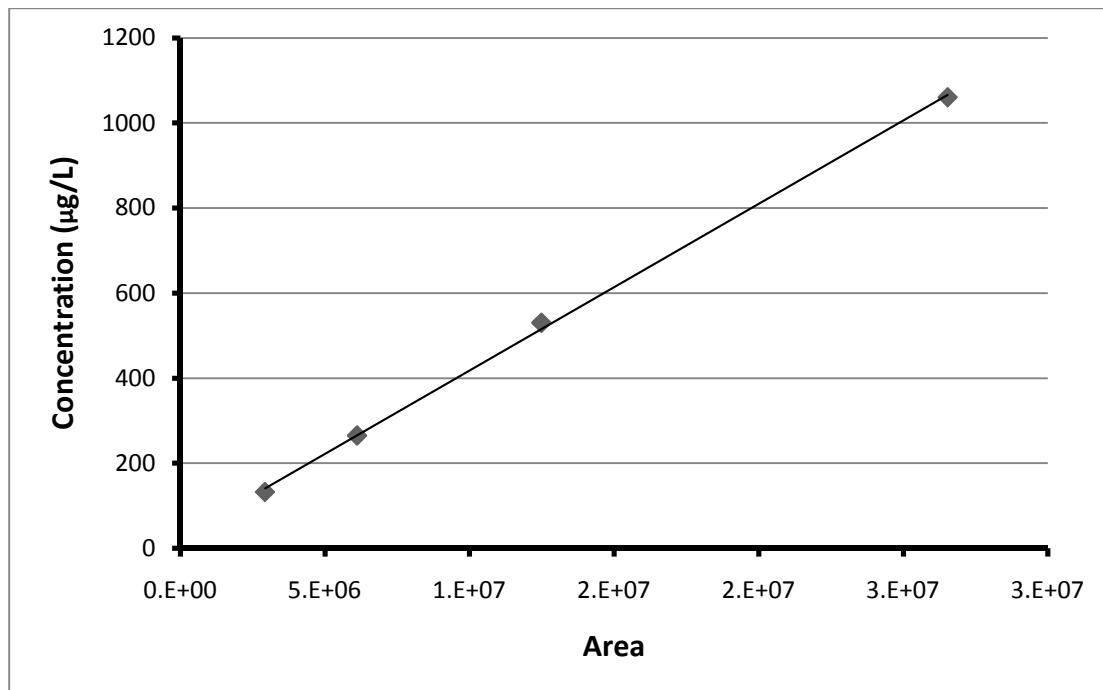


Figure 3.17: Calibration Factor Plot for N-(2-hydroxyethyl) benzamide

Table 3.10: Calibration Factors

Component	Calibration Factor
phenyl carb	9.03
1-methylethyl benzoate	4.62E-05
N-(2-hydroxyethyl) benzamide	3.92E-05

The calibration factors are used to determine the concentration of each of the components from the area under the chromatogram peak. An internal standard comprising of known concentration of all three components is injected after every 10 samples analysed to recalibrate the HPLC column. The inaccuracy in determining the concentration of phenyl carb is noticed in its calibration factor which is much larger than that of the other components. The reason for it is that a high enough concentration of it could not be prepared to improve the accuracy. It will however be shown in the next section that it has a similar repeatability accuracy than the other components.

3.8.4 MEA Error and Repeatability in Analysis

It is firstly desirable to study the repeatability of the mass precipitate formed in scavenging the unreacted MEA. A study was done at initial concentrations of $[MEA]_i = 2.5[CO_2]_i$ at 30 °C in the long residence time reactor at the lowest volumetric flow rate, adding 500 μ L of pure MEA to facilitate complete precipitation. The results obtained are tabulated in **Table 3.11**:

Table 3.11: Test for Repeatability of MEA Measurements

Volume of sample (L)	Mass Precipitate (g)	Deviation from Average (%)
0.059	1.98	1.00
0.061	2.03	-1.50
0.060	2.04	-2.00
0.060	1.99	0.50
0.061	1.96	2.00

From **Table 3.11** a repeatability in the mass of precipitate formed of within 2% is achieved. This is acceptable. The accuracy bias percentage for each component analysed, which is an indication of the repeatability for the HPLC analysis, is tabulated in **Table 3.12**:

Table 3.12: Repeatability of each Component analysed

Component	Accuracy Bias Range (%)
2-phenyl Carb	-3.42 - 9.9
1-methylethyl benzoate	-2.64 - 9.27
N-(2-hydroxyethyl) benzamide	-2.31 - 10.02

From **Table 3.12** an accuracy within 10.02% is achieved for each component. This was achieved by injecting six different concentrations of each component in triplicate and performing a statistical analysis on the concentrations determined with the calibration factors in **Table 3.10**. This is a large error band for a data set earmarked for model development. It should be noted that the error increased with a decrease in analyte concentration. For the concentrations of interest to this study the accuracy bias lies within 5.8%, which is not ideal, but deemed acceptable.

CHAPTER 4: DIFFUSIVE MASS TRANSFER

EXPERIMENTAL DESIGN AND PROCEDURE

The specific absorption of CO₂ into solutions of MEA/2-propanol was studied on a wetted wall experimental set-up. The wetted wall allows for the investigation of the absorption of a gas into a liquid on a known liquid transfer area. In order to be able to draw a comparison between absorption data and correlations, a very similar wetted wall experimental set-up to the one used by Erasmus 2004 was designed and constructed.

4.1.1 Wetted Wall Column Design

The design of the wetted wall column is based on the work of Roberts and Danckwerts (1962), Davies *et al.* (1967) and Erasmus (2004). Refer to Appendix E for a dimensioned mechanical drawing of the wetted wall set-up. A schematic of the wetted wall column assembly is illustrated in **Figure 4.1**:

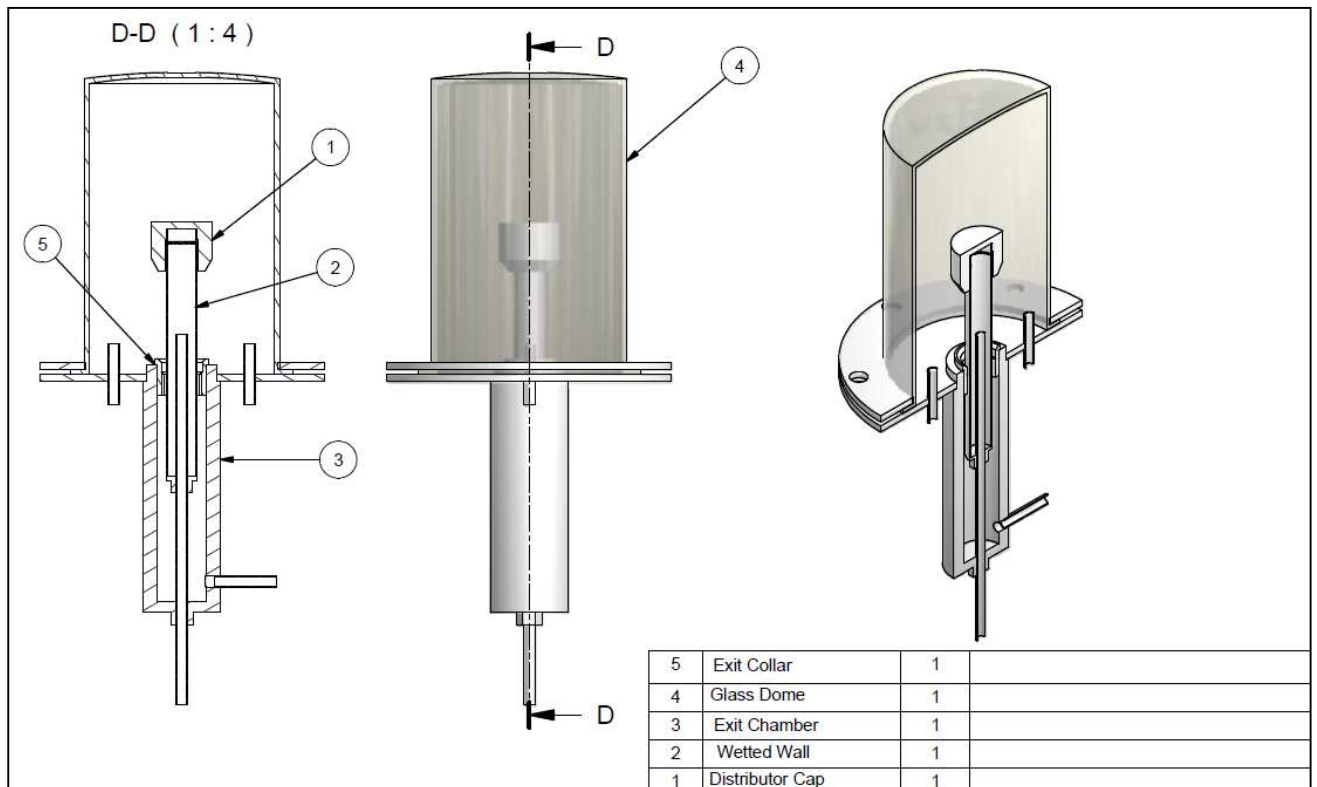


Figure 4.1: Schematic of the Wetted Wall Assembly

The column is basically a stainless steel pipe with an outside diameter of 25.4 mm. The liquid entering through the bottom of the pipe, exits through 24 evenly spaced holes at the top and is evenly distributed over the full circumference of the column by means of a stainless steel distributor cap fitted on top. The cap allows for a 0.2 mm annular gap, which is vital, because should the gap be too small, the liquid will not have enough space to pass freely past the cap's edge, resulting in droplet hold-up due to surface tension (see **Figure 4.2**) and should the gap be too large, the liquid wont distribute evenly with a uniform film thickness. The distributor cap serves a secondary purpose in covering the top 15 mm of the column, allowing for fully developed liquid flow close to the free film stream velocity of the liquid before any contact with the gas is made. The annular gap should thus also not be too big to prevent significant gas contact in the annulus. The liquid profile observed in the entrance region of the wetted wall is illustrated in **Figure 4.2**

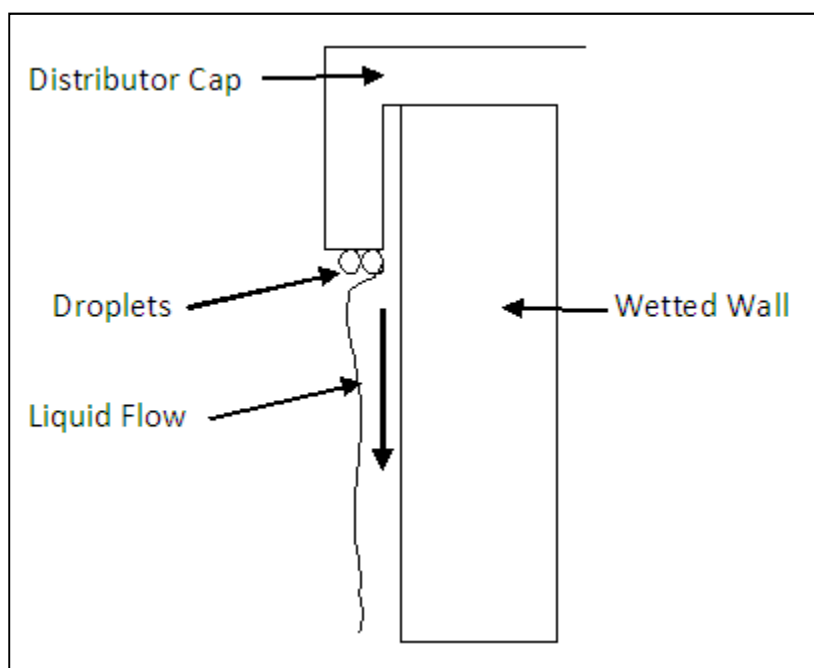


Figure 4.2: Schematic Showing Liquid Flow Profile at the Entrance of the Wetted Wall (Adapted from Wilkes and Nedderman, 1961)

Once absorption has taken place the loaded liquid exits through a stainless steel exit collar. A schematic of the exit collar is illustrated in **Figure 4.3:**

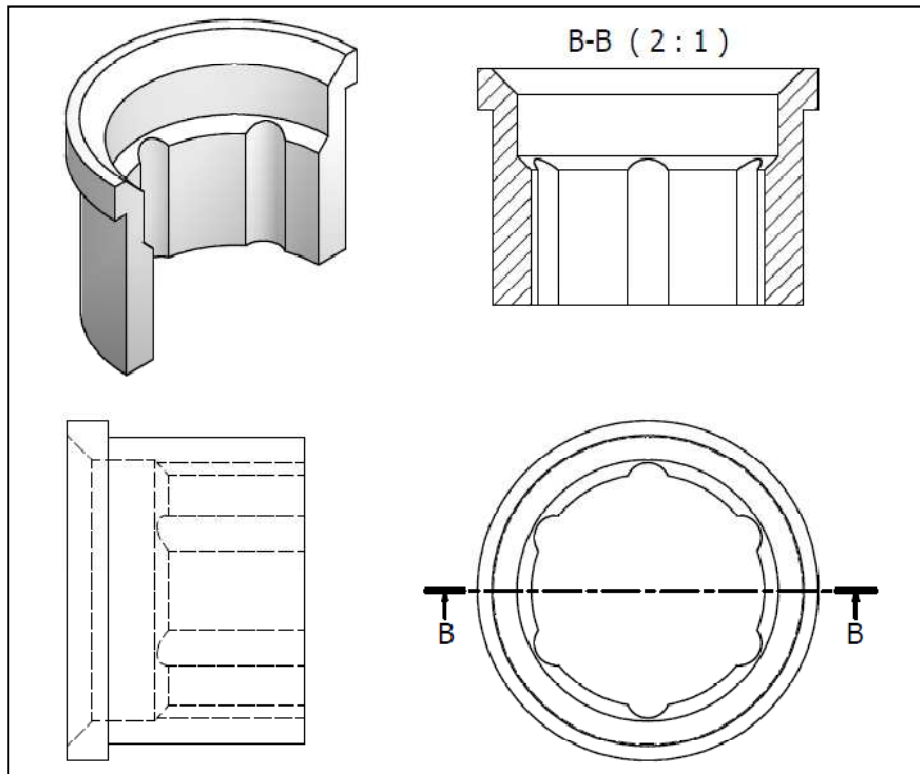


Figure 4.3: Schematic of Exit Collar

The design of the collar serves combined purposes. It firstly causes a slight liquid hold-up, which prevents the gas from getting into contact with the liquid which already exited the system into the base section. The collar secondly keeps the column in the same vertical orientation as the rest of the set-up, due to the fact that the column fits tightly in the collar. Roberts and Danckwerts used an exit collar of slightly different design. By cutting narrow grooves on the outer surface of their collar they prevented the stagnant liquid film caused by a build-up of surfactant at the base of the column (Roberts and Danckwerts, 1962). This study did not use surfactants, so the exit collar in **Figure 4.3** is deemed appropriate.

The base section screws into a 6 mm stainless steel flange on which the 3 mm thick glass dome is bolted in place. The flange is fitted with a gas entry and exit port. The tube in the entry port extends to the top of the dome where the gas is introduced to prevent short circuiting of the gas. In order to be able to study absorption rates for different column heights, it is important that the column can be extended from- and collapsed into the base section.

A common problem encountered with stainless steel wetted walls is that the liquid does not disperse uniformly across the entire surface of the column, but disperses in streaks. Another problem encountered at longer column heights and low liquid flow

rates is the formation of ripples at the base of the column which makes the interfacial area unknown. These effects were prevented by previous authors by introducing a surfactant (Danckwerts, 1970, Sada *et al.*, 1985). Erasmus found the surfactants to be ineffective (Erasmus, 2004) which forced him to use very short column heights. A solution to the streaking problem is to have a small annular gap and as many liquid exit holes as possible. The trick is then to have an initial liquid surge at high flow rates to overcome the surface tension of the dry wall. Once the wall has been wetted, the flow rate may be decreased to the desired operating rate. For column lengths longer than 105 mm and at low liquid flow rates (approximately 1mL/s) the formation of surface waves was considered to become significant. The maximum column length investigated was thus 105 mm. Absorption studies taking wave effects into account should form part a future investigation, since the turbulent flow in separation columns cause wave formation on the packing material, which enhances mass transfer and affects the effective interfacial mass transfer area.

4.1.2 Experimental Design Parameters

This study is aimed at showing that a fully functional wetted wall set-up could be constructed to produce repeatable absorption measurements. The experimental runs will thus be designed to imitate the results obtained by Erasmus, 2004. The experimental set-up was designed to incorporate two gas mass flow controllers/meters for fixing the inlet flow and measuring the outlet flow. This means that a CO₂ concentration analyser, which has a limit on the maximum flow rate it can handle, is not needed to measure for CO₂. Another advantage is that higher CO₂ gas concentrations can be studied since the concentration analyser cannot measure above 25 volume % CO₂ and is therefore not feasible when pure CO₂ absorption runs are performed. It is desirable to be able to study absorption rates over a wide concentration range to test the consistency of the rate expressions derived for determining effective interfacial mass transfer area.

Erasmus performed his absorption experiments for CO₂ mass percentages in the range 0.54% – 1.3% and for MEA concentrations in the range 0.2 – 0.3mol/L. This study will attempt experimental runs for some of his conditions in order to validate the results obtained at the proposed flow rates and concentrations. The gas side experimental design parameters for the proposed reaction runs are tabulated in **Table 4.1:**

Table 4.1: Gas Experimental Design Parameters

Mass% CO ₂	MFC _{out}	MFC _{CO₂,in}	P _{dome} (kPa)	P _{CO₂} (kPa)
100	2	2	104.72	104.72
78	2	1.7		80
55	2	1.3		55
30	2	0.8		30

It is important to note that these are not the actual mass flow rates of the gasses to the dome but merely the MFC readings. The actual mass flow rates are calculated by incorporating a calibration factor for each gas, since the MFC is originally calibrated for air. The total pressure in the dome was measured for the different flow rates and was found to remain fairly constant (deviating by ±1 % over the flow rate range). From **Table 3.10** it can be seen that the dome pressure exceeds standard atmospheric pressure by ±3%. This could not be avoided in order to be able to achieve the desired inlet concentration range.

It should further be noted that only the CO₂ inlet flow is fixed and the argon flow adjusted accordingly to achieve the desired CO₂ mass%. This means that the MFC_{out} reading will not always be exactly 2 at the start of a run, but as close as possible. Before the liquid side design parameters could be fixed it is necessary to decide on the temperature and initial MEA concentration range. In order to be consistent with both the reaction kinetic study as well as the temperatures and concentrations used by Erasmus (2004) it was decided to study the absorption rates of CO₂ at 25°C and 30°C and at MEA concentrations of 0.25 mol/L and 0.3 mol/L.

The next consideration is the gas-liquid contact time achieved per run. The contact time may be calculated from classic laminar falling film theory (Roberts and Danckwerts, 1969):

$$t_c = \frac{h}{u_i} = \frac{2h}{3} \left(\frac{3\mu_L}{\rho g} \right)^{1/3} \left(\frac{\pi d}{V} \right)^{2/3} \quad (4.1)$$

The density and viscosity in equation 4.1 is for the liquid mixture and were measured for each of the different mixtures at each of the operating temperatures. The density was determined with a density flask of known volume and measuring the mass of the mixture at the specific temperature. The viscosity was determined with a roto-visco meter. The measured properties are tabulated in **Table A.2** in Appendix A.

The gas – liquid contact time was varied by varying the volumetric liquid flow rate and column height. Liquid flow rates of 0.96 and 1.54 mL/s and column heights of 60, 90 and 105 mm were investigated.

Having a small annular gap (0.2 mm) would increase the liquid velocity in the entry region of the wetted wall. The effect of the increase in liquid velocity on the distance required for the liquid flow to become fully developed was investigated by Wilkes and Nedderman (1961). It is of great interest to be able to know if velocity will have an effect, since the laminar falling film theory used to calculate the gas liquid contact time may only be applied to fully developed laminar flow. The first condition to be satisfied would be to determine if the liquid flow is laminar. The Reynold's number for the highest liquid velocity was calculated to be in the region of 0.5 – 0.9, which indicates that the flow is indeed laminar. Similar liquid Reynold's numbers were investigated by Wilkes and Nedderman.

Wilkes and Nedderman investigated a velocity range of $u_{max}:u_{min}$ of 6.92. In this study, the velocity was calculated to be 1.755 times larger than the velocities investigated in previous studies with a larger annular gap (0.35 mm) (Erasmus, 2004). Based on the similar Reynold's number and a velocity increase within the range investigated by Wilkes and Nedderman, it is assumed that their findings are applicable to this study. They found that an increase in velocity has no significant effect on the distance required for fully developed laminar flow. The distance calculated in their study was approximately 7 mm. With the similarities in the Reynold's numbers, it is assumed that a similar distance was needed in this study. Another similarity found in this study is the bending of the liquid stream lines away from the wall in the entry region (see **Figure 4.2**). The immediate increase in film thickness contributes to the faster development of a fully developed velocity profile.

Based on these similarities it may be concluded that the falling film theory is applicable for determining gas-liquid contact times in this study. More experimentation on the size of the annular gap will be performed in future to increase the accuracy of the gas liquid contact times. The use of surfactants will also be investigated to improve the uniformity of the film thickness and liquid distribution on the wetted wall.

4.2 Diffusive Mass Transfer P&ID

The absorption study piping and instrumentation diagram (P&ID) is illustrated in **Figure 4.4**. The process fundamentals are as follows:

The inlet CO₂ gas flow rate is controlled by a gas mass flow controller (MFC) (FIC 01). The argon flow rate is adjusted to achieve the desired total gas flow rate before absorption. This is measured by the outlet MFC (FIC 02). The gas leaving the dome is analysed by means of a mass balance calculation. The gas is then vented to the atmosphere.

Calibration of the MFC for the mixed gas is achieved with the use of a positive displacement gas flow totaliser (E-6). The MEA/2-propanol mixture is pumped from its reservoir to the wetted wall where it is distributed evenly over the circumference of the tube allowing the gas to absorb through a known surface area.

The liquid flow rate is controlled by means of a liquid rotameter (E-5). The loaded liquid exits the bottom of the wetted wall set-up and is collected in a reservoir. A sample is drawn and analysed. The liquid may be regenerated for repeated use by means of gas stripping under vacuum. To ensure that isothermal conditions prevail, the whole set-up is submerged in a temperature controlled water bath. The liquid lines are circulated through the pre-heater and back to the reservoir to achieve the desired liquid temperature and maintain isothermal conditions.

G-1 CO₂ Gas Cylinder
G-2 Argon Gas Cylinder
E-1 Wetted Wall in Glass Dome
E-2 MEA/2- Propanol Reservoir
E-3 Exit Liquid Reservoir
E-4 Sampling Port
E-5 Rotameter
E-6 Positive Displacement Gas Flow Meter
P-101 Liquid Pump

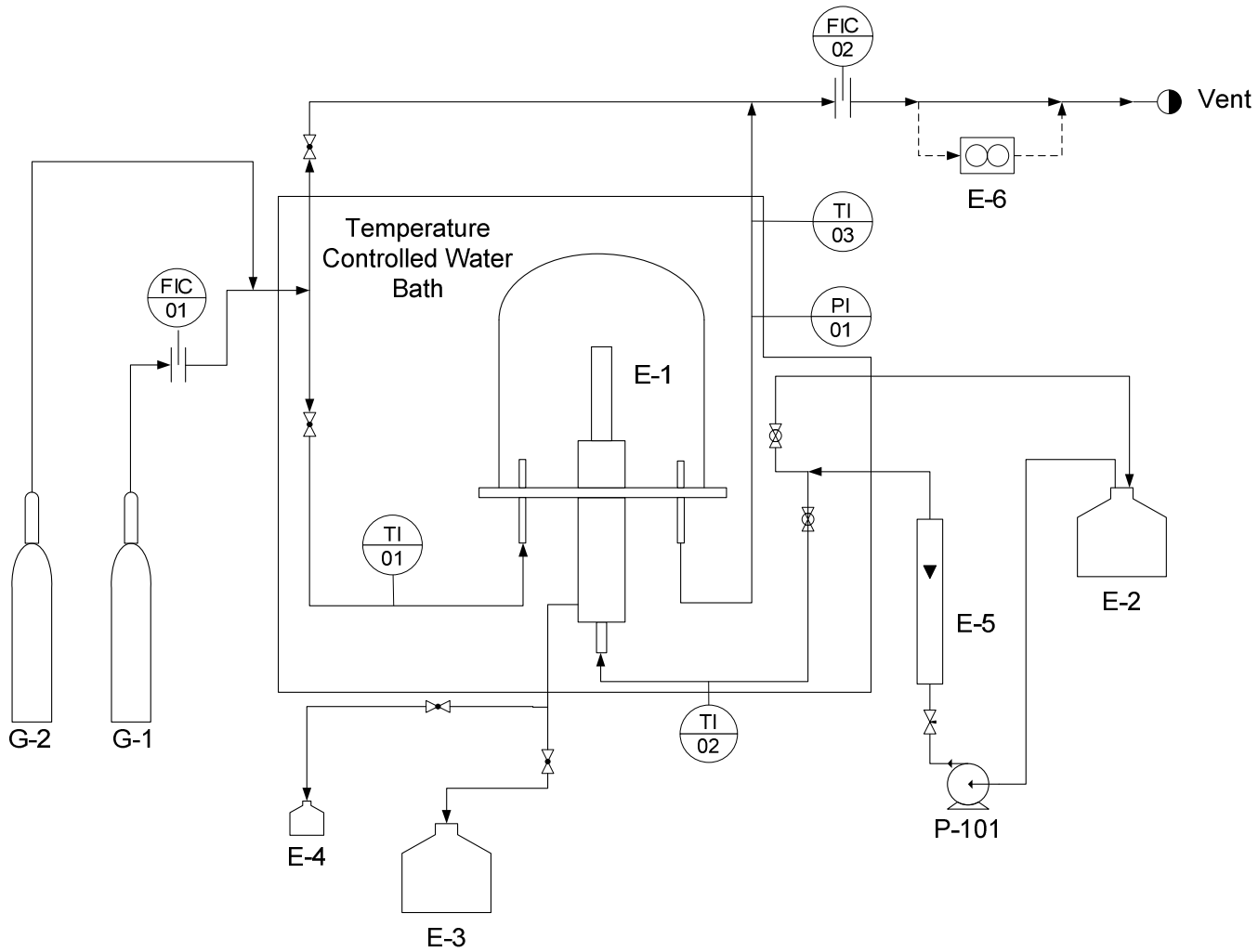


Figure 4.4: Wetted Wall P&ID

4.2.1 Materials of Construction

As stated before, the corrosive nature of MEA limits the choice for materials of construction:

- The wetted wall itself is constructed from 316-stainless steel, as is the distributor cap and the exit collar.
- The dome of the wetted wall is made from 6mm Pyrex glass to prevent rupture should a pressure surge be encountered.
- All the tubing is either form stainless steel 316 or silicone rubber. All the fittings and valves are made from stainless steel 316.
- The impellers of the centrifugal pump (P-101) are from stainless steel (unknown number type).
- All the reservoirs are made from glass.

4.2.2 Experimental Procedure and Control Philosophy

It is once again with safety and accuracy in mind that the experimental procedure and control philosophy for the wetted wall experimental set-up have been derived:

After fitting the wetted wall to the correct height and fixing the dome tightly in place, purge the dome with argon. Adjust the valves to have the gas bypass the wetted wall. The whole wetted wall set-up is set in an upright position.

Fill the water bath and pre-heater and switch on the elements and circulating pump. Take care in not overflowing the water bath. Enter the desired operating temperature as a set-point and check the temperature sensors. The elements are only functional if the water bath and pre-heater are filled to capacity. This should be checked regularly due to water evaporation.

Once thermal equilibrium has been reached, set the CO₂ MFC to the desired flow rate and open the CO₂ cylinder. Open the argon cylinder and adjust the regulator until the outlet MFC reads the desired flow rate. These flow rates are tabulated in **Table 4.1**. Adjust the valves to direct the gas flow to the dome. Allow enough time for the outlet MFC reading to stabilize and check the pressure inside the dome. If necessary, adjust the argon regulator to once again achieve the desired outlet MFC reading and dome pressure to ensure that CO₂ is fed at the desired mass%.

This prompts the introduction of the MEA/2-propanol to the system. Prepare the mixture to the desired MEA concentration and purge with argon to prevent reaction with atmospheric CO₂. Switch on the liquid pump and allow the mixture to circulate through the pre-heater to achieve thermal equilibrium. Adjust the rotameter needle valve to the desired flow rate.

Direct the liquid flow to the wetted wall once thermal equilibrium is reached. Set the wetted wall outlet valve to facilitate an outlet flow rate that ensures that the liquid exit chamber remains filled to the level of the exit collar. This will eliminate any gas-liquid interaction inside of the exit chamber. To ensure that steady state is achieved, allow for two exit chamber volumes of liquid to pass through the wetted wall and the outlet MFC reading to stabilize before logging any data.

4.3 Diffusive Mass Transfer Method of Analysis

4.3.1 CO₂ Analysis

The amount of CO₂ absorbed may be calculated from a mass balance performed on the MFC readings. Since the MFC's default calibration was done with air, it had to be recalibrated for both CO₂ and argon. This was simply achieved by placing the cylinders on a digital weighing scale and measuring the mass expelled by the cylinders at different time intervals, whilst noting the reading on the MFC. The time integral of the MFC reading vs. time curve summates the predicted total mass expelled which was correlated with a correction factor for the actual mass expelled. The correction factors are listed in **Table 4.2**:

Table 4.2: Correction Factors for Calibration of the MFC

Gas	Correction Factor	%Error	MFC Range
CO ₂	2.175	±0.39	0.1 - 5
Argon	3.241	±0.57	0.3 - 5

The factors were tested at higher and lower settings than calibrated for with a gas totaliser and held true. The correction factors of **Table 4.2** are implemented as follows:

$$m_{\text{Actual}} = f \cdot m_{\text{MFC}} \left(\frac{\text{kg}}{\text{hr}} \right) \tag{4.3}$$

The calibration was done for three different MFC settings within the range specified in **Table 4.2** with each resulting correction factor within the error percentage from the average. The factors are therefore assumed to be valid for this range, which is the operating range of the study. Refer to Appendix B for the calibration data of the MFCs.

Since the wetted wall set-up is equipped with two MFCs, absorption experiments with pure CO₂ are also possible. The mass flow controllers were calibrated for different gas mixtures by using a gas totaliser. The accuracy of the gas totalizer was tested by placing two in series and noting the same flow rate for each. This is an indication that the device operates correctly, since the probability that two totalisers will have the same inaccuracy is very small.

Before the calibration could be done, the effect of 2-propanol, evaporating from the surface of the wetted wall, on the MFC reading was investigated at the operating temperatures. The effect of 2-propanol on the MFC reading on the wetted wall was determined as follows: Argon was sent through the dome with no 2-propanol on the wetted wall to ensure that the inlet and outlet MFC gave identical readings before the test was done. 2-propanol was then distributed on the wetted wall at 30°C and 40°C to determine the temperature at which the amount of 2-propanol evaporated from the wetted wall to have a significant effect on the MFC measurement. Only argon was sent through the dome and the inlet and outlet MFC readings compared. The average of at least 60 readings at steady state for each gas flow rate at the longest column height (maximum evaporation area) is tabulated in **Table 4.3**:

Table 4.3: Effect of Evaporated 2-propanol on MFC Readings

30°		40°	
MFC _{inlet}	MFC _{outlet}	MFC _{inlet}	MFC _{outlet}
2.35	2.37	2.35	2.41
2	2	2.03	2.09
1.86	1.87	1.84	1.89
1.54	1.54	1.48	1.53

It can be seen from the data in **Table 4.3** that the amount of 2-propanol evaporated at 30 °C does not have a significant effect on the MFC reading. At 40°C the effect does become significant, but since the wetted wall experimental runs were performed at 30°C, the inaccuracy in the data caused by the evaporating 2-propanol is deemed insignificant within the error of the device ($\pm 0.55\%$ of the free stream flow rate). The test was repeated by

passing Argon through a 5L Erlenmeyer flask filled with 1L 2-propanol heated to the respected temperatures. This increased the evaporation surface area. The same results were obtained, even whilst shaking the flask periodically to entice more rapid evaporation of 2-propanol.

The gas mixture may therefore be assumed to consist of predominantly CO₂ and argon and the gas mixture calibration were done as follows: The inlet MFC were set to different CO₂ flow rates and the argon flow adjusted each time to achieve a reading of approximately 2 on the outlet MFC. This was done to be in the same range of the experimental runs as well as achieving the same total gas pressure as the experimental runs. The total gas flow rate was measured each time by allowing 10 L of gas to pass through the totalizer and noting the time. The runs were performed in triplicate, with pure CO₂ and argon runs also performed to test the validity of the correction factors in **Table 4.2**.

Since no absorption of CO₂ was allowed, a mass balance taking the gas mixture density at the average operating temperature of 27°C into account allows for calculating the mass flow rate of argon for each calibration run. The mass flow balance may be summarised as follows:

$$m_{\text{tot}} = m_{\text{CO}_2} + m_{\text{argon}} \quad (4.4)$$

where m_{CO_2} is calculated from the correction factor in **Table 4.2** and verified with the gas totaliser. The gas mixture density may be expressed in terms of the pure species densities:

$$\rho_{\text{mix}} = y_{\text{CO}_2} \cdot \rho_{\text{CO}_2} + (1 - y_{\text{CO}_2}) \cdot \rho_{\text{argon}} \quad (4.5)$$

and by assuming a negligible ΔV_{mix} for the gas the total mass flow rate may be expressed as:

$$m_{\text{tot}} = \rho_{\text{mix}} \cdot V \quad (4.6)$$

where V is the volumetric flow rate measured by the gas totaliser. Substituting equation 4.5 in equation 4.6 gives:

$$m_{\text{tot}} = V \cdot y_{\text{CO}_2} \cdot \rho_{\text{CO}_2} + V \cdot (1 - y_{\text{CO}_2}) \cdot \rho_{\text{argon}} \quad (4.7)$$

by substituting the mass fraction of CO₂:

$$y_{\text{CO}_2} = \frac{m_{\text{CO}_2}}{m_{\text{tot}}} \quad (4.8)$$

into equation 4.7 and simplifying, the following quadratic equation results:

$$m_{\text{tot}}^2 - V \cdot \rho_{\text{argon}} \cdot m_{\text{tot}} + \left[V \cdot m_{\text{CO}_2} \cdot (\rho_{\text{argon}} - \rho_{\text{CO}_2}) \right] = 0 \quad (4.9)$$

The negative root of equation 4.9 is rejected and the total mass flow rate calculated. The mass flow rate of argon is then calculated from equation 4.4. The mass flow rate of argon may now be expressed as a function of the difference in MFC readings:

$$\dot{m}_{\text{Ar}} = \alpha (\text{MFC}_{\text{outlet}} - \text{MFC}_{\text{CO}_2}) \quad (4.10)$$

Equation 4.10 is used to determine the mass flow rate of argon through the system at the start of the absorption experimental run and since argon is inert and found to have very low solubility in alcoholic solutions (Reid and Sherwood, 1966), it is assumed that its inlet and outlet mass flow rates are equal:

The total gas flow rate at any time may also be expressed as a function of the difference in MFC readings:

$$\dot{m}_{\text{tot}} = \beta (\text{MFC}_{\text{outlet}} - \text{MFC}_{\text{CO}_2}) + \gamma \quad (4.11)$$

Since the CO₂ mass flow controller delivers a constant flow, the mass of CO₂ absorbed may be calculated from the reading on the outlet MFC. Once the total outlet flow is known from equation 4.11, the outlet CO₂ flow rate is calculated with equation 4.4 and the mass of CO₂ absorbed calculated as follows:

$$m_{\text{CO}_2, \text{absorbed}} = \left(\frac{\dot{m}_{\text{CO}_2, \text{in}} - \dot{m}_{\text{CO}_2, \text{out}}}{3600} \right) \cdot t_c \quad (4.12)$$

Refer to Appendix B for the calibration curves. The calibration equations for the flow rate range investigated are as follows:

$$\dot{m}_{Ar} = 3.398(MFC_{outlet} - MFC_{CO_2}), \quad R^2 = 0.9921$$

$$\dot{m}_{tot} = 1.199(MFC_{outlet} - MFC_{CO_2}) + 4.415, \quad R^2 = 0.9347$$

Refer to Appendix B for the calibration data of the mass flow controllers. Refer to Appendix D for the sample calculations for determining the specific and absolute CO₂ absorption rates. Refer to Appendix E for the equipment specifications of the MFC.

4.3.2 MEA Analysis

The analysis of the unreacted MEA is based on the acid/base characteristics it possesses. As described in section 2.2.1, MEA may be classified as a text book Brønsted-Lawry base. The titration reaction with a weak hydrochloric acid (HCl) solution is as follows:



With the titration calculation based on the stoichiometric mole balance:

$$v_{MEA} \cdot C_{MEA} \cdot V_{MEA} = v_{HCl} \cdot C_{HCl} \cdot V_{HCl} \quad (4.14)$$

But since both stoichiometric coefficients are unity:

$$C_{MEA} = \frac{C_{HCl} \cdot V_{HCl}}{V_{MEA}} \quad \left(\frac{\text{mol}}{\text{L}} \right) \quad (4.15)$$

The indicator of choice is for the titration is congo red since it falls in the correct pH range (3.5 – 8) and shows great contrasting colours. Congo red is bright red in basic solutions and deep blue in acidic solutions with an end point indicated by a deep purple colouring. To ensure the best degree of titration accuracy and repeatability, the known initial concentration is titrated to reveal the reference colour for the endpoint reached. Each titration is then compared with the reference colouring to establish whether the end point has been reached.

It is important to note that the acid concentration used, depended on the estimated concentration range of MEA for the particular analysis and was calculated to be of similar order of magnitude, to allow for the least aggressive titration conditions

4.3.3 CO₂ Error and Sensitivity of Analysis

The error in CO₂ analysis is predominantly caused by the sensitivity of the MFC. To decrease the effect, the MFC was calibrated for both pure species and for gas mixtures. All data point consists of the average of at least 30 MFC reading, logged at steady state every 2 seconds during an experimental run. The average reading is then used unrounded in the calculations and along with the error in calibration; a resulting error of 5 – 7% is noted on the calculated specific absorption rates.

4.3.4 MEA Error and Sensitivity of Analysis

The error in determining the analysed MEA concentration for the absorption study lies mainly in the repeatability of the titration end point. It is however important to keep the number of significant figures in mind when expressing the titrated concentration. The most accurate volume measured from a burette is to the first decimal place, for example, 10.2mL and since all volumes used in the titration lies between 10 and 100mL, the number of significant figures for the calculated concentration is 3.

The error range for the experimentally determined MEA concentrations is thus the percentage variance of each repeated measurement from the average expressed to 3 significant figures.

CHAPTER 5: RESULTS AND DISCUSSION: REACTION KINETICS

The results obtained from the reaction kinetic experiments will be presented in this chapter. These results will be discussed in accordance with the accuracy of their determination as well as the physical and chemical significance based on the existing theory of reaction kinetics and the proposed mechanism for the reaction.

The results will then be subjected to the modelling of a reaction rate equation or series of equations. The main objectives of modelling the data is to critically assess and challenge the significance of existing rate models in describing the homogeneous non-aqueous reaction kinetics of CO₂ with MEA in 2-propanol solution.

5.1 Concentration – Residence Time Profiles

The main advantage of using a CSTR in this study is to have the ability to determine the concentration of either CO₂ or MEA at different specific residence times. As explained in section 3.3.1, by altering the reagent flow rates to the reactor, the residence time of each species is altered accordingly. If the reaction is stopped as the product stream exits the reactor and the product stream analysed, it becomes possible to plot a concentration profile for each species in terms of the average time spent within the reactor. In order to achieve and maintain a chronological order in the method of the data analysis, the data gathered from the experiment performed at 30°C and initial CO₂ and MEA concentrations of $[\text{MEA}]_i = 2.5[\text{CO}_2]_i$ will be presented as the reference example and is representative for all the other experiments. The reason for this is that the same procedures were followed throughout and therefore the same interpretation applies.

5.1.1 CO₂ Concentration Profiles

The CO₂ concentration profiles constructed rests heavily on the accuracy of the solubility data for CO₂ in 2-propanol as well as the repeatability of the product

stream composition. Since both reactor volumes are small enough to make this assumption at maximum stirring rate, an investigation was made by performing repeated runs through both reactors at a flow rate of 50 L/hr, maximum stirring, 30°C and initial concentrations of $[MEA]_i = 2.5[CO_2]_i$. The results obtained are tabulated in **Tables 5.1** and **5.2**:

Table 5.1: Short Residence Time Reactor Product Stream Repeatability

Volume of sample (L)	Mass Precipitate (g)	Deviation from Average (%)	Mass CaCO ₃ (g)	Deviation from Average (%)
0.059	2.61	-0.77	0.216	-0.935
0.061	2.63	-1.38	0.221	-3.271
0.060	2.58	0.39	0.209	2.336
0.060	2.55	1.69	0.211	1.402
0.061	2.6	-0.39	0.213	0.467

Table 5.2: Long Residence Time Reactor Product Stream Repeatability

Volume of sample (L)	Mass Precipitate (g)	Deviation from Average (%)	Mass CaCO ₃ (g)	Deviation from Average (%)
0.060	2.18	-0.46	0.138	-1.770
0.061	2.13	2.11	0.142	-4.720
0.061	2.21	-1.84	0.136	-0.295
0.059	2.19	-0.64	0.131	3.392
0.060	2.18	-0.46	0.131	3.392

The ‘deviation from average’ columns in **Tables 5.1** and **5.2** indicate the deviation of each mass measurement from the average mass for the 5 repetitions. From **Tables 5.1** and **5.2** it can be seen that the product stream repeatability is within 3.3 % for the short residence time reactor and within 3.4 % for the long residence time reactor. This information however only indicates that the same degree of mixing is achieved each time in the separate reactors. The validation of complete mixing is best achieved by an RTD study, but since it was not done, complete mixing is validated by examining the CO₂ and MEA concentration profiles.

The concentration profile of CO₂ at 30°C and initial concentrations of $[MEA]_i = 2.5[CO_2]_i$ is illustrated in **Figure 5.1**

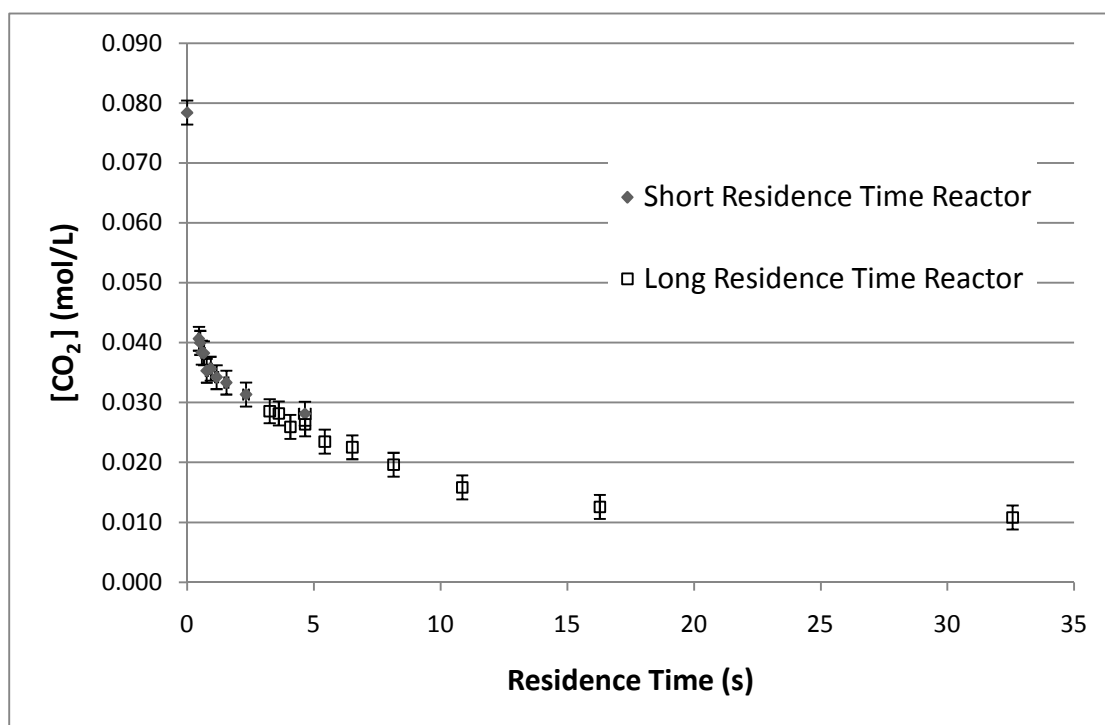


Figure 5.1 CO₂ Concentration Profile, 30°C, [MEA]_i = 2.5[CO₂]_i

Figure 5.1 illustrates the sharp initial decline in CO₂ concentration, which becomes more gradual with an increase in residence time. It also indicates the 0.002 mol/L confidence interval in the CO₂ concentration. A more advanced method of CO₂ analysis should greatly reduce this error. The data points collected for each of the reactors are presented separately to indicate that complete mixing is achieved within the reactors, since it is highly unlikely that such a good overlap in the data is possible if both reactors are not completely mixed.

5.1.2 MEA Concentration Profile

The concentration profile of MEA at 30°C and initial concentrations of [MEA]_i = 2.5[CO₂]_i is illustrated in **Figure 5.2**:

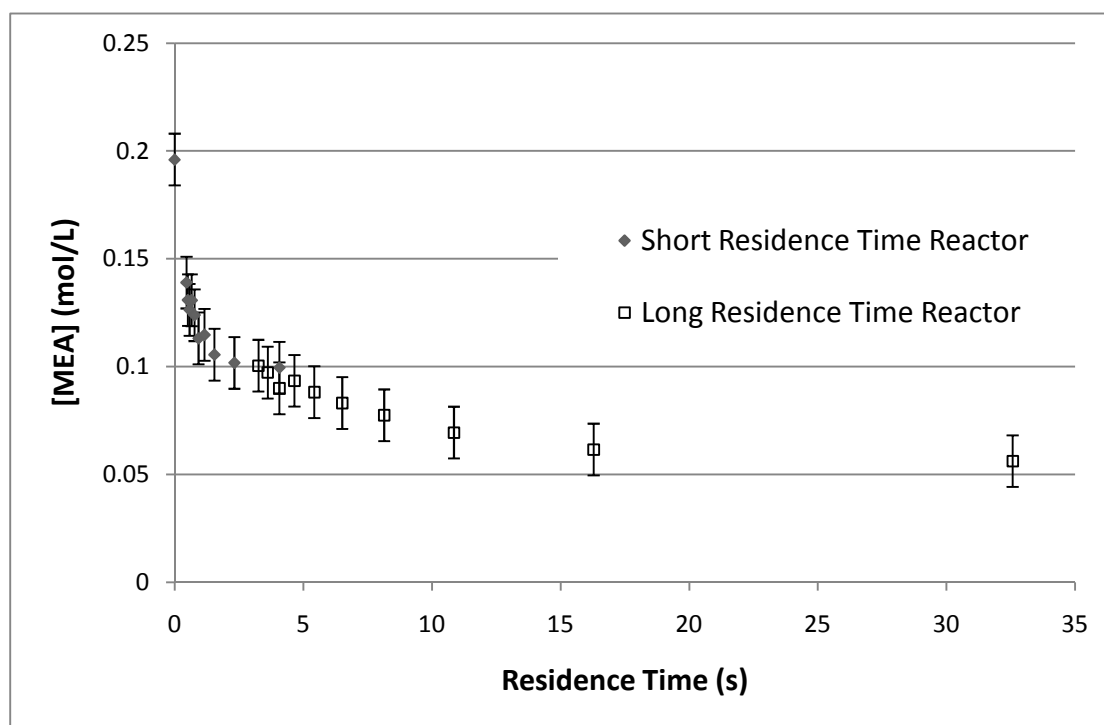


Figure 5.2: MEA Concentration Profile, 30°C, $[MEA]_i = 2.5[CO_2]_i$

A similar trend to that of the CO_2 concentration profile is illustrated in **Figure 5.2**. The error bars represent the confidence interval of 0.012 mol/L. This is a result of the error of 5.8% in the HPLC method of analysis. The overlap in the data from the different reactors is once again an indication of the complete mixing achieved within the reactors.

5.2 Conversion and Reaction Rate Profiles

This section is aimed at evaluating the concentration – residence time profiles determined in section 5.1 regarding the conversion profiles as well as the reaction rate profiles of both CO_2 and MEA. Once again, the data gathered from the experiments performed at 30 °C and initial concentrations of $[MEA]_i = 2.5[CO_2]_i$ will be presented as the reference example.

5.2.1 Conversion Profiles

The conversion of a reactant species is calculated with equation 3.17:

$$X_A = \frac{C_{A,in} - C_{A,out}}{C_{A,in}} \quad (3.17)$$

The conversion may be expressed as a fraction or a percentage of the initial concentration. In this thesis it will be presented as a percentage.

The conversion – residence time profiles for the measured CO₂ and MEA data at 30°C and initial concentrations of [MEA]_i = 2.5[CO₂]_i is illustrated in **Figure 5.3**:

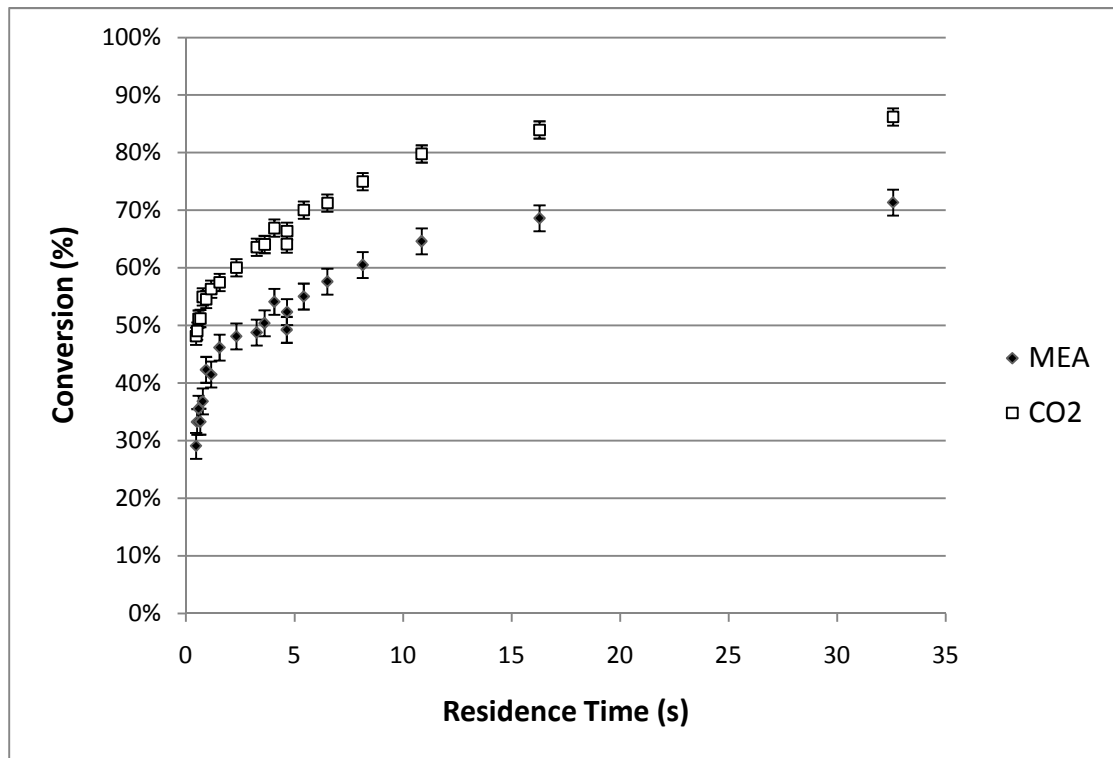
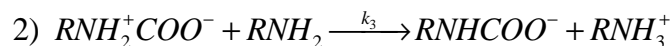
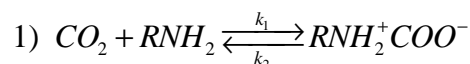


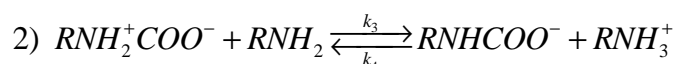
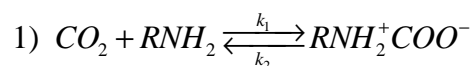
Figure 5.3: Conversion Profiles, 30°C, [MEA]_i = 2.5[CO₂]_i

Figure 5.3 illustrates the effect of the error in both MEA and CO₂ analysis on the species conversion. The conversion confidence interval for CO₂ is approximate 3% and approximately 4.5% for MEA at the specified conditions. Similar errors were noted throughout the temperature and concentration range. Before discussing the conversion or reaction rate profiles, it is necessary to re-introduce the proposed reaction rate mechanisms:

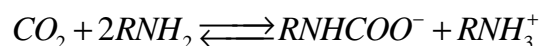
Mechanism A



Mechanism B



Overall Reaction



Conversion is a function of the relative initial concentrations of the reactants, with a higher conversion noted for the limiting reagent, CO₂, in **Figure 5.3**. The stoichiometry of the reaction is best illustrated when evaluating the relative reaction rate profiles of CO₂ and MEA. The effect of the experimental error will also be discussed then.

At 25°C and equal initial concentrations (Refer to **Table C1** in Appendix C) the MEA conversion strived towards 100%, but this could be as a result of experimental error. At all other temperatures and concentrations investigated in this study, neither CO₂ nor MEA achieved 100% conversion. The significance of this finding is that that for the overall reaction to be reversible, the second reaction in the mechanism must also be reversible. Mechanism B is therefore correct and should be the preferred mechanism to describe this reactive system. The modelling of the rate equation will therefore be based on mechanism B.

5.2.2 Reaction Rate Profiles

After calculating the conversion of the reacting species, it is possible to calculate the reaction rate of these species with equation 3.16:

$$-r_A = \frac{C_{A,in} \cdot X_A}{\tau} \quad (3.16)$$

The reaction rate profiles for the first 5 seconds residence time for the measured CO₂ and MEA data at 30°C and [MEA]_i = 2.5[CO₂]_i is illustrated in **Figure 5.4**:

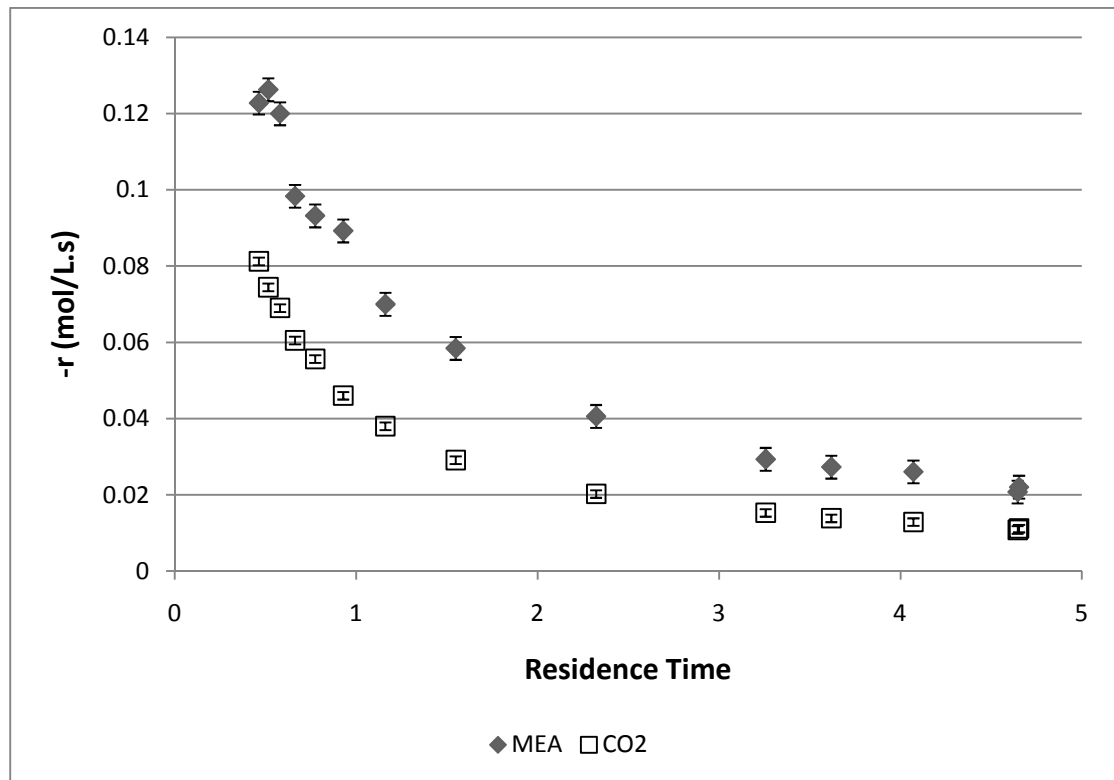


Figure 5.4: Reaction Rate Profiles up to 5 seconds Residence Time

The error bars in **Figure 5.4** shows the effect of the error in analysis on the reaction rate profiles. From **Figures 5.4** a sharp decrease in reaction rate is noticed until it tempers off as the reaction strives towards equilibrium. Extrapolation of the concentration data towards reaction initiation indicates a sharp increase in reaction rate, which may be noticed from the peak in the MEA reaction rate profile. Usually three data points is not considered the definition of a peak, but it is supported by the theory that the reaction rate initially increases rapidly until a maximum and then decreases as the reaction approaches equilibrium (Fogler, 1999). The significance of the peak will be discussed when modeling the rate data in Chapter 6

From **Figure 5.4** it is seen that the rate of MEA reaction is larger than the rate of CO₂ reaction. This is in accordance with the reaction stoichiometry. The magnitude of

this difference is noted when an evaluation of the relative reaction rates at 30 °C and $[\text{MEA}]_i = 2.5[\text{CO}_2]_i$ are done. A plot of the relative reaction rates vs. residence time is illustrated in **Figure 5.5**:

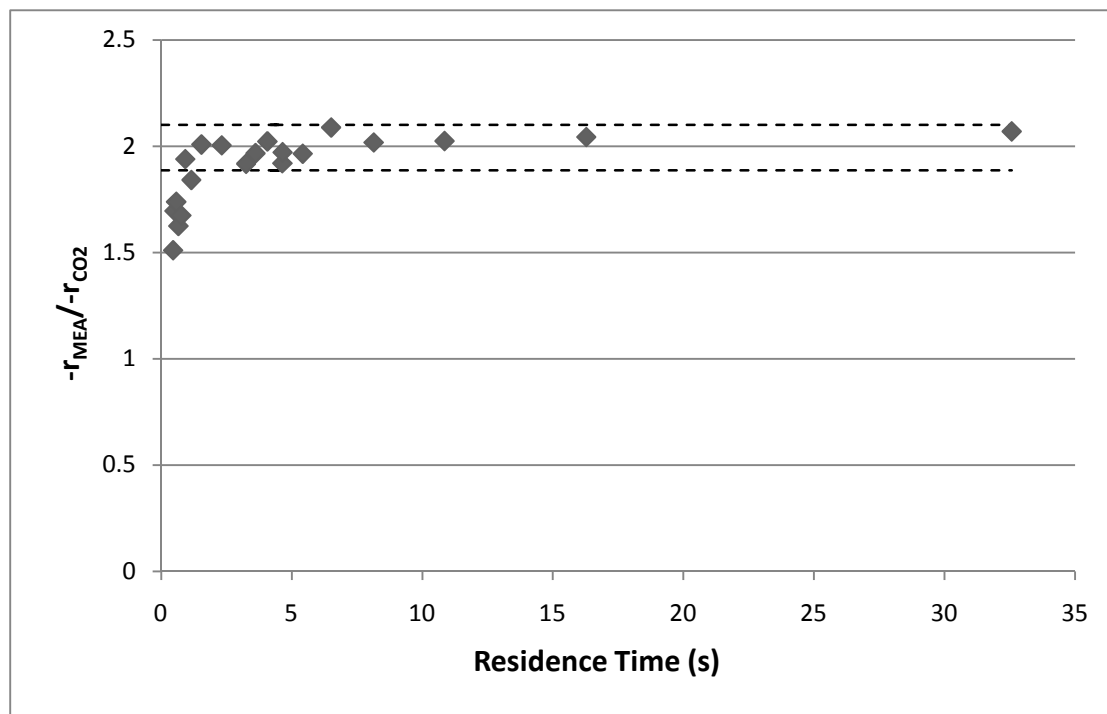


Figure 5.5: Relative Reaction Rate Profile, 30 °C, $[\text{MEA}]_i = 2.5[\text{CO}_2]_i$

From **Figure 5.5** it is noticeable that the relative reaction rates increases from approximately 1 and seemingly converges to a value of 2. This is in accordance with the reaction mechanism and the overall reaction stoichiometry at equilibrium. The dashed line indicates the 95% level of confidence interval, supported by the error of less than 4% on the reaction rate profiles over the entire temperature and concentration range due to the error in analysis. From **Figure 5.5** it may be noticed that all of the data points lie within the 95% confidence interval.

5.3 Temperature and Relative Initial Concentration Effect

The effect of temperature and concentration on the reaction of CO_2 and MEA will be discussed in tandem since the initial concentration of CO_2 is a function of temperature. The effect of the different initial relative concentrations at the same temperature will also be discussed.

The data selected for the temperature/concentration effect discussion is at $[\text{MEA}]_i = 2.5[\text{CO}_2]_i$ concentrations. This was arbitrarily chosen as the reference example since the same effects and trends are noticed throughout, but the effect is most clearly noticeable at these conditions. In order to maintain consistency with the previous profiles presented, the data selected for the effects of the different initial relative concentrations are at 30°C.

5.3.1 Temperature/Concentration Effect

The effect of temperature and thus concentration on the reagent concentration profiles is best illustrated graphically in **Figure 5.6**:

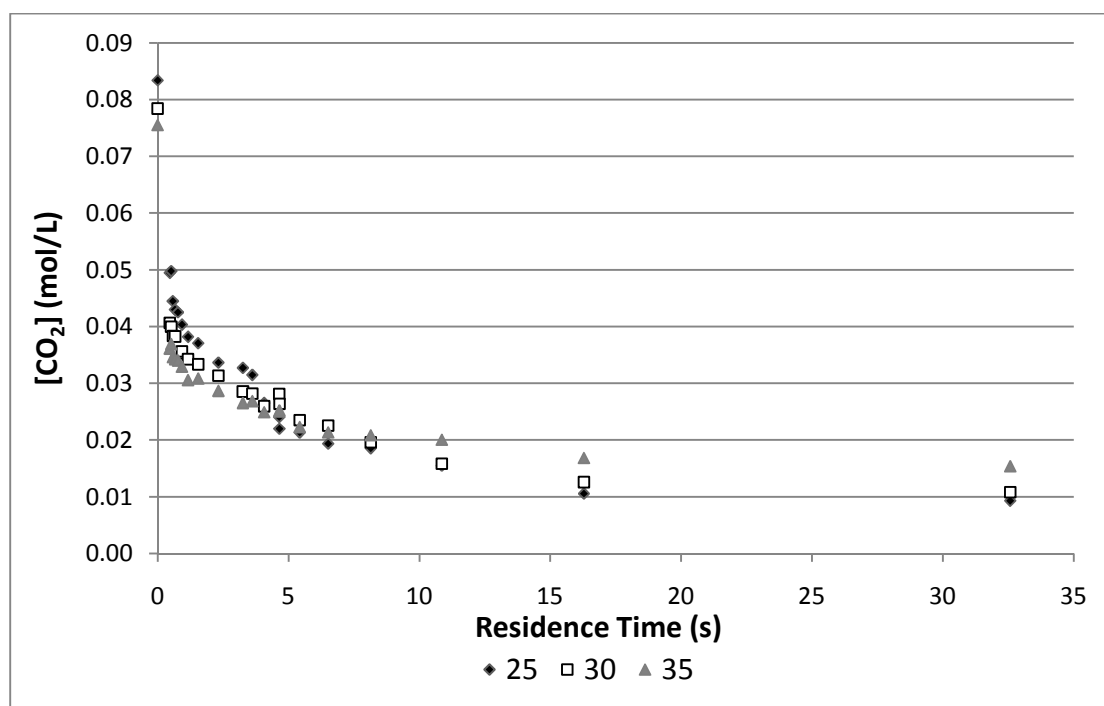


Figure 5.6: CO₂ Concentration Profiles at the Different Operating Temperatures

Since the same effect was noticed for the MEA concentration profiles, it is not presented. Efforts to improve the data visibility in **Figure 5.6** were made but no visual improvement could be found. These efforts include a log scale on the y-axis as well as plotting relative change in concentration with a change in temperature. This is the best representation. The effect of temperature may now be discussed:

An increase in temperature causes a decrease in the solubility of CO₂ in 2-propanol at 1 atm resulting in lower initial concentrations. It is however noticeable from

Figure 5.6 that the concentration gradient at the start of the reaction increases as the temperature increases indicating an increase in the rate of reaction. This lies beyond the error in analysis for CO₂ and may thus be a trustworthy conclusion (the error bars are not included to avoid cluttering). The error in MEA analysis is too large to make the same conclusion, but since it is true for CO₂, it is assumed to be true for MEA as well. It is difficult to accurately determine if reaction equilibrium will be achieved faster at higher temperatures, since a relatively narrow temperature range was used in this study. This should form part of future investigation.

The effect of temperature on the conversion profiles is illustrated in Figure 5.7:

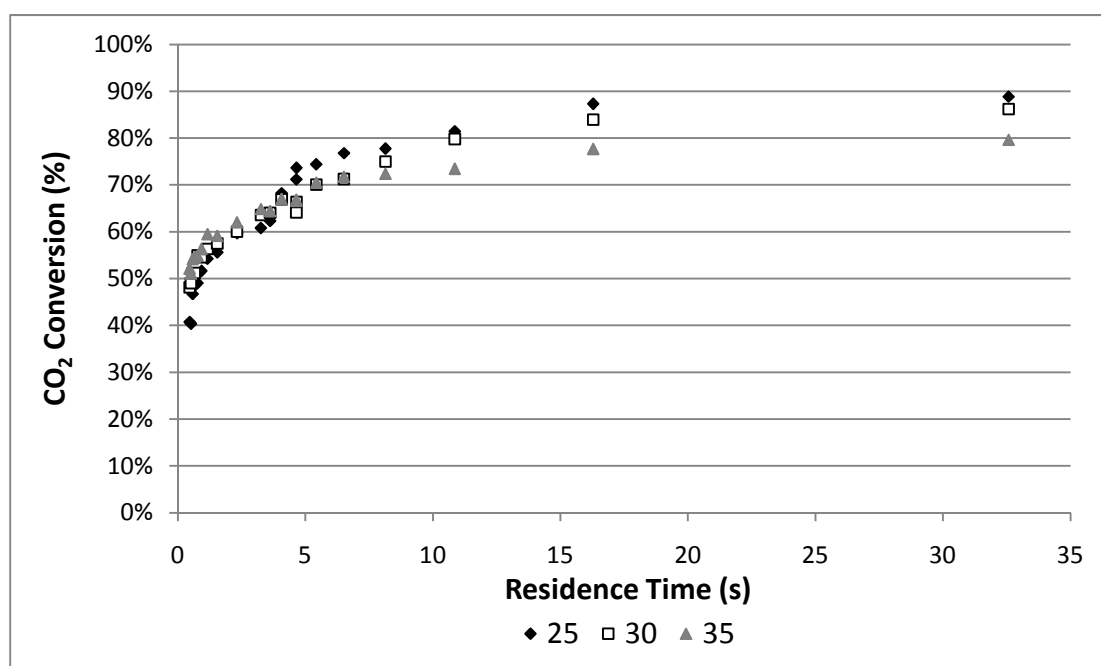


Figure 5.7: CO₂ Conversion Profiles at the Different Operating Temperatures

The same trends were once again noticed for MEA. The effect of temperature becomes more apparent after evaluating the conversion profiles of MEA and CO₂. Both MEA and CO₂ conversion initially increases with an increase in temperature and then decreases as the reaction strives towards equilibrium. Based on Le Chatelier’s principle this is consistent with an exothermic forward reaction. It is known that the absorption of CO₂ with MEA is in fact exothermic (Aresta, 2003), but the distinction between heat of mixing and heat of reaction could not be made. Since the conversion profiles overlap in the error range for both CO₂ and MEA, it cannot be concluded with a high level of certainty that the data indicates an exothermic reaction. Since the method used in this study eliminated the heat of mixing it may

be useful in determining the heat of reaction, but a wider temperature range will need to be considered. It also becomes apparent that equilibrium is achieved slightly faster at higher temperatures, but once again cannot be concluded with absolute certainty due to the experimental error.

The reaction rates of MEA and CO₂ for [MEA]_i = 2.5[CO₂]_i concentrations at the different operating temperatures are illustrated in **Figure 5.8**:

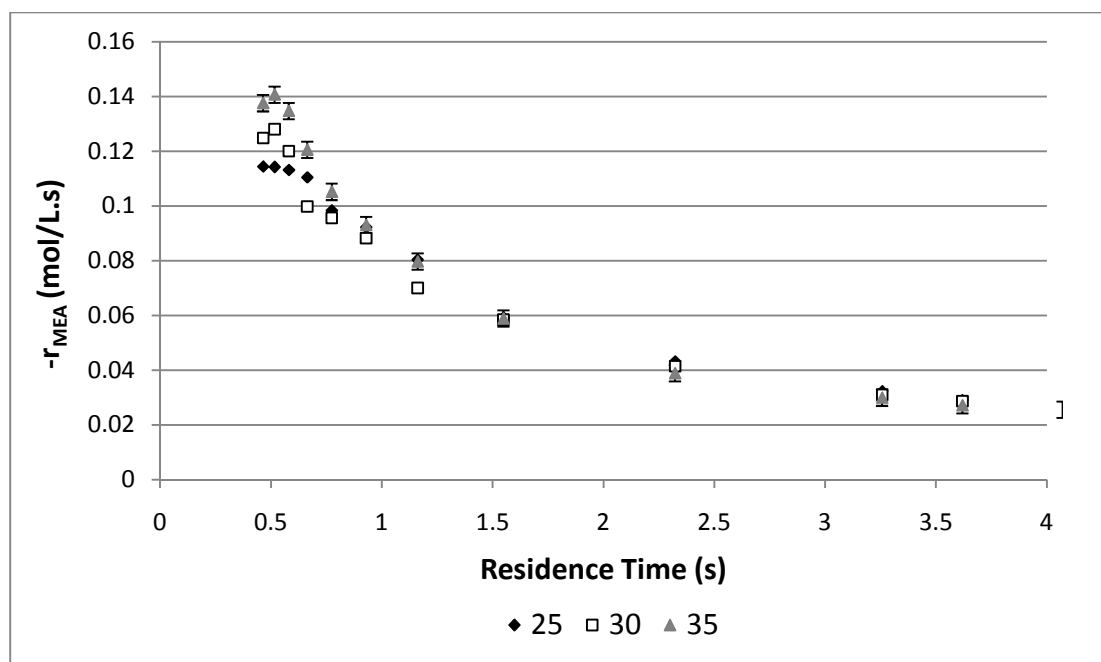


Figure 5.8: MEA Reaction Rate Profiles (First 4 seconds)

Figure 5.8 illustrates the existence of a relationship between concentration and temperature: From 1.5 seconds residence time onward the reaction rates are more or less equal over the temperature range. This is an indication of the cancellation effect that temperature and concentration have on the reaction rate. An increase in temperature causes an increase in reaction rate. This increase is, however, countered by a decrease in reaction rate due to the decrease in initial reagent concentration as the temperature increases, leaving equal reaction rate profiles over the temperature range.

An interesting effect is noticed regarding the peaks of the reaction rate profiles. **Figure 5.8** indicates a higher peak in the reaction rate profile at higher temperatures. This may be attributed to the increase in reaction rate with an increase in temperature. It indicates that the temperature effect trumps the concentration

effect during the initial stages of the reaction when only CO₂ and MEA are present. This effect may be concluded to a reasonable amount of certainty since the peaks are significant within the accuracy of the data as indicated by the reaction rate error bars at 35°C in **Figure 5.8**. The same trend is noticeable in the reaction rate profile of CO₂.

5.3.2 Relative Initial Concentration Effect

The use of the relative initial concentrations at each temperature is to facilitate a study of the reaction kinetics of CO₂ with MEA over a wide concentration range. The effect of this concentration range on the conversion, reaction rates and relative reaction rates will be discussed.

The temperature of reference is 30°C to remain in step with the profiles presented thus far in the thesis. The MEA concentration is varied relative to the concentration of CO₂ at 30°C. The CO₂ and MEA conversion profiles at the different initial concentrations are illustrated in **Figure 5.9** and **Figure 5.10**:

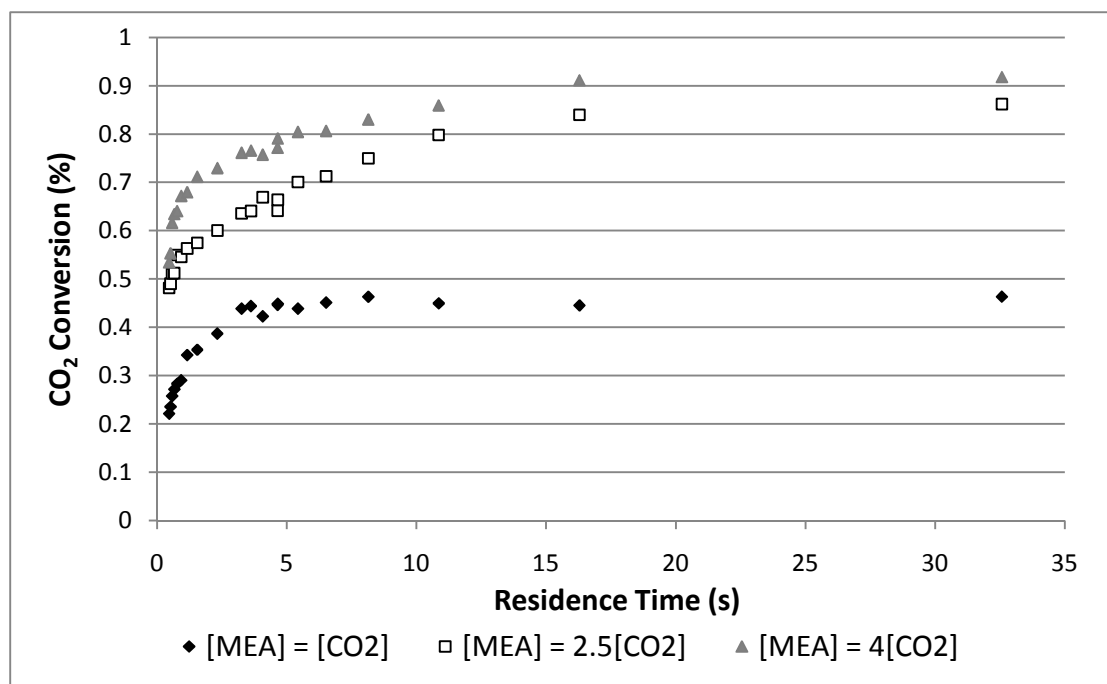


Figure 5.9: CO₂ Conversion Profile for Different Initial Concentrations

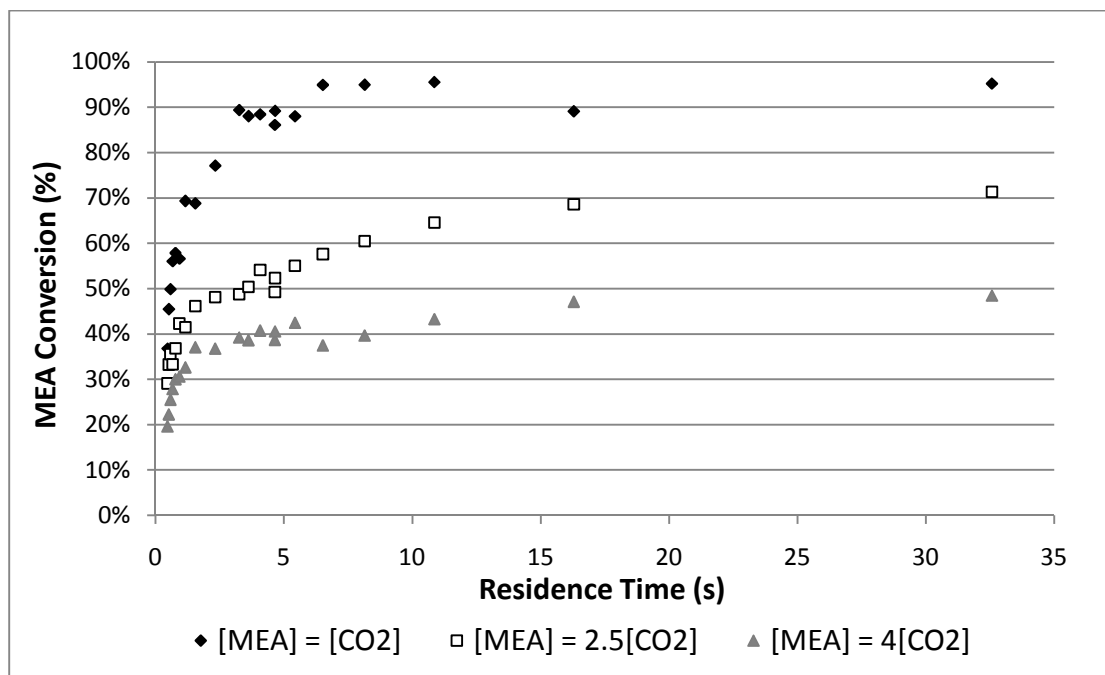


Figure 5.10: MEA Conversion Profile for Different Initial Concentrations

The legends in **Figures 5.9** and **5.10** refer to the initial concentration of MEA. As can be expected, the CO₂ conversion profiles increase with an increase in the concentration of MEA with the opposite being true for the MEA conversion profiles. It is however important to note that a 100% conversion for either species is not achieved at 30°C, indicating the system is in fact governed by an overall equilibrium reaction mechanism.

The change in equilibrium conversion (the average conversion for 8 seconds residence time and above) for both CO₂ and MEA at 30°C is illustrated in **Figure 5.11:**

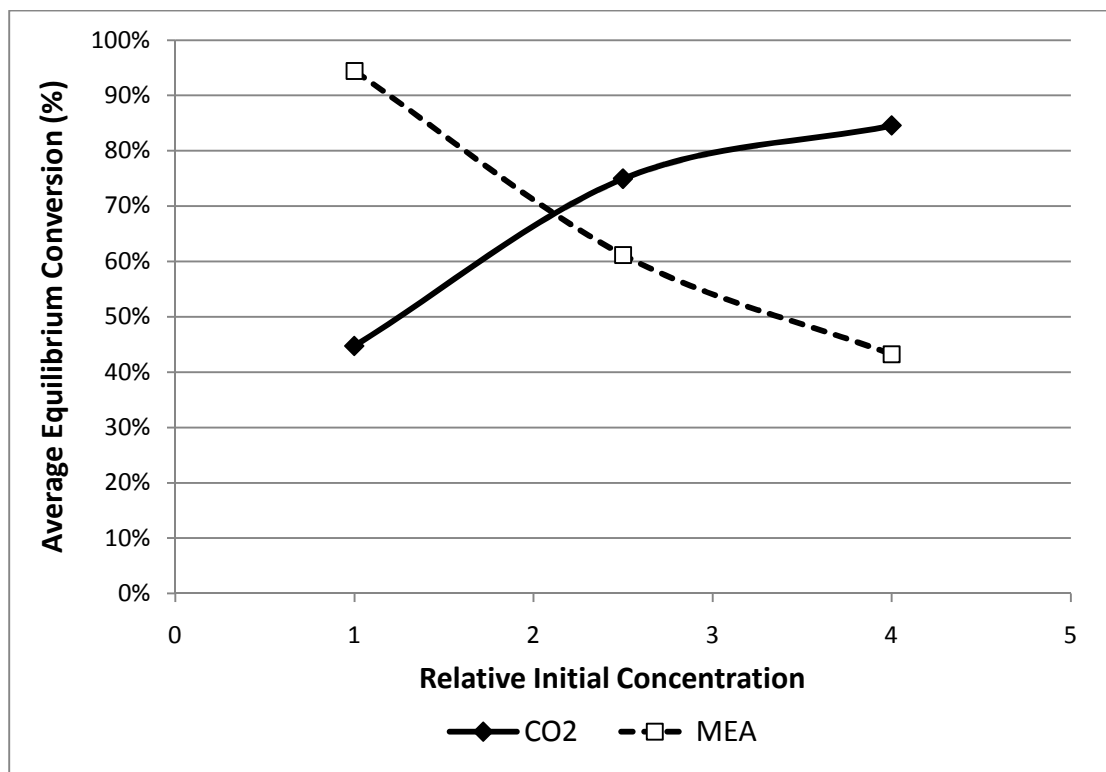


Figure 5.11: Equilibrium Conversions for the Relative Initial Concentration Range

Figure 5.11 illustrates the seemingly non-linear trend in the change of equilibrium conversion for both CO₂ and MEA for a change in relative initial concentration. This is an indication that the system is probably governed by higher order reaction kinetics, since first order systems would show a linear relationship between concentration and conversion. This means that the reaction rate expression should be expressed as a function of a CO₂ and MEA product term. The same trend is noticeable over the entire temperature range.

The concentration effect on the rates of reaction for CO₂ and MEA is illustrated in **Figure 5.12** and **Figure 5.13** respectively:

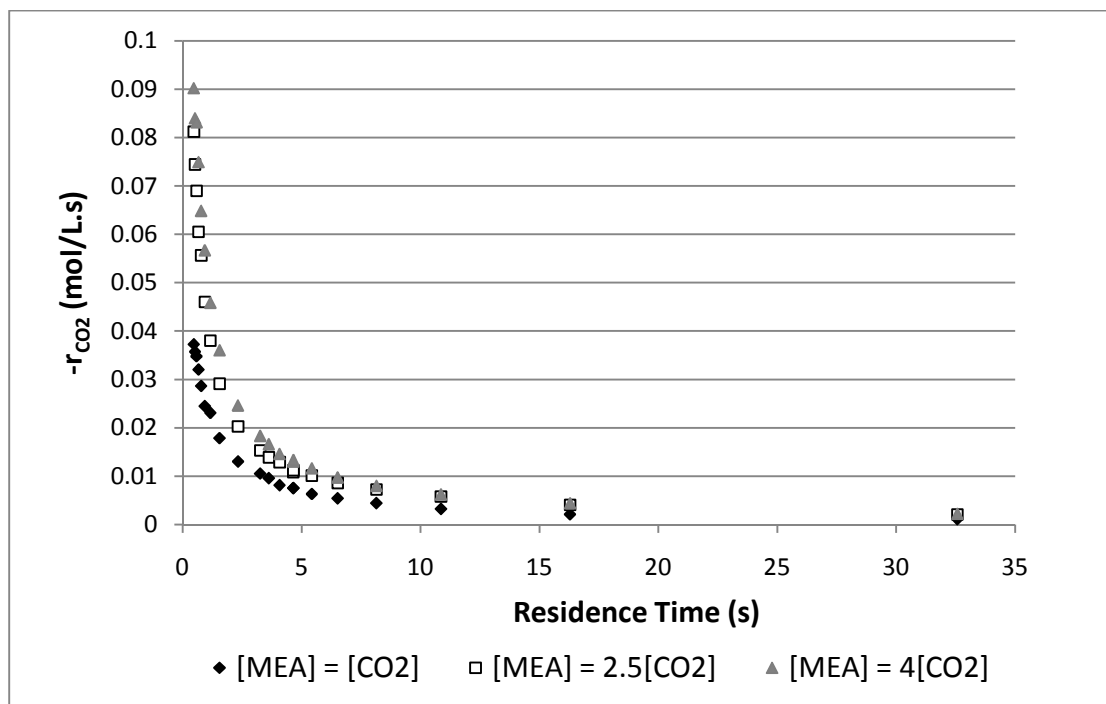


Figure 5.12: CO₂ Reaction Rate Profiles for Different Initial Concentrations

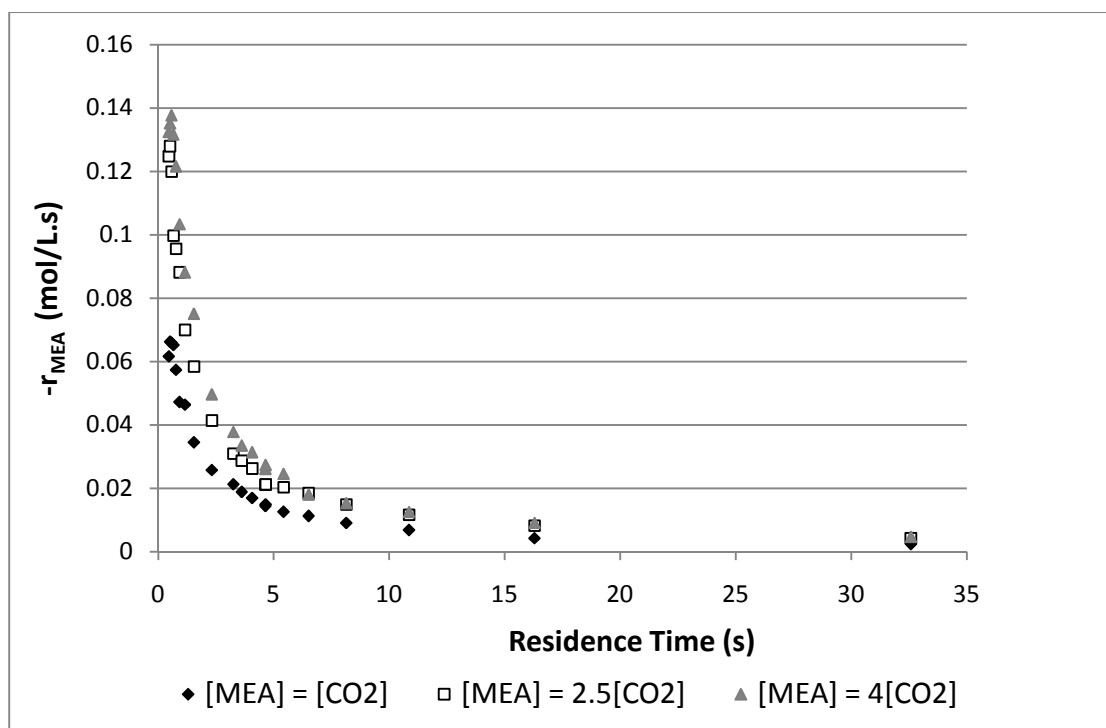


Figure 5.13: MEA Reaction Rate Profiles for Different Initial Concentrations

From **Figures 5.12** and **5.13** it is seen that the reaction rates for both CO₂ and MEA increases as the relative initial concentration of MEA increases. This is expected

since an increase in MEA concentration will result in more molecular interactions per volume and per time causing an increase in the reaction rate. It is meaningful to quantify the average relative increase in reaction rate with the increase in the relative initial MEA concentration. These relative reaction rates were calculated as follows:

$$r_{\text{Relative}} = \frac{\sum_1^N \left(\frac{-r_{i, [\text{MEA}] = a}}{-r_{i, [\text{MEA}] = [\text{CO}_2]_i}} \right)}{N} \quad (5.1)$$

$$a = [\text{CO}_2]; 2.5[\text{CO}_2]; 4[\text{CO}_2]$$

$$i = \text{CO}_2; \text{MEA}$$

$$N = \text{Number of Data Points} = 20$$

The average increase in reaction rate is best illustrated graphically in **Figure 5.14**:

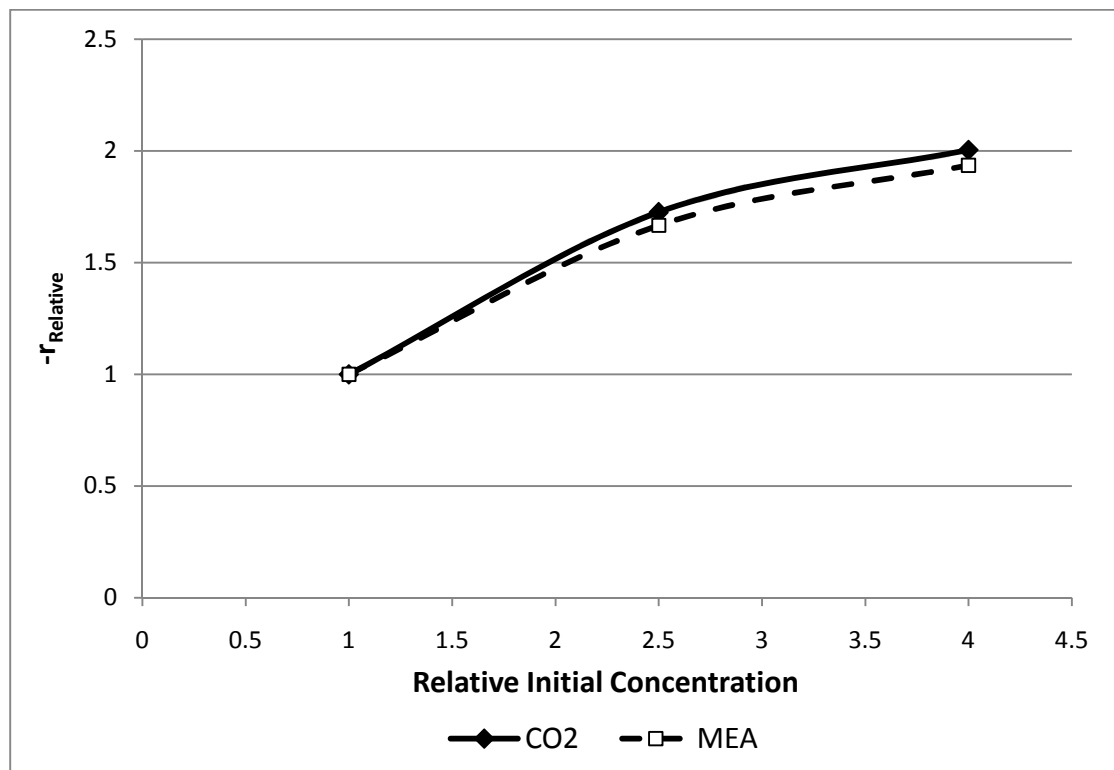


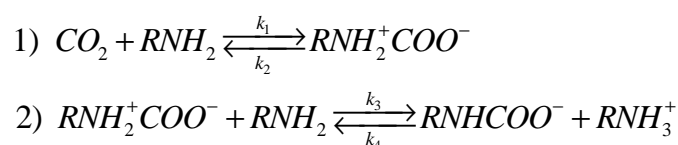
Figure 5.14: Increase in Reaction Rate for the Relative Initial Concentration Range

Figure 5.14 shows a seemingly non-linear increase in the reaction rates of both CO₂ and MEA as the relative initial concentration of MEA increases. It is further noticed

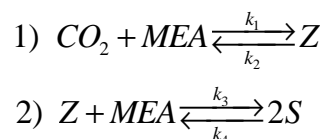
that the rates of CO₂ and MEA increases in approximately equal relative amounts. This should be true for reagents of the same reaction. This indicates that the orders of CO₂ and MEA maintain the same value over the concentration range (*m* and *n* maintain the same value for the concentration range).

5.4 Zwitterion and Salt Concentrations

Determining the concentration profiles of the zwitterion and salt products was one of the toughest challenges of this study. It should be emphasized early that the concentration validation method used is not in total agreement with the equations governing the operation of a CSTR, but the assumptions made are founded on sound physical feasibility. These assumptions will duly be noted. It is firstly necessary to re-introduce the governing reaction mechanism:



To simplify the syntax of the discussion the mechanism is rewritten as:



The difficulty in determining the concentration of Z arises from the fact that it is a reactive intermediate, with no indication of its selectivity to either react with MEA in reaction (2) or to decompose in reaction (1).

In section 3.5.2 mention is made of the assumption derived from the MS analysis (**Figure 3.10**) of a typical experimental run regarding the concentration of the zwitterion. In analyzing the HPLC concentrations determined for the zwitterion and salt precipitation product, it was found that the quantity of phenyl carb (peak 1 in the chromatogram) precipitate relates to a zwitterion concentration in the expected order of magnitude. It is therefore assumed that the species in the precipitate with a molecular weight of 314 g/mol (registering as 315 g/mol in the MS analysis) consist

of only scavenged zwitterion. This assumption is based on the fact that the salt product which has a molecular weight of 315 g/mol would register as 316 g/mol in **Figure 3.10** and since a very low relative concentration (less than 5%) of such a species is detected, the assumption is deemed reasonable. The low concentration resulting from the measured phenyl carb precipitate is most probably because complete precipitation of the zwitterion and salt was not achieved. The assumption thus stands but should be investigated and validated in future work.

Based on this assumption, the concentration profile of Z may be calculated from the concentration of the phenyl carb precipitate and is illustrated in **Figure 5.15**:

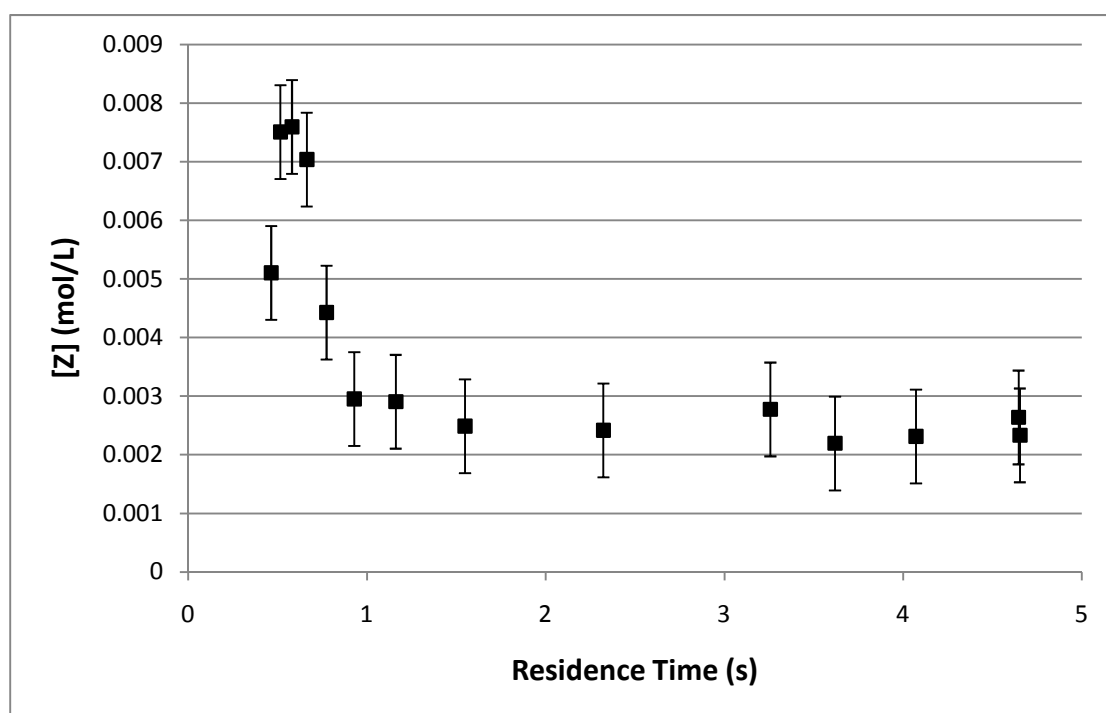


Figure 5.15: Zwitterion Concentration Profile, 30 °C, $[MEA]_i = 2.5[CO_2]_i$

From **Figure 5.15** it is noticed that the zwitterion concentration seems to increase sharply from zero and then decreases as the reaction strives to equilibrium. This is noticed throughout the temperature and concentration range. The first peak may be attributed to the first reaction overpowering the second reaction in the initial stages causing the formation of Z to be faster than its depletion. This is expected since only CO_2 and MEA are present initially, granting a great driving force for the forward reaction of reaction (1). The error range of ± 0.0008 mol/L resulting from the 10.02% error in the analysis of the phenyl carb concentration is illustrated in **Figure 5.15**. This error may even be larger, since the error in determining the calibration factor

for the phenyl carb HPLC analysis could not be determined. This large error does not instill much confidence in making conclusions with regards to the effect of concentration and temperature on the zwitterion concentration profiles and will thus not be discussed. It is, however, the best estimation of the zwitterion concentration profile and will therefore be used in the modeling of the reaction rate expressions. The effect of this error on the rate models will be discussed in Chapter 6.

With an estimation of the zwitterion concentration in place, it is now possible to estimate the salt concentration. This is simply done by means of a carbon or nitrogen balance on the system:

Carbon Balance:

$$n_{C,in} = n_{C,out}$$

$$n_{CO_2,in} = n_{CO_2,out} + n_Z + n_S \quad (5.19)$$

By assuming equal volume for all species:

$$[CO_2]_{in} - [CO_2]_{out} = [Z] + [S] \quad (5.20)$$

thus:

$$[Z] = [CO_2]_{in} - [CO_2]_{out} - [S] \quad (5.21)$$

Nitrogen Balance:

$$n_{N,in} = n_{N,out}$$

$$n_{RNH_2,in} = n_{RNH_2,out} + n_Z + 2n_S \quad (5.22)$$

thus for equal volume:

$$[S] = \frac{[\text{RNH}_2]_{\text{in}} - [\text{RNH}_2]_{\text{out}} - [Z]}{2} \quad (5.23)$$

The concentration profile for S is estimated as the average of the results obtained with equation 5.21 and equation 5.23. The difference between the results obtained with either of these equations is within 8% of their average. This may be attributed to the experimental error in determining the concentration of MEA, but since it is within this error of $\pm 10\%$ the estimation of the salt concentration is assumed to hold true.

The salt concentration profile at 30°C and $[\text{MEA}]_i = 2.5[\text{CO}_2]_i$ concentrations is illustrated in **Figure 5.23**:

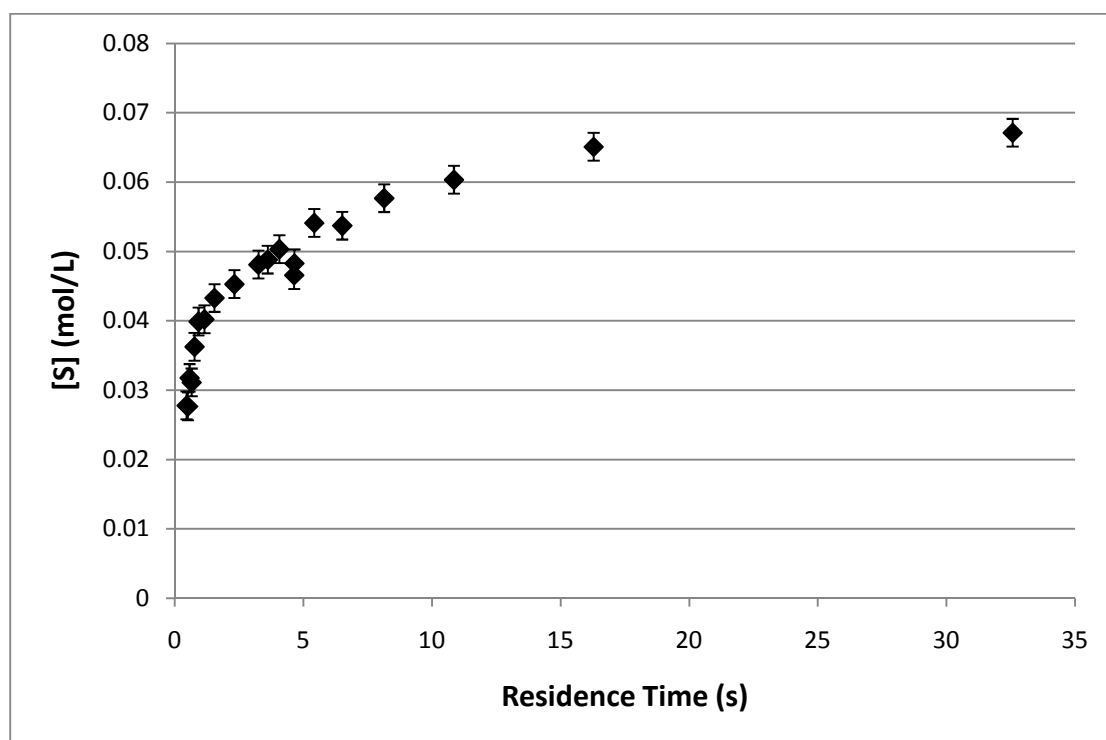


Figure 5.16: Estimated Salt Concentration Profile

From **Figure 5.16** it can be seen that the salt concentration increases from zero and seemingly strives to stability as the reaction approaches equilibrium. This is in accordance with what is expected. It is important to note that the salt concentration is of the same order of magnitude as the concentrations of CO_2 and MEA, with the zwitterion concentration an order of magnitude less. This is in accordance with the nature of a reactive intermediate to have an almost insignificant concentration at

equilibrium. For the purpose of modelling an applicable rate expression, it is assumed that the zwitterion concentration is significant. This assumption will be tested and investigated in Chapter 6.

The effect of temperature on the salt concentration profile is illustrated in **Figure 5.17**:

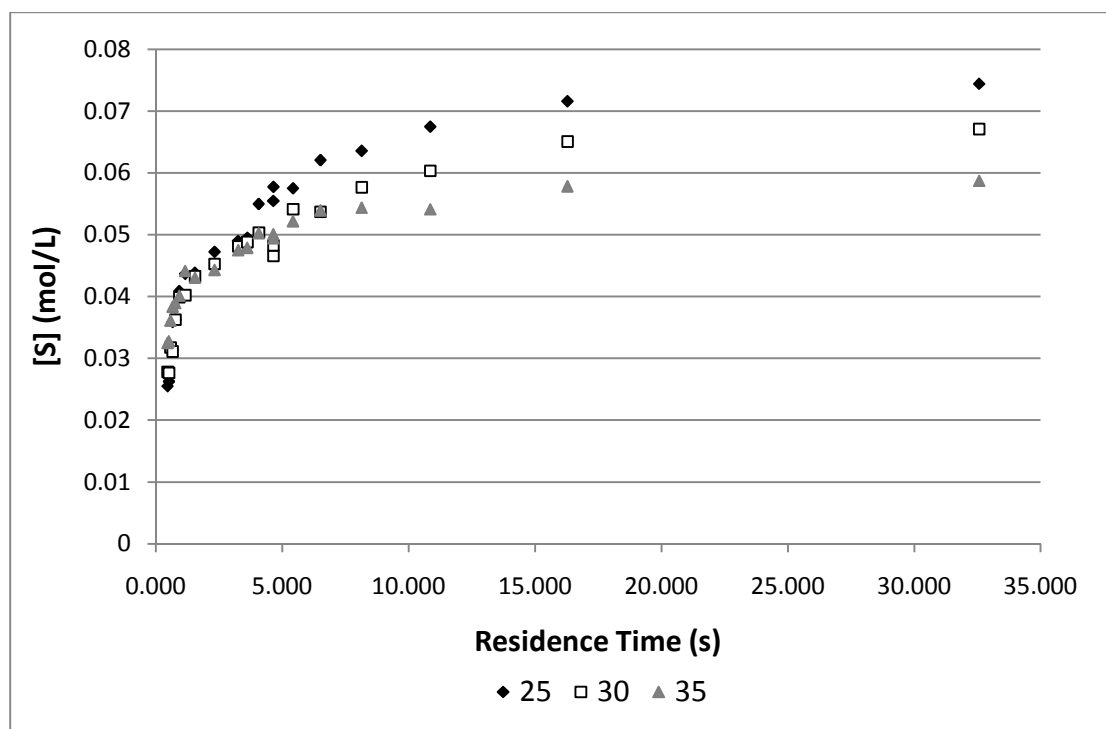


Figure 5.17: Temperature Effect on Salt Concentration Profile

From **Figure 5.17** it can be seen that the concentration of the salt product decreases with an increase in temperature. This is expected since the initial concentration of CO_2 decreases with an increase in temperature. This conclusion can be made with a reasonable degree of certainty with a confidence interval of ± 0.002 mol/L as indicated in **Figure 5.16**.

The effect of different relative initial concentrations is illustrated in **Figure 5.18**:

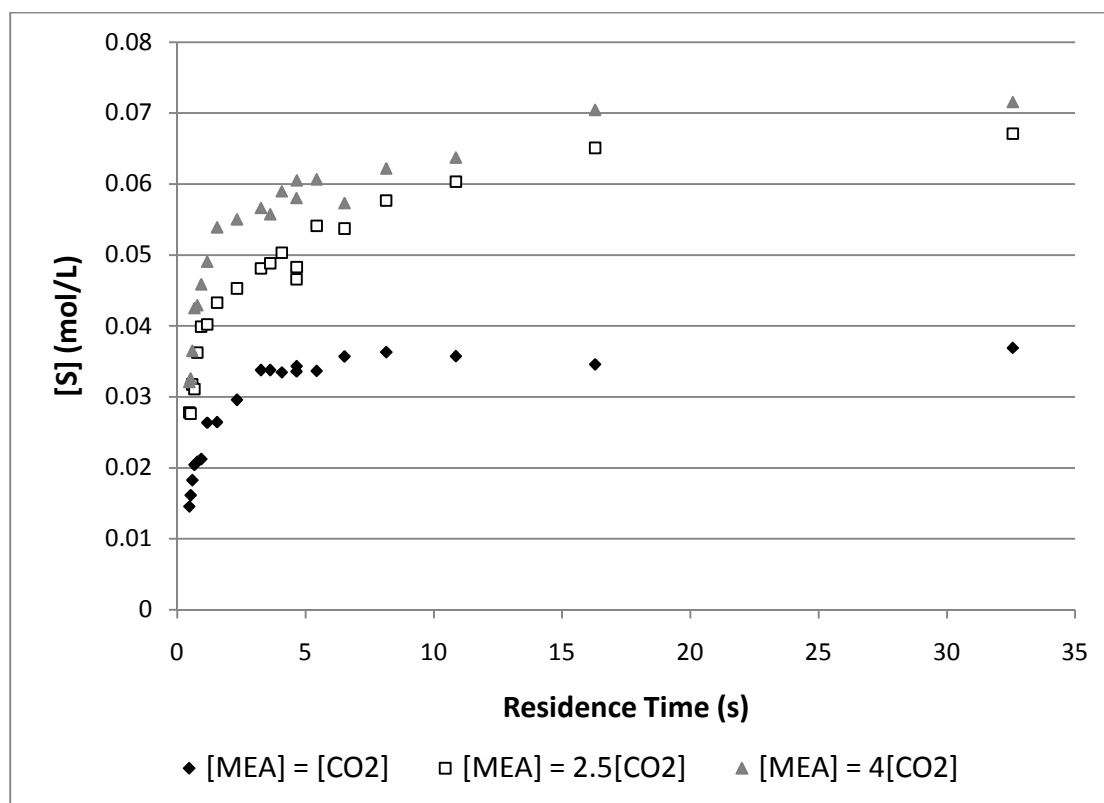


Figure 5.18: Salt Concentration Profiles for Different Initial Concentrations

From **Figure 5.18** it can be seen that the concentration of the salt product increases with an increase in MEA initial concentration. This is expected since more MEA is available to react with CO_2 and the formed zwitterion to form salt. Similar trends were noticed throughout the temperature range. The conclusion can once again be made with a reasonable amount of certainty.

5.5 Chapter Conclusions

The overlapping in the concentration profiles obtained from each CSTR indicates that complete mixing was achieved within both the reactors used in this study. The CO_2 and MEA profiles showed a sharp decline in concentration from reaction initiation which becomes more gradual as the reaction strives toward equilibrium. The error in CO_2 analysis resulted in a confidence interval of 0.002 mol/L for the CO_2 concentration profile and the error in MEA analysis resulted in a confidence interval of 0.012 mol/L for the MEA profile.

Neither CO₂ nor MEA achieved 100% conversion for the temperature and concentration range of this study. An MEA data point at 25°C and equal initial concentration of 98.3% conversion was noticed, but this could be due to experimental error. The rest of the data indicates that both reactions in the mechanism are reversible, which translates to the overall reaction mechanism being reversible as well.

Both reaction rates decrease as residence time increases. The reaction rate of MEA is greater than that of CO₂ over the entire temperature and concentration range. This is in accordance with the overall reaction stoichiometry. A peak is noticed on the MEA rate profile which indicates that the reaction rate increases initially, before it starts to decrease as the reaction strives towards equilibrium. The relative reaction rate profiles converge to a value of 2 as the reaction strives towards equilibrium, which is once again in agreement with the overall reaction stoichiometry.

An increase in temperature increases the initial rate of reaction. This could be concluded with a good degree of certainty based on the CO₂ concentration and reaction rate profiles, since the data trends fall outside of the error range for CO₂ analysis. An increase in temperature seemingly decreases the species conversion as the reaction strives to equilibrium, which is in agreement with the nature of an exothermic reaction, but it could not be concluded to a high degree of certainty due to the experimental error in the data. There is an increase in reaction rate with an increase in relative initial concentration of MEA:CO₂, which is expected.

Conclusions regarding the effect of temperature and concentration on the zwitterion concentration profile could not be made with a high level of certainty since its profiles have a relatively large error of 0.0008 mol/L. It was found that the salt concentration increases with an increase in relative initial concentration and decreased with an increase in temperature.

CHAPTER 6: MODELLING OF A REACTION RATE EXPRESSION

This section will address the main aims of the reaction kinetic study. These aims may be summarized shortly as:

1. Modelling and statistically evaluating the rate expressions proposed in literature. The results obtained will shed light on the validity of assuming these models as representative of this reactive system.
2. Investigating and statistically analyzing rate expressions for possible future implementation in a rate based model as well as determining the effective interfacial mass transfer area for the reactive absorption of CO₂ into a non-aqueous solution of MEA with 2-propanol.

Due to the fact that all of the reaction rate expressions under investigation are non-linear, it was decided to incorporate the non-linear estimation algorithm in MATLAB[®], which applies Levenberg-Marquard optimization of the loss function. The estimated parameters were also subject to certain constraints which were implemented as a penalty function to be added to the loss function if the algorithm estimated the parameters outside of the specified constraints. Simply put, if the algorithm estimated a parameter outside of its specified constraint, a large value is added to the loss function, forcing a significant change in the choice of parameter value for the next iteration.

The derived models will firstly be evaluated by the mean squared error (*mse*) and Pearson R^2 -value conveying the quality of the model fit. The fit will then be illustrated as a parity plot of the observed vs. the model predicted values as well as a fitted plot for visual comparison.

The estimated parameters will then be discussed in accordance with the structure and condition number of their *Jacobian* matrix. This will shed light on the confidence intervals obtained for each parameter. Refer to Appendix F for the description of these statistical parameters of interest during the model evaluation.

6.1 Power Rate Law Expression

The first rate expression to be investigated is the expression assumed by Danckwerts, Charpentier and Erasmus in deriving correlations for the rate of absorption of CO₂ into both aqueous and non-aqueous solutions of MEA. The rate expression proposed is based on the assumption of power rate law reaction kinetics governing the absorption process. The rate expression therefore is:

$$-r_{CO_2} = k [CO_2]^m [MEA]^n \quad (6.1)$$

Danckwerts indicated that a rate law of this form is only applicable to certain reagent concentrations and gas-liquid contact time. (Danckwerts,1970). This will be discussed after evaluating the rate law at different concentrations. Since the reaction rate of CO₂ was determined experimentally as well as concentration – residence time profiles for both CO₂ and MEA, all the information needed to model expression 6.1 is available. A non-linear estimation was employed for the entire temperature and relative concentration range. The investigation of the power rate law rate expression was done for two different sets of constraints on the parameters:

1. $k > 0, m > 0, n > 0$
2. $k > 0, 0.5 < m < 2, 0.5 < n < 2$

Constraint (1) firstly ensures that the reaction direction remains as specified in equation 6.1 by forcing k to be positive. It further serves the fundamental structure of the rate expression by forcing m and n to be positive, which ensures that the rate expression is in accordance with reaction kinetic theory.

Constraint (2) is a refinement of constraint (1). Constraint (2) is implemented to test the findings of Versteeg *et al.*, which stipulates that the order of reaction with regards to CO₂ and MEA is in the region of 1 – 2.

Constraint (2) was executed by forcing the non-linear estimation algorithm to stay within the parameter range specified. For example, if the parameter exceeded the maximum constraint, it is set equal to the maximum for the next iteration. The same concept was implemented on the minimum constraint.

The results of the model fit for constraint (1) at 30°C and equal initial reagent concentration are illustrated in **Figures 6.1** and **6.2** and tabulated in **Table 6.1**:

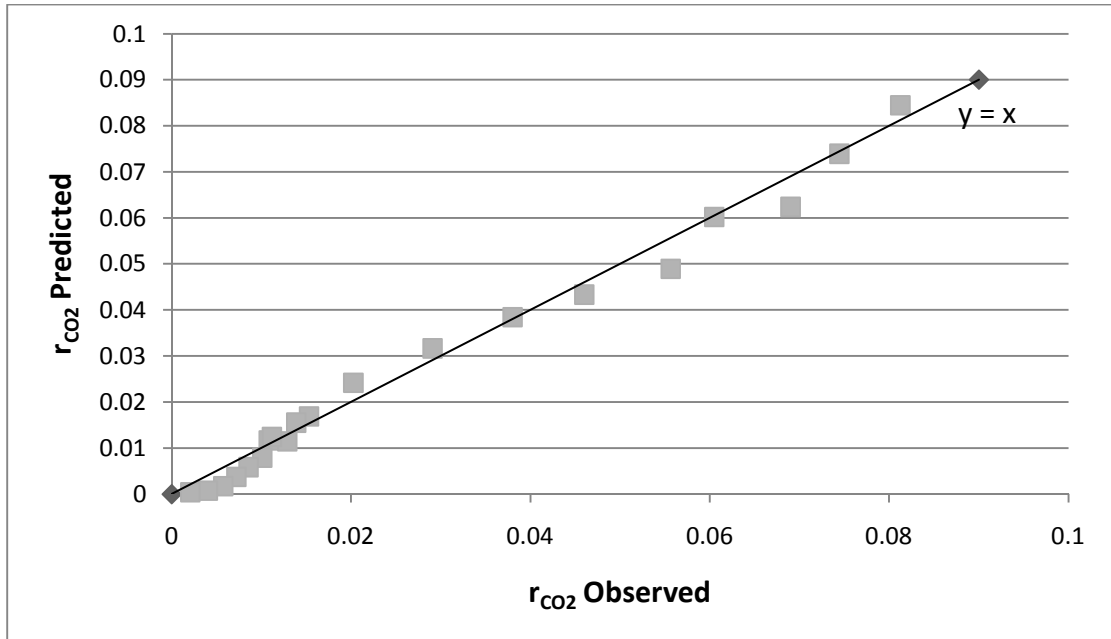


Figure 6.1: Parity plot of Power Rate Law Results, $T = 30^{\circ}\text{C}$, $[\text{MEA}]_i = 2.5[\text{CO}_2]_i$, Constraints: $k > 0$, $m > 0$, $n > 0$

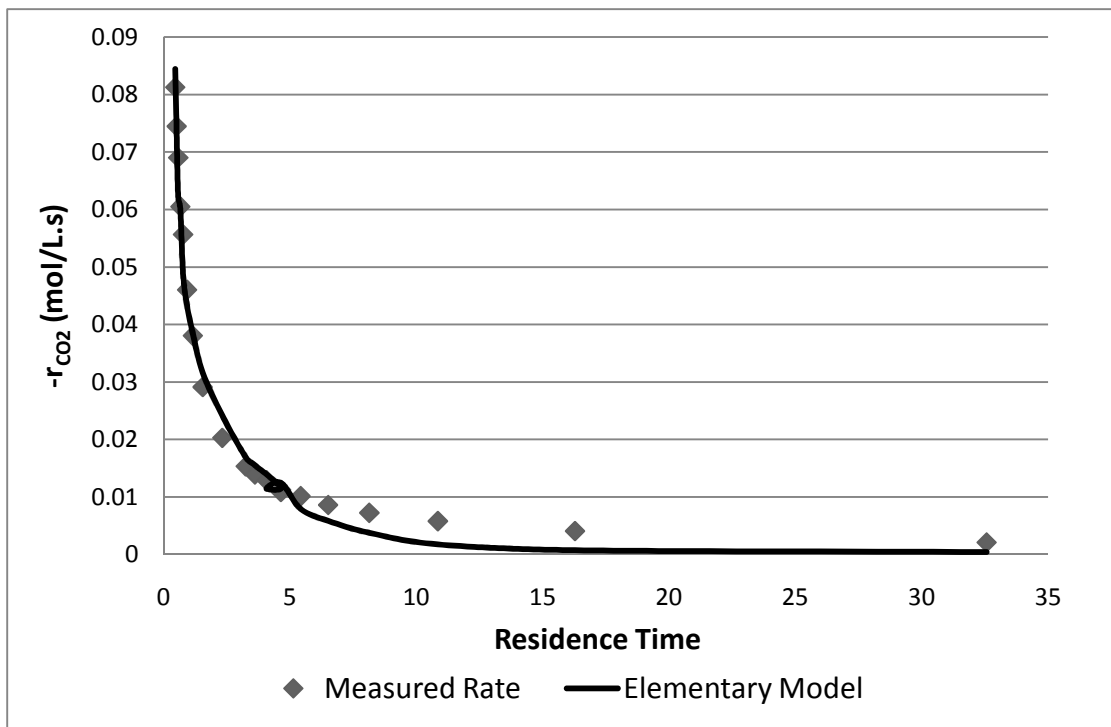


Figure 6.2: Fitted Plot of Power Rate Law Results, $T = 30^{\circ}\text{C}$, $[\text{MEA}]_i = 2.5[\text{CO}_2]_i$, Constraints: $k > 0$, $m > 0$, $n > 0$

Table 6.1: Power Rate Law Expression Results*

	k**	m	n
	3.00E+4	3.19	1.30
Lower limit	-5.61E+4	1.21	-0.62
Upper limit	11.6E+4	5.16	3.22
Mean Squared Error	1.87E-5		
Pearson R ²	0.9165		
Jacobian Condition	4.2E+13		

*T = 30°C, [MEA]_i = 2.5[CO₂]_i, Constraints: $k > 0$, $m > 0$, $n > 0$

**Units of $k \in \left[\frac{L^{(m+n)-1}}{\text{mol}^{(m+n)-1} \cdot s} \right]$

Figure 6.1 indicates that the power rate law rate expression provides a reasonable fit for the experimentally determined reaction rate profile. This is confirmed by the relatively low *mse* listed in **Table 6.1** as well as the R^2 value close to unity. Before discussing the parity plot it is firstly necessary to identify the regions of the plot. The upper right region represents the non-equilibrium data point and thus moving down and left negotiates to the data points striving towards equilibrium in the lower left region of the plot. This is applicable for all the parity plots illustrated in this study.

From the fitted plot in **Figure 6.2** it is seen that the shape of the curve correlates fairly well with the transition data. A deviation in the model data is noticed as the reaction strives to equilibrium. This is expected since it is of no use to model equilibrium data with the power rate law, because it does not account for the reverse reaction. The model is fitted on the CO₂ reaction rate profile, which is significant, since it does not show the peak that is visible in the MEA rate profiles. The CO₂ rate profiles is also suspected to have a peak, so the goodness of the power rate law fit is somewhat misleading. The power rate law will not be able to follow the peak in the non-equilibrium region and it is therefore necessary to investigate a non-elementary reaction rate expression as well.

When assessing the model parameters listed in **Table 6.1** it is firstly noted that the exponents are of reasonable order in magnitude, but the confidence interval (lower limit to upper limit) for exponents should preferably be smaller. The rate constant has a much larger than expected value, which causes an increase in the value of the concentration product term of CO₂ and MEA and thus improves its correlation with the dependant variable. This may indicate a compensation for the missing terms in the rate expression, but due to the experimental error in the data and the large

confidence interval of k , it cannot be concluded with absolute certainty. This also does not bode well for the model fit subject to constraint (2).

It is secondly noted from **Table 6.1** that the confidence interval for each parameter is very large. This is due to the very high condition number of the *Jacobian*. A section of the *Jacobian* is given by:

$$J = \begin{pmatrix} 2.81205E-06 & -0.270463173 & -0.167244684 \\ 2.46176E-06 & -0.238033704 & -0.150880014 \\ 2.07675E-06 & -0.203420452 & -0.129032838 \\ 2.13651E-06 & -0.209410051 & -0.131012767 \\ \vdots & \vdots & \vdots \end{pmatrix} \quad (6.2)$$

Each of the columns in matrix 6.2 is representative of the change in the predicted value of the dependant variable for a change in the iterative value of the parameter from one data point to the next. The first column is zero in the limit relative to the other columns relating to an ill-conditioned *Jacobian* which in turn relates to undesirably large confidence intervals for the model parameters (refer to Appendix F for statistical clarification). The large confidence intervals may also in part be attributed to the error in analysis. Since only 20 data points are available for the model fit and these points are spaced out in relatively large time step intervals for accurate modeling purposes, the error imposed on each data point plays a significant part in increasing the confidence interval.

Incorporating further constraints on the model parameters will almost definitely increase the condition number of the *Jacobian*, but for the sake of testing the assumptions made in literature with regards to the order of the rate expression, it is investigated.

The results of the model fit for constraint (2) at 30°C and equal initial reagent concentration is illustrated in **Figures 6.3** and **6.4** and tabulated in **Table 6.2**:

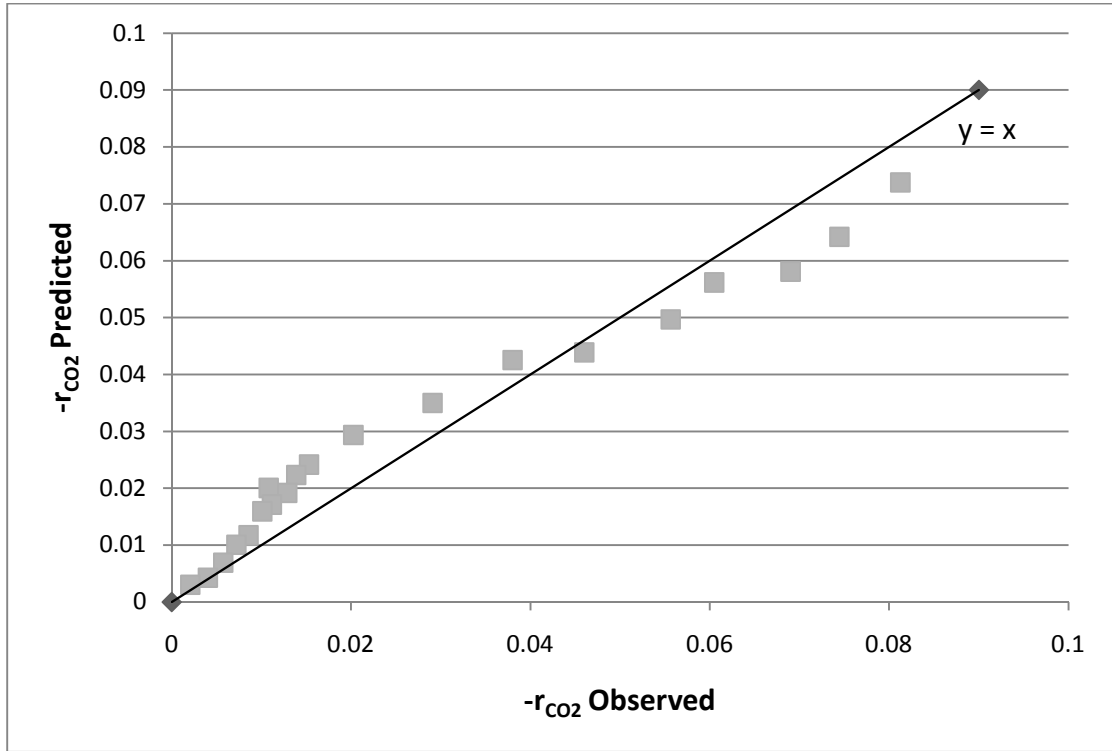


Figure 6.3: Parity plot of Power Rate Law Results, $T = 30^\circ\text{C}$, $[\text{MEA}]_i = 2.5[\text{CO}_2]_i$, Constraints: $k > 0$, $0.5 < m < 2$, $0.5 < n < 2$

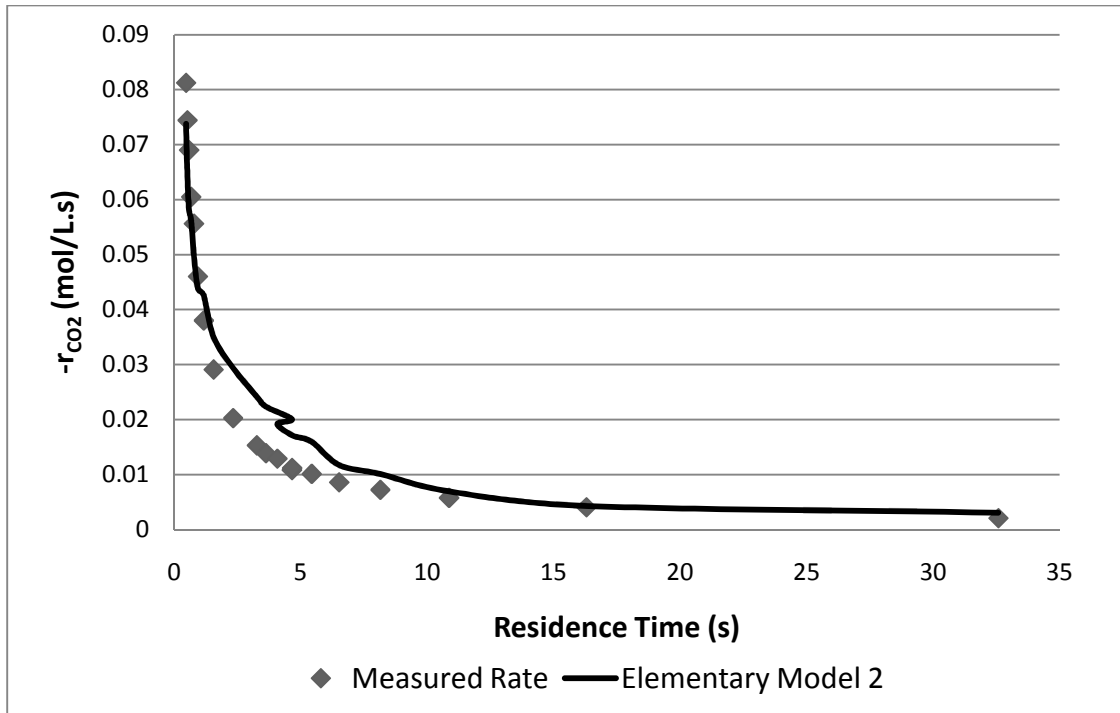


Figure 6.4: Fitted Plot of Power Rate Law Results, $T = 30^\circ\text{C}$, $[\text{MEA}]_i = 2.5[\text{CO}_2]_i$, Constraints: $k > 0$, $0.5 < m < 2$, $0.5 < n < 2$

Table 6.2: Power rate law Rate Expression Results*

	k	m	n
	111.72	1.05	2.00
Lower limit	-513.45	-0.74	2.00
Upper limit	736.89	2.84	2.00
Mean Squared Error	7.44E-05		
Pearson R²	0.84		
Jacobian Condition	6.09E+30		

* T = 30°C, [MEA]_i = [CO₂]_i, Constraints: $k > 0$, $0.5 < m < 2$, $0.5 < n < 2$

**Units of $k \in \left[\frac{L^{(m+n)-1}}{\text{mol}^{(m+n)-1} \cdot s} \right]$

As expected and as is illustrated in the parity plot of **Figure 6.3** the added constraints have resulted in a poorer fit as is indicated by the decrease in R^2 . The model now under predicts in the non-equilibrium region of the data and over predicts in the region approaching reaction equilibrium. The under prediction may be contributed to the constraints, not allowing the model to increase the correlation of the concentration product term with the dependant variable, $-r_{CO_2}$ sufficiently enough.

There is a decline in the accuracy of the more constrained model fit, but improvement in the magnitude and confidence interval of k . The confidence interval for each of the parameters is still too large to instill much confidence. This is once again a direct cause of the very high condition number of the *Jacobian*.

Another explanation may be that the rigid constraints imposed on the parameters have a dramatic and disruptive effect on the solution pathway along the model error surface. If the error in analysis is also considered, it results in great uncertainty in arriving at trustworthy estimated parameters.

It should be noted that a similar quality fit is achieved throughout the entire temperature and relative initial concentration range. To illustrate this, the effect of temperature on the estimated parameters for initial concentrations of [MEA]_i = 2.5[CO₂]_i is tabulated in **Table 6.3** and the model parameters at 30°C over the concentration range investigated is tabulated in **Table 6.4**:

Table 6.3: Effect of Concentration on Power Rate Law Parameters

Relative Concentration	Constraint 1			Constraint 2		
	1	2.5	4	1	2.5	4
k	19.22	3.00E+4	6.97E+03	19.22	112	3.16
m	1.53	3.19	2.70	1.53	1.05	0.50
n	0.64	1.30	1.27	0.64	2.00	0.89
Mean Squared Error	5.9E-6	1.87E-5	2.9E-5	5.9E-6	7.44E-5	3.63E-6
Pearson R ²	0.977	0.917	0.950	0.928	0.836	0.903

Table 6.4: Effect of Temperature on Power Rate Law Parameters

Temperature (°C)	Constraint 1			Constraint 2		
	25	30	35	25	30	35
k	58.80	3.00E+4	3.55E+6	64.08	112	611
m	0.98	3.19	4.88	0.99	1.05	1.45
n	1.97	1.30	0.64	2.00	2.00	2.00
Mean Squared Error	3.41E-5	1.87E-5	1.7E-5	3.43E-5	7.44E-5	1.01E-4
Pearson R ²	0.954	0.917	0.918	0.930	0.836	0.868

From **Table 6.3** it can be seen that there is inconsistency in the magnitude of the rate constant over the concentration range. This may be attributed to the large confidence interval for the estimated parameter resulting from the experimental error. For a kinetic model to be valid, the rate constant should be independent of concentration which does not instill a great deal of confidence in the validity of the fitted power rate law. From **Table 6.4** it may be seen that the rate constant seemingly increases exponentially with an increase in temperature. This is an expected result and may indicate that the trends in the experimental data are correct. More data points with greater accuracy and shorter time intervals may be required to improve the consistency of the rate constant.

Based on the model data presented it is hard to completely reject the power rate law. It does not represent the rate profile at reaction initiation, since it will not model the initial peak in the reaction rate profile. It does however give a reasonable fit on the data leading up to reaction equilibrium, since it is assumed for the reaction to be predominantly irreversible in this region (Danckwerts, 1970). It may therefore be concluded that the power rate law should still be considered when deriving rate expressions for developing a method for determining the effective interfacial mass transfer area.

6.2 Non-Elementary PSSH Rate Expression

Since many authors have already identified the non-elementary nature of the reaction mechanism of CO₂ with MEA, it is also necessary to model a rate expression based on the pseudo-steady state hypothesis (PSSH). From the analysis of the experimental data, especially in section 5.2, it was concluded that the reaction mechanism composes of two reversible reactions, rather than a reversible- followed by an irreversible reaction.

Based on this finding it is concluded that the PSSH model derived in equation 2.40 is not sufficient and must be updated. By following the same procedure in deriving equation 2.40 the following non-elementary rate expression may be derived:

$$-r_{MEA} = \frac{2 \left(\frac{k_1 k_3}{k_2} [CO_2] [RNH_2]^2 - k_4 [S]^2 \right)}{1 + \frac{k_3}{k_2} [RNH_2]} \quad (6.5)$$

Refer to Appendix C for the derivation of equation 6.5. This expression is similar in form to equation 2.40 but differs in that the dependant variable is now $-r_{MEA}$ instead of $-r_{CO_2}$ and it includes the concentration of the salt product, S , formed in the second reversible reaction. The reason for expressing equation 6.5 in terms of $-r_{MEA}$ instead of $-r_{CO_2}$ is to be able to compare this model expression with more fundamentally derived rate expression (evaluated in the next section). The lumped constants of this rate expression can only be solved by means of non-linear regression, which is the method that is incorporated. The constraints imposed on the model are as follows:

$$k_1 > 0, k_2 > 0, k_3 > 0, k_4 > 0$$

These constraints will of course ensure that the model correlates with and is representative of the proposed reaction mechanism resulting in physically feasible model results for discussion

The results of the PSSH model fit at 30°C and equal initial reagent concentration is illustrated in **Figures 6.5** and **6.6** and tabulated in **Table 6.5**:

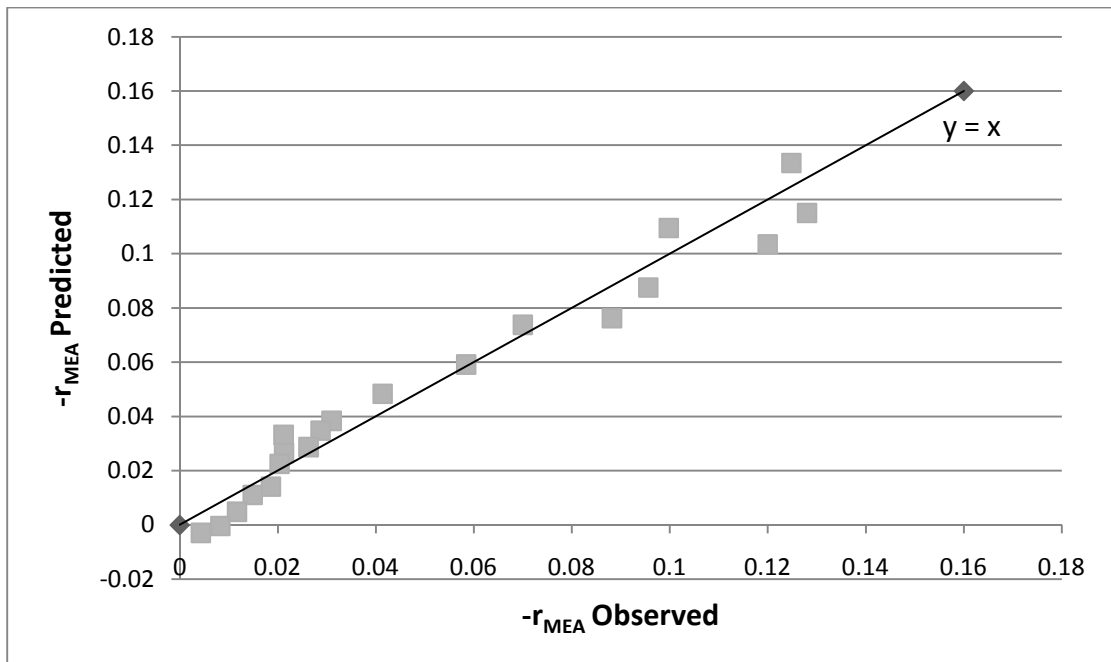


Figure 6.5: Parity plot for PSSH Model Results, $T = 30^\circ\text{C}$, $[\text{MEA}]_i = 2.5[\text{CO}_2]_i$, Constraints: $k_1 > 0, k_2 > 0, k_3 > 0, k_4 > 0$

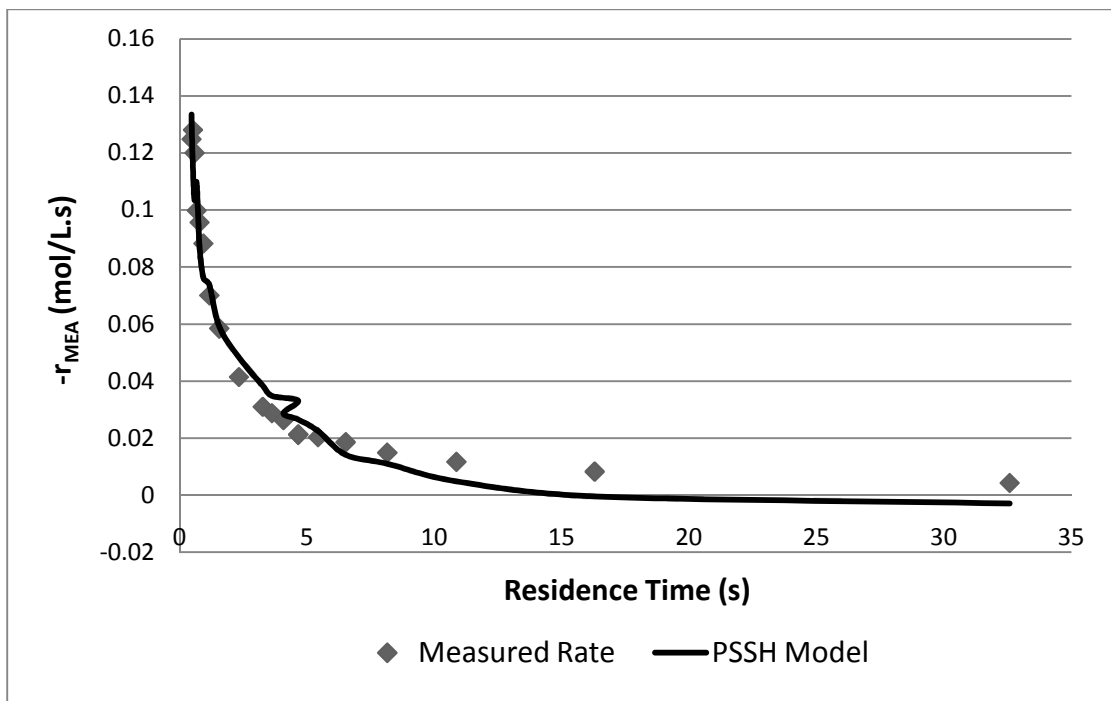


Figure 6.6: Fitted Plot for PSSH Model Results, $T = 30^\circ\text{C}$, $[\text{MEA}]_i = 2.5[\text{CO}_2]_i$, Constraints: $k_1 > 0, k_2 > 0, k_3 > 0, k_4 > 0$

Table 6.5: PSSH Model Results*

	$k_1 k_3 / k_2$	k_4	k_3 / k_2	k_1^{**}
	92.12	6.24E-10	8.61E-09	1.0
Lower limit	23.89	-3.92	-3.92	-1.48E+23
Upper limit	160.35	3.92	3.92	1.48E+23
Mean Squared Error	1.18E-03			
Pearson R²	0.9156			
Jacobian Condition	1.07E+19			

*T = 30°C, [MEA]_i = 2.5[CO₂]_i, Constraints: $k_1 > 0, k_2 > 0, k_3 > 0, k_4 > 0$

**Units of every $k \in \left[\frac{L^2}{\text{mol}^2 \cdot s} \right]$

It is firstly noted from the parity plot of **Figure 6.5** that the PSSH model provides a similar quality fit to that of the power rate law for the measured reaction rate. This is reflected in the R^2 -value and relatively high *mse* tabulated in **Table 6.5**. Since the model structure is strongly non-linear and only 20 data points are available to be fitted, it was found that the model predictions are strongly dependant on the initial estimates for iteration. These results are representative of the best fit obtained for a vast number of initial guesses. The model also fails to follow the peak in the reaction rate profile which means that for a similar quality fit, the power rate law will be preferred because of its greater simplicity.

From **Table 6.5** it can be seen that the model struggled considerably to obtain trustworthy parameter estimates as is indicated by the enormous confidence intervals. This may once again be attributed to the high condition number of the *Jacobian*. This may be improved by having more data point at a higher degree of accuracy available for modelling purposes.

This PSSH model shows a similar quality fit throughout the entire temperature and relative initial concentration range which leads to the conclusion that the PSSH model structure is not sufficient in representing the reaction kinetics of CO₂ with MEA in solution with 2-propanol.

6.3 Proposed Rate Expression

Keeping in mind that the modeled rate expression derived in this study is aimed at being incorporated in a method to determine the effective interfacial mass transfer area on structured packing material which will aid in deriving a more accurate rate based model for the reactive absorption of CO₂ into MEA; a rate expression with no over simplifying assumptions needs to be investigated. Refer to section 2.2.2.4 for all the fundamental expressions of interest. The one expression in the list that includes all the concentrations and all the parameters to be determined is equation 2.46:

$$-r_{RNH_2} = k_1 [CO_2]^m [RNH_2]^n - k_2 [Z]^p + k_3 [RNH_2]^q [Z]^v - k_4 [S]^w \quad (2.46)$$

A non-linear estimation technique will once again have to be incorporated to find the best fit. It was found that a poor model fit was achieved with equation 2.46, the reason for which is that 10 model parameters were estimated with only 20 data point available. The number of model parameters therefore needed to be decreased. This was achieved by examining the correlations of the independent and dependant variables.

A pre-requisite for a good model fit is to determine if a good correlation exists between the independent and dependant variables of the model expression. In this case the independent variables are the concentration product terms with the dependant variable being $-r_{MEA}$. These correlations for the temperature range at concentrations of $[MEA]_i = 2.5[CO_2]$ are tabulated in **Table 6.6**:

Table 6.6: Correlations of Dependant and Independent Variables

25 °C				
	CO ₂ x MEA	MEA x Z	Z	S ²
Correlation with r _{MEA}	95.97%	92.06%	84.58%	-90.84%
30 °C				
	CO ₂ x MEA	MEA x Z	Z	S ²
Correlation with r _{MEA}	95.41%	88.31%	84.71%	-88.06%
35 °C				
	CO ₂ x MEA	MEA x Z	Z	S ²
Correlation with r _{MEA}	96.03%	94.96%	89.33%	-92.68%

The cases in which a negative correlation is depicted, is merely an indication of the directionality of the correlation, the essential information is the magnitude of the value, where any correlation above 80% is deemed good.

In examining **Table 6.6** it is firstly noticeable that the CO₂ and MEA concentration product term has a good correlation with the dependant variable. This may be one of the reasons why previous authors deemed the power rate law rate expression to be sufficient.

Further examination of **Table 6.6** reveals that the zwitterion concentration has the weakest correlation. This may be attributed to the relative large experimental error in determining the zwitterion concentration. All the other independent variables show a good to very good correlation which invests confidence in the modeling of a fundamentally derived rate expression, such as Model 1:

$$-r_{\text{MEA}} = k_1 [\text{CO}_2][\text{RNH}_2] - k_2 [\text{Z}] + k_3 [\text{Z}][\text{RNH}_2] - k_4 [\text{S}]^2 \quad (\text{Model 1})$$

In order to ensure that the reaction mechanism structure is represented by the model, the model parameters are subject to the following constraints:

$$k_1 > 0, k_2 > 0, k_3 > 0, k_4 > 0$$

The results of Model 1 at 30°C and equal initial reagent concentration is illustrated in **Figures 6.7** and **6.8** and tabulated in **Table 6.7**:

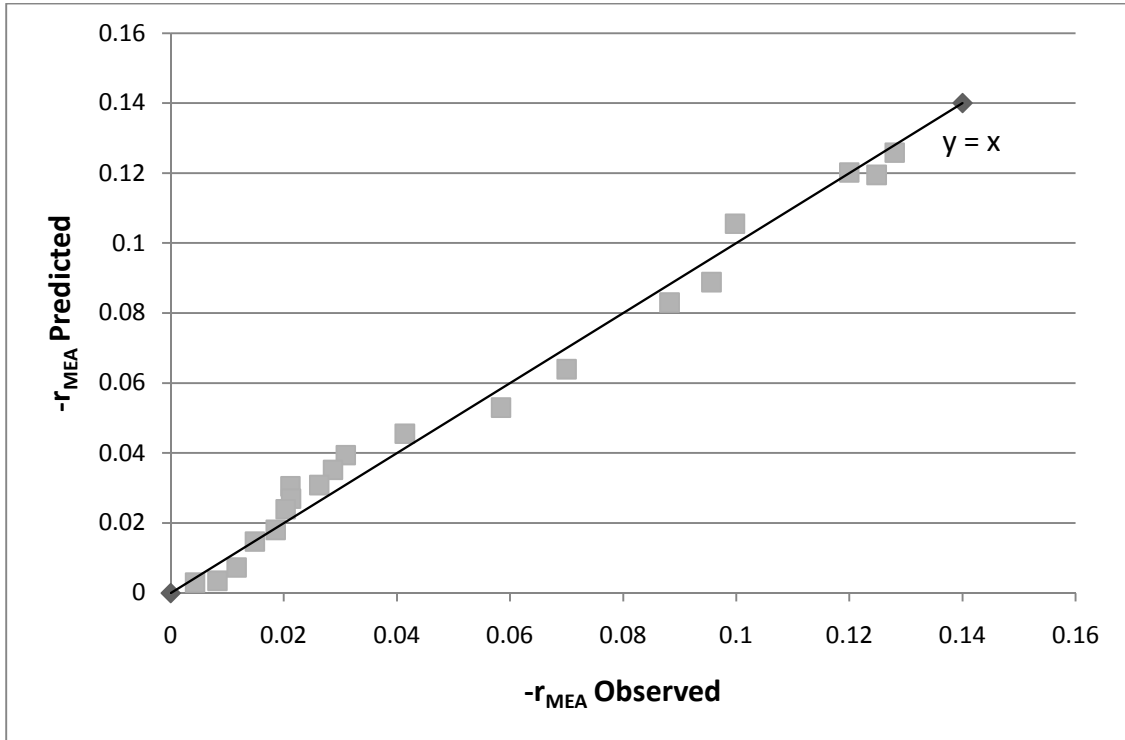


Figure 6.7: Parity plot for Model 1 Results, $T = 30^{\circ}\text{C}$, $[\text{MEA}]_i = 2.5[\text{CO}_2]_i$, Constraints: $k_1 > 0$, $k_2 > 0$, $k_3 > 0$, $k_4 > 0$

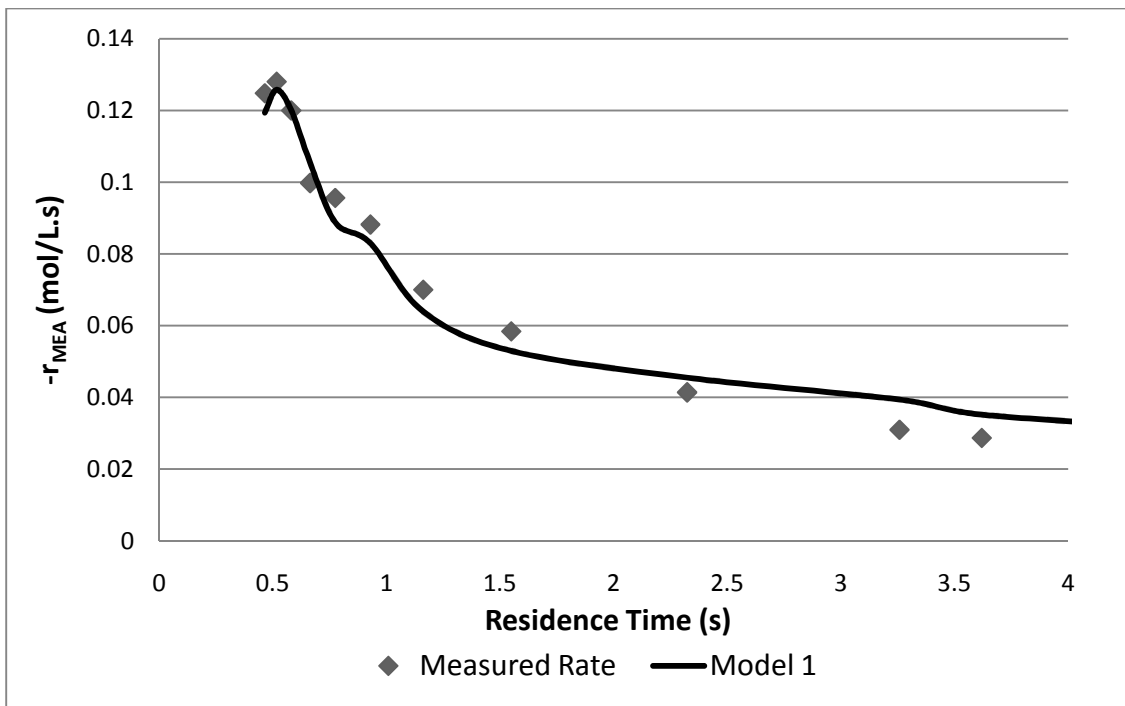


Figure 6.8: Fitted Plot for Model 1 Results, $T = 30^{\circ}\text{C}$, $[\text{MEA}]_i = 2.5[\text{CO}_2]_i$, Constraints: $k_1 > 0$, $k_2 > 0$, $k_3 > 0$, $k_4 > 0$

Table 6.7: Model 1 Results*

	k_1^{**}	k_2	k_3	k_4
	12.60	10.35	139	1.14
Lower limit	7.18	-13.67	-53	-7.06
Upper limit	18.03	34.37	331	9.34
Mean Squared Error	1.75E-03			
Pearson R²	0.9947			
Jacobian Condition	41580			

*T = 30°C, [MEA]_i = 2.5[CO₂]_i, Constraints: $k_1 > 0, k_2 > 0, k_3 > 0, k_4 > 0$

**Units of every $k \in \left[\frac{L^2}{\text{mol}^2 \cdot s} \right]$

From the parity plot in **Figure 6.7** it can immediately be seen that Model 1 is a reasonable, but not absolutely accurate fit and judging by the *mse* and *R²*-value in **Table 6.7** it shows some improvement with respect to the power rate law and PSSH models. The confidence interval for the estimated parameters has improved greatly from that of the power rate law and PSSH models. This may be attributed to the relatively low *Jacobian* number. A section of the *Jacobian* reads:

$$J = \begin{pmatrix} 0.005610809 & -0.005613268 & 0.000774727 & -0.000850263 \\ 0.005192365 & -0.00794052 & 0.001031649 & -0.000886936 \\ 0.004841452 & -0.00833393 & 0.001052805 & -0.000973775 \\ 0.004963398 & -0.007011361 & 0.000909973 & -0.0009843 \\ \vdots & \vdots & \vdots & \vdots \end{pmatrix} \quad (6.7)$$

The values in matrix 6.7 are of similar order in magnitude, which means that the outer product matrix is well behaved. This instills confidence in the estimated model parameters. **Figure 6.8** only illustrates the first four seconds in residence time to better illustrate that Model 1 does follow the peak in the rate profile. A matter of concern regarding Model 1 is of course the incorporation of the zwitterion concentration. Determining the zwitterion concentration rests on assumptions that could not be validated to a high degree of certainty (refer to Chapter 5). This resulted in a relatively large error in its determined concentration profile. Since its concentration has a reasonable correlation with $-r_{MEA}$, it was included in the model fit, but its influence on the model fit should form part of a future investigation.

The effect of temperature on the estimated parameters for initial concentrations of $[MEA]_i = 2.5[CO_2]_i$ is tabulated in **Table 6.8**:

Table 6.8: Effect of Temperature on Model 1 Parameters

Temperature (°C)	25	30	35
k_1	3.40	12.60	26.44
k_2	2.90	10.35	22.97
k_3	5.43E-09	139	230
k_4	4.16E-10	1.14	5.43
Mean Squared Error	1.82E-03	1.75E-03	2.33E-04
Pearson R^2	0.9707	0.9947	0.9994

From **Table 6.8** it seems that there is an exponential increase in each model parameter with an increase in temperature. This is in accordance with an Arrhenius type of expression and may be used for determining the activation energy of the reaction, but since the quality of the model fit is not the same across the concentration range, this will be left for future investigation. The model parameters at 30°C over the concentration range investigated is tabulated in **Table 6.9**:

Table 6.9: Effect of Concentration on Model 1 Parameters

Relative Concentration	1	2.5	4
k_1	26.59	12.60	15.70
k_2	1.50E-12	10.35	5.37E-12
k_3	2.38E-10	139.2	8.20
k_4	3.04E-14	1.14	5.64
Mean Squared Error	6.11E-04	1.75E-03	7.55E-04
Pearson R^2	0.9995	0.9947	0.9362

From **Table 6.9** it is seen that the model parameters differ greatly over the concentration range. This is unexpected since the rate constant is not a function of concentration. This is an indication that the model is too sensitive with too few data points available for a fundamental model fit. This renders an Arrhenius analysis of the rate constants untrustworthy and will thus not be attempted in this study.

Based on the concentration effect noticed in **Table 6.9**, an investigation was made into fitting all the concentration data at each temperature to try and find model parameters that are consistent over a concentration range. This model fit would provide rate constants which are independent of concentration which was deemed the correct procedure for trying to derive a fundamental model fit of the data. The

resulting fits for Model 1 on the data at 30°C are illustrated in **Figure 6.9** and the model parameters over the temperature range tabulated in **Table 6.10**:

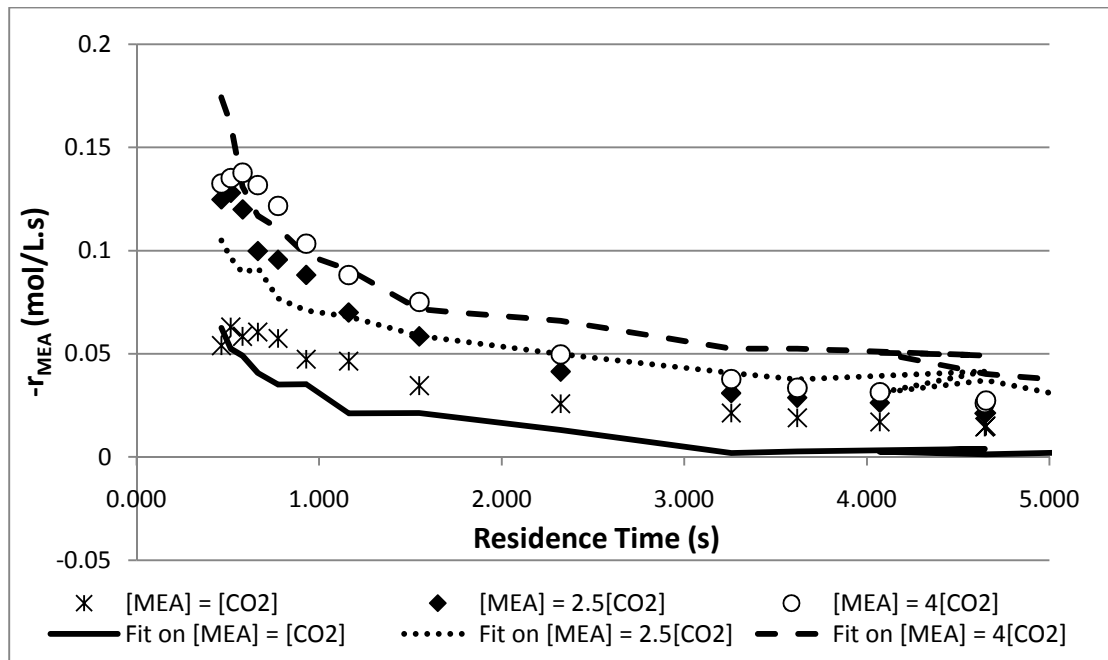


Figure 6.9: Model Fits at 30°C imposing model parameters of $[MEA]_i = 2.5[CO_2]_i$ on $[MEA]_i = [CO_2]_i$ and $[MEA]_i = 4[CO_2]_i$.

Table 6.10: Model 1 Parameters

Temperature (°C)	k_1	k_2	k_3	k_4	mse	R^2
25	13.06	4.64E-14	1.16E-10	0.93	9.06E-04	0.624
30	19.51	7.43E-14	6.52E-11	5.32	8.06E-04	0.612
35	24.57	1.09E-08	2.68	6.86E-13	1.62E-03	0.571

From **Figure 6.9** it may be seen that the model fit is poor. This is reflected in **Table 6.10** which shows the high mse and the R^2 – values that deviate significantly from unity. Only the first 5 seconds in residence time is illustrated. This shows that the trend in the model fit deviates from the fit achieved in **Figure 6.8** by not following the initial peak well. Between 1 and 2 seconds residence time, it may be seen that the model fits reasonably well. This is of significance, since it falls in the contact time region investigated in the absorption study (Chapter 7). It was therefore decided to investigate the fit of the power rate law on the lumped temperature data. A comparison with Model 1 at $T = 30^\circ\text{C}$, $[MEA]_i = 2.5[CO_2]_i$ for the lumped data fit is illustrated in **Figure 6.10** and the power rate law parameters for the fit at each temperature is tabulated in **Table 6.11**.

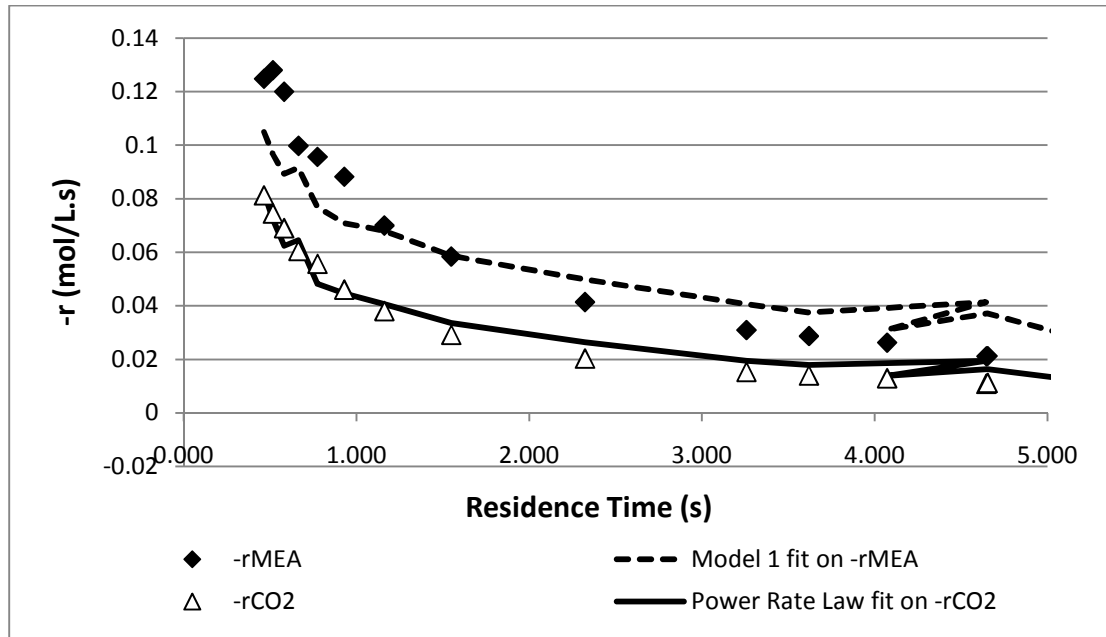


Figure 6.10: Power Rate Law and Model 1 Comparison

Table 6.11: Power Rate Law Parameters

Temperature (°C)	k	m	n	mse	R ²
25	27.87	1.61	0.67	2.56E-05	0.856
30	5089	2.52	1.49	3.56E-05	0.813
35	130500	3.33	1.55	2.76E-05	0.786

From **Figure 6.10** and **Table 6.11** it may be seen that the power rate law provides a better quality fit than Model 1. The fit is however of similar quality between 1 and 2 seconds residence time. It may therefore be concluded that the power rate law should not be rejected, but still considered for modeling the data for short contact times. It may further be concluded that more data with a higher level of accuracy is needed for both model fit qualities to be improved. This may be achieved by gathering continuous time data:

It is important to note that all of the data gathered is modeled on residence time and not continuous time. This may have a significant effect on the model parameters estimated in this study. Once a concentration profile is represented in continuous time, it may be expressed as a continuous curve and therefore allows for an abundant amount of data points available for modelling purposes. The difficulty lies in accurately gathering concentration- continuous time data. It will have to be done in a semi-batch, micro-reactor.

6.4 Chapter Conclusions

By implementing a non-linear regression technique and utilizing the Levenberg-Marquard optimization algorithm, the experimentally determined rate data could be modeled on various reaction rate expressions.

The power rate law gives a reasonable fit of the CO₂ rate data. The confidence intervals of the model parameters are large, which is not desirable. This is mainly due to the relatively small number of data points available for the model fit as well as the experimental error imposed on the data. The power rate law is not completely rejected, since it is a well behaved function, but since it will not follow the expected peak in the rate data, other non-elementary models were investigated.

The PSSH model provides the same quality fit as the power rate law model on the MEA rate data. It fails to follow the peak in the rate curve and its lumped rate constants have a large confidence interval. This is once again due to the error in and lack of data point available for modeling. The PSSH model is therefore rejected, since it is too complicated and tedious for no noticeable improvement on the simpler power rate law.

The correlation of the concentration product terms, [CO₂][MEA], [Z][MEA] and [S]² with the independent variable, $-r_{MEA}$, is in the order of 90 – 96% with the correlation of [Z] being above 80%. A fundamentally derived rate expression, Model 1, was investigated and it gave a reasonably good model fit, following the peak in the rate profile. The confidence intervals for the model parameters are however still too large. An attempt was made to achieve consistency in the rate constants of Model 1 and the power rate law over a concentration range. This was done by fitting all the concentration data at one temperature and evaluating the estimated model parameters for each lumped model fit over the temperature range. The model fits were reasonable, but can still be improved considerably. The model structures stayed reasonably intact, leading to the conclusion that more accurate data is required. This may be achieved by gathering concentration data from a semi-batch reactor to be able to study continuous- instead of residence time data.

CHAPTER 7: RESULTS AND DISCUSSION: REACTIVE ABSORPTION

The results obtained from the experimental runs performed on the wetted wall experimental set-up will be presented in this chapter. The validation of the set-up will firstly be discussed in comparison with results obtained in the study performed by Erasmus, 2004. The effect of temperature and gas or liquid side concentrations on the absolute and specific rate of CO₂ absorption will be investigated and discussed. The relevance of the reaction kinetic study will be introduced and discussed. Based on the findings, recommendations for future investigations will be made.

7.1 Validation Results

In order to be able to present meaningful absorption experimental results, an experimental set-up validation must firstly be done. This was achieved by completing runs at similar conditions to Erasmus, 2004. In order to achieve the CO₂ mass percentages for the comparison study, the CO₂ MFC readings was in the order of 0.1 which is the minimum trustworthy reading of the device and is hard to control the flow rate at this low value. The argon flow rate had to be increased. This increased the total gas flow rate to the dome to MFC readings in the range of 4.45 – 4.9 which increased the dome pressure to 112.3 kPa. This is one of the drawbacks of the current experimental set-up and will form part of a future optimization investigation to be able to study absorption rates at lower CO₂ mass percentages.

The amount of CO₂ absorbed was determined as described in section 4.3.1 but a different calibration equation for the total mass flow had to be used. The calibration was done in the same way as for the lower flow rates and the resulting equations are as follows:

$$\dot{m}_{Ar} = 3.231(\text{MFC}_{\text{outlet}} - \text{MFC}_{\text{CO}_2}), \quad R^2 = 0.9756 \quad (7.1)$$

$$\dot{m}_{\text{tot}} = 1.051(\text{MFC}_{\text{outlet}} - \text{MFC}_{\text{CO}_2}) + 9.57, \quad R^2 = 0.9021 \quad (7.2)$$

The specific absorption rate is calculated from:

$$N_{\text{CO}_2} = \frac{n_{\text{CO}_2}}{A_{\text{wetted wall surface}}} \left(\text{mol}/\text{m}^2\text{s} \right) \quad (7.3)$$

where

$$n_{\text{CO}_2} = \frac{n_{\text{CO}_2, \text{absorbed}}}{t_c} \left(\text{mol}/\text{s} \right) \quad (7.4)$$

The results obtained at 30°C and [MEA] = 0.3 mol/L are illustrated in **Figure 7.1**:

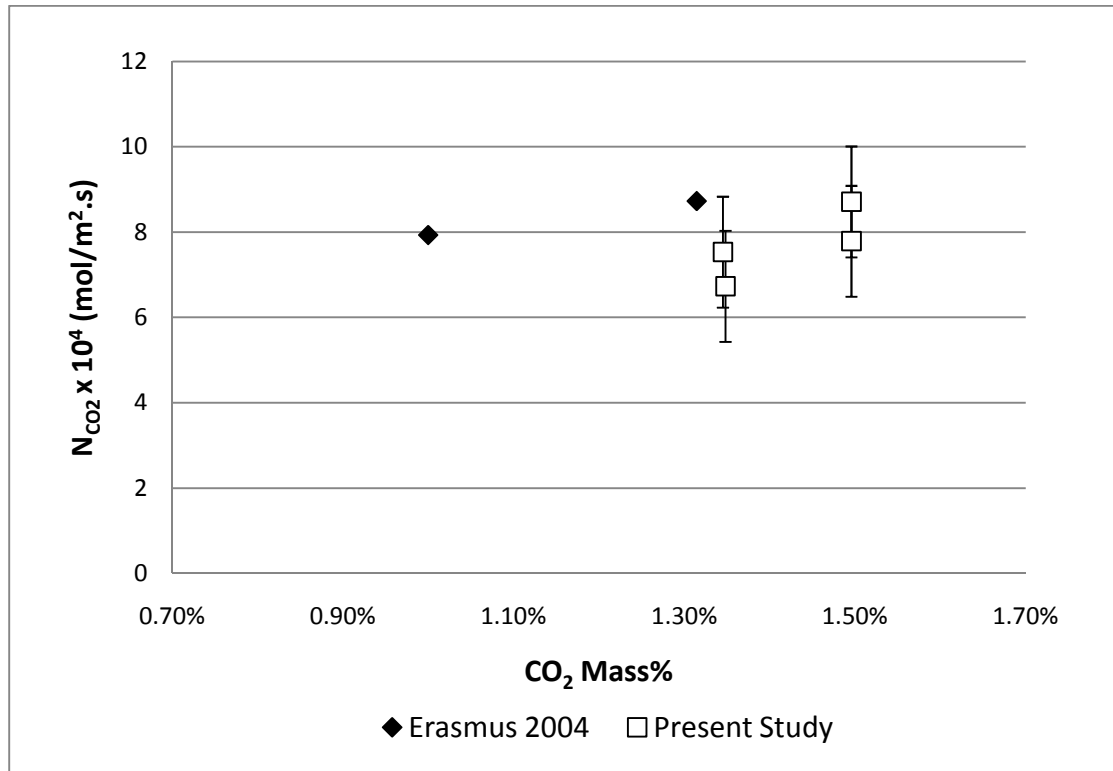


Figure 7.1: Wetted Wall Comparative Results at 30°C and [MEA] = 0.3 mol/L

From **Figure 7.1** it can be seen that the results obtained in this study correlates fairly well with the absorption data from Erasmus, considering the error due to the sensitivity of the MFC at these low CO₂ mass percentages. The sensitivity is indicated by the error bars. The data presented represents many experimental repetitions and the average of the logged data to the third decimal place. The accuracy of these runs will be greatly improved by designing the set-up to be able to conduct accurate

runs at low CO₂ mass percentages. This may be achieved with soap bubble flow meters for accurate flow measurement at low argon and CO₂ flow rates. This will also allow for the runs to be conducted near 1 atm dome pressure instead of the 112.3 kPa pressure at which these runs were conducted.

It may be noticed from **Figure 7.1** that the absorption rates determined in this study is predominantly lower than that determined by Erasmus. This may be due to the fact that CO₂ is less soluble in 2-propanol than in n-propanol, since 2-propanol is more polar than n-propanol and CO₂ is more solvent in non-polar liquids. Tokunaga, 1975 found that CO₂ is approximately 7.7% more soluble in n-propanol than 2-propanol at 30°C and 1 atm. Due to the error in the absorption data, the effect of solubility could however not be concluded to a high degree of certainty.

In order to be able to validate the specific absorption rates to higher degree of certainty, it will be necessary to stop the reaction with benzoyl chloride and analyze the liquid phase for CO₂ and MEA concentration to be able to characterize the reaction rate effect. The wetted wall set-up should also be modified to be able to perform both high and low CO₂ concentration studies. This will form part of a future investigation.

Further proposed evidence regarding the validation of the wetted wall runs is achieved by investigating the dependence of the specific absorption rate on gas-liquid contact time. This is illustrated in **Figure 7.2** with a plot of specific absorption rate vs. CO₂ mass% at 25°C and [MEA]_i = 0.25mol/L:

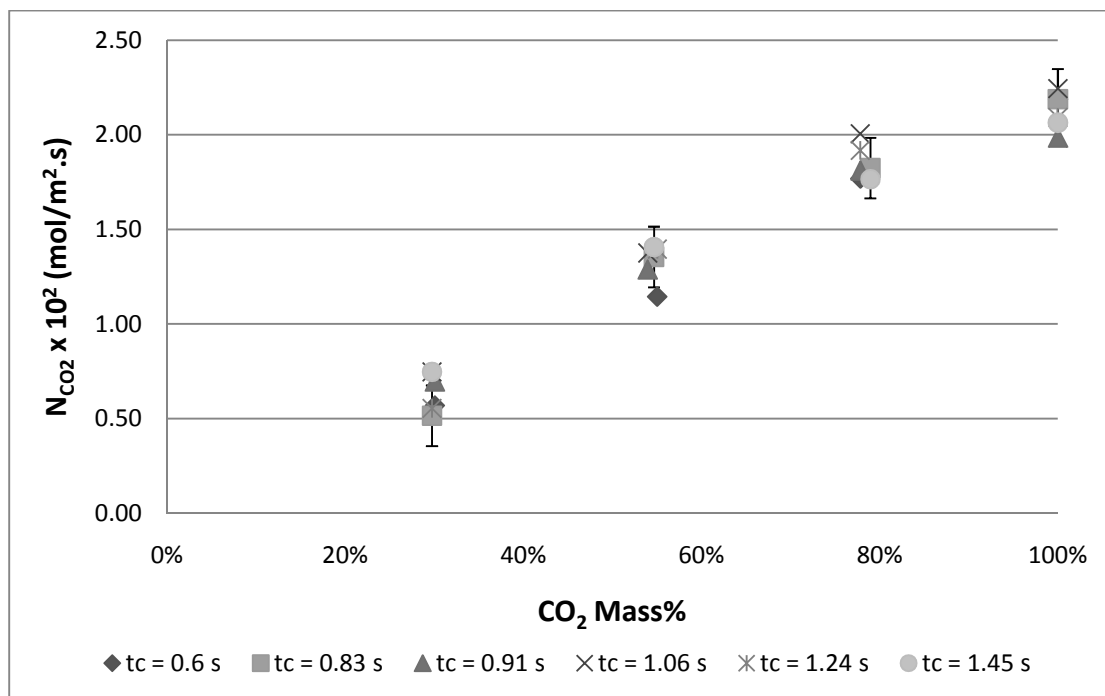


Figure 7.2: Dependence of Specific Absorption Rate on Contact Time

The error bars in **Figure 7.2** indicates the sensitivity of the MFC reading according to the calibration done with the positive displacement gas flow meter. From **Figure 7.2** it is noticed that the specific absorption rate is independent of contact time. Due to the rapid nature of the reaction of CO₂ with MEA this is expected. This was noticed for both temperatures and MEA initial concentrations. This also correlates well with the results obtained by Erasmus (2004) which serves as evidence towards supporting the validation of the wetted wall experimental results obtained in this study.

For further validation purposes, the effect of liquid surface area on the absolute absorption rate of CO₂ was investigated. The results at 25°C, an initial MEA concentration of 0.25mol/L and a liquid flow rate of 1.54mL/s are illustrated in **Figure 7.3:**

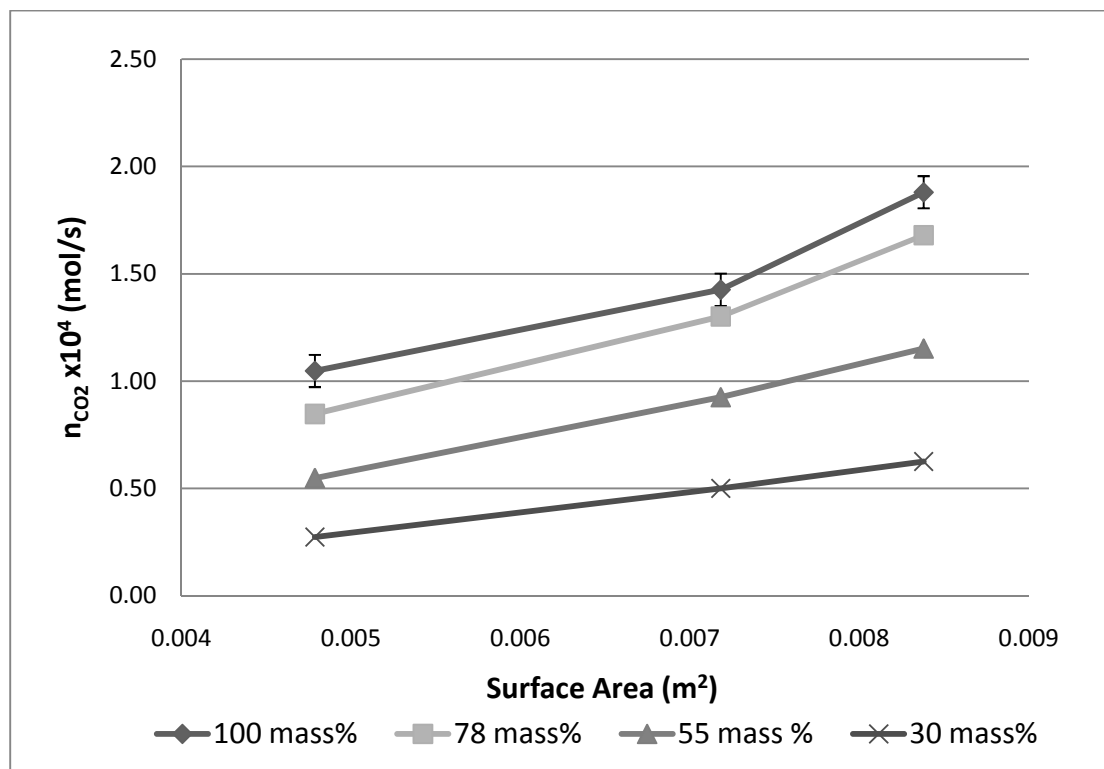


Figure 7.3: Absorption Rates vs. Surface Area

From **Figure 7.3** it can be seen that the absolute absorption rate increases seemingly non-linearly with an increase in the exposed liquid surface area. This is an expected result. With only three column lengths investigated, the true trend of the absorption rate could not be determined to a degree of certainty.

It should be noted that a 100% validation of the wetted wall experimental set-up could not be confirmed, but based on the evidence presented in this section; the trends noticed from this study may be deemed representative of the reactive absorption of CO₂ into solutions of MEA/2-propanol.

7.2 Temperature/Concentration Effect

The effect of temperature and initial MEA concentration on the specific absorption rate of CO₂ was investigated in this study. The concentration effect will be discussed first and the results obtained at 25°C are illustrated in **Figure 7.4**:

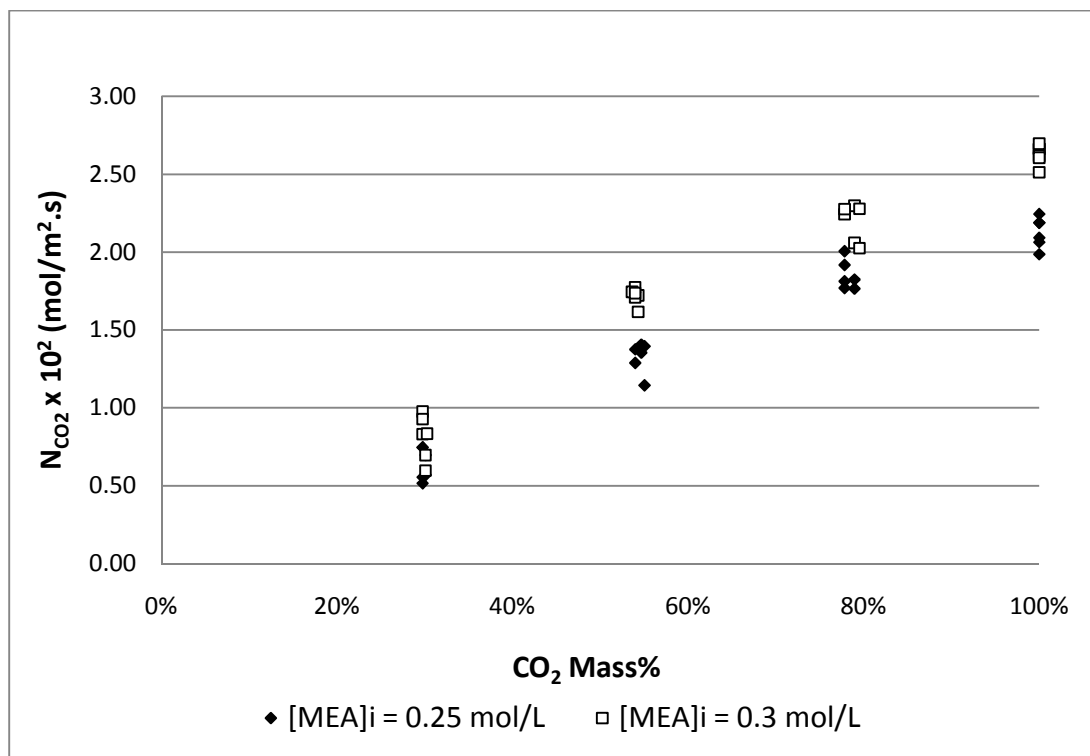


Figure 7.4: MEA Concentration Effect on the Specific Rate of Absorption.

From **Figure 7.4** it is seen that the specific rate of absorption increases with an increase in both CO₂ mass% and MEA concentration. This may be attributed to the increase in the reaction rate within the liquid which is in accordance with the findings in section 5.3.2.

It was decided to conduct a run at an MEA concentration of 1mol/L and 25°C to confirm the concentration effect. The results obtained are illustrated in **Figure 7.5**:

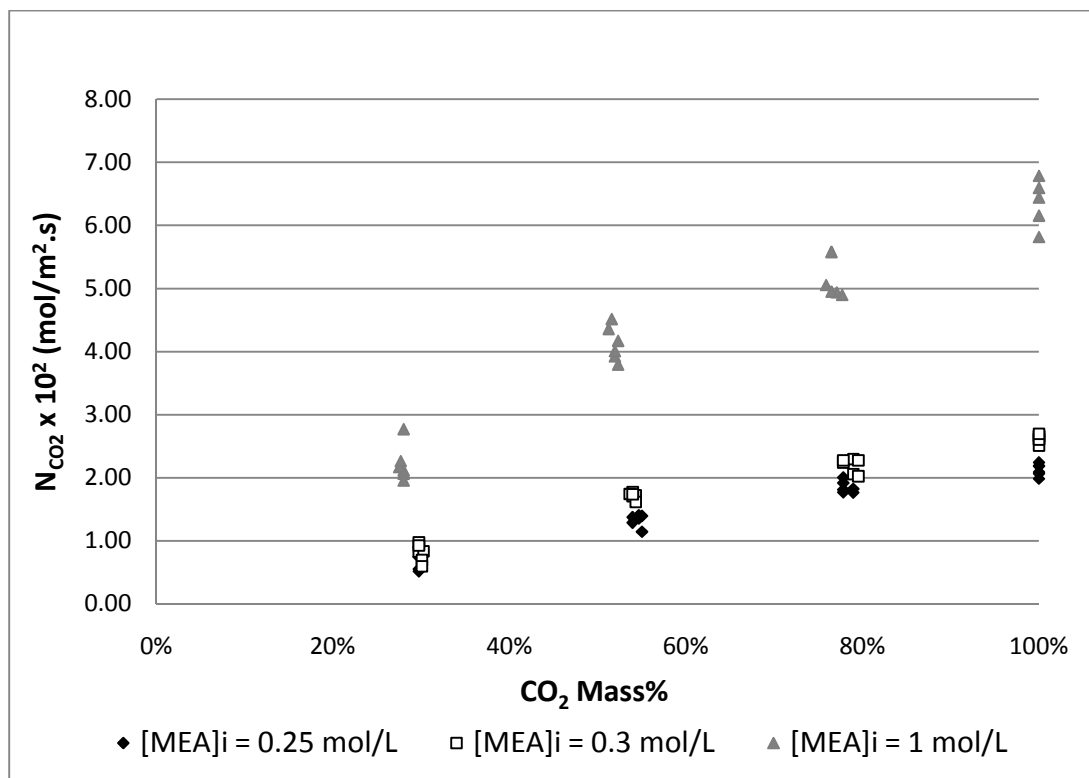


Figure 7.5: Concentration Effect with added [MEA]_i = 1mol/L

From **Figure 7.5** the increase in absorption rate for an increase in MEA concentration is confirmed. This result is in good agreement with the conclusion made in Chapter 5 that the reaction rate in the liquid phase increases exponentially with an increase in reagent initial concentration. It may therefore indicate that the absorption kinetics is defined by a reaction rate law of similar structure to the rate laws examined in Chapter 6. This will be investigated in a future study when rate expressions will be derived to enable the determination of effective interfacial mass transfer area. Being able to study a wider CO₂ and MEA concentration range is beneficial for developing a method for determining effective interfacial mass transfer area, since it will provide a wide concentration range to test the consistency of the rate expression governing the reactive absorption.

The effect of temperature on the specific rate of absorption is investigated next. The results obtained at an initial MEA concentration of 0.3 mol/L are illustrated in **Figure 7.6:**

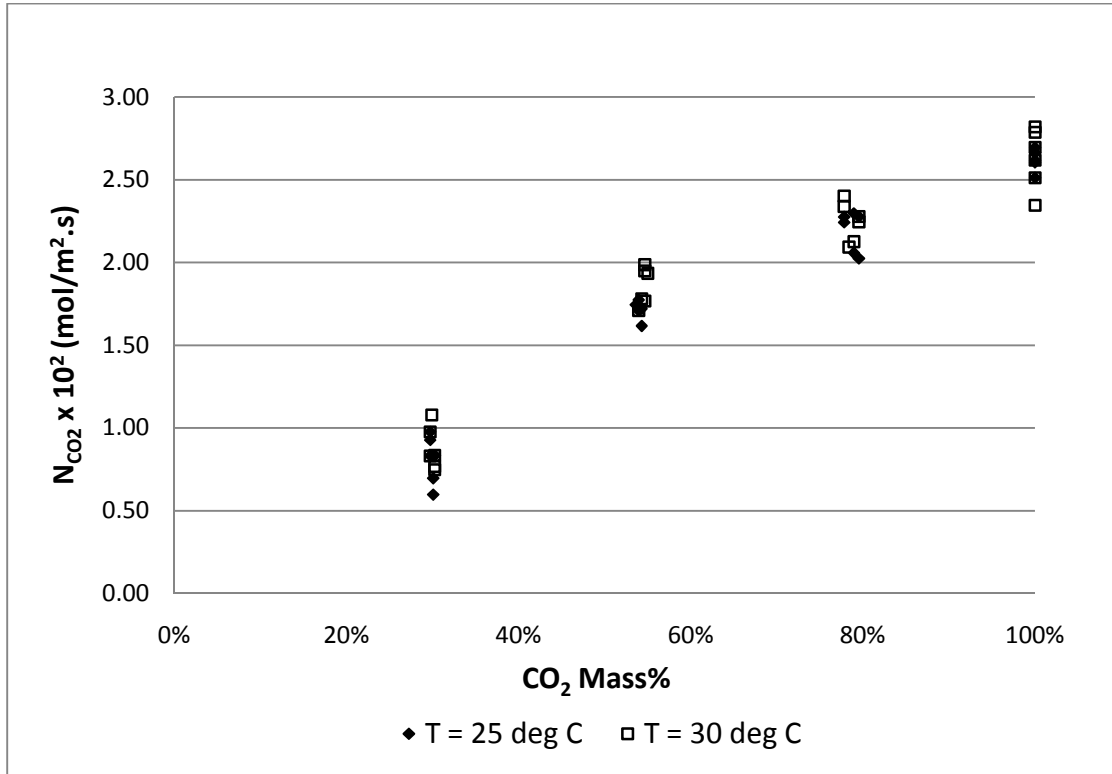


Figure 7.6: Temperature Effect on the Specific Absorption Rate

From **Figure 7.6** it can be seen that for a constant pressure a change in temperature has no significant effect on the specific rate of absorption. The dual effect of CO₂ solubility and the rate of reaction must be considered when the effect of temperature is evaluated. An increase in temperature causes a decrease in CO₂ solubility which decreases the specific absorption rate. An increase in temperature does however cause an increase in the liquid phase reaction rate, which facilitates an increase in the specific rate of absorption. The true temperature effect should become evident when a wider temperature range is considered. The characterization of the temperature effect on the absorption rate will become vital when deriving rate expressions to determine effective interfacial mass transfer area. If, as suspected, the rate expressions are of the same form as in Chapter 6, the rate constants will be dependent on temperature according to an Arrhenius type expression.

7.3 Specific Absorption Model Proposed by Erasmus, 2004

After evaluating the temperature and concentration effect on the specific rate of absorption, Erasmus proceeded to model a power rate expression on his experimental data:

$$N_{\text{CO}_2} = k \cdot p_{\text{CO}_2}^{0.9} \cdot C_{\text{MEA}}^{0.93} \quad (2.98)$$

with the temperature dependence of the specific absorption rate modeled with a rate constant of the form:

$$k = -3.818 \times 10^{-6} \cdot T + 2.985 \times 10^{-3} \quad (2.99)$$

The results obtained from a model fit of equation 2.98 on the data obtained at 25°C and an MEA concentration of 0.25mol/L is illustrated in **Figure 7.7**:

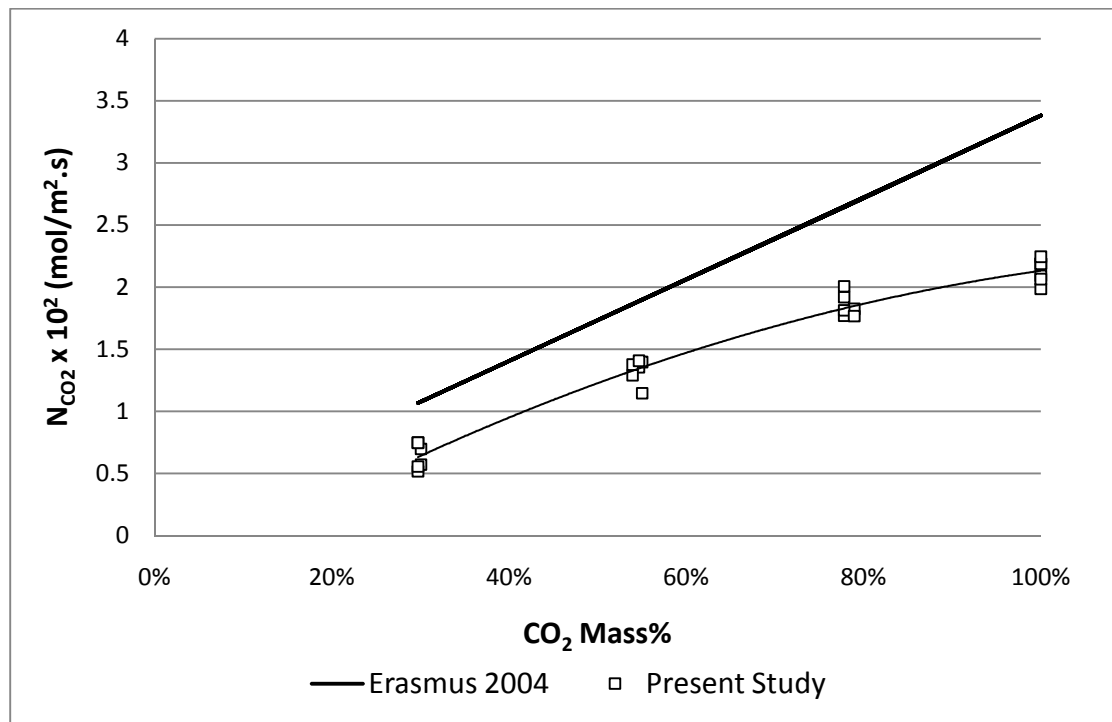


Figure 7.7: Model Fit of Equation 2.98 at 25°C, [MEA]_i = 0.25mol/L

From **Figure 7.7** it can be seen that the experimentally determined specific absorption rates are lower than the rates calculated with equation 2.98 at higher

CO₂ mass%. This may be due to the fact that equation 2.98 was extrapolated well outside of the concentration range that it was derived for. It may also be that the difference in solvent used causes the over prediction of the model, since it has already been stated that CO₂ is 7.7 – 7.8% more soluble in less polar solvent such as n-propanol relative to 2-propanol. It may further be noticed from **Figure 7.7** that the trends in the data are different. Equation 2.98 follows a near linear trend whilst the data in this study shows a parabolic trend. This may be due to the difference in CO₂ concentrations investigated. Equation 2.98 is derived for low CO₂ concentrations, where the absorption rate may be approximated with a near linear correlation. As the CO₂ concentration increases the rate of absorption strives towards a maximum at each MEA concentration. This trend may also be as a result of the high CO₂ concentrations absorbing into relatively low MEA concentrations. The MEA concentration will decrease very rapidly which will slow the reaction rate after a very short time and allow the liquid side mass transfer resistance to control the absorption rate.

It may therefore indicate that the derivation of an alternative rate expression for different solvent systems should be investigated and tested over a wide range of CO₂ and MEA concentrations. This rate expression will form the basis for the method of determining the effective interfacial mass transfer area over a wide CO₂ and MEA concentration range. This will be investigated in future work.

7.4 Relevance of Reaction Kinetics

Equation 2.98 may be used to estimate the effective interfacial mass transfer area on structured packing material. This is achieved by performing a material balance for CO₂ over the length of a short piece of structured packing. The material balance results in equation 2.102 for determining the effective interfacial mass transfer area:

$$a_e = \frac{n_{\text{CO}_2}}{A_s \int_{z=0}^{z=h} N_{\text{CO}_2} dz} \quad (2.102)$$

By measuring the difference in CO₂ gas concentration over the packing material and by estimating the contact time, the rate of CO₂ absorption, n_{CO_2} , can be determined.

Using short sections of packing material, it may be assumed that a linear concentration profile exists for both species over the length of the packing material.

By determining the specific absorption rate for various CO₂ and MEA concentrations along their respective linear concentration profiles with equation 2.98, the integral in equation 2.102 could be solved numerically to determine the effective interfacial mass transfer area.

Absorption experiments at three different wetted wall column heights were conducted to test the assumption of linear CO₂ and MEA concentration profiles. As already indicated in **Figure 7.3** the rate of CO₂ absorption seemingly increases non-linearly with an increase in the exposed liquid surface area. The liquid surface area is a function of the column height, so it may be deduced that an increase in the column length results in a non-linear increase in the amount of CO₂ absorbed per time. This indicates a non-linear CO₂ concentration profile along the length of the column.

Since the liquid was not analysed for CO₂ concentration, the amount of CO₂ reacted could not be determined, which means that an accurate CO₂ concentration profile cannot be presented. The liquid was however analyzed for MEA and an MEA concentration profile over the length of the wetted wall column could be constructed. The profiles at 25°C, an initial MEA concentration of 0.25mol/L and a liquid flow rate of 1.54mL/s are illustrated in **Figure 7.8**:

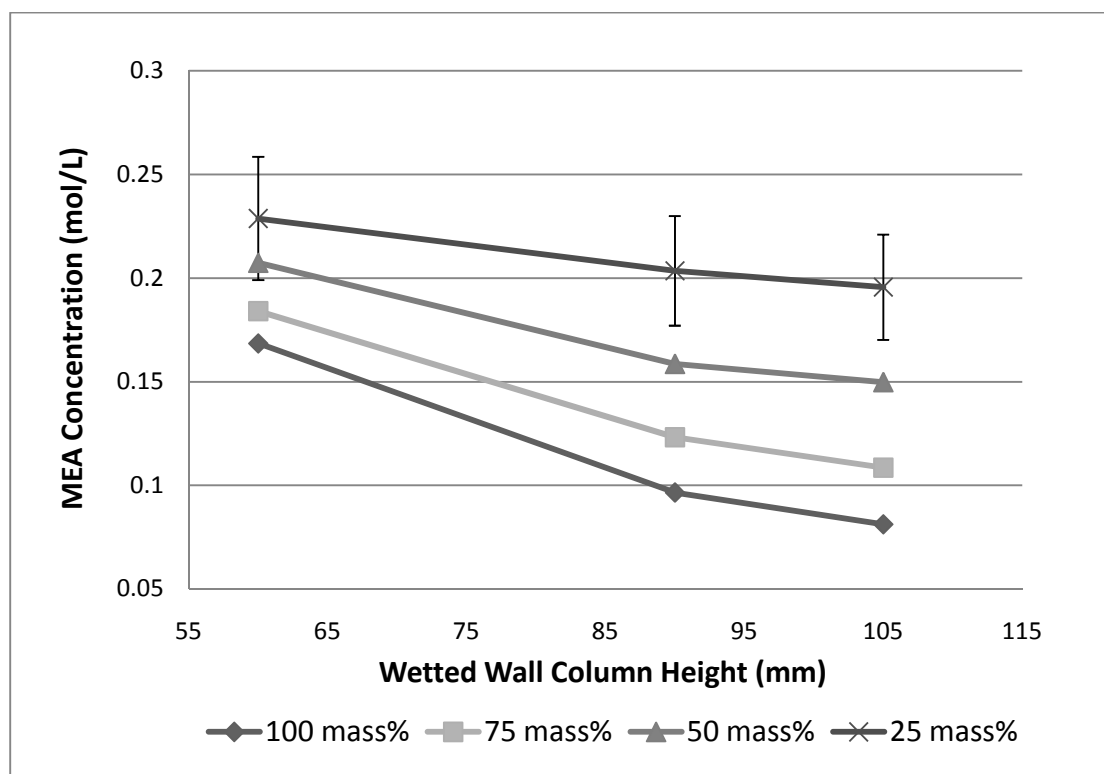


Figure 7.8: MEA Concentrations for Different Column Heights

From **Figure 7.8** the expected decrease in MEA concentration with an increase in column height can be seen. The error bars in **Figure 7.8** represent the 13% repeatability range achieved in the titration analysis of the MEA concentration. The exponential decline in the MEA concentrations is not obvious from **Figure 7.8** but it may be concluded that a linear concentration profile is also not obvious. Based on the MEA concentration profiles obtained in the reaction kinetic study, the assumption of a linear concentration profile is rejected.

Based on the evaluation of the absorption rate expression proposed by Erasmus and the discussion concerning the concentration profiles of CO_2 and MEA along the length of the wetted wall column the relevance of the reaction kinetic comes into play: By incorporating a technique for analysing both CO_2 and MEA concentrations in the liquid phase it will firstly be possible to derive a more accurate absorption rate expression. The liquid analysis will secondly shed light on accurately determining the CO_2 and MEA concentration profiles, eliminating the need to assume a linear profile. With these two discoveries working in tandem, the effective interfacial mass transfer area in equation 2.102 may be determined accurately. Refer to Chapter 9 for the recommended future investigations based on the results obtained in this reactive absorption study.

CHAPTER 8: CONCLUSIONS

Based on the results obtained in the reactive absorption study of CO₂ into a solution of MEA/2-propanol the following may be concluded:

An isothermal CSTR experimental set-up was successfully constructed to conduct the homogeneous liquid phase reaction kinetic study. The method of analysis was designed to stop the reaction after set contact times to enable the construction of a concentration – residence time profile for both CO₂ and MEA.

Both CO₂ and MEA concentration profiles show a sharp decline in concentration from reaction initiation which becomes more gradual as the reaction strives toward equilibrium. The error in CO₂ analysis resulted in a confidence interval of 0.002 mol/L for the CO₂ concentration profile and the error in MEA analysis resulted in a confidence interval of 0.012 mol/L for the MEA profile.

Based on the conversion profiles obtained for CO₂ and MEA it was found that 100% conversion of the limiting reactant was not achieved for the operating conditions specified in this study. It is thus concluded that the governing reaction mechanism consists of two consecutive reversible reactions instead of a reversible followed by an irreversible reaction as suggested in literature.

It was found that the reaction rate increases with an increase in temperature and an increase in the initial concentrations of both species. This could be concluded with a good degree of certainty based on the CO₂ concentration and reaction rate profiles, since the data trends fall outside of the error range for CO₂ analysis. A peak is noticed on the MEA rate profile which indicates that the reaction rate increases initially, before it starts to decrease as the reaction strives towards equilibrium. The relative reaction rate profiles seemingly converges to a value of 2 as the reaction strives towards equilibrium, which is once again in agreement with the overall reaction stoichiometry.

An increase in temperature increases the initial rate of reaction. An increase in temperature seemingly decreases the species conversion as the reaction strives to equilibrium, which is in agreement with the nature of an exothermic reaction, but it could not be concluded to a high degree of certainty due to the experimental error

in the data. There is an increase in reaction rate with an increase in relative initial concentration of MEA:CO₂, which is expected.

Conclusions regarding the effect of temperature and concentration on the zwitterion concentration profile could not be made with a high level of certainty since its profiles has a relatively large error of 0.0008 mol/L. It was found that the salt concentration increases with an increase in relative initial concentration and decreased with an increase in temperature.

By implementing a non-linear regression technique and utilizing the Levenberg-Marquard optimization algorithm, the experimentally determined rate data could be modeled on various reaction rate expressions. It was found that both the power rate law gives a reasonable fit of the data, but does not follow the peak in the reaction rate profile. It is therefore not completely rejected, since it is an easy model structure to work with and it does fit the data leading up to reaction equilibrium well. The pseudo-steady state hypothesis (PSSH) rate expressions proved to be insufficient in modelling the data.

A fundamental model structure derived from first principles was found to give a reasonably accurate fit of the experimental data. The proposed model structure is as follows:

$$-r_{\text{MEA}} = k_1 [\text{CO}_2][\text{RNH}_2] - k_2 [\text{Z}] + k_3 [\text{Z}][\text{RNH}_2] - k_4 [\text{S}]^2 \quad (\text{Model 1})$$

Model 1 provides for good fit over the entire temperature and concentration range of this study. Due to the fact that only 20 data points were available to estimate 4 model parameters over a highly non-linear model error surface, some of the model parameters determined cannot be deemed trustworthy because of large confidence intervals resulting. For this reason a temperature dependence of the estimated parameters could not be determined.

The specific absorption rate of CO₂ into various solutions of MEA/2-propanol on a wetted wall experimental set-up was firstly found to be independent of contact time, which supports the rapid nature of the reaction, secondly to increase with an

increase in MEA concentration, supporting the findings in the reaction kinetic study and thirdly to be independent of temperature.

The absorption rate expression derived by Erasmus (2004) for low CO₂ concentrations over predicts the specific absorption rate at high concentrations. The over prediction may also be due to the fact that CO₂ is 7% less soluble in 2-propanol than n-propanol at the temperatures investigated in this study. Erasmus used n-propanol as solvent. Based on this finding, an alternative rate expression should be derived for use at high CO₂ mass percentages, with 2-propanol as solvent. This expression will form the basis of a method to determine the effective interfacial mass transfer on structured packing material.

It may finally be concluded that the assumption of linear CO₂ and MEA liquid concentration profiles for determining the effective interfacial mass transfer area on structured packing is an over-simplification.

CHAPTER 9: RECOMMENDED FUTURE WORK

Based on the conclusions made from the results obtained in both studies, certain areas of interest have been identified for future investigation. These areas will briefly be discussed in this chapter.

9.1 Continuous Time Concentration Profiles

All the concentration data in this study is determined with respect to residence time and not continuous time. This may have a significant effect on the model parameters estimated in this study. Once a concentration profile is represented in continuous time, it may be expressed as a continuous curve and therefore allows for an abundant amount of data points available for modelling purposes. The difficulty lies in accurately determining the concentration- continuous time data. It is recommended that a semi-batch, micro-reactor is used incorporating the method of MEA scavenging with benzoyl chloride. Different solvents, preferably with a high CO₂ solubility should also be investigated.

9.2 Effective Interfacial Mass Transfer Area

It is recommended that the technique of MEA scavenging with benzoyl chloride be implemented to stop the absorption reaction at various wetted wall column heights. This will allow for the accurate determination of the absorption rate expression from reactive absorption data as well as the CO₂ and MEA concentration profiles along the height and width of the separation column. With these expressions known, it will firstly be possible to determine the effective interfacial mass transfer area on the structured packing material and secondly to model the mass transfer on a reaction rate basis.

It will however firstly be necessary to determine the effective interfacial mass transfer area of the structured packing by studying the reactive absorption of CO₂ into a primary amine solution (Danckwerts, 1979, Charpentier, 1981 and Erasmus,

2004), deriving the appropriate specific absorption rate expression based on non-power rate law kinetics and evaluating equation 2.116. This may be achieved on the same wetted wall experimental set-up.

9.3 Modifications of the Wetted Wall Set-up

Based on the results obtained in Chapter 7 and for the purpose of determining the effective interfacial mass transfer area on structured packing material, the wetted wall set-up will be subject to certain improvements and modifications.

It is firstly recommended that both CO₂ and the solute gas inlet flow rates are controlled with mass flow controllers. The outlet gas should preferably not be analysed with a MFC, since its sensitivity promotes error in the measurements. It is recommended that the outlet gas be analysed with a gas totaliser and either a CO₂ concentration analyser that can measure the full range of CO₂ volume fractions or by means of gas chromatography techniques. The low CO₂ concentration study should incorporate soap bubble flow meters to avoid the inaccuracies of calibrating electronic equipment. This may solve the sensitivity situation encountered at the low CO₂ mass percentages investigated. This, accompanied with the MEA scavenging technique, should provide for more accurate absorption data.

Absorption runs at longer column lengths should be investigated. To avoid liquid surface waves, the use of a surfactant should be investigated. The effect of the surfactant on the absorption rate of CO₂ should be investigated as well as its effect on the effective interfacial mass transfer area on structured packing material.

It is recommended that the wetted wall set-up is also modified to evenly distribute liquid on a section of packing material wrapped around the base column. The liquid distribution will be achieved by means of a distribution cap with channels designed specifically to achieve even distribution on packing material. The exit collar will also be modified to accommodate the packing material. These small scale experiments for determining the effective interfacial mass transfer area will be repeated on a distillation column with larger sections of packing material to verify the results obtained.

REFERENCES

Alvarez-Fuster, C., Midoux, N., Laurent, A. and Charpentier, J.C. (1980). "Chemical Kinetics of the Reaction of Carbon Dioxide with Amines in Pseudo m, n^{th} Order Conditions in Aqueous and Organic Solutions", *Chem. Eng. Sci.*, **35**, 1717.

Alvarez-Fuster, C., Midoux, N., Laurent, A. and Charpentier, J.C. (1981). "Chemical Kinetics of the Reaction of Carbon Dioxide with Amines in Pseudo m, n^{th} Order Conditions in Polar and Viscous Organic Solutions", *Chem. Eng. Sci.*, **36**, 1513.

Aresta, M, *Carbon Dioxide Recovery and Utilization*, Springer, 2003

Astarita (1967), G. *Mass Transfer with Chemical Reaction*, Elsevier, Amsterdam.

Barth, D., Tondre, C. and Delpuech, J.J., (1984). "Kinetics and Mechanisms of the Reactions of Carbon Dioxide with Alkanolamines: A Discussion Concerning the Cases of MDEA and DEA", *Chem. Eng. Sci.*, **39**, 1753.

Blauwhoff, P.M.M., Versteeg, G.F. and van Swaaij, W.P.M. (1982). "A Study on the Reaction between CO_2 and Alkanolamines in Aqueous Solutions", *Chem. Eng. Sci.*, **39**, 207.

Bratzler, K. and Doerges, A. (1974). "Amisol Process Purifies Gases", *Hydrocarbon Proc*, **1974**, 78

Bretsznajder, S.. *Prediction of Transport and Other Physical Properties of Fluids*, Volume 11, Pergamon Press, New York (1971).

Caplow, M., (1968). "Kinetics of carbamate formation and breakdown", *J. Am. chem. Soc.* **90**, 6795 – 6803.

Charpentier, J.C. (1981). "Mass Transfer Rates in Gas-Liquid Absorbers", *Advances in Chemical Engineering*, Vol. 11 Academic Press, New York.

Danckwerts, P.V. (1970). *Gas-Liquid Reactions*, McGraw-Hill, New York.

Danckwerts, P.V. and Sharma, M.M. (1966). "The Absorption of Carbon Dioxide into solutions of Alkalis and amines", *The Chemical Engineer*, **44**, CE244.

Danckwerts, P.V. (1979). "The Reaction of CO₂ with Ethanolamines", *Chem. Eng. Sci.*, **34**, 443.

Davies, R.A., Ponter, A.B and Craine, K. (1967). "The Diffusion of Carbon Dioxide in Organic Liquids", *Can. J. Chem. Eng.*, **45**, 372.

Davis, R.A. and Sandall, O.C. (1993). "Kinetics of the Reaction of Carbon Dioxide with Secondary Amines in Polyethylene Glycol", *Chem. Eng. Sci.*, **48**, 3187.

Erasmus, A.B. (2004) *Mass Transfer in Structured Packing*, PhD Dissertation Stellenbosch, University of Stellenbosch,

Fogler, H.S. (1999) *Elements of Chemical Reaction Engineering*, Third Edition, Prentice-Hall International, Inc. New Jersey.

Hikita, H., Asai, S., Ishikawa, H. and Honda, M. (1976). "The Kinetics of Reactions of Carbon Dioxide with Monoethanolamine, Diethanolamine and Triethanolamine by Rapid Mixing Method", *Chem. Eng. Journal*, **13**, 7.

Hikita, H., Asai, S., Ishikawa, H. and Honda, M. (1977). "The Kinetics of Reactions of Carbon Dioxide with Monoisopropanolamine, Diglycolamine and Ethylenediamine by Rapid Mixing Method", *Chem. Eng. Journal*, **14**, 27.

Joosten, G.E.H. and Danckwerts, P.V. (1972), "Chemical Reaction and Effective Interfacial Areas in Gas Absorption", *Chem. Eng. Sci.*, **28**, 453.

Laddha, S.S., Danckwerts, P.V. (1980). "Reaction of CO₂ with Ethanolamines: Kinetics from Gas-Absorption", *Chem. Eng. Sci.*, **36**, 479.

Little, R.J., Versteeg, G.F. and van Swaaij, W.P.M. (1991). "Physical Absorption into Non-aqueous Solutions in a Stirred Cell Reactor", *Chem. Eng. Sci.*, **46**, 3308.

Little, R.J., Versteeg, G.F. and van Swaaij, W.P.M. (1992). "Kinetics of CO₂ with Primary and Secondary Amines in Aqueous Solutions – Zwitterion Deprotonation Kinetics for DEA and DIPA in Aqueous Blends of Alkanolamines", *Chem. Eng. Sci.*, **47**, 2027.

- McMurry, J. (2004) *Organic Chemistry*, 6th Edition, Brooks/Cole, Belmont, USA
- Morcuende, A., Ors, M., Valverde, S. and Herradon, B. (1996). "Microwave-Promoted Transformations: Fast and Chemoselective N-Acylation of Amino Alcohols Using Catalytic Amounts of Dibutyltin Oxide. Influence of the Power Output and the Nature of the Acylating Agent on the Selectivity", *J. Org. Chem.*, **61**, 5264 – 5270.
- Onda, K., Sada, E., Kobayashi, T. and Fujine, M. (1969), "Gas Absorption Accompanied by Complex Chemical Reactions – I Reversible Chemical Reactions", *Chem. Eng. Sci.*, **25**, 753.
- Onda, K., Sada, E., Kobayashi, T. and Fujine, M. (1969), "Gas Absorption Accompanied by Complex Chemical Reactions – II Consecutive Chemical Reactions", *Chem. Eng. Sci.*, **25**, 761.
- Onda, K., Sada, E., Kobayashi, T. and Fujine, M. (1970), "Gas Absorption Accompanied by Complex Chemical Reactions – III Parallel Chemical Reactions", *Chem. Eng. Sci.*, **25**, 1023.
- Onda, K., Sada, E., Kobayashi, T. and Fujine, M. (1969), "Gas Absorption Accompanied by Complex Chemical Reactions – IV Unsteady State", *Chem. Eng. Sci.*, **27**, 247.
- Oyevaar, M.H, Morssinkhof, R.W.J. and Westerterp, K. R. (1990) "The Kinetics of the Reaction Between CO₂ and Diethanolamine in Aqueous Ethyleneglycol at 298 K: A Viscous Gas-liquid Reaction System for the Determination of Interfacial Areas in Gas-liquid Contactors" *Chem. Eng. Sci.*, **45**, 3283.
- Puranik, S.A., Sharma, M.M. (1969), "Effective Interfacial Area in Packed Liquid Extraction Columns:", *Chem. Eng. Sci.*, **25**, 257.
- Reid, R.C., Sherwood, T.K. (1966), *The Properties of Gases and Liquids*, Second Edition, McGraw-Hill, New York.
- Roberts, D. and Danckwerts, P.V. (1962). " Kinetics of CO₂ absorption in alkaline solutions – I Transient absorption rates and catalysis by arsenite", *Chem. Eng. Sci.*, **17**, 961

- Sada, E., Kumazawa, H. and Butt, M.A. (1976). "Gas Absorption with Consecutive Chemical Reaction: Absorption of Carbon dioxide into Aqueous Amine solutions", *Can. J. Chem Eng.*, **54**, 421.
- Sada, E., Kumazawa, H., Han, Z.Q. and Matsuyama, H. (1985). "Chemical Kinetics of the Reaction of Carbon Dioxide with Ethanolamines in Nonaqueous Solvents", *AIChE J.*, **31**, 1297.
- Sridharan, K. and Sharma, M.M. (1976). "New Systems and Methods for the Measurement of Effective Interfacial Area and Mass Transfer Coefficients in Gas Liquid Contactors", *Chem. Eng. Sci.*, **31**, 767.
- Tokunaga, J. (1975), "Solubilities of Oxygen, Nitrogen, and Carbon Dioxide in Aqueous Alcohol Solutions", *J. Chem. and Eng. Data*, **20**, 41.
- Vas Bhat, R.D., Kuipers, J.A.M., Versteeg, G.F. (1999), "Mass Transfer with Complex Chemical Reaction in gas-Liquid Systems: Two-Step Reversible Reactions with Unit Stoichiometric and Kinetic Orders", *Chem. Eng. Jour.*, **76**, 127.
- Versteeg, G.F. and van Swaaij, P.M. (1988a). "On the Kinetics between CO₂ and Alkanolamines both in aqueous and Non-aqueous solutions – I. Primary and Secondary Amines", *Chem. Eng. Sci.*, **43**, 573.
- Versteeg, G.F. and van Swaaij, P.M. (1988b). "On the Kinetics between CO₂ and Alkanolamines both in aqueous and Non-aqueous solutions – II. Tertiary Amines", *Chem. Eng. Sci.*, **43**, 573.
- Versteeg, G.F. and Oyevaar (1988), M.H. "The Reaction Between CO₂ and Diethanolamine at 298 K", *Chem. Eng. Sci.*, **44**, 1264.
- Versteeg, G.F., Kuipers, J.A.M., van Beckhum, F.P.H. and van Swaaij, W.P.M.(1989), "Mass Transfer with Complex Reversible Chemical Reactions – II. Parallel Reversible Chemical Reactions.", *Chem. Eng. Sci.*, **45**, 183
- Wilkes, J.O. and Nedderman, R.M. (1961). "The Measurement of Velocities in Thin Films of Liquid", *Chem. Eng. Sci.*, **17**, 177.

APPENDIX

Table of Contents

APPENDIX A: Physical and Chemical Properties

APPENDIX B: Calibration Data and Design Calculations

APPENDIX C: Reaction Kinetics Experimental Data and Sample Calculations

APPENDIX D: Absorption Experimental Data and Sample Calculations

APPENDIX E: Equipment Specifications and Illustrations

APPENDIX F: Statistical Parameters of Interest for Model Evaluation

APPENDIX G: Model Data

APPENDIX A: PHYSICAL AND CHEMICAL PROPERTIES

A.1 Properties of CO₂ (g)

Molecular Weight	44.01
Specific Gravity	1.52
Specific Volume @ 21°C (m ³ /kg)	0.547
Density @ 15°C (kg/m ³)	1.87
Viscosity @ 0°C (cP)	0.014
Specific Heat, c _p (J/kgK)	0.037
Specific heat Ratio, c _p /c _v	1.32
Sublimation Point, 1atm (°C)	-78.5
Latent H _{vap} (J/kg)	571.08
Critical Temperature (°C)	31
Critical Pressure (MPa)	7.38
Critical Volume (m ³ /kg)	0.002155
Vapour Pressure @ 20°C (bar)	58.5

A.2 Properties of Argon

Molecular Weight	39.948
Specific Gravity	1.38
Specific Volume (m ³ /kg)	0.622
Density @ 25°C (kg/m ³)	1.4
Viscosity @ 25°C (cP)	0.02
Specific Heat, c _p (J/kgK)	523
Specific Heat Ratio, c _p /c _v	1.67
Boiling Point, 1atm (°C)	-186
Latent H _{vap} (J/kg)	1.63 E05
Melting Point, 1atm (°C)	-189.2
Critical Temperature (°C)	122
Critical Pressure (MPa)	4.87
Critical Volume (m ³ /kg)	0.00186

A.3 Properties of MEA

Molecular Weight	61.1
Specific Gravity	1.02
Specific Volume (m ³ /kg)	0.000988
Density @ 25°C (kg/m ³)	1012
Viscosity @ 25°C (cP)	19.37
Boiling Point, 1atm (°C)	170.5
Melting Point, 1atm (°C)	10.3
Vapour Pressure @ 20°C (Pa)	25
Corrosive	yes
Toxicology	Irritant to eyes, skin and lungs, toxic
Flammable	moderate fire hazard

A.4 Properties of 2-Propanol

Molecular Weight	60.1
Specific Gravity	0.786
Specific Volume (m ³ /kg)	0.001272
Density @ 25°C (kg/m ³)	786
Viscosity @ 25°C (cP)	1.96
Boiling Point, 1atm (°C)	82.3
Vapour Pressure @ 20°C (bar)	0.042
Melting Point, 1atm (°C)	-89
Flammable	yes

A.5 Properties of Benzoyl Chloride

Molecular Weight	140.57
Specific Gravity	1.21
Specific Volume (m ³ /kg)	0.0008264
Density @ 25°C (kg/m ³)	1210
Viscosity @ 25°C (cP)	1.2442
Boiling Point, 1atm (°C)	197.2

Corrosive	yes
Toxicology	Irritant to eyes, skin and lungs, toxic
Vapour Pressure @ 20°C (bar)	0.001
Melting Point, 1atm (°C)	-1

A.6 Density and Viscosity Data for MEA/2-propanol mixtures

The viscosities were determined with a roto-visco meter whilst a density flask of known volume (50mL exactly) was used to determine the densities. The density and viscosity data for the three concentrations of MEA in 2-propanol at the two operating temperatures is tabulated in **Table A1**:

Table A1: Density and Viscosity Data

MEA Concentration (mol/L)	Temperature (°C)	Viscosity (mPa.s)	Density (kg/m ³)
0.25	25	3.31	790
	30	3.02	784
0.3	25	3.36	792
	30	3.08	786
1	25	3.81	798
	30	3.36	796

The temperature and concentration dependence of both viscosity and density is illustrated in **Figure A1** and **Figure A2**:

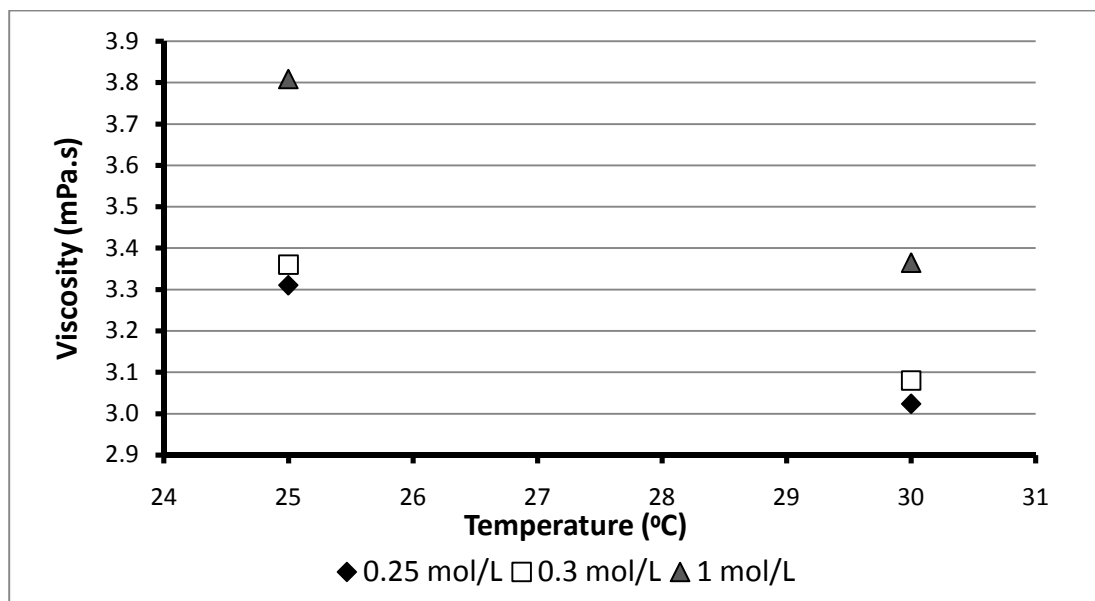


Figure A1: Temperature Dependence of Viscosity

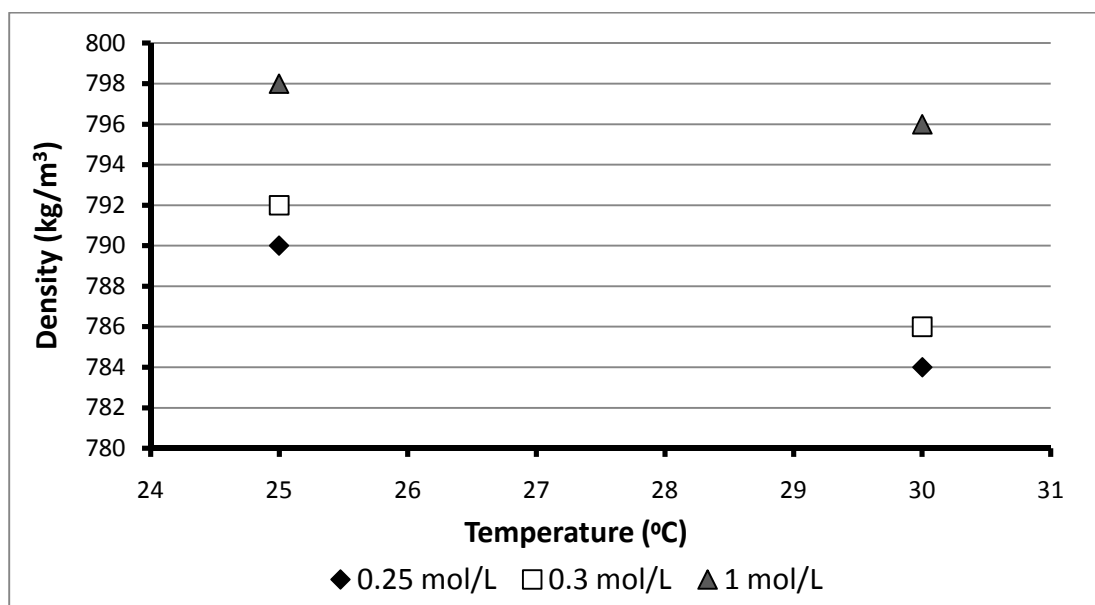


Figure A2: Temperature Dependence of Density

As expected, both density and viscosity decrease with an increase in temperature and both increase with an increase in MEA concentration.

APPENDIX B: CALIBRATION DATA AND DESIGN CALCULATIONS

B.1 Reaction Kinetics Pump Calibration

The calibration curves of the Sera pumps, 50L/hr capacity for 2-propanol liquid are illustrated in **Figures B1** and **B2**:

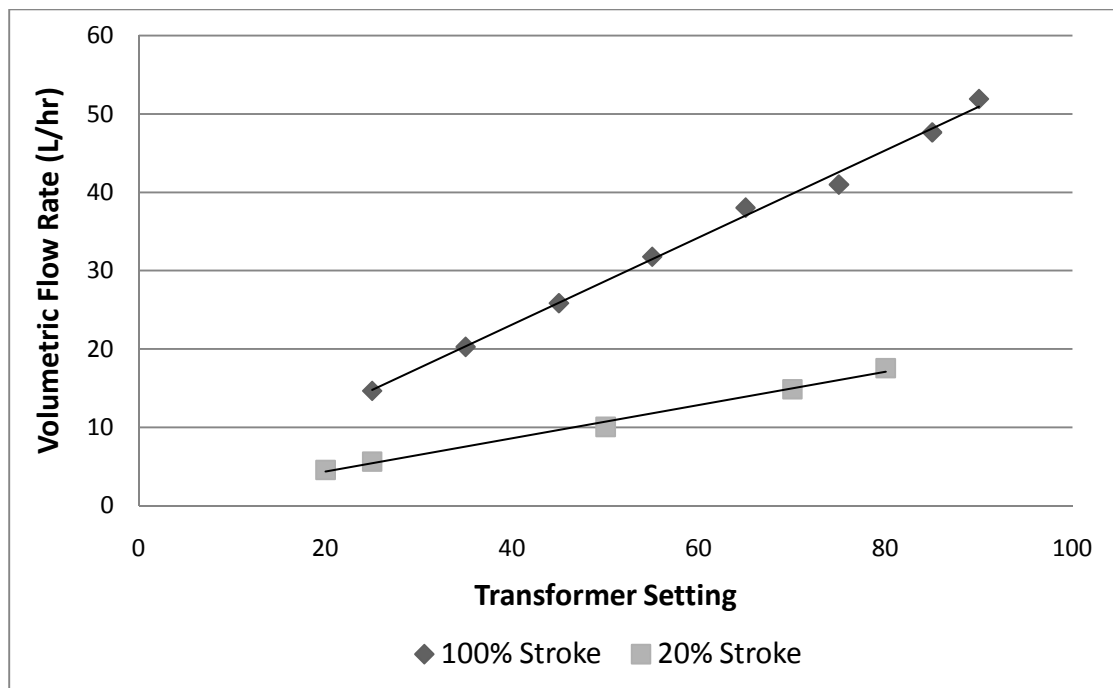


Figure B1: CO₂/2-propanol Pump Calibration Curve

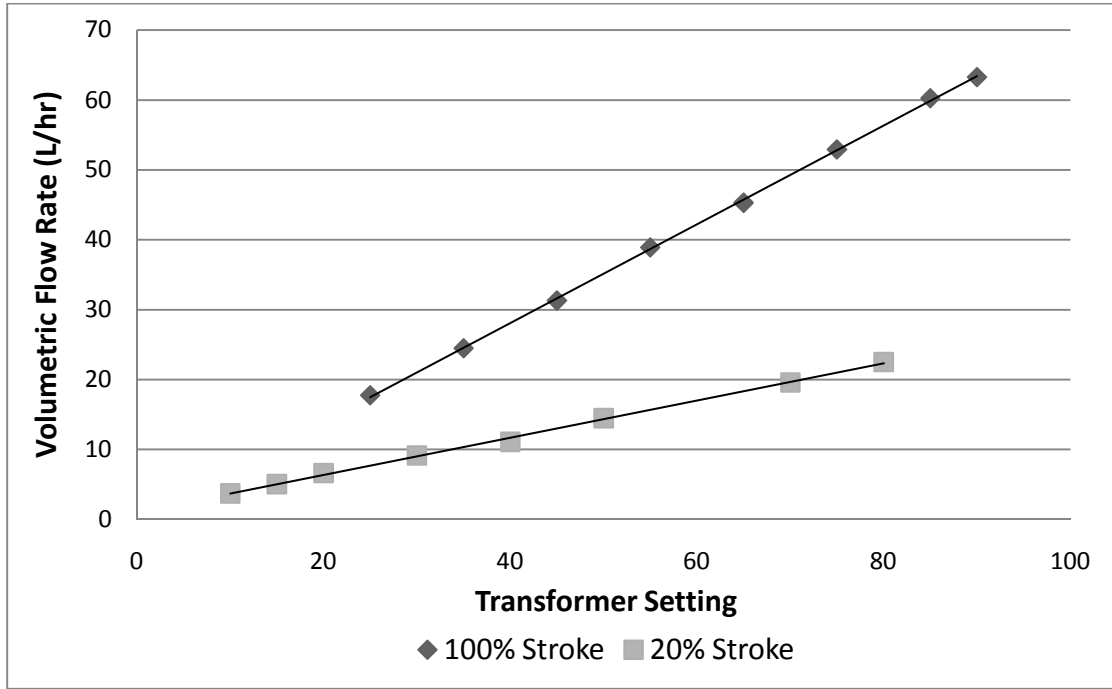


Figure B2: MEA/2-propanol Pump Calibration Curve

The calibration equations are (where x denotes the transformer setting):

CO₂/2-propanol 100% Stroke Length:

$$Q = 0.5567x + 0.8419 \quad R^2 = 0.9959 \quad (\text{B.1})$$

CO₂/2-propanol 20% Stroke Length:

$$Q = 0.2124x + 0.1311 \quad R^2 = 0.994 \quad (\text{B.2})$$

MEA/2-propanol 100% Stroke Length:

$$Q = 0.7065x - 0.1726 \quad R^2 = 0.9997 \quad (\text{B.3})$$

MEA/2-propanol 20% Stroke Length:

$$Q = 0.2661x + 1.0494 \quad R^2 = 0.9985 \quad (\text{B.4})$$

B.2 Sample Collection Times in Scavenging Unit

The times required for the collection of 60 mL of reactor effluent to the scavenging unit is tabulated in **Table B.1**:

Table B.1 Times per Run

Run #	Pump Stroke (%)	CO ₂ Pump Setting	MEA pump Setting	Total Flow Rate (mL/s)	Time/60ml sample (s)
1	100	88.3	71.0	27.77	2.16
2	100	79.3	63.9	24.99	2.4
3	100	70.3	56.9	22.22	2.7
4	100	61.4	49.8	19.45	3.08
5	100	52.4	42.7	16.67	3.6
6	100	43.4	35.6	13.88	4.32
7	100	34.4	28.6	11.12	5.4
8	20	70.0	52.4	8.33	7.2
9	20	46.5	33.6	5.56	10.8
10	20	22.9	14.8	2.77	21.64

B.3 Mass Flow Controller Calibration Data

The mass flow controllers had to be calibrated for both CO₂ and argon. This was achieved by placing the gas cylinder on a scale and noting the change in mass over time. This revealed the actual mass expelled from the cylinder over time. The MFC reading was noted at the same time intervals and a MFC reading vs. time profile constructed. The time integral of this profile revealed the mass expelled predicted by the MFC. The correction factor was calculated from:

$$f = \frac{m_{\text{Actual}}}{m_{\text{MFC}}} \quad (\text{B.5})$$

As an example, the MFC reading vs. time profile and scale reading vs. time profile for one of the CO₂ calibrations is illustrated in **Figures B3** and **B4** respectively:

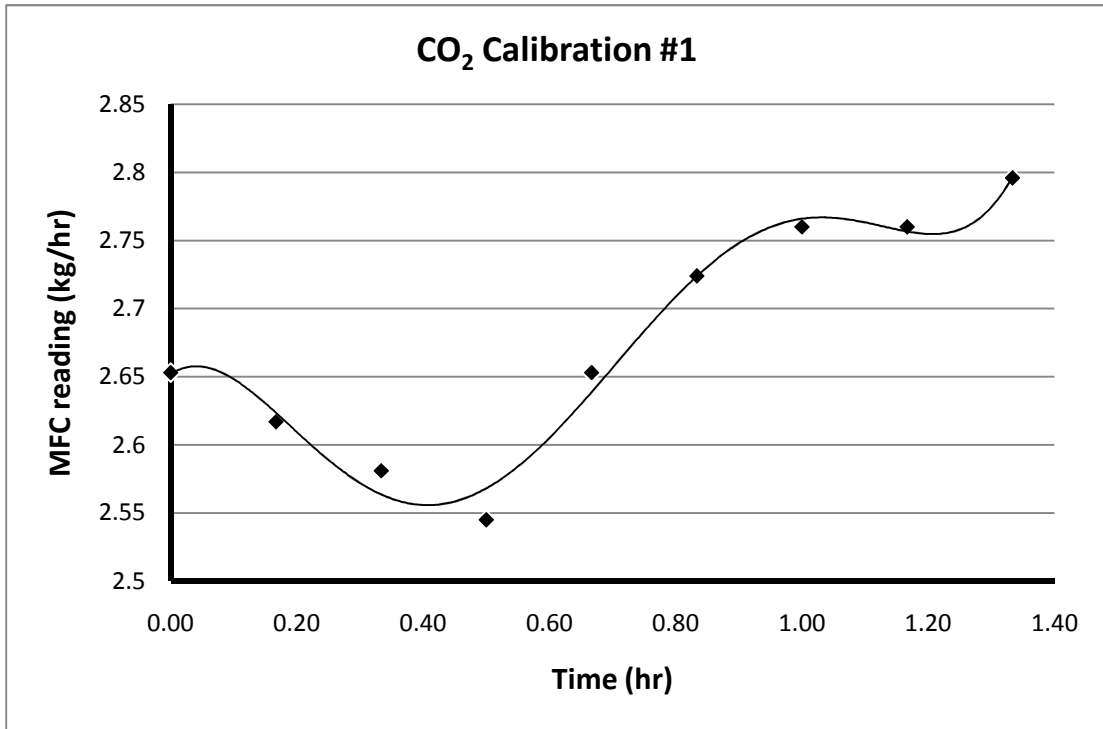


Figure B3: MFC reading vs. Time for CO₂ Calibration #1

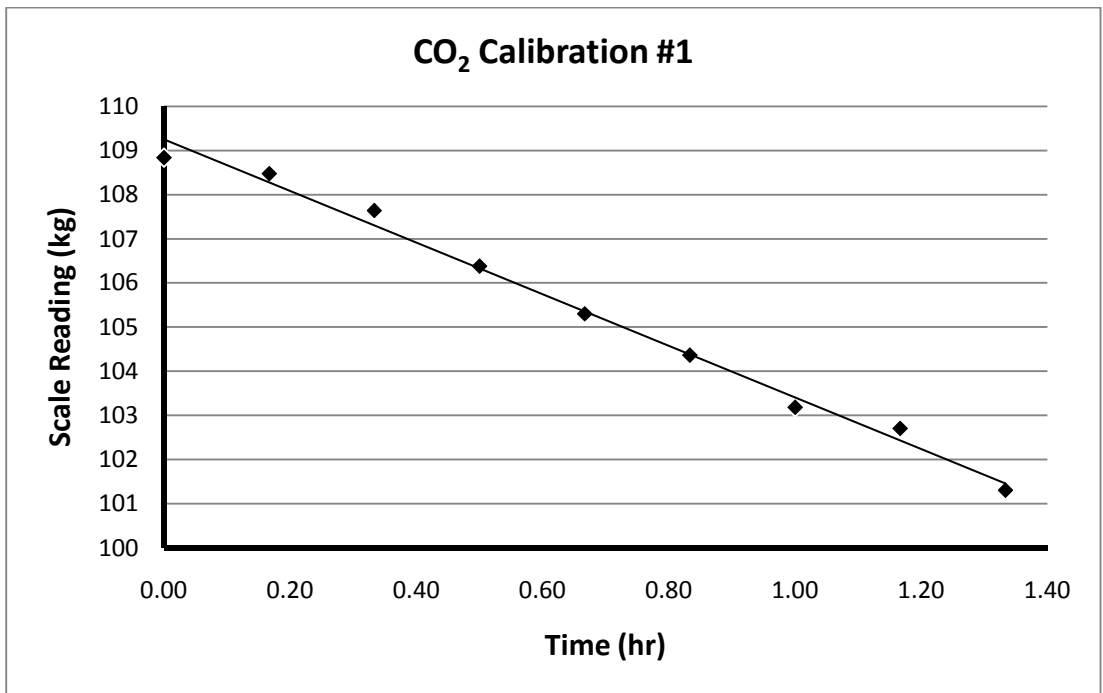


Figure B4: Scale Reading vs. Time for CO₂ Calibration #1

The calibration data for the mass flow controllers for both CO₂ and argon are tabulated in **Table B1** to **Table B5**:

Table B1: CO₂ Calibration Data for Calibration #1

Time (min)	Time (hr)	MFC setting (kg/hr)	Scales (kg)
0	0.00	0.52	79.24
10	0.17	0.54	78.96
15	0.25	0.55	78.89
20	0.33	0.56	78.78
25	0.42	0.55	78.73
30	0.50	0.54	78.65
Mass Expelled According to MFC (kg)			0.27
Actual Mass Expelled (kg)			0.59
Correction Factor			2.17

Table B2: CO₂ Calibration Data for Calibration #2

Time (min)	Time (hr)	MFC (kg/hr)	Scale (kg)
0	0.00	1.36	101.54
10	0.17	1.36	101.14
20	0.33	1.36	100.34
30	0.50	1.36	99.62
40	0.67	1.36	99.16
50	0.83	1.40	98.02
60	1.00	1.43	97.36
70	1.17	1.47	96.66
80	1.33	1.51	95.82
90	1.50	1.51	94.76
Mass Expelled According to MFC (kg)			3.13
Actual Mass Expelled (kg)			6.78
Correction Factor			2.17

Table B3: CO₂ Calibration Data for Calibration #3

Time (min)	Time (hr)	MFC (kg/hr)	Scale (kg)
0	0.00	2.65	108.84
10	0.17	2.62	108.48
20	0.33	2.58	107.64
30	0.50	2.55	106.38
40	0.67	2.65	105.3
50	0.83	2.72	104.36
60	1.00	2.76	103.18
70	1.17	2.76	102.7
80	1.33	2.80	101.1
Mass Expelled According to MFC (kg)			3.56
Actual Mass Expelled (kg)			7.74
Correction Factor			2.17

Table B4: Argon Calibration Data for Calibration #1

Time (min)	Time (hr)	MFC setting (kg/hr)	Scales (kg)
0	0.00	0.52	79.24
10	0.17	0.54	78.96
15	0.25	0.56	78.8
20	0.33	0.56	78.64
25	0.42	0.55	78.48
30	0.50	0.53	78.36
Mass Expelled According to MFC (kg)			0.27
Actual Mass Expelled (kg)			0.88
Correction Factor			3.23

Table B5: Argon Calibration Data for Calibration #2

Time (min)	Time (hr)	MFC setting (kg/hr)	Scales (kg)
0	0.00	1.51	78.26
10	0.17	1.51	77.44
15	0.25	1.51	77.04
20	0.33	1.51	76.62
Mass Expelled According to MFC (kg)			0.50
Actual Mass Expelled (kg)			1.64
Correction Factor			3.26

Table B6: Argon Calibration Data for Calibration #3

Time (min)	Time (hr)	MFC setting (kg/hr)	Scales (kg)
0	0.00	2.55	95.3
5	0.08	2.55	94.48
10	0.17	2.57	93.72
15	0.25	2.62	93
20	0.33	2.67	92.32
25	0.42	2.71	91.78
Mass Expelled According to MFC (kg)			1.09
Actual Mass Expelled (kg)			3.52
Correction Factor			3.24

The factors were tested and confirmed at lower and higher flow rates. A summary of the correction factors are tabulated in **Table B7**:

Table B7: Summary of MFC Calibration Correction Factors

Gas	Correction Factor	%Error	MFC Range
CO ₂	2.175	±0.39	0.1 - 5
Argon	3.241	±0.57	0.3 - 5

B.4 Gas Mixture Calibration Data

The calibration data for the gas mixture flow rates are tabulated in **Table B11**:

MFC _{CO2}	MFC _{outlet}	m _{CO2,in} (kg/hr)	Time for 10 L gas to flow through (s)	Gas Density x 10 ⁶ (kg/L)	m _{tot} (kg/hr)	m _{Ar} (kg/hr)
2.03	2.03	4.42	14.58	1.79	4.42	0
1.81	2.04	3.94	13.69	1.74	4.57	0.63
1.58	1.99	3.44	12.61	1.68	4.80	1.36
1.38	2.01	3.00	11.75	1.63	5.01	2.01
1.21	2.01	2.63	10.12	1.58	5.63	3.00
1.04	2.05	2.26	9.51	1.55	5.88	3.61
0.81	2.01	1.76	9.05	1.52	6.03	4.27
0	2.01	0.00	7.68	1.4	6.58	6.58

The calibration curves are illustrated in **Figures B5** and **B6** respectively:

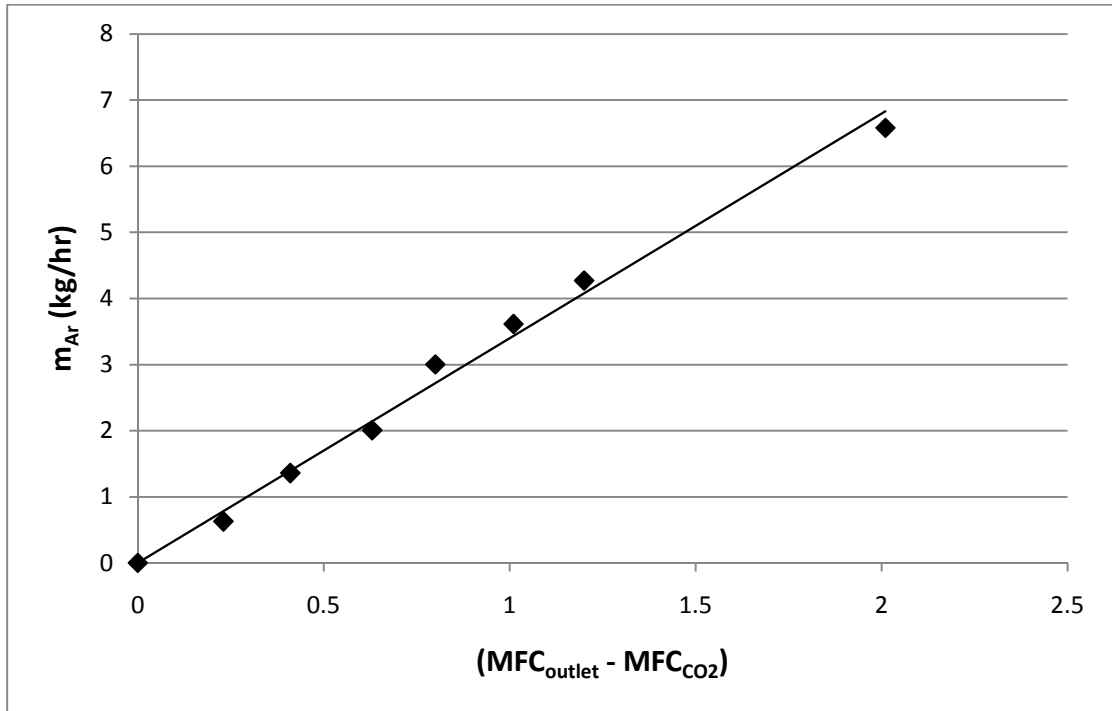


Figure B5: Calibration Curve for Argon Mass Flow Rate

Calibration equation from **Figure B5**:

$$\dot{m}_{Ar} = 3.398(MFC_{outlet} - MFC_{CO_2}), \quad R^2 = 0.9921 \quad (B6)$$

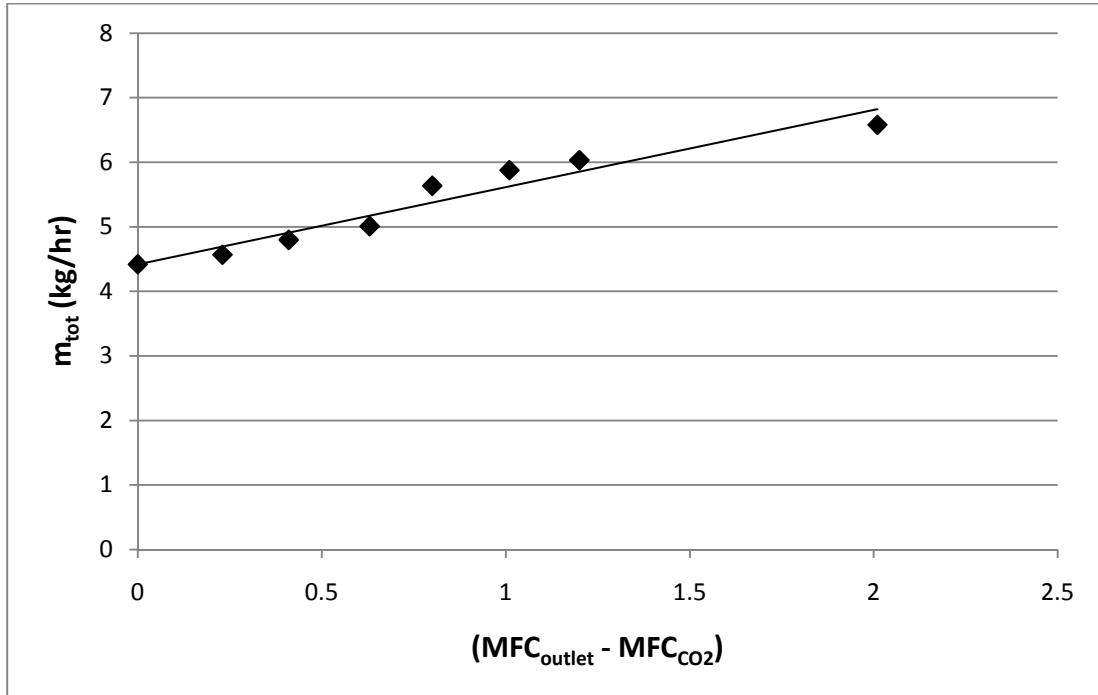


Figure B6: Calibration Curve for Total Mass Flow Rate

Calibration equation from **Figure B6**:

$$\dot{m}_{\text{tot}} = 1.199(\text{MFC}_{\text{outlet}} - \text{MFC}_{\text{CO}_2}) + 4.415, \quad R^2 = 0.9347 \quad (\text{B7})$$

B.5 Calculating CSTR Water Jacket Flow Rate

The minimum flow rate to the water jacket to prevent any significant temperature change with reaction is calculated from equation 3.25:

$$n_{\text{water}} = \frac{F_{\text{CO}_2, \text{in}} \cdot X \cdot \Delta H_{\text{rxn}}(T)}{c_{P, \text{water}} \cdot \Delta T_{\text{water}}} \quad (3.25)$$

to find the minimum flow rate, the conversion is assumed to be 1 and the maximum CO₂ flow rate of is applied. The heat of reaction was found in literature (Aresta, 2003). The maximum flow rate of CO₂ was taken to be its flow rate at 25°C when it is at its maximum solubility. The flow rate of water may now be calculated as follows:

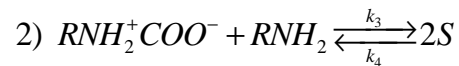
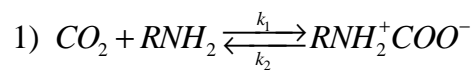
$$n_{\text{water}} = \frac{0.183 \times 1 \times 1919}{4.81 \times 0.5} = 146 \text{ kg/hr}$$

APPENDIX C: REACTION KINETICS EXPERIMENTAL DATA AND SAMPLE CALCULATIONS

C.1 Derivation of the PSSH Rate Expression

The pseudo-steady state rate expression of equation 6.5 is derived as follows:

Starting with the reaction rate expression:



The rate of disappearance of RNH_2 is:

$$-r_{\text{RNH}_2} = k_1 [\text{CO}_2] [\text{RNH}_2] - k_2 [\text{RNH}_2^+ \text{COO}^-] + k_3 [\text{RNH}_2^+ \text{COO}^-] [\text{RNH}_2] - k_4 [\text{S}]^2 \quad (1)$$

The rate of disappearance of CO_2 is:

$$-r_{\text{CO}_2} = \frac{(-r_{\text{RNH}_2})}{2} \quad (2)$$

The PSSH states that the rate of zwitterion formation is zero:

$$r_z = 0 = k_1 [\text{CO}_2] [\text{RNH}_2] - k_2 [\text{RNH}_2^+ \text{COO}^-] - k_3 [\text{RNH}_2^+ \text{COO}^-] [\text{RNH}_2] + k_4 [\text{S}]^2$$

rearranging:

$$[\text{RNH}_2^+ \text{COO}^-] = \frac{k_1 [\text{CO}_2] [\text{RNH}_2] + k_4 [\text{S}]^2}{k_2 + k_3 [\text{RNH}_2]} \quad (3)$$

substituting (3) into (1) and rearranging:

$$-r_{RNH_2} = \frac{2(k_1k_3[CO_2][RNH_2]^2 - k_2k_4[S]^2)}{k_2 + k_3[RNH_2]}$$

$$\therefore -r_{RNH_2} = \frac{2\left(\frac{k_1k_3}{k_2}[CO_2][RNH_2]^2 - k_4[S]^2\right)}{1 + \frac{k_3}{k_2}[RNH_2]} \quad (6.5)$$

If it is desired to express equation 6.5 in terms of CO₂, substitute (2) into (6.5):

$$-r_{CO_2} = \frac{\frac{k_1k_3}{k_2}[CO_2][RNH_2]^2 - k_4[S]^2}{1 + \frac{k_3}{k_2}[RNH_2]}$$

C.2 Calculating MEA Concentration from HPLC Data

The concentration of the unreacted MEA at 30°C, [MEA]_i = 2.5[CO₂] and a flow rate of 50 L/hr through the short residence time reactor will serve as reference for the sample calculation:

It was found from HPLC analysis that the precipitate was well mixed and the species evenly distributed. This was achieved by comparing the chromatograms of fragments of the precipitate and finding very similar species concentrations, within 5% of one another, which is within the 10.02% repeatability error presented in **Table 3.12**. The value of this is that a fraction of the total precipitate may now be dissolved in methanol, saving on methanol volumes used in the analysis.

Start with the sample mass (sm) dissolved in 5 ml methanol:

$$sm = 0.5078 \text{ g}$$

From the concentration of N-(2-hydroxyethyl) benzamide determined with HPLC, it is possible to determine the mass of N-(2-hydroxyethyl) benzamide in the sample:

$$m_{\text{N-(2-hydroxyethyl) benzamide}} = \frac{\text{HPLC concentration} \times \text{Total Sample Volume}}{10^6}$$

$$\therefore m_{\text{N-(2-hydroxyethyl) benzamide}} = \frac{89882.197 \times 5}{10^6} = 0.4494 \text{ g}$$

By adding 500 μ L of pure MEA to facilitate complete precipitation, enough N-(2-hydroxyethyl) benzamide is formed to render the mass of phenyl carb precipitate insignificant to the total mass of precipitate. The amount of N-(2-hydroxyethyl) benzamide representing the unreacted MEA in the precipitate may now be approximated by subtracting the N-(2-hydroxyethyl) benzamide formed from the added MEA from the total mass of precipitate. The fraction of this approximated amount in the total precipitate was found to exist in the sample as well. The approximated N-(2-hydroxyethyl) benzamide (NHB) from unreacted MEA in the sample may thus be calculated from:

$$\text{Approx. } m_{(\text{NHB})_{\text{Unreacted MEA}}} \text{ in sample} = \frac{(\text{Precipitate mass}) - (\text{NHB})_{\text{Added MEA}}}{(\text{Precipitate mass})} \times m_{\text{NHB in sample}}$$

$$\therefore \text{Approx. } m_{(\text{NHB})_{\text{Unreacted MEA}}} \text{ in sample} = \frac{2.63 - 0.506}{2.63} \times 0.4494$$

$$\therefore \text{Approx. } m_{(\text{NHB})_{\text{Unreacted MEA}}} \text{ in sample} = 0.218 \text{ g}$$

The actual mass of N-(2-hydroxyethyl) benzamide from unreacted MEA in the total precipitate can now be calculated from the fraction of this approximated mass in the sample:

$$\text{Mass } (\text{NHB})_{\text{Unreacted MEA}} \text{ in precipitate} = \frac{\text{Approx. } (\text{NHB})_{\text{Unreacted MEA}} \text{ in sample}}{\text{Mass of Sample}} \times \text{Precipitate mass}$$

$$\therefore \text{Mass } (\text{NHB})_{\text{Unreacted MEA}} \text{ in precipitate} = \frac{0.218}{0.5078} \times 2.63 = 1.13 \text{ g}$$

The mass of N-(2-hydroxyethyl) benzamide is converted to moles and applying the 1:1 mole ratio of MEA: N-(2-hydroxyethyl) benzamide the number of moles of unreacted MEA is calculated. The concentration of MEA is then determined by dividing the number of moles by the volume passed through the reactor:

$$n_{\text{N-(2-hydroxyethyl) benzamide}} = \frac{1.13}{165} = n_{\text{MEA}}$$

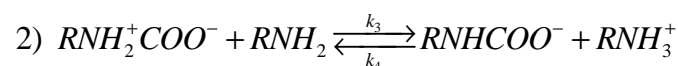
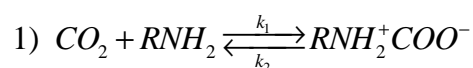
$$[\text{MEA}] = \frac{n_{\text{MEA}}}{0.061} = 0.113 \text{ mol/L}$$

C.3 Calculating Zwitterion and Salt Concentrations from HPLC Data

The zwitterion concentration is calculated by determining the mass of phenyl carb precipitate in the total precipitate. It is assumed that the phenyl carb concentration only consists of zwitterion. The mass of phenyl carb in the sample is calculated similarly to that of N-(2-hydroxyethyl) benzamide. The fraction of phenyl carb in the sample was found to hold true in the total precipitate from where the mass of phenyl carb in the precipitate can be calculated. The mass is converted to moles and by applying the 1:1 mole ratio of zwitterion:phenyl carb the number of moles of zwitterion is calculated. The zwitterion concentration is then determined by dividing the number of moles by the volume passed through the reactor

With the zwitterion concentration calculated, it is possible to calculate the salt concentration from a carbon and nitrogen balance:

Start with the reaction mechanism:



$$\text{Let } Z = \text{RNH}_2^+ \text{COO}^- \text{ and } S = \text{RNHCOO}^- = \text{RNH}_3^+$$

Carbon balance:

$$n_{\text{CO}_2, \text{begin}} = n_{\text{CO}_2, \text{end}} + n_{\text{RN}_2^+ \text{COO}^-} + n_{\text{RNHCOO}^-}$$

$$\therefore n_{\text{CO}_2, \text{begin}} = n_{\text{CO}_2, \text{end}} + n_Z + n_S$$

Since the volume is the same for all species:

$$[\text{CO}_2]_{\text{begin}} = [\text{CO}_2]_{\text{end}} + [\text{Z}] + [\text{S}] \quad (\text{C7})$$

rearranging (C7):

$$[\text{S}] = [\text{CO}_2]_{\text{begin}} - [\text{CO}_2]_{\text{end}} - [\text{Z}] \quad (\text{C8})$$

Nitrogen balance:

Following the same procedure as for the carbon balance, the following may be derived from a nitrogen balance:

$$[\text{S}] = \frac{[\text{RNH}_2]_{\text{begin}} - [\text{RNH}_2]_{\text{end}} - [\text{Z}]}{2} \quad (\text{C9})$$

the concentration of S may now be calculated from:

$$[\text{S}] = \frac{[\text{S}]_{(\text{C8})} + [\text{S}]_{(\text{C9})}}{2} \quad (\text{C10})$$

C.4 Reaction Kinetic Data at 25°C

Table C1: Reaction Kinetic Data, T = 25°C, [MEA]_i = [CO₂]_i

τ (s)	[CO ₂] (mol/L)	X _{CO2} (%)	-r _{CO2} (mol/L.s)	[MEA] (mol/L)	X _{MEA} (%)	-r _{MEA} (mol/L.s)	-r _{MEA} /-r _{CO2}	[Z] (mol/L)	[S] (mol/L)
0.000	0.083			0.083					
0.465	0.068	18.4%	0.033	0.059	29.3%	0.053	1.59	1.379E-03	0.013
0.516	0.065	22.1%	0.036	0.050	40.4%	0.065	1.83	2.094E-03	0.016
0.581	0.063	24.5%	0.035	0.044	47.1%	0.068	1.92	1.704E-03	0.019
0.664	0.060	28.1%	0.035	0.038	53.9%	0.068	1.92	9.409E-04	0.022
0.774	0.057	31.6%	0.034	0.033	60.2%	0.065	1.90	5.271E-04	0.025
0.929	0.058	31.0%	0.028	0.032	61.5%	0.055	1.98	4.198E-04	0.025
1.161	0.054	35.7%	0.026	0.026	69.3%	0.050	1.94	3.079E-04	0.029
1.549	0.054	35.3%	0.019	0.025	69.8%	0.038	1.98	6.281E-04	0.029
2.323	0.051	38.3%	0.014	0.017	79.8%	0.029	2.08	8.270E-04	0.032
3.257	0.051	39.1%	0.010	0.014	83.3%	0.021	2.13	2.309E-04	0.033
3.619	0.050	40.3%	0.009	0.012	86.1%	0.020	2.13	3.566E-04	0.035
4.646	0.049	41.3%	0.007	0.014	83.3%	0.015	2.02	3.570E-04	0.034
4.072	0.045	45.7%	0.009	0.005	94.3%	0.019	2.06	1.173E-03	0.038
4.653	0.043	48.2%	0.009	0.003	96.3%	0.017	2.00	6.600E-04	0.040
5.429	0.044	47.2%	0.007	0.002	97.2%	0.015	2.06	7.052E-04	0.039
6.514	0.043	48.4%	0.006	0.003	95.8%	0.012	1.98	2.705E-04	0.040
8.143	0.042	49.5%	0.005	0.002	98.2%	0.010	1.98	6.487E-04	0.041
10.857	0.043	48.3%	0.004	0.002	98.1%	0.008	2.03	6.615E-04	0.040
16.286	0.043	47.9%	0.002	0.002	97.1%	0.005	2.03	5.804E-04	0.040
32.572	0.042	49.5%	0.001	0.002	98.3%	0.003	1.98	6.083E-04	0.041

Table C2: Reaction Kinetic Data, T = 25°C, [MEA]_i = 2.5[CO₂]_i

τ (s)	[CO ₂] (mol/L)	X _{CO2} (%)	-r _{CO2} (mol/L.s)	[MEA] (mol/L)	X _{MEA} (%)	-r _{MEA} (mol/L.s)	-r _{MEA} /-r _{CO2}	[Z] (mol/L)	[S] (mol/L)
0.000	0.083			0.209					
0.465	0.049	40.7%	0.073	0.155	25.5%	0.114	1.57	6.334E-03	0.026
0.516	0.050	40.3%	0.065	0.150	28.3%	0.114	1.75	7.035E-03	0.026
0.581	0.044	46.7%	0.067	0.143	31.5%	0.113	1.69	5.602E-03	0.032
0.664	0.043	48.5%	0.061	0.135	35.1%	0.110	1.81	3.469E-03	0.036
0.774	0.043	49.0%	0.053	0.132	36.5%	0.098	1.86	4.325E-03	0.036
0.929	0.040	51.6%	0.046	0.123	41.1%	0.092	1.99	2.739E-03	0.041
1.161	0.038	54.2%	0.039	0.115	44.7%	0.080	2.06	2.993E-03	0.044
1.549	0.037	55.6%	0.030	0.117	43.9%	0.059	1.98	2.975E-03	0.044
2.323	0.034	59.7%	0.021	0.108	48.2%	0.043	2.02	3.654E-03	0.047
3.257	0.033	60.8%	0.016	0.103	50.4%	0.032	2.07	3.498E-03	0.049
3.619	0.031	62.3%	0.014	0.103	50.5%	0.029	2.03	3.676E-03	0.050
4.646	0.024	71.2%	0.013	0.099	52.6%	0.024	1.85	2.179E-03	0.055
4.072	0.027	68.2%	0.014	0.091	56.2%	0.029	2.06	3.667E-03	0.055
4.653	0.022	73.7%	0.013	0.094	55.0%	0.025	1.87	2.131E-03	0.058
5.429	0.021	74.4%	0.011	0.092	56.0%	0.022	1.88	3.618E-03	0.058
6.514	0.019	76.8%	0.010	0.079	62.2%	0.020	2.03	3.177E-03	0.062
8.143	0.019	77.8%	0.008	0.074	64.3%	0.016	2.07	3.170E-03	0.064
10.857	0.015	81.4%	0.006	0.067	68.0%	0.013	2.09	2.530E-03	0.068
16.286	0.011	87.3%	0.004	0.060	71.1%	0.009	2.04	2.536E-03	0.072
32.572	0.009	88.9%	0.002	0.053	74.6%	0.005	2.10	2.036E-03	0.074

Table C3: Reaction Kinetic Data, T = 25°C, [MEA]_i = 4[CO₂]_i

τ (s)	[CO ₂] (mol/L)	X _{CO2} (%)	-r _{CO2} (mol/L.s)	[MEA] (mol/L)	X _{MEA} (%)	-r _{MEA} (mol/L.s)	-r _{MEA} /-r _{CO2}	[Z] (mol/L)	[S] (mol/L)
0.000	0.083			0.334					
0.465	0.048	42.6%	0.077	0.282	15.5%	0.112	1.46	9.375E-03	0.026
0.516	0.045	46.0%	0.074	0.265	20.6%	0.133	1.80	1.083E-02	0.028
0.581	0.043	48.7%	0.070	0.259	22.4%	0.129	1.84	8.482E-03	0.032
0.664	0.041	51.3%	0.064	0.255	23.7%	0.119	1.85	8.166E-03	0.035
0.774	0.038	55.0%	0.059	0.242	27.6%	0.119	2.01	5.614E-03	0.040
0.929	0.035	57.5%	0.052	0.234	29.9%	0.107	2.08	6.061E-03	0.042
1.161	0.032	61.4%	0.044	0.230	31.0%	0.089	2.02	5.610E-03	0.046
1.549	0.032	62.1%	0.033	0.233	30.2%	0.065	1.95	3.450E-03	0.048
2.323	0.028	66.7%	0.024	0.222	33.6%	0.048	2.01	4.510E-03	0.051
3.257	0.023	72.2%	0.018	0.210	37.0%	0.038	2.05	3.433E-03	0.057
3.619	0.020	76.2%	0.018	0.200	40.1%	0.037	2.10	2.711E-03	0.061
4.646	0.017	79.7%	0.014	0.201	39.7%	0.029	1.99	3.794E-03	0.063
4.072	0.017	79.5%	0.016	0.192	42.3%	0.035	2.13	2.753E-03	0.064
4.653	0.015	81.9%	0.015	0.192	42.5%	0.030	2.08	3.058E-03	0.065
5.429	0.014	83.1%	0.013	0.193	42.1%	0.026	2.03	2.970E-03	0.066
6.514	0.013	83.9%	0.011	0.192	42.3%	0.022	2.02	4.142E-03	0.066
8.143	0.014	83.7%	0.009	0.194	41.9%	0.017	2.00	4.206E-03	0.066
10.857	0.010	87.7%	0.007	0.187	44.0%	0.014	2.01	3.250E-03	0.070
16.286	0.006	92.9%	0.005	0.173	48.2%	0.010	2.07	3.831E-03	0.074
32.572	0.004	94.8%	0.002	0.168	49.7%	0.005	2.09	3.072E-03	0.076

C.5 Reaction Kinetic Data at 30°C

Table C4: Reaction Kinetic Data, T = 30°C, [MEA]_i = [CO₂]_i

τ (s)	[CO ₂] (mol/L)	X _{CO₂} (%)	-r _{CO₂} (mol/L.s)	[MEA] (mol/L)	X _{MEA} (%)	-r _{MEA} (mol/L.s)	-r _{MEA} /-r _{CO₂}	[Z] (mol/L)	[S] (mol/L)
0.000	0.078			0.078					
0.465	0.061	22.1%	0.037	0.050	36.6%	0.062	1.66	2.102E-03	0.015
0.516	0.060	23.5%	0.036	0.044	43.7%	0.066	1.86	3.088E-03	0.016
0.581	0.058	25.8%	0.035	0.040	48.9%	0.066	1.90	2.152E-03	0.018
0.664	0.057	27.1%	0.032	0.035	55.3%	0.065	2.04	1.608E-03	0.020
0.774	0.056	28.3%	0.029	0.034	56.7%	0.057	2.00	2.116E-03	0.021
0.929	0.056	29.0%	0.024	0.034	56.1%	0.047	1.93	1.632E-03	0.021
1.161	0.052	34.2%	0.023	0.024	68.8%	0.046	2.01	8.671E-04	0.026
1.549	0.051	35.3%	0.018	0.025	68.3%	0.035	1.93	1.194E-03	0.026
2.323	0.048	38.7%	0.013	0.018	76.5%	0.026	1.98	9.226E-04	0.030
3.257	0.044	43.8%	0.011	0.009	88.5%	0.021	2.02	1.166E-03	0.034
3.619	0.044	44.4%	0.010	0.010	87.4%	0.019	1.97	1.132E-03	0.034
4.646	0.043	44.7%	0.008	0.011	85.8%	0.014	1.92	1.112E-03	0.034
4.072	0.045	42.3%	0.008	0.009	88.2%	0.017	2.09	6.297E-04	0.033
4.653	0.043	44.8%	0.008	0.009	89.0%	0.015	1.98	1.045E-03	0.034
5.429	0.044	43.8%	0.006	0.010	87.4%	0.013	1.99	9.931E-04	0.034
6.514	0.043	45.1%	0.005	0.005	94.2%	0.011	2.09	7.863E-04	0.036
8.143	0.042	46.3%	0.004	0.004	94.5%	0.009	2.04	6.063E-04	0.036
10.857	0.043	44.9%	0.003	0.004	95.0%	0.007	2.11	8.142E-04	0.036
16.286	0.043	44.5%	0.002	0.009	89.0%	0.004	2.00	4.562E-04	0.035
32.572	0.042	46.3%	0.001	0.004	95.5%	0.002	2.15	9.077E-04	0.037

Table C5: Reaction Kinetic Data, T = 30°C, [MEA]_i = 2.5[CO₂]_i

τ (s)	[CO ₂] (mol/L)	X _{CO2} (%)	-r _{CO2} (mol/L.s)	[MEA] (mol/L)	X _{MEA} (%)	-r _{MEA} (mol/L.s)	-r _{MEA} /-r _{CO2}	[Z] (mol/L)	[S] (mol/L)
0.000	0.078			0.196					
0.465	0.041	48.1%	0.081	0.138	29.6%	0.125	1.54	5.211E-03	0.028
0.516	0.040	49.0%	0.074	0.130	33.7%	0.128	1.72	7.749E-03	0.028
0.581	0.038	51.1%	0.069	0.126	35.5%	0.120	1.74	7.595E-03	0.032
0.664	0.038	51.2%	0.061	0.130	33.8%	0.100	1.65	7.037E-03	0.031
0.774	0.035	55.0%	0.056	0.122	37.8%	0.096	1.72	4.429E-03	0.036
0.929	0.036	54.5%	0.046	0.113	41.8%	0.088	1.92	2.953E-03	0.040
1.161	0.034	56.3%	0.038	0.115	41.5%	0.070	1.84	2.906E-03	0.040
1.549	0.033	57.5%	0.029	0.106	46.2%	0.058	2.01	2.488E-03	0.043
2.323	0.031	60.0%	0.020	0.100	49.1%	0.041	2.04	2.418E-03	0.045
3.257	0.029	63.6%	0.015	0.095	51.5%	0.031	2.02	2.709E-03	0.048
3.619	0.028	64.1%	0.014	0.092	53.0%	0.029	2.07	2.169E-03	0.049
4.646	0.028	64.1%	0.011	0.098	50.2%	0.021	1.96	2.672E-03	0.047
4.072	0.026	66.9%	0.013	0.089	54.6%	0.026	2.04	2.343E-03	0.050
4.653	0.026	66.4%	0.011	0.097	50.5%	0.021	1.90	2.401E-03	0.048
5.429	0.023	70.0%	0.010	0.086	56.3%	0.020	2.01	1.256E-03	0.054
6.514	0.023	71.3%	0.009	0.075	61.7%	0.019	2.17	3.259E-03	0.054
8.143	0.020	75.0%	0.007	0.075	61.8%	0.015	2.06	1.801E-03	0.058
10.857	0.016	79.8%	0.006	0.069	64.6%	0.012	2.02	3.464E-03	0.060
16.286	0.013	84.0%	0.004	0.062	68.6%	0.008	2.04	1.914E-03	0.065
32.572	0.011	86.2%	0.002	0.056	71.3%	0.004	2.07	2.179E-03	0.067

Table C6: Reaction Kinetic Data, T = 30°C, [MEA]_i = 4[CO₂]_i

τ (s)	[CO ₂] (mol/L)	X _{CO2} (%)	-r _{CO2} (mol/L.s)	[MEA] (mol/L)	X _{MEA} (%)	-r _{MEA} (mol/L.s)	-r _{MEA} /-r _{CO2}	[Z] (mol/L)	[S] (mol/L)
0.000	0.078			0.314					
0.465	0.036	53.5%	0.090	0.252	19.6%	0.132	1.47	5.677E-03	0.032
0.516	0.035	55.3%	0.084	0.244	22.3%	0.135	1.61	8.726E-03	0.033
0.581	0.030	61.6%	0.083	0.234	25.5%	0.138	1.66	1.023E-02	0.036
0.664	0.029	63.4%	0.075	0.226	27.9%	0.132	1.76	5.636E-03	0.042
0.774	0.028	64.1%	0.065	0.219	30.0%	0.122	1.88	7.660E-03	0.043
0.929	0.026	67.2%	0.057	0.218	30.6%	0.103	1.82	5.987E-03	0.046
1.161	0.025	68.0%	0.046	0.211	32.6%	0.088	1.92	4.213E-03	0.049
1.549	0.023	71.2%	0.036	0.197	37.1%	0.075	2.08	4.073E-03	0.054
2.323	0.021	72.9%	0.025	0.198	36.8%	0.050	2.02	3.182E-03	0.055
3.257	0.019	76.1%	0.018	0.191	39.2%	0.038	2.06	5.300E-03	0.057
3.619	0.018	76.6%	0.017	0.192	38.6%	0.033	2.02	6.100E-03	0.056
4.646	0.018	77.2%	0.013	0.192	38.7%	0.026	2.01	3.427E-03	0.058
4.072	0.019	75.7%	0.015	0.186	40.8%	0.031	2.15	3.553E-03	0.059
4.653	0.016	79.1%	0.013	0.186	40.6%	0.027	2.05	3.032E-03	0.061
5.429	0.015	80.4%	0.012	0.180	42.5%	0.025	2.11	5.535E-03	0.061
6.514	0.015	80.6%	0.010	0.196	37.5%	0.018	1.86	4.910E-03	0.057
8.143	0.013	83.0%	0.008	0.189	39.7%	0.015	1.91	1.922E-03	0.062
10.857	0.011	85.9%	0.006	0.178	43.3%	0.013	2.02	5.138E-03	0.064
16.286	0.007	91.1%	0.004	0.166	47.1%	0.009	2.07	2.904E-03	0.070
32.572	0.006	91.8%	0.002	0.162	48.5%	0.005	2.11	3.207E-03	0.072

C.6 Reaction Kinetic Data at 35°C

Table C7: Reaction Kinetic Data, T = 35°C, [MEA]_i = [CO₂]_i

τ (s)	[CO ₂] (mol/L)	X _{CO2} (%)	-r _{CO2} (mol/L.s)	[MEA] (mol/L)	X _{MEA} (%)	-r _{MEA} (mol/L.s)	-r _{MEA} /-r _{CO2}	[Z] (mol/L)	[S] (mol/L)
0.000	0.076			0.076					
0.465	0.058	22.7%	0.037	0.051	32.2%	0.052	1.42	1.534E-03	0.014
0.516	0.056	25.7%	0.038	0.042	44.4%	0.065	1.73	4.377E-03	0.015
0.581	0.053	29.5%	0.038	0.035	53.5%	0.070	1.81	2.574E-03	0.019
0.664	0.053	29.6%	0.034	0.031	58.4%	0.066	1.97	1.880E-03	0.021
0.774	0.052	30.9%	0.030	0.028	62.9%	0.061	2.04	1.805E-03	0.022
0.929	0.051	33.0%	0.027	0.030	60.4%	0.049	1.83	2.050E-03	0.022
1.161	0.050	33.3%	0.022	0.026	65.5%	0.043	1.97	8.580E-04	0.024
1.549	0.050	34.0%	0.017	0.024	68.2%	0.033	2.01	8.045E-04	0.025
2.323	0.047	37.3%	0.012	0.017	77.9%	0.025	2.09	6.303E-04	0.028
3.257	0.046	39.7%	0.009	0.015	80.3%	0.019	2.02	7.411E-04	0.030
3.619	0.043	42.8%	0.009	0.011	84.9%	0.018	1.98	6.927E-04	0.032
4.646	0.044	41.4%	0.007	0.014	80.9%	0.013	1.95	9.527E-04	0.030
4.072	0.043	42.4%	0.008	0.011	85.2%	0.016	2.01	1.507E-03	0.031
4.653	0.044	42.3%	0.007	0.006	91.7%	0.015	2.17	9.707E-04	0.033
5.429	0.043	43.2%	0.006	0.012	83.6%	0.012	1.93	3.144E-04	0.032
6.514	0.043	43.7%	0.005	0.009	87.5%	0.010	2.00	7.065E-04	0.032
8.143	0.042	44.1%	0.004	0.007	90.2%	0.008	2.04	7.061E-04	0.033
10.857	0.043	42.9%	0.003	0.012	83.5%	0.006	1.95	6.206E-04	0.032
16.286	0.043	43.1%	0.002	0.012	84.1%	0.004	1.95	5.548E-04	0.032
32.572	0.043	43.7%	0.001	0.009	88.3%	0.002	2.02	3.918E-04	0.035

Table C8: Reaction Kinetic Data, T = 35°C, [MEA]_i = 2.5[CO₂]_i

τ (s)	[CO ₂] (mol/L)	X _{CO2} (%)	-r _{CO2} (mol/L.s)	[MEA] (mol/L)	X _{MEA} (%)	-r _{MEA} (mol/L.s)	-r _{MEA} /-r _{CO2}	[Z] (mol/L)	[S] (mol/L)
0.000	0.076			0.189					
0.465	0.036	52.1%	0.085	0.125	33.9%	0.138	1.62	4.259E-03	0.032
0.516	0.037	51.1%	0.075	0.116	38.5%	0.141	1.88	6.267E-03	0.033
0.581	0.035	54.2%	0.070	0.111	41.4%	0.135	1.91	5.228E-03	0.036
0.664	0.034	54.6%	0.062	0.109	42.4%	0.121	1.94	3.029E-03	0.038
0.774	0.034	54.9%	0.054	0.107	43.1%	0.105	1.96	2.885E-03	0.039
0.929	0.033	56.4%	0.046	0.102	45.8%	0.093	2.03	3.685E-03	0.040
1.161	0.031	59.5%	0.039	0.096	49.0%	0.080	2.06	1.963E-03	0.044
1.549	0.031	59.1%	0.029	0.098	48.3%	0.059	2.04	2.792E-03	0.043
2.323	0.029	62.0%	0.020	0.098	47.9%	0.039	1.93	2.284E-03	0.044
3.257	0.027	64.9%	0.015	0.091	51.7%	0.030	1.99	1.871E-03	0.047
3.619	0.027	64.4%	0.013	0.090	52.2%	0.027	2.03	1.427E-03	0.048
4.646	0.025	66.8%	0.011	0.086	54.6%	0.022	2.04	1.219E-03	0.050
4.072	0.025	67.0%	0.012	0.085	55.2%	0.026	2.06	1.457E-03	0.050
4.653	0.025	66.6%	0.011	0.084	55.4%	0.022	2.08	2.510E-03	0.049
5.429	0.022	70.5%	0.010	0.080	57.6%	0.020	2.04	2.152E-03	0.052
6.514	0.021	71.7%	0.008	0.078	58.5%	0.017	2.04	9.923E-04	0.054
8.143	0.021	72.4%	0.007	0.077	59.4%	0.014	2.05	1.289E-03	0.054
10.857	0.020	73.4%	0.005	0.078	58.9%	0.010	2.01	1.877E-03	0.054
16.286	0.017	77.7%	0.004	0.070	62.8%	0.007	2.02	1.539E-03	0.058
32.572	0.015	79.6%	0.002	0.069	63.3%	0.004	1.99	1.575E-03	0.059

Table C9: Reaction Kinetic Data, T = 35°C, [MEA]_i = 4[CO₂]_i

τ (s)	[CO ₂] (mol/L)	X _{CO2} (%)	-r _{CO2} (mol/L.s)	[MEA] (mol/L)	X _{MEA} (%)	-r _{MEA} (mol/L.s)	-r _{MEA} /-r _{CO2}	[Z] (mol/L)	[S] (mol/L)
0.000	0.076			0.302					
0.465	0.029	62.0%	0.101	0.234	22.4%	0.146	1.45	6.835E-03	0.035
0.516	0.027	64.4%	0.094	0.224	25.9%	0.152	1.61	1.755E-02	0.031
0.581	0.024	68.3%	0.089	0.205	32.1%	0.167	1.88	1.059E-02	0.042
0.664	0.024	68.5%	0.078	0.203	32.8%	0.149	1.91	9.722E-03	0.043
0.774	0.023	69.3%	0.068	0.199	34.1%	0.133	1.97	1.277E-02	0.042
0.929	0.021	72.6%	0.059	0.190	37.2%	0.121	2.05	5.321E-03	0.052
1.161	0.020	73.4%	0.048	0.188	37.6%	0.098	2.05	4.407E-03	0.053
1.549	0.019	74.2%	0.036	0.187	38.1%	0.074	2.05	2.898E-03	0.055
2.323	0.020	74.0%	0.024	0.189	37.4%	0.049	2.02	3.338E-03	0.054
3.257	0.019	74.7%	0.017	0.186	38.3%	0.035	2.05	4.726E-03	0.054
3.619	0.018	76.3%	0.016	0.186	38.4%	0.032	2.01	2.552E-03	0.056
4.646	0.017	76.9%	0.012	0.180	40.3%	0.026	2.10	2.077E-03	0.058
4.072	0.019	75.0%	0.014	0.193	36.0%	0.027	1.92	2.821E-03	0.053
4.653	0.018	76.4%	0.012	0.188	37.7%	0.024	1.97	2.403E-03	0.056
5.429	0.016	79.3%	0.011	0.181	40.2%	0.022	2.03	2.964E-03	0.058
6.514	0.015	80.1%	0.009	0.184	39.1%	0.018	1.95	2.994E-03	0.057
8.143	0.014	81.7%	0.008	0.182	39.6%	0.015	1.94	2.646E-03	0.059
10.857	0.012	84.3%	0.006	0.174	42.5%	0.012	2.02	2.371E-03	0.062
16.286	0.010	86.9%	0.004	0.175	42.1%	0.008	1.94	4.404E-03	0.061
32.572	0.010	87.2%	0.002	0.162	46.3%	0.004	2.12	3.456E-03	0.065

APPENDIX D: ABSORPTION EXPERIMENTAL DATA AND SAMPLE CALCULATIONS

D.1 Calculating Specific Absorption Rate

As an example, the data entry in **Table D1** for a column height of 60mm, a volumetric flow rate of 0.96mL/s and a CO₂ mass% of 78.95% will be used in the sample calculation of the specific rate of CO₂ absorption.

The mass flow rate of CO₂ and argon may be calculated from equations 4.3 and 4.4:

$$\dot{m}_{\text{CO}_2, \text{in}} = 2.175(\text{MFC}_{\text{inlet}})$$

$$\therefore \dot{m}_{\text{CO}_2, \text{in}} = 2.175 \cdot 1.7 = 3.6975 \text{ kg/hr}$$

$$\dot{m}_{\text{Ar, in}} = 3.398(\text{MFC}_{\text{outlet}} - \text{MFC}_{\text{inlet}})$$

$$\therefore \dot{m}_{\text{Ar, in}} = 3.79(1.99 - 1.7) = 0.98542 \text{ kg/hr}$$

From equation 4.5 the total inlet gas mass flow rate is thus:

$$\dot{m}_{\text{in}} = 3.6975 + 0.98542 = 4.68292 \text{ kg/hr}$$

Assuming that no argon absorbs:

$$\dot{m}_{\text{Ar, in}} = \dot{m}_{\text{Ar, out}} = 0.98542 \text{ kg/hr}$$

Taking the average of the 30 MFC_{outlet} reading during steady state absorption conditions, the total outlet flow rate may be calculated:

$$\dot{m}_{\text{tot}} = 1.199(\text{MFC}_{\text{outlet}} - \text{MFC}_{\text{CO}_2}) + 4.415$$

$$\therefore \dot{m}_{\text{tot}} = 1.199(1.912 - 1.7) + 4.415 = 4.669 \text{ kg/hr}$$

the outlet CO₂ mass flow rate may now be calculated:

$$\dot{m}_{\text{CO}_2,\text{out}} = \dot{m}_{\text{out}} - \dot{m}_{\text{Ar},\text{out}}$$

$$\therefore \dot{m}_{\text{CO}_2,\text{out}} = 4.669 - 0.98542 = 3.6837 \text{ kg/hr}$$

The mass CO₂ absorbed may now be calculated:

$$m_{\text{CO}_2,\text{absorbed}} = \left(\frac{\dot{m}_{\text{CO}_2,\text{in}} - \dot{m}_{\text{CO}_2,\text{out}}}{3600} \right) \cdot t_c$$

$$\therefore m_{\text{CO}_2,\text{absorbed}} = \left(\frac{3.6975 - 3.6837}{3600} \right) \cdot 0.83 = 3.12 \times 10^{-6} \text{ kg}$$

The number of moles absorbed is thus:

$$n_{\text{CO}_2,\text{absorbed}} = \frac{m_{\text{CO}_2,\text{absorbed}}}{M_{r,\text{CO}_2}} = \frac{3.185 \times 10^{-6}}{44.01} \times 1000 = 7.24 \times 10^{-5} \text{ mol}$$

The specific absorption rate may now be calculated from a combination of equations 7.1 and 7.2

$$N_{\text{CO}_2} = \frac{n_{\text{CO}_2,\text{absorbed}}}{A_{\text{wetted wall surface}} \cdot t_c}$$

$$\therefore N_{\text{CO}_2} = \frac{7.24 \times 10^{-5}}{\pi \left(\frac{25.4}{1000} \right)^2 \cdot \left(\frac{60}{1000} \right) \cdot 0.83} = 1.82 \times 10^2 \text{ mol/m}^2 \cdot \text{s}$$

D.2 Absorption Experimental Data

Table D1: Absorption Data, 25°C, [MEA]_i = 0.25 mol/L

h_{col} (mm)	V_L (mL/s)	t_c (s)	MFC _{CO₂}	P_{dome} (kPa)	Mass% CO ₂	P_{CO_2} (kPa)	MFC _{outlet} *	$n_{CO_2, absrd}$ x10 ⁵ (mol)	$N_{CO_2} \times 10^2$ (mol/m ² .s)	[MEA] _{out} (mol/L)
60	1.54	0.60	2.00	104.72	100.00%	104.72	1.932	6.32	2.19	0.168
60	1.54	0.60	1.70	104.75	77.82%	79.72	1.969	5.11	1.77	0.184
60	1.54	0.60	1.30	104.66	55.02%	55.06	1.896	3.31	1.14	0.207
60	1.54	0.60	0.80	104.69	30.08%	29.39	1.938	1.65	0.57	0.229
60	0.96	0.83	2.00	104.72	100.00%	104.72	1.932	8.67	2.19	0.119
60	0.96	0.83	1.70	104.69	78.95%	80.92	1.912	7.22	1.82	0.141
60	0.96	0.83	1.30	104.69	54.66%	54.70	1.923	5.36	1.35	0.169
60	0.96	0.83	0.80	104.75	29.73%	29.06	1.995	2.04	0.52	0.219
90	1.54	0.91	2.00	104.72	100.00%	104.72	1.927	12.92	1.99	0.097
90	1.54	0.91	1.70	104.75	77.82%	79.72	1.963	11.79	1.81	0.123
90	1.54	0.91	1.30	104.75	53.95%	53.98	1.976	8.38	1.29	0.159
90	1.54	0.91	0.80	104.69	30.08%	29.39	1.935	4.53	0.70	0.204
90	0.96	1.24	2.00	104.72	100.00%	104.72	1.926	18.64	2.09	0.062
90	0.96	1.24	1.70	104.75	77.82%	79.72	1.962	17.09	1.92	0.078
90	0.96	1.24	1.30	104.66	55.02%	55.06	1.89	12.44	1.40	0.125
90	0.96	1.24	0.80	104.75	29.73%	29.06	1.993	4.94	0.55	0.200
105	1.54	1.06	2.00	104.72	100.00%	104.72	1.921	19.87	2.24	0.081
105	1.54	1.06	1.70	104.75	77.82%	79.72	1.958	17.75	2.00	0.109
105	1.54	1.06	1.30	104.75	53.95%	53.98	1.973	12.18	1.38	0.150
105	1.54	1.06	0.80	104.75	29.73%	29.06	1.99	6.61	0.75	0.196
105	0.96	1.45	2.00	104.72	100.00%	104.72	1.923	25.04	2.06	0.034
105	0.96	1.45	1.70	104.69	78.95%	80.92	1.904	21.41	1.77	0.065
105	0.96	1.45	1.30	104.69	54.66%	54.70	1.916	17.07	1.41	0.103
105	0.96	1.45	0.80	104.75	29.73%	29.06	1.99	9.06	0.75	0.172

*After Absorption

Table D2: Absorption Data, 30°C, [MEA]_i = 0.25 mol/L

h_{col} (mm)	V_L (mL/s)	t_c (s)	MFC _{CO2}	P_{dome} (kPa)	Mass% CO ₂	P_{CO2} (kPa)	MFC _{outlet} *	$n_{CO2, absrd} \times 10^5$ (mol)	$N_{CO2} \times 10^2$ (mol/m ² .s)	[MEA] _{out} (mol/L)
60	1.54	0.61	2.00	104.72	100.00%	104.72	1.929	7.73	2.66	0.21
60	1.54	0.61	2.01	104.75	77.82%	79.72	1.966	6.51	2.24	0.23
60	1.54	0.61	2.00	104.72	54.30%	54.34	1.949	5.00	1.72	0.25
60	1.54	0.61	2.01	104.75	29.73%	29.06	1.993	2.41	0.83	0.28
60	0.96	0.83	2.00	104.72	100.00%	104.72	1.929	10.59	2.66	0.16
60	0.96	0.83	1.99	104.69	78.95%	80.92	1.909	9.14	2.30	0.19
60	0.96	0.83	2.01	104.75	53.95%	53.98	1.977	7.06	1.77	0.22
60	0.96	0.83	1.98	104.66	30.26%	29.56	1.908	3.32	0.83	0.26
90	1.54	0.91	2.00	104.72	100.00%	104.72	1.922	16.41	2.51	0.17
90	1.54	0.91	1.99	104.69	78.95%	80.92	1.904	13.45	2.06	0.19
90	1.54	0.91	2.01	104.75	53.95%	53.98	1.972	11.17	1.71	0.23
90	1.54	0.91	2.01	104.75	29.73%	29.06	1.989	6.38	0.98	0.26
90	0.96	1.25	2.00	104.72	100.00%	104.72	1.921	23.44	2.62	0.09
90	0.96	1.25	1.98	104.66	79.53%	81.53	1.876	18.12	2.02	0.12
90	0.96	1.25	2.02	104.78	53.60%	53.63	2.01	15.62	1.74	0.17
90	0.96	1.25	1.99	104.69	30.08%	29.39	1.935	6.23	0.70	0.24
105	1.54	1.06	2.00	104.72	100.00%	104.72	1.917	23.17	2.61	0.12
105	1.54	1.06	1.98	104.66	79.53%	81.53	1.87	20.25	2.28	0.16
105	1.54	1.06	2.00	104.72	54.30%	54.34	1.942	14.38	1.62	0.20
105	1.54	1.06	2.01	104.75	29.73%	29.06	1.988	8.24	0.93	0.25
105	0.96	1.45	2.00	104.72	100.00%	104.72	1.916	32.85	2.70	0.02
105	0.96	1.45	2.01	104.75	77.82%	79.72	1.955	27.73	2.28	0.08
105	0.96	1.45	2.01	104.75	53.95%	53.98	1.969	21.16	1.74	0.14
105	0.96	1.45	1.99	104.69	30.08%	29.39	1.935	7.27	0.60	0.22

*After Absorption

Table D3: Absorption Data, 25°C, [MEA]_i = 0.3 mol/L

h_{col} (mm)	V_L (mL/s)	t_c (s)	MFC _{CO2}	P_{dome} (kPa)	Mass% CO ₂	P_{CO_2} (kPa)	MFC _{outlet} *	$n_{CO_2, absrd}$ x10 ⁵ (mol)	$N_{CO_2} \times 10^2$ (mol/m ² .s)	[MEA] _{out} (mol/L)
60	1.54	0.59	2.00	104.72	100.00%	104.72	1.931	6.59	2.35	0.162
60	1.54	0.59	1.70	104.75	77.82%	79.72	1.97	4.53	1.61	0.190
60	1.54	0.59	1.30	104.69	54.66%	54.70	1.921	4.70	1.67	0.188
60	1.54	0.59	0.80	104.69	30.08%	29.39	1.937	2.05	0.73	0.223
60	0.96	0.80	2.00	104.72	100.00%	104.72	1.932	8.43	2.19	0.119
60	0.96	0.80	1.70	104.75	77.82%	79.72	1.969	6.81	1.77	0.144
60	0.96	0.80	1.30	104.75	53.95%	53.98	1.979	5.62	1.46	0.163
60	0.96	0.80	0.80	104.75	29.73%	29.06	1.994	2.59	0.67	0.210
90	1.54	0.88	2.00	104.72	100.00%	104.72	1.925	13.89	2.20	0.127
90	1.54	0.88	1.70	104.72	78.38%	80.31	1.934	11.91	1.88	0.145
90	1.54	0.88	1.30	104.75	53.95%	53.98	1.974	9.48	1.50	0.166
90	1.54	0.88	0.80	104.72	29.90%	29.23	1.962	5.29	0.84	0.203
90	0.96	1.21	2.00	104.72	100.00%	104.72	1.924	19.95	2.30	0.043
90	0.96	1.21	1.70	104.75	77.82%	79.72	1.961	17.53	2.02	0.068
90	0.96	1.21	1.30	104.69	54.66%	54.70	1.92	10.57	1.22	0.141
90	0.96	1.21	0.80	104.75	29.73%	29.06	1.993	4.81	0.55	0.200
105	1.54	1.03	2.00	104.72	100.00%	104.72	1.918	21.66	2.52	0.086
105	1.54	1.03	1.70	104.75	77.82%	79.72	1.963	13.37	1.55	0.149
105	1.54	1.03	1.30	104.78	53.60%	53.63	1.996	15.99	1.86	0.129
105	1.54	1.03	0.80	104.66	30.26%	29.56	1.903	8.00	0.93	0.189
105	0.96	1.41	2.00	104.72	100.00%	104.72	1.919	28.61	2.43	0.038
105	0.96	1.41	1.70	104.72	78.38%	80.31	1.935	17.97	1.52	0.090
105	0.96	1.41	1.30	104.75	53.95%	53.98	1.969	20.49	1.74	0.068
105	0.96	1.41	0.80	104.69	30.08%	29.39	1.935	7.04	0.60	0.187

*After Absorption

Table D4: Absorption Data, 30°C, [MEA]_i = 0.3 mol/L

h_{col} (mm)	V_L (mL/s)	t_c (s)	MFC _{CO₂}	P_{dome} (kPa)	Mass% CO ₂	P_{CO_2} (kPa)	MFC _{outlet} *	$n_{CO_2, absrd} \times 10^5$ (mol)	$N_{CO_2} \times 10^2$ (mol/m ² .s)	[MEA] _{out} (mol/L)
60	1.54	0.59	2.00	104.72	100.00%	104.72	1.928	7.97	2.82	0.195
60	1.54	0.59	1.70	104.75	77.82%	79.72	1.965	6.79	2.40	0.210
60	1.54	0.59	1.30	104.69	54.66%	54.70	1.919	5.62	1.99	0.226
60	1.54	0.59	0.80	104.66	30.26%	29.56	1.908	2.36	0.83	0.269
60	0.96	0.81	2.00	104.72	100.00%	104.72	1.931	9.09	2.35	0.160
60	0.96	0.81	1.70	104.66	79.53%	81.53	1.881	8.70	2.25	0.166
60	0.96	0.81	1.30	104.66	55.02%	55.06	1.891	7.50	1.94	0.184
60	0.96	0.81	0.80	104.75	29.73%	29.06	1.993	3.22	0.83	0.250
90	1.54	0.89	2.00	104.72	100.00%	104.72	1.921	16.66	2.62	0.153
90	1.54	0.89	1.70	104.75	77.82%	79.72	1.958	14.88	2.34	0.169
90	1.54	0.89	1.30	104.75	53.95%	53.98	1.972	10.88	1.71	0.204
90	1.54	0.89	0.80	104.75	29.73%	29.06	1.989	6.21	0.98	0.245
90	0.96	1.21	2.00	104.72	100.00%	104.72	1.922	21.91	2.51	0.074
90	0.96	1.21	1.70	104.72	78.38%	80.31	1.932	18.25	2.09	0.112
90	0.96	1.21	1.30	104.72	54.30%	54.34	1.943	15.52	1.78	0.140
90	0.96	1.21	0.80	104.66	30.26%	29.56	1.906	6.69	0.77	0.231
105	1.54	1.03	2.00	104.72	100.00%	104.72	1.916	23.35	2.70	0.124
105	1.54	1.03	1.70	104.66	79.53%	81.53	1.87	19.72	2.28	0.151
105	1.54	1.03	1.30	104.69	54.66%	54.70	1.912	15.31	1.77	0.185
105	1.54	1.03	0.80	104.72	29.90%	29.23	1.958	9.34	1.08	0.230
105	0.96	1.42	2.00	104.72	100.00%	104.72	1.915	33.06	2.79	0.008
105	0.96	1.42	1.70	104.69	78.95%	80.92	1.9	25.23	2.13	0.077
105	0.96	1.42	1.30	104.69	54.66%	54.70	1.91	23.12	1.95	0.096
105	0.96	1.42	0.80	104.66	30.26%	29.56	1.905	8.88	0.75	0.222

*After Absorption

Table D5: Absorption Data, 25°C, [MEA]_i = 1 mol/L

h_{col} (mm)	V_L (mL/s)	t_c (s)	MFC _{CO2}	P_{dome} (kPa)	Mass% CO ₂	P_{CO2} (kPa)	MFC _{outlet} *	$n_{CO2, absrd} \times 10^5$ (mol)	$N_{CO2} \times 10^2$ (mol/m ² .s)	[MEA] _{out} (mol/L)
60	1.54	0.61	2.00	104.72	100.00%	104.72	1.974	17.83	6.15	0.694
60	1.54	0.61	1.70	104.75	75.89%	77.58	1.88	14.65	5.06	0.749
60	1.54	0.61	1.30	104.69	51.95%	51.85	1.83	11.37	3.92	0.805
60	1.54	0.61	0.80	104.66	28.01%	27.31	1.852	8.02	2.77	0.862
60	0.96	0.83	2.00	104.72	100.00%	104.72	1.973	25.58	6.44	0.486
60	0.96	0.83	1.70	104.69	77.09%	78.86	1.865	19.61	4.94	0.606
60	0.96	0.83	1.30	104.66	52.32%	52.21	1.82	16.56	4.17	0.667
60	0.96	0.83	0.80	104.66	28.01%	27.31	1.854	8.40	2.11	0.831
90	1.54	0.91	2.00	104.72	100.00%	104.72	1.961	42.99	6.59	0.508
90	1.54	0.91	1.70	104.72	76.48%	78.21	1.861	36.38	5.58	0.584
90	1.54	0.91	1.30	104.72	51.59%	51.49	1.83	29.44	4.51	0.663
90	1.54	0.91	0.80	104.75	27.51%	26.83	1.88	14.13	2.17	0.838
90	0.96	1.24	2.00	104.72	100.00%	104.72	1.96	60.63	6.78	0.188
90	0.96	1.24	1.70	104.72	76.48%	78.21	1.861	49.86	5.58	0.332
90	0.96	1.24	1.30	104.75	51.24%	51.13	1.84	38.93	4.36	0.479
90	0.96	1.24	0.80	104.66	28.01%	27.31	1.851	18.44	2.06	0.753
105	1.54	1.06	2.00	104.72	100.00%	104.72	1.96	51.62	5.82	0.494
105	1.54	1.06	1.70	104.66	77.70%	79.51	1.845	43.47	4.90	0.574
105	1.54	1.06	1.30	104.69	51.95%	51.85	1.82	35.56	4.01	0.651
105	1.54	1.06	0.80	104.72	27.67%	26.99	1.868	20.10	2.26	0.803
105	0.96	1.45	2.00	104.66	101.77%	106.70	1.951	71.25	5.86	0.182
105	0.96	1.45	1.70	104.72	76.48%	78.21	1.86	60.21	4.95	0.309
105	0.96	1.45	1.30	104.66	52.32%	52.21	1.812	46.13	3.79	0.470
105	0.96	1.45	0.80	104.66	28.01%	27.31	1.85	23.79	1.96	0.727

*After Absorption

APPENDIX E: EQUIPMENT SPECIFICATIONS AND ILLUSTRATIONS

E.1 Mass Flow Controller

The MFC Type 8626 is compact devices with which the mass flow of gases is controlled. It controls to a preset set point value, independent of disturbances such as pressure variations or flow resistances that vary with time, e.g. as a result of filter contamination. The MFC contain the components flow rate sensor (Q sensor), electronics (with the functions signal processing, control and valve drive), and a proportional solenoid valve as the servo component. These components are illustrated in **Figure E1**:

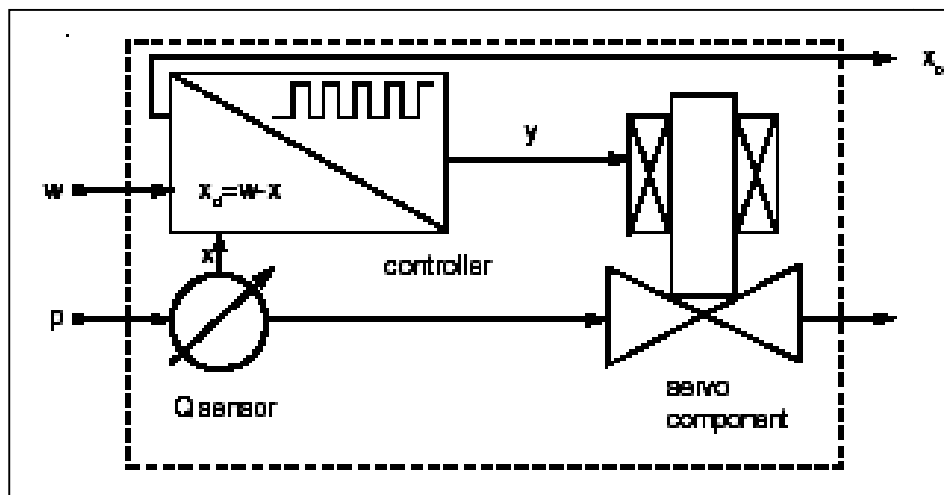


Figure E1: Components of MFC

The set point value (w) is set electrically via a standard signal or a field bus. The process value (x) measured by the sensor is compared in the controller with the set point value. The correcting variable is sent as a plus-width modulated voltage signal to the servo component. The pulse-duty factor of the voltage signal is varied according to the control deviation determined.

The process value, in addition, is sent out via an analog electrical interface or a field bus and is available to the user for monitoring purposes or further evaluation (e.g. calculation of consumption by integration).

The thermal measurement principle guarantees that the MFC control to the required mass flow to a large extent independently of pressure and temperature variations in the respective application.

The Mass Flow Controller in-line sensor is illustrated in **Figure E2**:

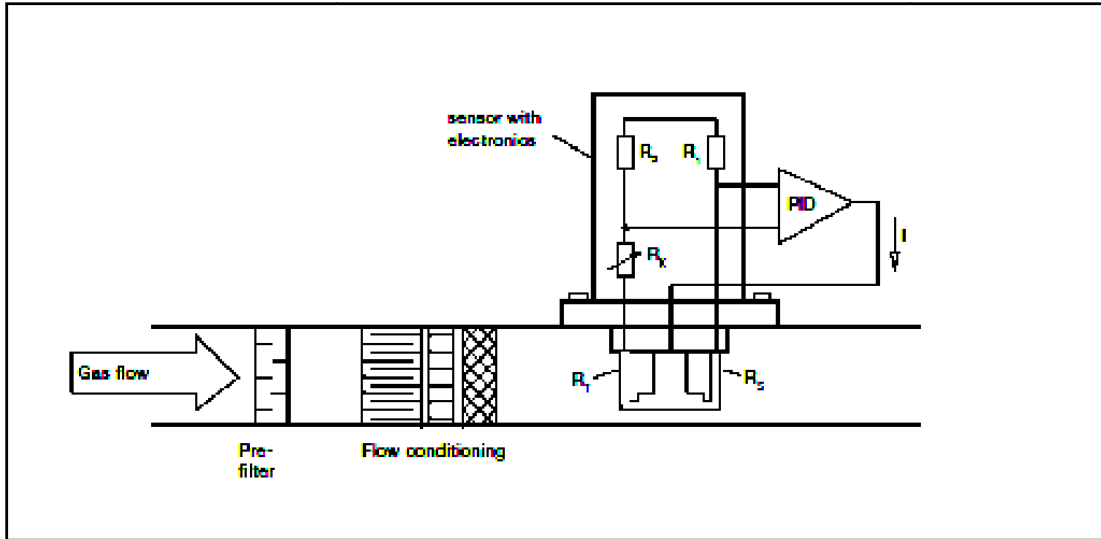



Figure E2: Functional Diagram of the In-line Sensor in the MFC

This sensor works as a hot-film anemometer in the so-called CTA operational mode (Constant Temperature Anemometer). To do this, two resistors with precisely specified temperature coefficients located directly in the media flow and three resistors located outside the flow are connected together to form a bridge.

The first resistor in the medium flow (R_T) measures the fluid temperature, while the second, low-value resistor (R_S) is heated so that it is maintained at a fixed, predefined over temperature with respect to the fluid temperature. The heating current required to maintain this is a measure of the heat being removed by the flowing gas, and represents the primary measurement.

An adequate flow conditioning within the MFC and the calibration with high-quality flow standards ensure that the mass of gas flowing per time unit can be derived from the primary signal with great accuracy. (Adapted from the instruction manual that arrived with the MFC)

The Calibration Data Supplied by Burkert is as follows:

 FLUID CONTROL SYSTEMS	Bürkert Fluid Control Systems Bürkert S.A.S BP 21 F-67220 Triembach au Val Info-Center: +33 388 58 91 11 burkert.france@buerkert.com www.buerkert.com
---	---

Calibration Protocol Mass Flow Controller type 8626

Order No.: 06920381
 Device Ident No: 00203219
 Nominal Flow Rate: 30.00 kg/h
 InputSignal: 4...20 mA
 Output Signal: 4...20 mA
 Serial No.: 001000
 Software Revision: A.00.82.00

 Calibration Reference: Mass Flow Meter 8006
 ID153911, SN010079, MB 0-600 NI/min
 Operating Gas: Air
 Calibration Gas: Air

 Inlet Pressure: 2.00 bar (g) referred to operating gas
 Leak-Tight Pressure: > 8.0 bar (g)
 Temperature: 22,7 °C
 Installation Position: horizontal

Calibration Data:

Flow Rate [%]	Reference [kg/h]	Deviation [% F.S.]	Allowed Dev. [% F.S.]
0.00	0.000	0.00	0.30
25.00	7.365	0.45	0.68
50.00	14.835	0.55	1.05
75.00	22.431	0.23	1.43
100.00	29.952	0.16	1.80

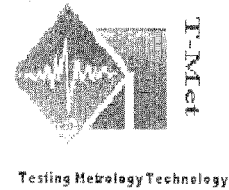
Calibration Date: 04/06/2008 Calibrator: 04000225

These data refer to the time and conditions of calibration.
 Reference conditions (NI/min): 273,15 K, 1.013,25 mbar (a)
 This report is produced by an electronic system and is valid without signature.

E.2 Temperature Sensors



Testing Metrology Technology cc t/a T-Met
 PO Box 3822, Durbanville, 7550.
 Unit G1, Centurion Business Park, Milnerton.
 Tel /Fax Fax (021) 551 4595.
 Vat No : 4360219325.
 Registration no: CK2004/122069/23cc



Certificate of Calibration

SANAS accredited laboratory no 155/355

The South African National Accreditation Service (SANAS) is a member of the International Laboratory Accreditation Cooperation (ILAC) Mutual Recognition Agreement (MRA). This arrangement allows for the mutual recognition of technical test and calibration data by the member accreditation bodies worldwide. For more information on the arrangement please consult www.ilac.org

Manufacturer : Unknown
 Description : Temperature Probes
 Model No : PT100 (IEC751 / 385)
 Serial No : TM07
 Calibrated for : N&Z Instrumentation
 : Parrow
 Temperature : 23 °C ± 3 °C
 Relative humidity : 55 %RH ± 2 %RH
 Date of calibration : 12 December 2007
 Issue Date : 13 December 2007
 Calibrated by : ZW de Witt

This certificate is issued without alteration, and in accordance with the conditions of accreditation granted by the SANAS. It is a correct record of the measurements made at the time of calibration. Copyright of this certificate is owned jointly by T Met and may not be reproduced other than in full, except with the prior written approval of T-Met. The values given in this certificate were correct at the time of calibration. Subsequently the accuracy will depend on factors such as care exercised in handling the instrument and frequency of use. Recalibration should be performed after a period, which has been chosen to ensure that, under normal circumstances, the instruments accuracy remains within the desired limits. The accuracies of all measurements were traceable to the national measuring standards as maintained in South Africa, unless otherwise noted. The uncertainties of measurement were estimated for a coverage factor of k=2 which approximates a 95% confidence level.

Authorised Signatory
 ZW de Witt
 Certificate no TM12402

Certificate of Calibration

1. **Standards and equipment**

Ref	Make	Model	Description	Serial no
74	Fluke	741B	Process Calibrator	8572023
18	Fluke	7103	Stirred Liquid Bath	A5B833
57	Hart Scientific	5699	SPRT Probe	0085
228	Guildline	9540	Resistance Thermometer	228
35	Hart Scientific	1620 (2626-H)	Thermo hygrometer @ Probe	A53650

2. **Procedure**

2.1.1 The UUT (Unit under Test) was in compliance to the International Temperature Scale of 1990 (ITS-90) and the manufacturers tolerance specifications

2.1.1 The UUT Temperature probe was inserted to an approximate depth of 100 mm into the temperature calibrator and calibrated in terms of its typical accuracy specification with reference to procedure no TM P3 000

3. **Results**

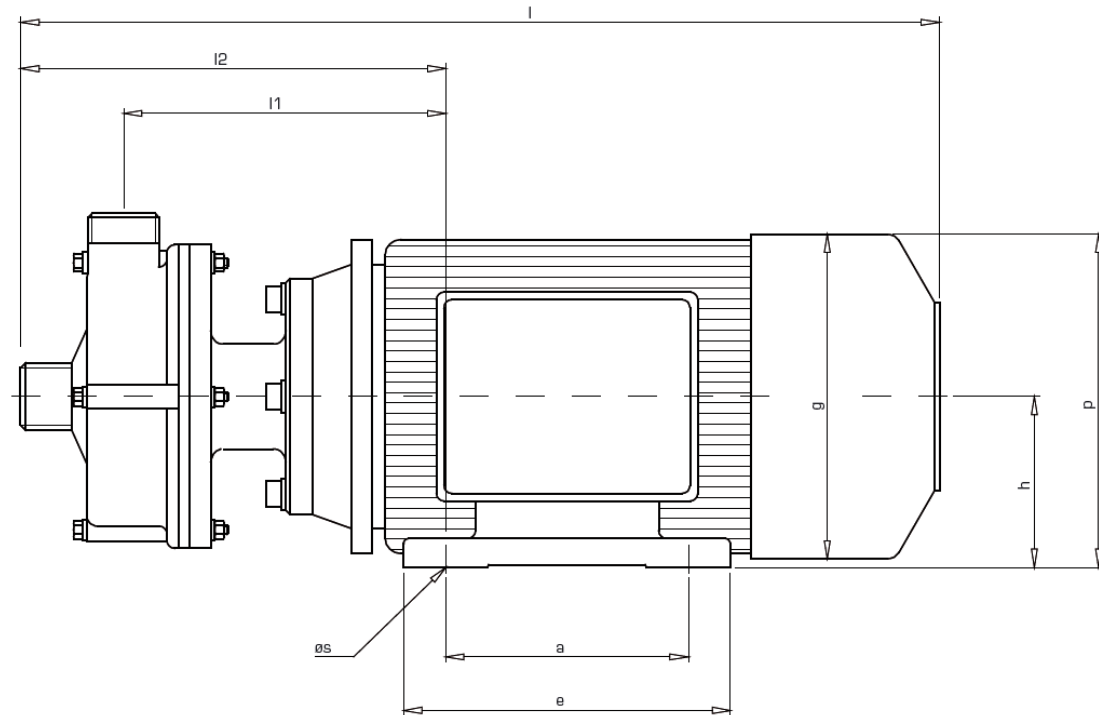
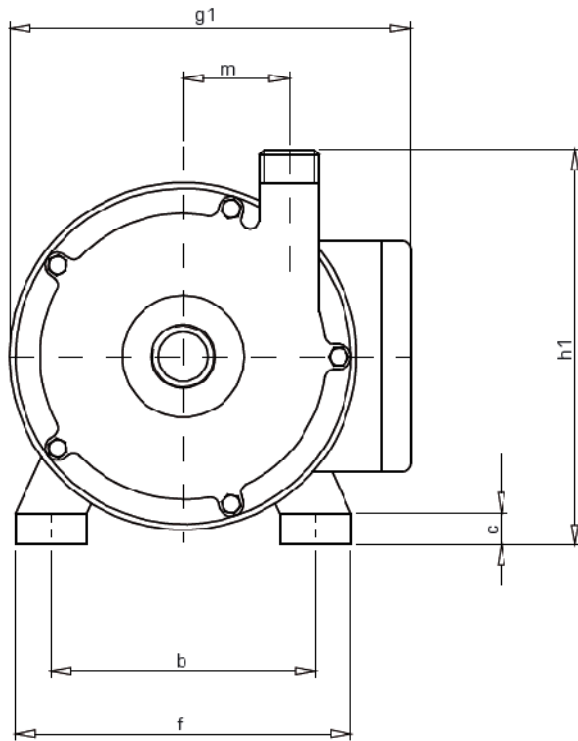
Range (°C)	Nominal Input (°C)	Applied Input (°C)	Tolerance (°C)	UUT Reading (°C)	Difference (°C)	Measurement uncertainty
-20 to 100	-20	-20.00	-20.25 to -19.75	-19.9	- 0.1	+ 0.5 °C
	0	0.000	-0.15 to 0.15	0.1	- 0.1	± 0.5 °C
	50	50.00	49.6 to 50.4	50.1	- 0.1	± 0.5 °C
	100	100.00	99.35 to 100.65	100.1	- 0.1	± 0.5 °C

4. **Comments**

4.1 **Bold** – highlights where applicable indicate out of tolerance values.

Authorised Signatory
 ZW de Witt
 Certificate no TM12402

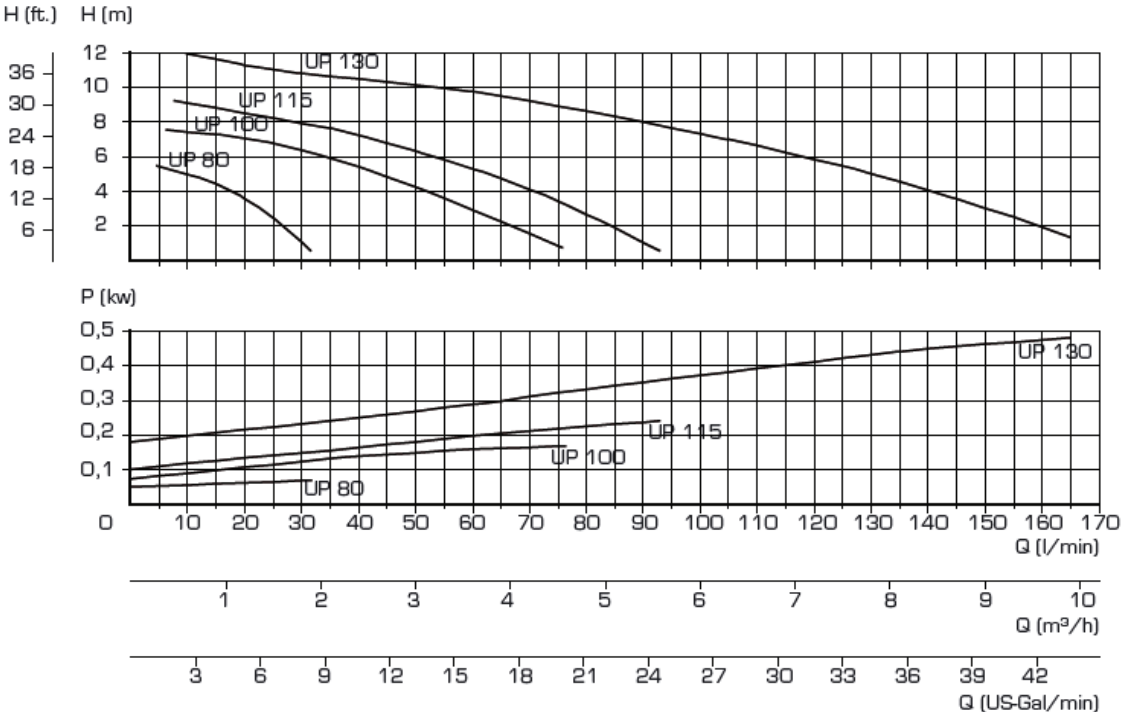
E.3 Wetted Wall Liquid Pump



UP80 Model: Material of Construction: Stainless Steel 1.4581

APPENDIX E: EQUIPMENT SPECIFICATIONS AND ILLUSTRATIONS

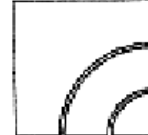
Type	h	h1	l	l1	l2	g	g1	p	a	b	e	f	c	ø s	m	Saugseite		Saugseite		Gewicht kg
																DN	AG	DN	AG	
UP 80	56	121	277	104	143	111	163	113	71	90	90	112	8	6	32	10	G 1/2"	10	G 1/2"	5,2
UP 100	56	126	281	106	147	111	163	113	71	90	90	112	8	6	35	15	G 3/4"	15	G 3/4"	5,6
UP 115	63	140	315	119	164	126	156	125	80	100	97	116	6	7	35	15	G 3/4"	15	G 3/4"	6,4
UP 130	71	157	343	127	172	139	191	140	90	112	108	140	10	7	42	20	G 1"	20	G 1"	9,9
UP 150	80	176	388	152	203	157	209	159	100	125	125	160	11	10	47	25	G 1 1/2"	20	G 1"	16,3
UP 170	90	200	453	175	234	177	235	180	125	140	152	180	14	11	55	32	G 1 1/2"	25	G 1 1/4"	24,4
UP 190	100	220	481	182	241	198	256	200	140	160	175	205	14	12	60	32	G 1 1/2"	25	G 1 1/4"	29,7
UP 210	112	242	508	189	253	220	279	224	140	190	180	232	15	12	70	40	G 2"	32	G 1 1/2"	39,4



E.4 Reaction Kinetics Pump

sera

Dosieren
Fördern
Verdichten



PRODUCT DESCRIPTION IQS20551

COMM. NO. : 5584470

4.03.04 bt/bc

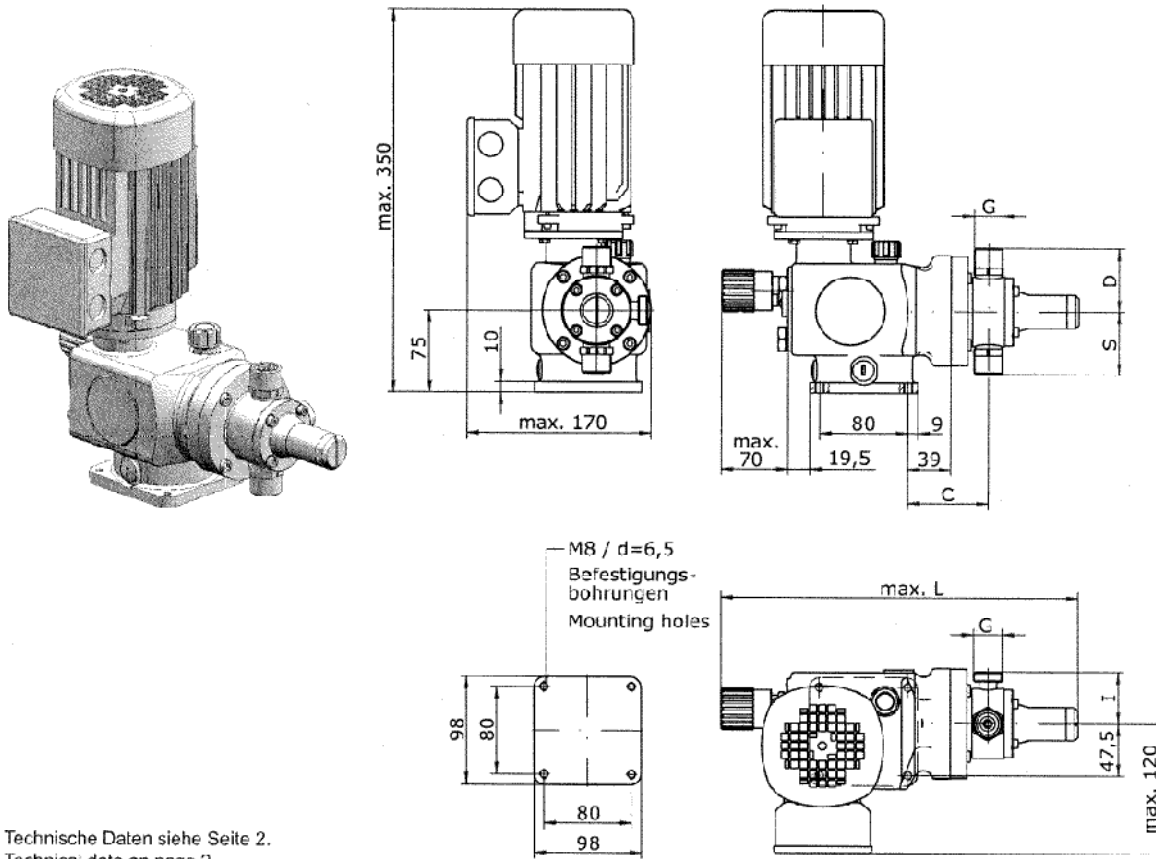
PAGE: 1

QTY

techn. contact: sales engineering
comm. contact: Mr Bürgel

- 2 Double diaphragm pump net
 RF 409.1 - 18
 Serial-No.276859- 276860
 Pump body: 1.4571
 with integrated relief valve
 Diaphragm: PTFE-faced
 Double valves: 1.4571/1.4581
 Valve balls: 1.4401
 Intern.diaphragm: PTFE
 Working diaphragm: PTFE-faced W
 Valve sealings: FEP-covered
 Connection thread: G 3/4
 Nom.no.of strokes: 0 - 50 L/h (QM) at 100 Hz
 Suction head: 3 MWC
 Manometr.pressure: 10 bar (P2 Max)
 Nom.No.of strokes: 300 l/Min at 100 Hz
 Buffer fluid: 13,5 cm glycerine
 Medium: ? solution without solids, approx. 20°C,
 max. 100 mPas
- 2 80180126 3-phase motor / size 63 0,180 KW
 230/400 V 50 HZ 1,13/ 0,65 A IP 55 ISO-XL F
 1370 UPM BAUFORM V18
- suitable for converter operation 5-100 Hz
 with integrated PTC-positors
- 6 Set net
 unit nut G 3/4 1.4571
 with pipe socket 1.4571 d-17,2

Documentation according to s e r a - standard
 3-fold English



Technische Daten siehe Seite 2.
 Technical data on page 2.

Dimensions in mm

Abmessungen / Dimensions											
Typ Type	G	C	FP, PVC, PVDF	I 1.457*	L	S Standard-Ventile / -valves			D Standard-Ventile / -valves		
						PVC	1.4571/ 1.4581	... - GFK ... - FRP	PVC	1.4571/ 1.4581	... - GFK ... - FRP
R 4C9.2 - 4,0 e	G 3/4	71	47	52	332	52	57	56	65	57	56
R 4C9.2 - 4,0	G 3/4	83	47	52	344	52	57	56	65	57	56
R 4C9.2 - 7,0 e	G 3/4	71	47	52	332	52	57	56	65	57	56
R 4C9.2 - 7,0	G 3/4	83	47	52	344	52	57	56	65	57	56
R 4C9.2 - 12 e	G 3/4	69	47	52	329	52	61	56	65	61	56
R 4C9.2 - 12	G 3/4	83	47	52	343	52	61	56	65	61	56

E.5 Mechanical Drawings of CSTRs and Wetted Wall

APPENDIX F: STATISTICAL PARAMETERS OF INTEREST FOR MODEL EVALUATION

In order to be able to critically assess and comment on the accuracy of the model fitted to the experimental data an understanding of the statistical parameters associated with the model fit must firstly be achieved. This section will briefly define these parameters.

F.1 Mean Squared Error

The mean squared error (mse) of a model fit is defined as:

$$\text{mse} = \frac{1}{N} \sum_1^N (y - y_{\text{pred}})^2 \quad (\text{F.1})$$

where

y = Observed or Experimental Data

y_{pred} = Model Predicted Data

N = Number of Data Points

This parameter is an indication of the average error of the predicted data to the observed data. A small mse ($<10^{-6}$) is desirable but it does not grant absolute clarity on the quality of the model fit, it merely indicates that the predicted values, on average, do not differ greatly from the observed values.

F.2 Pearson R^2 -value

The goodness of the model fit is deduced from the value of R^2 . R^2 is computed from the sum of the squares of the distances of the observed data from the best-fit curve determined by nonlinear regression. This sum-of-squares value is called SS_{reg} . To turn R^2 into a fraction, the predicted data are normalized to the sum of the square of the distances of the observed data from a horizontal line through the mean of all

observed values. This value is called SS_{tot} . If the curve fits the data well, SS_{reg} will be much smaller than SS_{tot} . The equation for determining R^2 is as follows:

$$R^2 = 1 - \frac{SS_{reg}}{SS_{tot}} \quad (F.2)$$

It is important to note that if SS_{reg} is larger than SS_{tot} , R^2 will be negative; this merely indicates a very poor fit.

F.3 Jacobian Matrix

For a regression function of the form:

$$y = \beta_1 x_1 + \beta_2 x_2 + \beta_3 x_3 + \dots + \beta_n x_n \quad (F.3)$$

The *Jacobian* matrix may be defined as:

$$J = \begin{pmatrix} \frac{\partial y_1}{\partial \beta_1} & \frac{\partial y_1}{\partial \beta_2} & \frac{\partial y_1}{\partial \beta_3} & \dots & \frac{\partial y_1}{\partial \beta_n} \\ \frac{\partial y_2}{\partial \beta_1} & \frac{\partial y_2}{\partial \beta_2} & \frac{\partial y_2}{\partial \beta_3} & \dots & \frac{\partial y_2}{\partial \beta_n} \\ \vdots & \vdots & \vdots & \vdots & \vdots \\ \frac{\partial y_n}{\partial \beta_1} & \frac{\partial y_n}{\partial \beta_2} & \frac{\partial y_n}{\partial \beta_3} & \dots & \frac{\partial y_n}{\partial \beta_n} \end{pmatrix} \quad (F.4)$$

where

$y_1, y_2, y_3, \dots, y_n$ are the predicted values for the dependant variable after optimizing the loss function of each model iteration. The *Jacobian* thus gives an indication of the change noticed in the predicted value with a change in the estimated model parameter. The confidence interval for each estimated model parameter rests strongly on the condition of the *Jacobian*. Large condition numbers and thus large confidence intervals are encountered when the columns of the *Jacobian* matrix differ greatly in order of magnitude or if one or more of the columns are zero or striving towards zero.

A large difference in order of magnitude indicates that for a change in one of the model parameters a large change results in the predicted value and vice versa, causing much doubt in the value of the parameters. A column of zeros indicates no change in the predicted value for any parameter value, which of course results in an astronomical confidence interval for that parameter.

The reason for obtaining large condition numbers for these cases is because the determinant of the outer dot product matrix becomes zero in the limit:

$$\lim \left| [J]' \cdot [J] \right| = 0 \quad (F.5)$$

which of course relates to a singular matrix with an undeterminable inverse. This causes great uncertainty in the estimation of the model parameters since the Levenberg-Marquard algorithm incorporates the inverse of the outer dot product matrix to optimization the loss function.

APPENDIX G: MODEL DATA

The model data for **Model 1** is tabulated in **Tables G1 – G9**:

Table G1: Model 1 Data, 25°C, $[\text{MEA}]_i = [\text{CO}_2]_i$

	k_1	k_2	k_3	k_4
	27.98	1.12E-13	2.69E-09	1.66E-14
Lower limit	15.65	-1.70E-14	-1.69E-09	-1.09E-14
Upper limit	41.70	2.30E-13	3.69E-09	2.69E-14
Mean Squared Error	7.9927E-04			
Pearson R²	0.8447			
Jacobian Condition	65535			

**Units of every $k \in \left[\frac{L^2}{\text{mol}^2 \cdot s} \right]$

Table G2: Model 1 Data, 25°C, $[\text{MEA}]_i = 2.5[\text{CO}_2]_i$

	k_1	k_2	k_3	k_4
	18.67	2.90	-5.43E-09	-4.16E-10
Lower limit	15.65	-1.91	-3.69	-3.69
Upper limit	21.70	7.72	3.69	3.69
Mean Squared Error	1.82E-03			
Pearson R²	0.9707			
Jacobian Condition	2.00E+18			

**Units of every $k \in \left[\frac{L^2}{\text{mol}^2 \cdot s} \right]$

Table G3: Model 1 Data, 25°C, $[\text{MEA}]_i = 4[\text{CO}_2]_i$

	k_1	k_2	k_3	k_4
	12.53	6.32	18.59	0.44
Lower limit	9.52	-25.90	-109.22	-5.15
Upper limit	15.53	38.54	146.41	6.03
Mean Squared Error	1.926E-03			
Pearson R²	0.9907			
Jacobian Condition	21468			

**Units of every $k \in \left[\frac{L^2}{\text{mol}^2 \cdot s} \right]$

Table G4: Model 1 Data, 30°C, [MEA]_i = [CO₂]_i

	k₁	k₂	k₃	k₄
	26.59	1.50E-12	2.38E-10	3.04E-14
Lower limit	-2.52E+16	-2.33E+22	-5.47E+37	-5.47E+37
Upper limit	2.52E+16	2.33E+22	5.47E+37	5.47E+37
Mean Squared Error	6.11E-04			
Pearson R²	0.8747			
Jacobian Condition	65535			

**Units of every $k \in \left[\frac{L^2}{\text{mol}^2 \cdot s} \right]$

Table G5: Model 1 Data, 30°C, [MEA]_i = 2.5[CO₂]_i

	k₁	k₂	k₃	k₄
	12.60	10.35	139	1.14
Lower limit	7.18	-13.67	-53	-7.06
Upper limit	18.03	34.37	331	9.34
Mean Squared Error	1.75E-03			
Pearson R²	0.9947			
Jacobian Condition	41580			

**Units of every $k \in \left[\frac{L^2}{\text{mol}^2 \cdot s} \right]$

Table G6: Model 1 Data, 30°C, [MEA]_i = 4[CO₂]_i

	k₁	k₂	k₃	k₄
	15.70	5.37E-12	8.20	5.64
Lower limit	10.69	-2.65E+06	-10.04	2.29
Upper limit	20.72	2.65E+06	26.44	8.98
Mean Squared Error	2.166E-03			
Pearson R²	0.9882			
Jacobian Condition	3.49E+18			

**Units of every $k \in \left[\frac{L^2}{\text{mol}^2 \cdot s} \right]$

Table G7: Model 1 Data, 35°C, [MEA]_i = [CO₂]_i

	k₁	k₂	k₃	k₄
	33.41	3.53	141.10	1.67E-13
Lower limit	18.51	-3.97	-46.13	-2.97E+06
Upper limit	48.31	11.04	328.33	2.97E+06
Mean Squared Error	7.55E-03			
Pearson R²	0.8678			
Jacobian Condition	65535			

**Units of every $k \in \left[\frac{L^2}{\text{mol}^2 \cdot s} \right]$

Table G8: Model 1 Data, 35°C, [MEA]_i = 2.5[CO₂]_i

	k₁	k₂	k₃	k₄
	26.44	22.97	230	5.43
Lower limit	16.83	-2.59	-6.93	-6.31
Upper limit	36.04	48.53	467	17.17
Mean Squared Error	2.33E-04			
Pearson R²	0.9922			
Jacobian Condition	42168.93			

**Units of every $k \in \left[\frac{L^2}{\text{mol}^2 \cdot s} \right]$

Table G9: Model 1 Data, 55°C, [MEA]_i = 4[CO₂]_i

	k₁	k₂	k₃	k₄
	28.01	-8.1E-08	39.81	-5.17E-10
Lower limit	3.98	-6.77	-17.27	-6.77
Upper limit	52.05	6.77	96.89	6.77
Mean Squared Error	3.753E-03			
Pearson R²	0.8432			
Jacobian Condition	2.41E+18			

**Units of every $k \in \left[\frac{L^2}{\text{mol}^2 \cdot s} \right]$